Investigating resting-state and motor-related brain dynamics using multimodal neuroimaging data

Alba Xifra Porxas

Graduate Program in Biological and Biomedical Engineering

McGill University, Montreal, Quebec, Canada

August 2020

A thesis submitted to McGill University in partial fulfillment

of the requirements of the degree of Doctor of Philosophy

Abstract

Coherent neural oscillations are distributed spatially and emerge even at rest, giving rise to the so-called brain networks. This fundamental characteristic of brain function is termed functional connectivity and has been widely investigated using neuroimaging modalities such as magnetoencephalography (MEG), electroencephalography (EEG) and functional magnetic resonance imaging (fMRI). This thesis capitalized on all the aforementioned neuroimaging modalities to investigate different facets of brain dynamics and estimates of functional connectivity.

The first work of this thesis examines age-related differences in spontaneous and motor-related brain dynamics. It particularly focuses on the effects of healthy aging on beta oscillations and its potential link to motor performance. Movement-related beta oscillations are a brain phenomenon that has been extensively studied and is known to be aberrant in multiple movement disorders. During movement there is a strong decrease in beta oscillatory activity known as movement related beta desynchronization (MRBD), which dissipates shortly after movement cessation. Conversely, during sustained muscle contractions, there is a relative increase in beta oscillatory activity with respect to MRBD levels. Using MEG recordings from young and older adults performing sustained and dynamic hand contractions, we demonstrate that older adults exhibit a more pronounced modulation of beta oscillations during movement execution compared to their younger counterparts.

The second work of this thesis switches the focus on the neural and physiological contributions on estimates of functional connectivity measured with fMRI data. fMRI is a complex signal that infers changes in neuronal activity via changes in local cerebral blood flow. However, physiological processes and motion artifacts can also induce variations in the fMRI signal, which can in turn lead to artifactual estimates of functional connectivity. In this work, we develop an innovative framework to characterize the spatial signature of head motion and physiological processes (cardiac and breathing activity) on estimates of functional connectivity. Capitalizing on a large cohort from the Human Connectome Project,

we show that a substantial variance of functional connectivity measures can be attributed to non-neural processes. We also assess the performance of several state-of-the-art preprocessing strategies in mitigating the effects of nuisance processes. Interestingly, we find that these non-neural functional connectivity patterns are to some extent subject specific; however, fMRI data corrected for these confounds improves subject discriminability, which suggests that neural-related functional connectivity patterns are characterized by an even stronger subject specificity.

The third study of this thesis investigates the effect of global signal regression (GSR) on fMRI studies. GSR is a widely used preprocessing method that consists in regressing out the mean time-series across all fMRI voxels with the goal of removing global confounds. However, its usage is controversial since it is not clear whether GSR also removes neuronal-related signal of interest. Capitalizing on a dataset with simultaneous EEG-fMRI and physiological recordings, we examine the processes underpinning the global fMRI signal and the implications of GSR for functional connectivity studies. We show that physiological fluctuations explain a much larger fraction of the global fMRI signal variations compared to electrophysiological fluctuations, both at rest and during a behavioural task. Furthermore, we demonstrate that GSR effectively reduces the artifactual connectivity arising from systemic fluctuations, while preserving the connectivity patterns associated with alpha and beta power activity.

Résumé

Les oscillations neuronales cohérentes sont réparties spatialement dans le cerveau. Elles sont présentes au repos et sont à la base des soi-disant réseaux cérébraux. Cette caractéristique fondamentale de la fonction cérébrale est appelée connectivité fonctionnelle. Elle a été largement étudiée grâce aux données recueillies à l'aide des modalités de neuroimagerie telles que la magnétoencéphalographie (MEG), l'électroencéphalographie (EEG) et l'imagerie par résonance magnétique fonctionnelle (IRMf). Cette thèse capitalise sur les modalités de neuroimagerie susmentionnées qui permettent d'étudier les différentes facettes de la dynamique cérébrale et sur les modèles qui permettent d'estimer la connectivité fonctionnelle.

La première partie de cette thèse examine les différences liées à l'âge quant à la dynamique spontanée du cerveau dans le cadre des fonctions motrices. Elle se concentre en particulier sur les effets du vieillissement sain sur les oscillations du rythme bêta et son lien potentiel avec les performances motrices. Les oscillations du rythme bêta liées au mouvement représentent un phénomène cérébral qui a été largement étudié et qui est reconnu pour être altéré en présence de pathologies qui affectent le mouvement. Pendant le mouvement, une forte diminution de l'activité oscillatoire bêta connue sous le nom de désynchronisation bêta liée au mouvement (MRBD) est observée. Cette activité se dissipe peu de temps après l'arrêt du mouvement. Inversement, lors de contractions musculaires prolongées, une augmentation relative de l'activité oscillatoire du rythme bêta est observée par rapport au niveau d'activité présent lors du MRBD. Les signaux de MEG enregistrés lors de contractions de la main soutenues et dynamiques chez de jeunes adultes et chez des sujets plus âgés, nous a permis de démontrer que les personnes âgées présentaient une modulation plus prononcée des oscillations du rythme bêta pendant l'exécution du mouvement par rapport à leurs homologues plus jeunes.

La deuxième partie de cette thèse se concentre sur les contributions neuronales et physiologiques lors d'estimations de la connectivité fonctionnelle à partir de données obtenues à l'aide de l'IRMf. L'IRMf est un signal complexe qui infère des changements de l'activité neuronale via des fluctuations du flux sanguin cérébral local. Cependant, les

processus physiologiques et les artefacts associés au mouvement peuvent aussi induire des variations du signal IRMf, ce qui peut conduire à des estimations artéfactuelles de la connectivité fonctionnelle. Dans ce chapitre, nous avons développé un cadre innovant pour caractériser la signature spatiale associée au mouvement de la tête et aux processus physiologiques (activités cardiaque et respiratoire) lors d'estimations de la connectivité fonctionnelle. Capitalisant sur l'utilisation de données recueillies chez une large cohorte de sujets accessible dans le cadre du projet *Human Connectome*, nous démontrons qu'une variance substantielle des mesures de connectivité fonctionnelle peut être attribuée à des processus qui ne sont pas d'origine neuronale et évaluons la performance de plusieurs stratégies de prétraitement de données de pointe afin d'atténuer les effets de ces processus nuisibles. Fait intéressant, les modèles de connectivité fonctionnelle qui ne sont pas d'origine neuronale sont dans une certaine mesure spécifique à chaque sujet; cependant, les données d'IRMf corrigées en tenant compte de ces facteurs de confusion améliorent la discrimination des sujets, ce qui suggère que les modèles de connectivité fonctionnelle qui tiennent comptent de l'activité neuronale sont caractérisés par une spécificité du sujet encore plus marquée.

La troisième partie de cette thèse étudie l'effet de la régression du signal global (GSR) dans le cadre d'études IRMf. Le GSR est une méthode de prétraitement largement utilisée qui consiste à régresser la série temporelle moyenne sur tous les voxels d'IRMf dans le but d'éliminer les facteurs de confusion globaux. Cependant, son utilisation est controversée car il n'est pas clair si la GSR supprime également le signal d'intérêt lié à l'activité neuronale. Capitalisant sur un ensemble de données obtenues à partir d'enregistrements simultanés d'EEG-IRMf et de signaux physiologiques, nous examinons les processus qui sous-tendent le signal IRMf global et les implications du GSR dans le contexte d'études de connectivité fonctionnelle. Nous montrons que les fluctuations physiologiques expliquent une partie beaucoup plus grande des variations globales du signal IRMf par rapport aux fluctuations électrophysiologiques, à la fois au repos et pendant une tâche comportementale. De plus, nous démontrons que le GSR réduit efficacement la connectivité artéfactuelle résultant des fluctuations systémiques, tout en préservant les patrons de connectivité associés à la puissance de l'activité des rythmes alpha et bêta.

Original contributions

Study I (Chapter 3). Older adults exhibit a more pronounced modulation of beta oscillations when performing sustained and dynamic handgrips.

- To the best of our knowledge, this study is the first to investigate the beta rhythm (~20 Hz) modulations that occur during sustained contractions in the context of healthy aging.
- We provide original results from a MEG experiment including young and aging adults designed to elicit modulations in sensorimotor beta oscillations by requiring participants to sequentially produce sustained and dynamic hand contractions.
- Our study revealed that, during sustained contractions, there seems to be no significant differences in beta power between age groups beyond the ones observed at rest. Conversely, during dynamic contractions, we observed a stronger beta desynchronization in older adults, consistent with earlier studies. The finding that both age groups return to resting levels of beta activity during sustained contractions is particularly novel, as together with the established evidence that older adults exhibit increased beta suppression during dynamic contractions it demonstrates that aging adults produce a larger modulation of beta activity compared to their younger counterparts.
- We also show that, during dynamic contractions, age-related differences in the magnitude of beta desynchronization are not restricted to primary motor cortices but rather extend and are stronger in frontal and premotor areas.
- Our study included both unimanual and bimanual hand contractions, showing consistent findings between the two paradigms.

Study II (Chapter 4). Physiological and head motion signatures in static and time-varying functional connectivity.

- We describe a novel methodology for the characterization of physiological and head motion biases on estimates of functional connectivity at the individual level.

- Using multisession resting-state fMRI data from a large cohort, we demonstrate the biases in whole-brain functional connectivity profiles induced by the main fMRI confounds, namely head motion, systemic low-frequency fluctuations, breathing motion and cardiac pulsatility. Both static and time-varying measures of functional connectivity were investigated.
- The study further provides a comprehensive assessment of state-of-the-art fMRI denoising strategies in terms of reducing the effects caused by head motion and physiological noise and enhancing subject discriminability.
- Finally, we evaluate the potential subject specificity of the connectivity profiles associated with physiological and motion confounds, along with their role as hypothetical contributors to connectome fingerprinting accuracy.

Study III (Chapter 5). Does global signal regression alter fMRI connectivity related to EEG activity? An EEG-fMRI study in humans.

- We provide original results from a simultaneous EEG-fMRI experiment with concurrent physiological recordings regarding the validity of global signal regression (GSR), which is a preprocessing method based on regressing out the mean average signal across all fMRI voxels.
- We demonstrate quantitatively that physiological fluctuations related to changes in heart rate and breathing patterns account for a larger fraction of fMRI global fluctuations compared to fluctuations in electrophysiological (EEG) signal power, which is more directly related to the underlying neural activations, within specific bands.
- We further capitalize on the methodology developed in Study II (Chapter 4) to quantify the effects of GSR on whole-brain functional connectivity patterns associated with neural activity and physiological fluctuations. We show that GSR effectively removes the effects induced by changes in heart rate and breathing patterns, consistent with our results in Study II (Chapter 4), while not significantly altering the fMRI-based connectivity profiles associated with EEG activity.

Contributions of Authors

The main body of work presented in this manuscript-based thesis comprises three scholarly articles. All the work presented was authored by myself, in collaboration with my supervisor G. D. Mitsis and co-supervisor MH. Boudrias, as well as several other co-authors. Listed below are the specific contributions of the authors for each manuscript. An account of the author roles following CRediT taxonomy can be found in the preface of each manuscript.

Chapter 3 is based on the following article:

Xifra-Porxas, A., Niso, G., Larivière, S., Kassinopoulos, M., Baillet, S., Mitsis, G. D., Boudrias, M-H. (2019). Older adults exhibit a more pronounced modulation of beta oscillations when performing sustained and dynamic handgrips. NeuroImage 201, 116037. https://doi.org/10.1016/j.neuroimage.2019.116037

Alba Xifra-Porxas recruited the participants, contributed to the study design, implementation of the experimental paradigm and conceptualization of the research, participated in data collection, preprocessed and analyzed the data, designed the figures, interpreted the results, drafted the manuscript and arranged the final version.

Guiomar Niso participated in the study design and implementation of the experimental paradigm, contributed to the data analysis, aided in interpreting the results, and edited the manuscript.

Sara Larivière helped with participant recruitment and participated in data collection.

Michalis Kassinopoulos helped with the implementation of the experimental paradigm and assisted in data collection**.**

Sylvain Baillet contributed to the conceptualization of the research and edited and reviewed the manuscript.

Georgios D. Mitsis contributed to the conceptualization of the research, supervised the findings, and edited and reviewed the manuscript.

Marie-Hélène Boudrias contributed to the study design and conceptualization of the research, supervised the findings, and edited and reviewed the manuscript.

Chapter 4 is based on the following article:

Xifra-Porxas*, A., Kassinopoulos*, M., Mitsis, G. D. (under review). Physiological and head motion signatures in static and time-varying functional connectivity. * equal contribution. *Available as a preprint in bioRxiv*: https://doi.org/10.1101/2020.02.04.934554

Alba Xifra-Porxas contributed to the conceptualization of the research, performed the data curation, developed the methodology, preprocessed and analyzed the data, designed the figures, interpreted the results, drafted the manuscript and arranged the final version.

Michalis Kassinopoulos contributed to the conceptualization of the research, helped with the data curation, participated in the development of the methodology, aided in interpreting the results, and edited and reviewed the manuscript.

Georgios D. Mitsis contributed to the conceptualization of the research, supervised the findings, and edited and reviewed the manuscript.

Chapter 5 is based on the following article:

Xifra-Porxas, A., Kassinopoulos, M., Prokopiou, P., Boudrias, M-H., Mitsis, G. D. (in preparation). Does global signal regression alter fMRI connectivity patterns related to EEG activity? An EEG-fMRI study in humans.

Alba Xifra-Porxas recruited the participants, contributed to the study design and conceptualization of the research, participated in data collection, preprocessed and analyzed the data, designed the figures, interpreted the results, drafted the manuscript and arranged the final version.

Michalis Kassinopoulos contributed to the conceptualization of the research, implemented the experimental paradigm and set up the data acquisition framework, participated in data collection, assisted in data preprocessing, aided in interpreting the results, and edited and reviewed the manuscript.

Prokopis Prokopiou participated in data collection, assisted in data preprocessing, and aided in interpreting the results.

Marie-Hélène Boudrias contributed to the study design and edited the manuscript.

Georgios D. Mitsis contributed to the conceptualization of the research, supervised the findings, and edited and reviewed the manuscript.

Acknowledgments

First and foremost, I would like to thank my supervisor Georgios D. Mitsis, for giving me the freedom to explore and find my own research path, and co-supervisor Marie-Hélène Boudrias, for supporting my development during these past years. Your patience, encouragements and guidance helped me in all steps of my doctoral research.

I am also extremely grateful to my PhD committee members, Sylvain Baillet, Henrietta L. Galiana, and David J. Ostry, for their insightful comments and invaluable discussions. I may have dreaded your sharp questions, but I always left our meetings extra motivated and confident on what to do next.

To all the members of the lab, the ones who graduated and the new wave of students, as well as the ones that came for briefer periods. I appreciate all the conversations, advice and friendship in the past five years. Particular thanks to Kiki, Prokopis and Arna, who have endured me the longest hours. You made my PhD experience so much better.

Thank you also to all the volunteers that participated in my research. Without their patience and commitment this work would not have been possible.

To my friends back home, particularly Alba, Laura, Mònica and Núria, who helped me stay sane and get through this rollercoaster despite our geographical distance. You realise you have the best friends in the world when they turn the discouraging scenario of writing a thesis in the middle of a pandemic into an experience involving so much “online” laughter and joy.

To everyone at Cause4paws, for sending the most adorable cats to foster. They provided the best company during Montreal’s long winters and periodically walked on the keyboard to fix my writing.

To Michalis, for all our endless discussions about science, and because without your support none of this would have been possible. How you can stay positive and optimistic about everything I will never know, but I am so grateful to have you cheering me on. Thank you for

sharing this wild journey with me and filling these years with sweet memories. Can't wait to see what the future has in store for us!

Finally, my heartfelt gratitude and love to my late parents, for so many, many reasons, particularly for encouraging me to pursue whatever career I wanted from a very young age, and for spending way too much money on books for me. I wish you could see this achievement; I know you would have been so proud. Us trobo molt a faltar.

Contents

1

Introduction

1.1 MOTIVATION

Many electrophysiological studies have reported age-related changes in resting and task-related neural dynamics (Susi et al., 2019). However, there are still many aspects of the healthy aging process that need to be elucidated to differentiate it from pathological aging. Given the prevalence of motor control impairments in older adults, it is vital to characterize the motor-related neural correlates of healthy ageing in order to differentiate normal from aberrant neural oscillations that are present in several movement disorders (Crowell et al., 2012; Heinrichs-Graham et al., 2014; Kondylis et al., 2016; Proudfoot et al., 2017). The first goal of this thesis was to investigate age-related differences in spontaneous and motor-related brain dynamics. Specifically, we were interested in the effects of aging on the modulation of beta oscillations during sustained and dynamic hand contractions that has been observed in younger adults (Kilner et al., 2003; van Wijk et al., 2012).

Functional magnetic resonance imaging (fMRI) has also been used to elucidate age-related patterns of altered brain function, for instance differences in functional connectivity (Grady, 2012; Sala-Llonch et al., 2015). However, many confounds arise when using an indirect measure of brain activity such as fMRI, particularly when comparing populations that exhibit differences in vascular health, breathing and heart rhythms (e.g. young vs. aging adults). The validity of such studies critically depends on the extent to which fMRI accurately reflects neural activity, rather than physiological-related fluctuations or motion. The second objective of this thesis was to disentangle the neural and physiological influences on

functional connectivity profiles when using fMRI data. First, we sought to characterize the signatures of common sources of noise such as global systemic fluctuations, head motion, breathing motion and cardiac pulsatility on estimates of functional connectivity. Second, we aimed to demonstrate the performance of state-of-the-art denoising strategies with respect to removing these confounds. Popular denoising approaches to remove these artifacts rely on data-driven techniques such as independent component analysis (Pruim et al., 2015; Salimi-Khorshidi et al., 2014) and principal component analysis (Behzadi et al., 2007; Muschelli et al., 2014). However, it is not precisely clear which sources of noise these techniques account for. While there is evidence that data-driven techniques mitigate head motion artifacts (Ciric et al., 2017; Kassinopoulos and Mitsis, 2019a; Parkes et al., 2018), it still needs to be addressed whether physiological noise is also reduced. Our goal was to investigate to what extent data-driven denoising strategies reduce physiological noise and head motion artifacts.

A common yet controversial denoising method in fMRI is global signal regression (GSR). GSR consists in regressing out the mean BOLD signal averaged across all voxels with the goal of removing global physiological confounds and head motion. However, it is an open question whether GSR also removes neuronal-related activity. Most studies investigating the putative neural contributions on fluctuations of the global fMRI signal have related these neural variations to vigilance levels and arousal (C. W. Wong et al., 2016; Wong et al., 2013). However, these studies did not account for the possibility that the observed global fluctuations could be due to changes in physiological processes (e.g. heart rate), that are strongly linked to arousal levels (Bonnet and Arand, 1997; Olbrich et al., 2011). The third objective of this thesis was to investigate the physiological and neural basis of global fMRI fluctuations. Furthermore, GSR has been criticized with respect to possibly introducing artifactual negative correlations between the fMRI signals of different brain regions and consequently distorting functional connectivity measures (Murphy et al., 2009; Parkes et al., 2018; Power et al., 2014a). Nonetheless, these studies did not employ concurrent direct measurements of neural activity, and therefore were not able to address the question whether GSR is indeed distorting connectivity patterns of neural activity. Using simultaneous

EEG-fMRI data, we aimed to quantify the effects of GSR on connectivity profiles associated with EEG activity.

1.2 OVERVIEW OF THE THESIS

Ensuing chapters in this dissertation are organized as follows. Chapter 2 provides an overview of the principles behind the functional brain imaging techniques used in this thesis and offers background material in topics related to neural oscillations and functional connectivity. In Chapter 3, we use MEG recordings from 24 healthy young and older adults to investigate the impact of aging on resting and motor-related beta activity. Chapters 4 and 5 describe efforts to characterize major confounds in fMRI, specifically head motion and physiological noise. In Chapter 4, we propose a framework to quantify the effects of nuisance processes on estimates of functional connectivity. We further provide a comprehensive assessment of the performance of fMRI denoising strategies in terms of mitigating the evaluated artifacts using a large-scale multisession dataset. In Chapter 5, we investigate the physiological and neural substrates of the global fMRI signal capitalizing on EEG-fMRI and physiological recordings. Finally, chapter 6 provides a high-level summary of the key findings presented in this dissertation and outlines potential future directions.

2

Background

2.1 FUNCTIONAL BRAIN IMAGING MODALITIES

The quest to understand the human brain has been a scientific driver for centuries. This driving force has pushed boundaries in many scientific disciplines to develop new instrumentation and signal analysis techniques to measure neural activity *in vivo*. Noninvasive functional imaging methods are markedly crucial to unfold the mysteries of the human mind and have tremendously advanced in the past 25 years. These powerful tools allow researchers to study large-scale brain dynamics to improve our understanding of cognitive processes and better characterize normal and pathological brain function. Albeit functional neuroimaging techniques share the same goal, that is to measure brain activity, each method relies on different neurophysiological aspects associated with neural activity to achieve it (**Figure 2-1A**), which bestows each method with key advantages as well as limitations compared to other recording techniques (**Figure 2-1B**). Among the existing neuroimaging modalities, magnetoencephalography (MEG) and electroencephalography (EEG) uniquely have temporal resolutions below 100 ms, at the expense of low spatial resolution. Conversely, whole-brain functional magnetic resonance imaging (fMRI) provides spatial resolutions as high as 1 mm, however the temporal resolution is limited by the sluggishness of hemodynamic responses. Functional near infrared imaging (fNIRS) is based on similar principles as fMRI and hence has limited temporal resolution, besides low spatial coverage, but is sometimes preferred as it is portable and more affordable.

The following sections will provide introductory materials for the three non-invasive techniques employed in this thesis, namely MEG, fMRI and EEG, along with the basics of simultaneous EEG-fMRI acquisition.

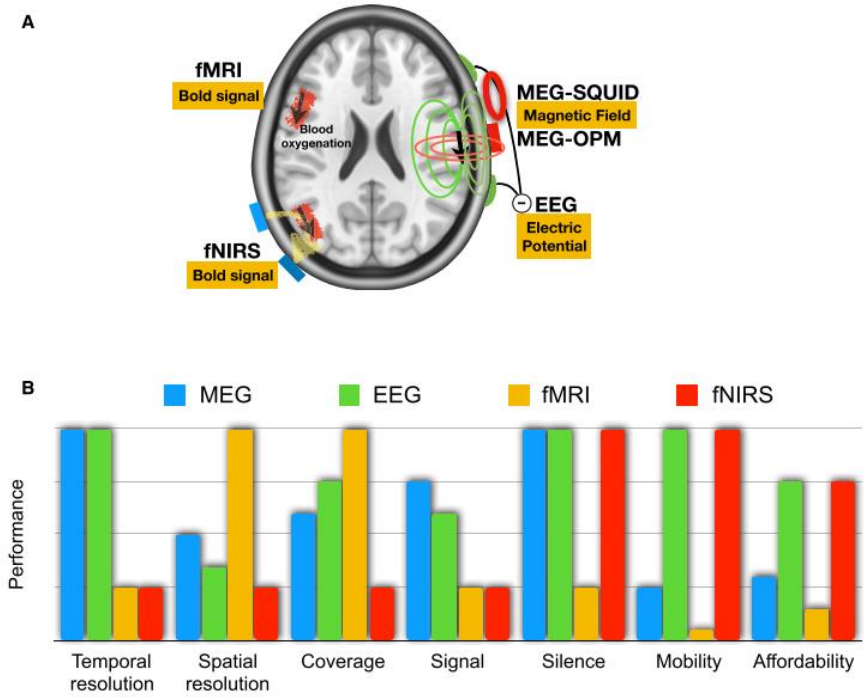

Figure 2-1. (A) Schematic figure illustrating how the most commonly used neuroimaging techniques measure brain activity. Black arrows denote current flow, which generate magnetic fields that can be recorded with MEG sensors and secondary currents that can be recorded as potential differences between EEG electrodes. fMRI and fNIRS are sensitive to changes in blood oxygenation triggered by neural activity. **(B)** Qualitative comparative ranking between MEG, EEG, fMRI and fNIRS. High bars indicate high performance. Reproduced from (Gross, 2019) with permission.

2.1.1 Electromagnetic brain imaging

Neuronal communication entails minute ionic currents that give rise to both electrical potentials on the scalp and magnetic induction outside the head, measurable by means of EEG and MEG, respectively. Thus, EEG and MEG are closely related noninvasive techniques whose signals are originated from the same neural cell assemblies. Their main differences arise as a result of the singular nature in which electric and magnetic fields spread. Both

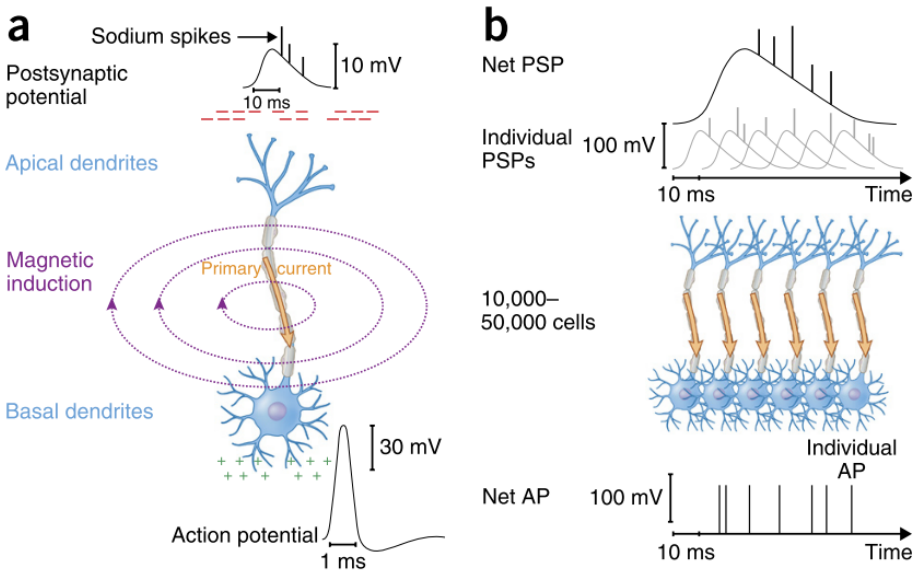

Figure 2-2. (a) Cellular origins of electromagnetic signals. **(b)** The summation of postsynaptic potentials (PSPs) from a large number of pyramidal neurons is needed to detect electromagnetic signals with EEG and MEG. Reproduced from (Baillet, 2017) with permission.

neurophysiological techniques are used to obtain novel insights into brain function, with particular emphasis on the temporal aspect of neuronal dynamics.

Now let's look more closely at the electrophysiological basis of EEG and MEG signals. We will focus on cortical pyramidal cells, which are neurons with a pyramidal shaped soma and two distinct dendritic trees: apical and basal dendrites, which receive input from other cells. Neuronal communication is achieved via action potentials. When an action potential from a neighbor or remotely located neuron arrives at a pyramidal neuron's apical dendrites, postsynaptic potentials (PSPs) are generated. PSPs induce an imbalance in electrical potentials between the apical dendritic arborescence of a pyramidal cell and its soma, which generates a current commonly referred as "primary current" (yellow arrow in **Figure 2-2a**). The primary current induces a magnetic induction perpendicular to the primary current flow (purple circles), as well as secondary electric currents (not pictured), which are the signal origins of MEG and EEG, respectively. Because of the elongated shape of pyramidal neurons and their spatial alignment perpendicular to the surface, at a large-scale the summation of slow and somewhat synchronous PSPs from tens of thousands of pyramidal cells produce signals detectable with EEG and MEG (**Figure 2-2b**). Therefore, it is mainly the slow PSPs

from populations of pyramidal cells in layers 3-6 which are considered the main neural generators of EEG and MEG, rather than action potentials (Baillet et al., 2001; Buzsáki et al., 2012), and importantly, the amplitude of EEG and MEG signals is largely based on the degree of neuronal synchrony. This has important implications as the synaptic input is far more energetically demanding (and thus likely to generate a hemodynamic response) than the synchronous activity. As a result, it is possible that a brain area may receive considerable input, though not yield a detectable electromagnetic signal (Butler et al., 2017).

The first human electroencephalogram was recorded by (Berger, 1929), even though at that time it was already known that the brain produced electrical fields that exhibit oscillations (Caton, 1875). Over the years, it has become an important brain imaging tool used both in neuroscience research and in the clinic. EEG measures brain electrical fields via electrodes attached to the scalp, and can thought of as a spatiotemporally smoothed version of local field potentials. Specifically, it measures voltage differences of the order of 50-100 μV between two electrodes at a time. Inhomogeneities in electrical conductivity (such as the skull and scalp) distort and smeared electrical currents, hampering identification of the underlying neural generators of EEG signals.

The possibility to measure extracranial magnetic inductions was then very appealing to researchers, as magnetic permittivity is, unlike electrical conductivity, homogeneous and identical across tissue compartments, and thus magnetic signals are less smeared and distorted by the skull (Okada et al., 1999). However, the weak magnetic inductions from the human brain are about 10^8 times smaller compared to the steady magnetic field of the earth. To measure them, a multilayered magnetically-shielded room is necessary to eliminate or dampen the environmental magnetic disturbances, as well as a pick-up coil through which the magnetic flux flows and induces an electrical current readily measurable. The first demonstration that measuring extracranial magnetic inductions was possible came around 40 years after Berger's first human electroencephalogram (Cohen, 1968). These early measurements required elaborate signal averaging to reveal the alpha rhythm with eyes closed, as the detectors used were not sensitive enough. Luckily, around that time a team of physicists had just developed an extremely sensitive device called SQUID (Superconducting Quantum Interference Device) (Zimmerman et al., 1970), which greatly improved the

sensitivity of MEG (Cohen, 1972). State-of-the-art commercial MEG systems feature a helmet with 306 SQUID detectors surrounding the head. For cooling purposes, the sensing apparatus is contained in a large liquid helium dewar (i.e. vacuum-insulated tank) within the gantry, which slowly boils away and needs to be replenished with about 70-100 fresh liters every week. This results in substantial operating costs, above the initial capital investment that is estimated around $3 million, which makes MEG considerably more expensive relative to EEG.

Both MEG and EEG sensor data record the evolution of brain activity at millisecond temporal resolution. Based on the measured EEG and MEG signals ("sensor space"), the generator currents may be inferred through source imaging ("source space"), usually in combination with structural MRI scans to account for individual variations in brain gyrification. Source imaging is an ill-posed problem as an infinite number of source models can fit the sensor data equivalently well (Hamalainen et al., 1993). Computing the most likely generator sources (i.e. the inverse solution) is therefore challenging, albeit relatively more straightforward for MEG, since additional assumptions about head-tissue layer conductivities are required in EEG. A variety of methods have been proposed to solve the inverse problem (Baillet, 2015). The approach later used in Chapter 3 is a beamforming method (Van Veen et al., 1997), which is a popular technique for source imaging that scans through a mesh of the brain surface to evaluate how a dipole at a specific location would fit the data while avoiding the crosstalk from other brain regions.

2.1.1.1 Differences between EEG and MEG

Consider a current dipole in the cortex with either of two orientations: radial or tangential to the surface of the head. Based on electromagnetic laws, the radial dipole produces no external magnetic field, whereas the tangential dipole does produce a magnetic field measurable outside the head. Conversely, both orientations do produce a surface potential. This results in an important difference between EEG and MEG signals: EEG is able to measure both tangential and radial dipoles, while MEG can only measure tangential dipoles. If we consider the gyrification of the brain and that pyramidal cells are oriented vertically to the cerebral cortex, dipoles located in the gyri are radial to the skull, and dipoles located in the sulci are tangential to the skull. Therefore, this means that MEG is more sensitive to neural

activity originating from sulcal walls, whereas EEG is sensitive to both (though slightly more sensitive to currents from gyral crowns because they are closer to the electrodes). This has implications regarding selective cancelation of EEG and MEG signals from extended sources (Ahlfors et al., 2010). Another consequence of MEG not being sensitive to radial sources is that activity from deep sources is also greatly suppressed, since they can be considered radial to the surface of the head. Coupled with the fact that the signal-to-noise ratio in MEG decreases faster with source depth, it is commonly believed that MEG cannot detect activity deep into the brain (but see recent advances in (Andersen et al., 2020; Pizzo et al., 2019)).

Given this, are the costs of purchasing and maintaining a MEG system worthwhile? As mentioned earlier, EEG signals are smeared by the high-resistivity skull and estimates of the tissue conductivities are necessary to localize neural activity, whereas MEG signals are not smeared and the head can be modelled as a single layer. All things equal, this would indicate that MEG localizes neural activity better than EEG, which is mostly true for tangential dipoles. Thus, because of skull smearing, EEG localization accuracy is about ± 9mm, whereas MEG localization accuracy can reach the sub-millimeter scale (Bonaiuto et al., 2018; Nasiotis et al., 2017). Furthermore, contributions from physiological contaminants such as ocular, cardiac and muscular artifacts are more easily removed in MEG compared to EEG, as in the latter is more difficult to distinguish between artifact components and high-frequency brain signals. However, ferromagnetic elements used in dental works and implants can cause complex artifacts in MEG, which is quite problematic when scanning older populations.

Another difference is that the magnetic induction measured by MEG is readily measurable in absolute physical quantities of the order of 100 fT, as it is proportional to the induced electric current on the pick-up coils. On the other hand, EEG signals are relative to a common reference electrode.

Moreover, there are evident practical differences between the two modalities. Subject preparation times are much shorter in MEG than in EEG, as MEG sensors are not attached to the scalp and therefore gel-free, eliminating the time spend in EEG for electrode positioning and impedance verification. However, this advantage comes at a price, as head movements during MEG acquisition considerably hinder data quality and comparisons between scans.

Subjects inside the MEG are therefore asked to keep their heads still, and real-time measurements of head movement and registration of head positions between participants are important factors for reliable MEG measurements. Conversely, during EEG recording subjects are relatively free to move, which permits recordings in real-life settings. EEG is also more versatile in terms of hyperscanning (Babiloni and Astolfi, 2014) and can be more easily combined with fMRI or stimulation techniques; for example, simultaneous EEG-fMRI is a powerful clinical tool for epilepsy (Krakow et al., 1999), whereas combining MEG with fMRI is rather unfeasible unless perhaps in the ultra-low field regime (Espy et al., 2013).

Overall, EEG and MEG are complementary modalities for noninvasive electrophysiology and imaging to explore the dynamics of the brain, and link those to cognition and disease (Baillet, 2017; Gross, 2019; Hari and Puce, 2017; Lopes da Silva, 2013).

2.1.2 Functional magnetic resonance imaging (fMRI)

Functional magnetic resonance imaging (fMRI) is based on the blood-oxygenation-level-dependent (BOLD) contrast mechanism (Ogawa et al., 1990). As the name suggests, fMRI detects changes in blood oxygenation induced by neural activity using a magnetic resonance scanner (Glover, 2011; Huettel et al., 2014; Nikos K Logothetis, 2008). Over the last few decades, fMRI has gained increased popularity as the standard technique to noninvasively study brain function, partly due to its high spatial resolution.

The fMRI signal is based on the principles of nuclear magnetic resonance, picking up local inhomogeneities in the magnetic field. An MR signal is localized in the three-dimensional space by the use of three gradient coils, through the processes of slice-selection, frequency encoding and phase encoding. Initially, proton spins in the brain are aligned with the static magnetic field and precess at the same frequency (known as the Larmor frequency). Next, a gradient magnetic field is superimposed along the z-axis, which causes spins to vary their precess frequency depending on their location with respect to the z-axis. Then, to select (i.e. excite) a specific slice, a radiofrequency pulse is delivered in the range of frequencies that the spins within that slice are precessing. Subsequently, the gradient coils along the x- and y-axis are superimposed at different times and strengths in order to modulate the precession frequency of the spins on the two-dimensional (2D) plane of a slice. Note that the modulation

of the gradients along the x- and y-directions is also referred to as frequency and phase encoding, respectively. The MR signal that is detected while the x and y gradient coils are changing corresponds to the 2D Fourier representation of the slice (i.e. k-space). Therefore, in the final step, the inverse Fourier transform of the MR signal is estimated to reconstruct the image of the slice.

The local inhomogeneities in the magnetic field are relevant to brain function as they reflect changes in metabolic activity through variations in the concentration of deoxyhemoglobin. Hemoglobin is a protein in the blood that transports oxygen from the lungs to the rest of the body to facilitate metabolism and carries carbon dioxide from the tissues to the lungs. Hemoglobin has different magnetic properties depending on whether it is bound to oxygen (oxyhemoglobin) or not (deoxyhemoglobin): oxyhemoglobin is weakly diamagnetic, whereas deoxyhemoglobin is paramagnetic (Pauling and Coryell, 1936). Inside the MR scanner, deoxyhemoglobin is weakly attracted to the magnetic fields, which induces local field distortions (Thulborn et al., 1982).

The role of hemoglobin in studying brain activity was recognised in the 1990s (Bandettini et al., 1992; Ogawa et al., 1990). Cerebral tissue is metabolically expensive, as the brain is only about 2% of the body weight but consumes about 20% of total blood flow. Further, the brain reserve of energy is very small, relying on continuous perfusion of blood from the vascular system to extract oxygen and glucose. Under resting conditions, oxyhemoglobin is converted to deoxyhemoglobin at a constant rate within the capillary bed. When there is a local increase in neural activity, however, a cascade of events are triggered that increase the vascular supply of oxygen-rich blood delivered to the activated region through vasodilatory processes that locally increase cerebral blood flow (Iadecola, 2017). For reasons not well understood, an overabundance of oxyhemoglobin is delivered to the brain tissue, which transiently increases the concentration of oxyhemoglobin (**Figure 2-3**). The result is a decrease in the amount of deoxygenated hemoglobin and a corresponding decrease in the

signal loss due to field distortions, leading to an increase in the BOLD signal [1]. Thus, fMRI can serve as a marker of neural activity via changes in local blood flow.

A central challenge in fMRI studies is distinguishing these neuronal-related signal fluctuations from the effects of motion, physiology and other sources of noise (Caballero-Gaudes and Reynolds, 2017). Head motion inside the scanner causes the content of an fMRI voxel to change and leads to spin-history effects (Friston et al., 1996). Volume realignment is regularly applied to account for head displacements and ensure that an fMRI voxel time-series corresponds to the brain activity of a specific region, however it does not account for spin-history effects and perturbations in the static magnetic field (B_0) after shimming correction. The motion parameters obtained from rigid-body volume realignment are often regressed out from fMRI time-series to correct for the remaining motion artifacts, however it has been shown that a considerable amount of motion-related variance still remains (Power et al., 2014b). Recent approaches such as volume censoring (Lemieux et al., 2007; Power et al., 2015) and ICA-AROMA (Pruim et al., 2015) have been identified as efficient strategies for motion correction (Parkes et al., 2018).

Non-neuronal physiological fluctuations are another source of noise that needs to be considered in fMRI studies. These fluctuations account for a fraction of the BOLD signal that is often comparable to that of neuronal-related activity. Cardiac pulsatility of blood flow in the brain generates brain tissue deformations, particularly in regions close to large arteries, and cerebrospinal fluid movement (Dagli et al., 1999). Breathing also corrupts the BOLD signal as it induces head motion and generates B_0 inhomogeneities through lung expansion (Power et al., 2015; Raj et al., 2001). The noise introduced by both cardiac pulsation and breathing motion is instantaneous and time-locked to the cardiac (~1 Hz) and respiratory (~0.3 Hz) cycles, respectively. The effects of cardiac pulsatility and breathing motion in the BOLD signal are frequently corrected using RETROICOR (Glover et al., 2000), considering that long repetition times (TR) can cause aliasing of these effects and thus low-pass filtering of the BOLD data is not an option. Finally, low-frequency cardiac and breathing activity, such

[1] Note that BOLD signal increases are readily observed in capillary vessels on the venous side of the cerebral vasculature rather than the arterial side, as venous blood contains both oxygenated and deoxygenated hemoglobin and therefore has a dynamic range, whereas arterial blood contains only oxygenated hemoglobin.

as variations in heart rate (Shmueli et al., 2007) and breathing patterns (Birn et al., 2006), also induces non-neuronal fluctuations in the BOLD signal, presumably through changes in blood flow (Tong et al., 2019). Heart rate and respiratory volume are usually extracted from concurrent physiological recordings and convolved with physiological response functions to account for low-frequency physiological noise (Birn et al., 2008b; Chang et al., 2009). Note that other blood-borne effects are also reflected on the BOLD signal, such as variations in levels of carbon dioxide (Wise et al., 2004) and changes in arterial blood pressure (Whittaker et al., 2019).

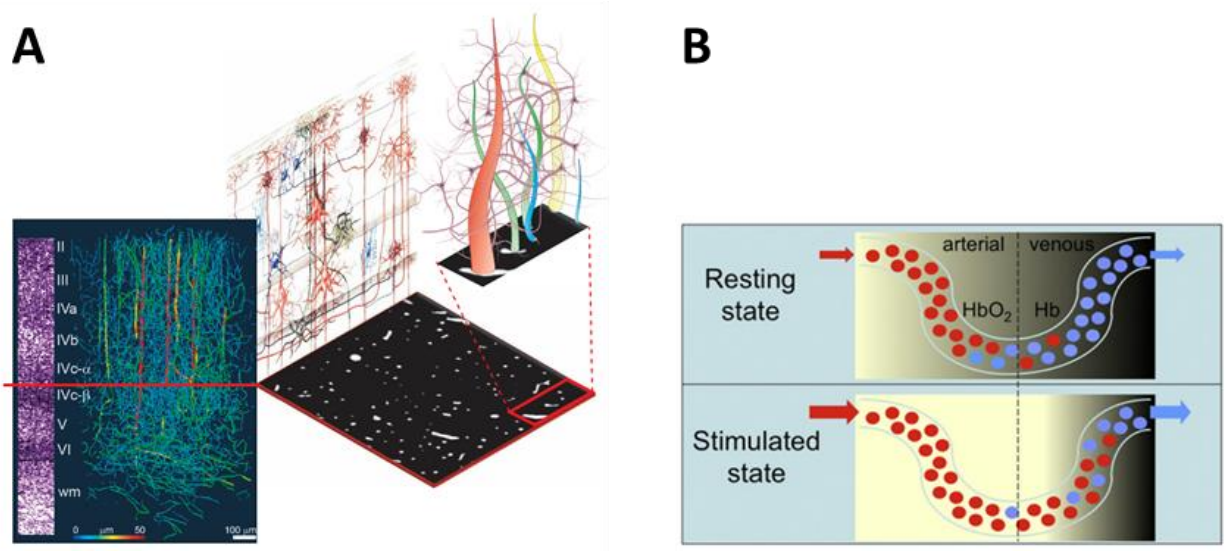

Figure 2-3. (A) Neural and vascular contents of an fMRI voxel. The left panel shows the dense vascular mesh of a monkey's visual cortex, color-coded by vessel diameter, as well as a Nissl slice from the same area showing neural density. The right figure illustrates a cross-sectional representation of a voxel, where white spots indicate small vessels. Note that the density of vessels is quite low (<3%), with an average distance between capillaries of about 50 μm. Neurons, synapses and glia occupy most of the intervascular space. Reproduced from (Logothetis 2008) with permission. **(B)** Drawing of a capillary when neurons are at rest (top) and active (bottom). Red circles represent oxyhemoglobin (HbO_2) and blue circles represent deoxyhemoglobin (Hb). At rest, the MRI signal is reduced in the venous side due to distortions of the magnetic field by paramagnetic Hb (darker background). When neurons become active blood flow increases, causing a transient increase in HbO_2 that sweeps out Hb and results in a BOLD signal increase (mostly on the venous side, note background change). Reproduced from (Glover 2011) with permission.

2.1.3 Simultaneous EEG-fMRI

As mentioned in the previous sections, scalp EEG provides millisecond temporal resolution but relatively poor spatial resolution, whereas BOLD fMRI offers excellent spatial resolution but poor temporal resolution. Simultaneous acquisition of both modalities provides a great opportunity to integrate their complementary characteristics towards improving our understanding of brain function (Mulert and Lemieux, 2010). For example, concurrent EEG-fMRI recordings have proved to be effective in studying epilepsy (Gotman et al., 2006; Krakow et al., 1999). However, their multimodal integration comes with many challenges as the MRI environment introduces several different types of artifacts in the EEG signals, among them the gradient and ballistocardiogram (BCG) artifacts (D. Mantini et al., 2007). The gradient artifact is induced by the switching of gradient magnetic fields used for spatial encoding of MRI signals, and is several orders of magnitude larger than the EEG signal (**Figure 2-4a**). Yet, its predictability and reproducibility in terms of shape and amplitude makes it relatively easy to remove postprocessing. The BCG artifact arises from slight electrode motion in the static magnetic field, as a result of the subject's pulsatile scalp and blood movement, and is of comparable or slightly higher magnitude than that of EEG (**Figure 2-4b**). Techniques such as average template subtraction are essential to remove these artifacts (Allen et al., 1998). Nonetheless, further preprocessing is usually required to remove traces of the gradient and BCG artifacts, as well as ocular artifacts (**Figure 2-4b**), commonly achieved using independent component analysis.

Currently, noninvasive simultaneous scalp EEG–fMRI experiments provide the best opportunity to examine the relationship between neural and hemodynamic fluctuations in humans because simultaneous, invasive intracranial EEG–fMRI measurements are not easily feasible.

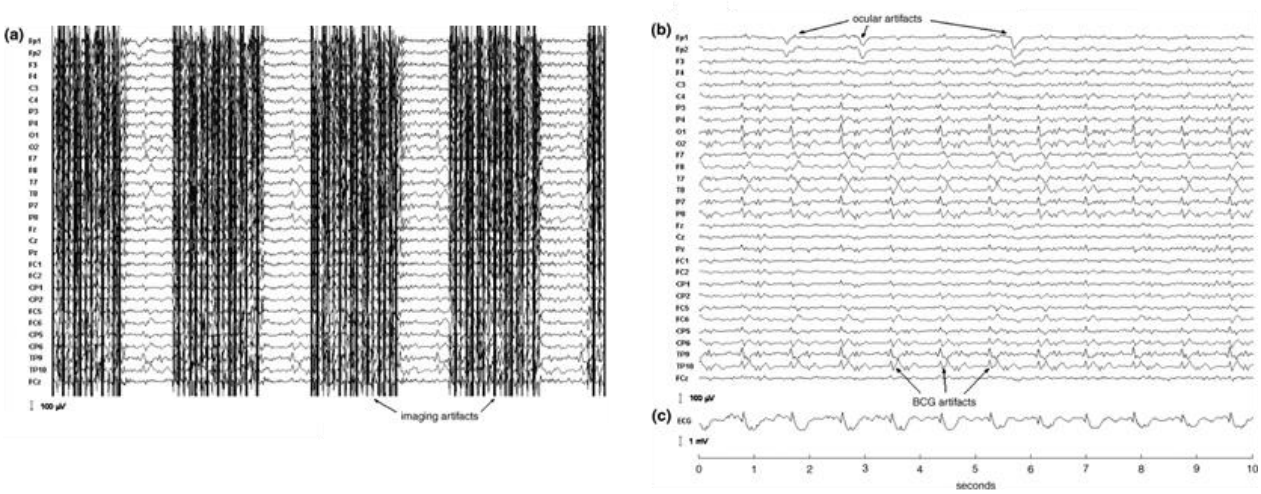

Figure 2-4. (a) Gradient artifacts. **(b)** BCG artifacts. Note that it is aligned to the cardiac cycle shown in **(c)** from an ECG recording. Reproduced from (Mantini et al. 2007) with permission.

2.2 OSCILLATORY ACTIVITY IN THE SENSORIMOTOR CORTEX

Brain rhythmic activities are widely implicated in cognition and in neural computations. Neural oscillations are usually categorized into the following frequency bands: delta (1-4 Hz), theta (4-8 Hz), alpha (8-13 Hz), beta (14-30 Hz) and gamma (>30 Hz). The reactivity of different brain rhythms can be quantified by computing their amplitude envelopes and monitoring their changes. Two well-known brain rhythms that arise within the sensorimotor cortex are the alpha (sometimes referred as "mu") and beta rhythms. Beta rhythms arising in the precentral gyrus of humans at rest were first described by (Berger, 1929), (Jasper and Penfield, 1949) subsequently detailed the transient blocking of the beta sensorimotor rhythm during voluntary movements, and (Chatrian et al., 1959) demonstrated a concurrent blocking of the mu rhythm as well as a transient increase in beta activity following movement termination.

Following these founding studies, the time-locked modulations of 10 Hz and 20 Hz oscillatory activity in response to movement has been extensively reproduced and are highly reliable (Cheyne, 2013; Espenhahn et al., 2017) (**Figure 2-5A**). Specifically, during preparation and execution of actions, there is a strong decrease in mu and beta activity relative to resting levels that begins about 1 s prior to movement onset [2], known as movement-related beta desynchronization (MRBD). Mu power suppression associated with the initiation of movement is widespread and bilateral (Alegre et al., 2004), whereas beta power attenuation is more restricted over sensorimotor areas (Alegre et al., 2004) and strongest contralateral to movement (Jurkiewicz et al., 2006) (**Figure 2-5B**). The mu power attenuation is sustained throughout movement and dissipates shortly after its termination (Pfurtscheller and Lopes da Silva, 1999). The decrease in beta oscillations lasts as long as there are continuous changes in muscle contraction (Erbil and Ungan, 2007; Omlor et al., 2011), whereas beta activity displays a relative increase in power during sustained contractions (Baker, 2007; Cassim et al., 2000; Kilner et al., 2003, 1999; Spinks et al., 2008; van Wijk et al., 2012). After movement, beta oscillations exhibit a period of increased amplitude relative to resting levels, known as post-movement beta rebound (PMBR)

[2] Note that if the interstimulus intervals are jittered across trials the desynchronization starts at movement onset (Alegre et al., 2003; Kilavik et al., 2013).

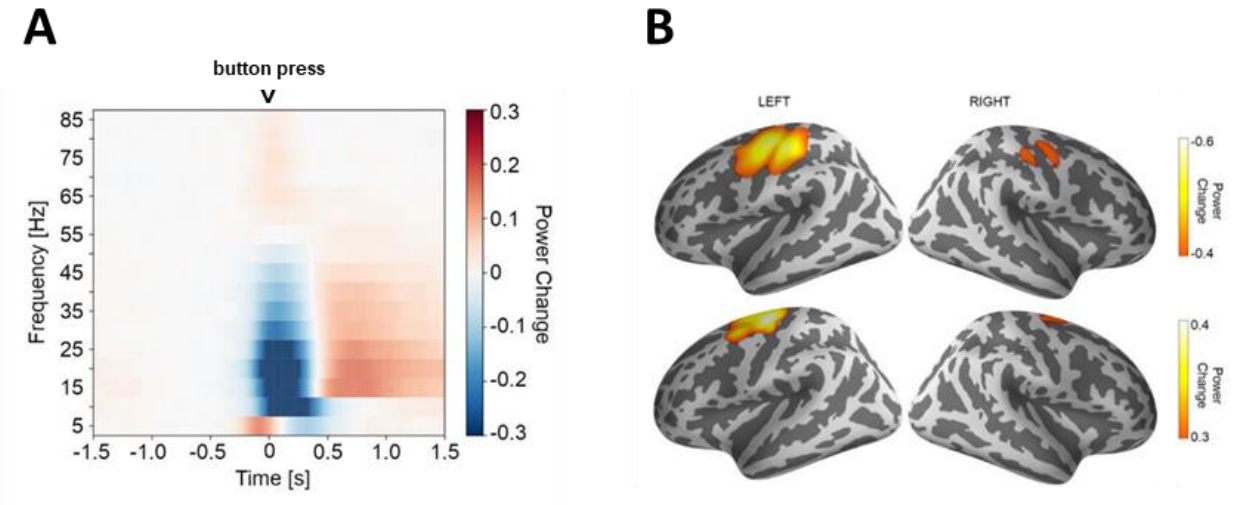

Figure 2-5. (A) Time-frequency response of the induced response to a button press at the contralateral primary motor cortex. Desynchronization of mu and beta rhythms are evident, as well as the beta rebound after movement cessation. **(B)** Localization of beta desynchronization (upper row) and beta rebound (lower row) of a right-hand button press. Adapted from (Bardouille et al. 2019) with permission.

(**Figure 2-5A**). PMBR overshoots around 1-2 seconds after movement cessation and is strongest in the hemisphere contralateral to the limb performing the movement (Fry et al., 2016; Jurkiewicz et al., 2006) (**Figure 2-5B**). Finally, recent evidence pointed at a direct relationship between spontaneous beta power and beta ERD (Heinrichs-Graham et al., 2018; Heinrichs-Graham and Wilson, 2016); specifically, greater beta suppression during movement seems to be associated with more pronounced spontaneous beta oscillations.

Developmental and aging studies have shown that motor-related beta oscillatory patterns change as a function of age. For example, during typical development from child to adolescent, the magnitude of MRBD and PMBR increases (Gaetz et al., 2010). Likewise, aging has been associated with stronger MRBD and spontaneous beta power (Bardouille et al., 2019; Heinrichs-Graham and Wilson, 2016; Rossiter et al., 2014), and PMBR seems to decrease with age (Bardouille et al., 2019). A recent study across the lifespan provided further evidence of the linear increase in the magnitude of MRBD (Heinrichs-Graham et al., 2018). Taken together, these studies provide substantial evidence that there are major neurophysiological changes related to sensorimotor oscillatory activity that occur throughout the lifespan.

2.3 FUNCTIONAL CONNECTIVITY

Sensory information from the periphery reaches the cerebral cortex via thalamocortical connections (except olfaction). Despite acting as a relay station, the thalamus receives ~10 times more afferents from the cortex than from the periphery, and input from thalamic nuclei forms only 1% of all input the cortex receives (Braitenberg, 1974). It therefore seems that much of the local cortical activity depends on inputs from other parts of the cortex.

Growing interest in the integrated activity among cortical brain regions has prompted increasing attention towards brain connectivity (Sporns, 2013; Suárez et al., 2020). Functional connectivity measures the statistical interdependence between time-series from distinct brain regions and is commonly studied using fMRI. Even in the absence of overt behaviour, resting-state networks fluctuate together at frequencies between [0.01, 0.1 Hz] that strongly overlap with brain regions commonly modulated during behavioral tasks (Biswal et al. 1995; Fox & Raichle 2007) (**Figure 2-6**). Presence of anticorrelations between large-scale brain networks have been reported, the most predominant being the default mode network routinely exhibiting deactivation during a task and activation during rest, and task-related networks exhibiting activation during a task and deactivation during rest (Fox et al., 2005).

To date, functional connectivity has largely been studied under the assumption that it is relatively static during a scanning session. However, several studies challenged this assumption (Chang and Glover, 2010; Sakoglu et al., 2010), and recently the community has developed an increasing interest in the time-varying characteristics of connectivity within a single scanning session (Hutchison et al., 2013; Lurie et al., 2019). Existing approaches to measure changes in functional connectivity use techniques such as sliding-window correlations between brain regions or networks (Allen et al., 2014), hidden Markov models (Vidaurre et al., 2017), and time-frequency approaches (Chang and Glover, 2010). Regardless of how fluctuations in whole-brain functional connectivity are estimated, an interesting avenue is to capture the spatiotemporal organization of functional connectivity to describe how connectivity patterns change over time (Hansen et al., 2015).

Interestingly, whole-brain functional connectivity profiles exhibit high subject specificity (Finn et al., 2015; Gratton et al., 2018; Seitzman et al., 2019), have been associated to behavioral measures (Finn et al., 2015; Li et al., 2019b; Smith et al., 2015), and seem to be promising biomarkers for disease (Brennan et al., 2019; Gratton et al., 2019a, 2019b; Xia et al., 2018).

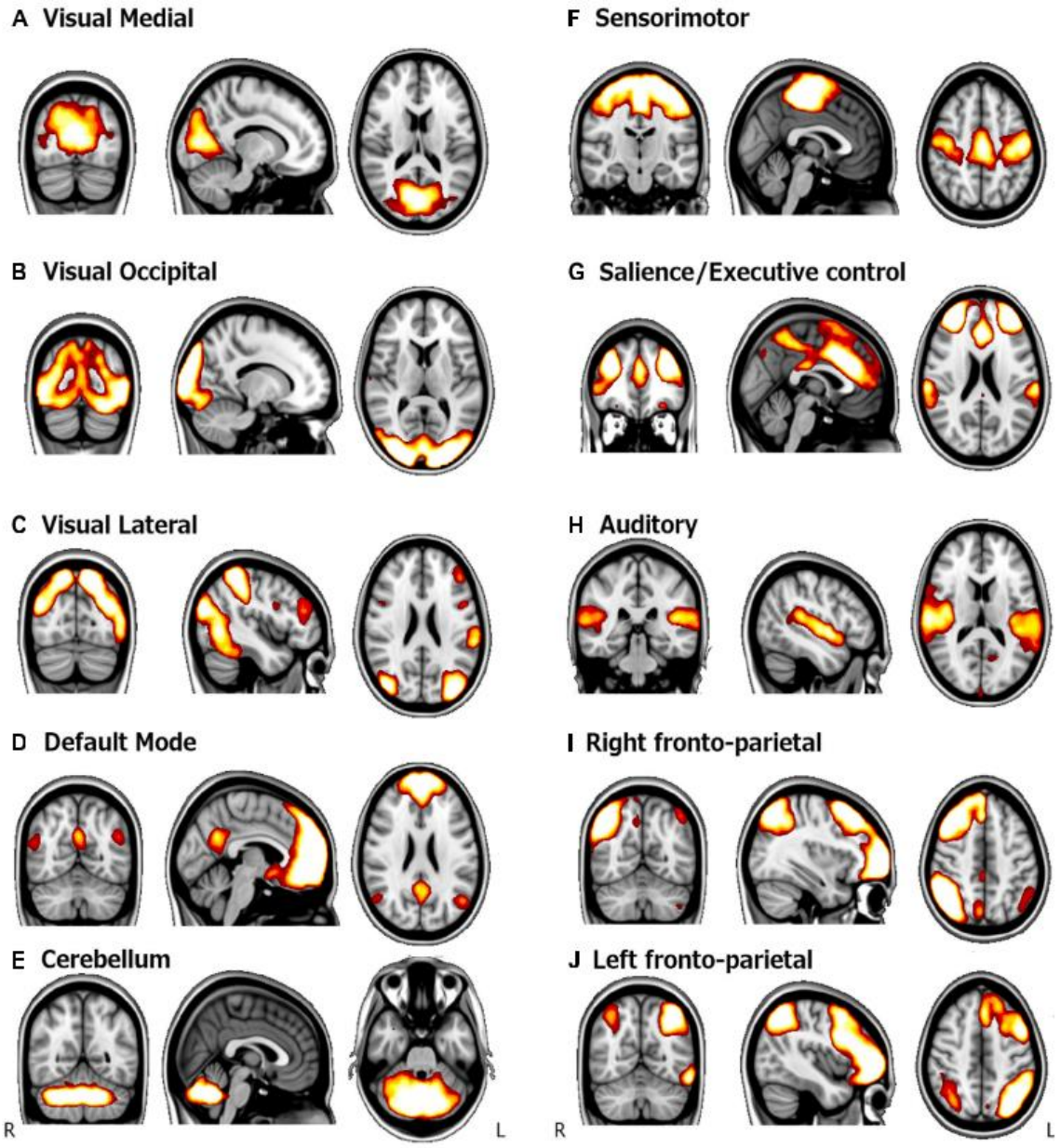

Figure 2-6. Large-scale brain networks identified by independent component analysis using resting-state fMRI data. Reproduced from (Sala-Llonch et al. 2015) with permission.

3

Older adults exhibit a more pronounced modulation of beta oscillations when performing sustained and dynamic handgrips

The following chapter was published as:

Xifra-Porxas, A., Niso, G., Larivière, S., Kassinopoulos, M., Baillet, S., Mitsis, G.D., Boudrias, MH. (2019). Older adults exhibit a more pronounced modulation of beta oscillations when performing sustained and dynamic handgrips. NeuroImage 201, 116037. https://doi.org/10.1016/j.neuroimage.2019.116037

CRediT authorship contribution

A. Xifra-Porxas: Conceptualization, Software, Investigation, Formal analysis, Data curation, Project administration, Visualization, Writing - original draft, Writing - review & editing. **G. Niso:** Conceptualization, Software, Formal analysis, Writing - review & editing. **S. Lariviere:** Investigation. **M. Kassinopoulos:** Software, Investigation. **S. Baillet:** Funding acquisition, Writing - review & editing. **G. D. Mitsis:** Funding acquisition, Supervision, Writing - review & editing. **MH. Boudrias:** Conceptualization, Funding acquisition, Supervision, Writing - review & editing.

3.1 PREFACE

The manuscript in this chapter describes an investigation of age-related changes in beta oscillations in the context of motor control, and its relationship with motor behaviour. Specifically, we examined a cohort of younger and older adults performing sustained and dynamic hand contractions. We used magnetoencephalography (MEG) and a paradigm that consisted of resting-state periods and unimanual and bimanual handgrips to characterize the effects of aging on the modulations of beta oscillations. This chapter provides new empirical evidence that older adults exhibit a more pronounced modulation of beta oscillations during movement execution compared to their younger counterparts. These results shed new light to the age-related neural correlates of motor control, which could be possibly used to design new therapeutic interventions using non-invasive brain stimulation techniques.

3.2 ABSTRACT

Muscle contractions are associated with a decrease in beta oscillatory activity, known as movement-related beta desynchronization (MRBD). Older adults exhibit a MRBD of greater amplitude compared to their younger counterparts, even though their beta power remains higher both at rest and during muscle contractions. Further, a modulation in MRBD has been observed during sustained and dynamic pinch contractions, whereby beta activity during periods of steady contraction following a dynamic contraction is elevated. However, how the modulation of MRBD is affected by aging has remained an open question. In the present work, we investigated the effect of aging on the modulation of beta oscillations and their putative link with motor performance. We collected MEG data from younger and older adults during a resting-state period and motor handgrip paradigms, which included sustained and dynamic contractions, to quantify spontaneous and motor-related beta oscillatory activity. Beta power at rest was found to be significantly increased in the motor cortex of older adults. During dynamic hand contractions, MRBD was more pronounced in older participants in frontal, premotor and motor brain regions. These brain areas also exhibited age-related decreases in cortical thickness; however, the magnitude of MRBD and cortical thickness were not found to be associated after controlling for age. During sustained hand contractions, MRBD exhibited a decrease in magnitude compared to dynamic contraction periods in both groups and did not show age-related differences. This suggests that the amplitude change in MRBD between dynamic and sustained contractions is larger in older compared to younger adults. We further probed for a relationship between beta oscillations and motor behaviour and found that greater MRBD in primary motor cortices was related to degraded motor performance beyond age, but our results suggested that age-related differences in beta oscillations were not predictive of motor performance.

3.3 INTRODUCTION

Aging is a multifaceted process, which involves alterations in brain structure and biochemistry. It is associated with reduced grey matter volume, cortical thinning, decreases of white matter myelination and neurotransmitter depletion (Minati et al., 2007). Motor functions tend to decline in old age in a broad array of motor tasks, manifesting in decline of fine motor control and coordination, slowing of movements, and impairments related to gait and balance, which in turn affect quality of life (Maes et al., 2017; Rosso et al., 2013; Seidler et al., 2010). Most common motor tasks require the combination of different types of muscle contraction, in which switches from static to dynamic force production occur frequently. However, age-related effects in brain dynamics during complex contraction sequences remain largely unknown.

Understanding how aging affects motor-related neural oscillations is fundamental to better understand the mechanisms of motor control in humans. A robust brain response induced by motor tasks is the modulation of beta sensorimotor rhythms. Beta oscillations are stronger during rest and are abolished during preparation and execution of motor tasks. This strong decrease in beta power relative to resting levels is known as movement-related beta desynchronization (MRBD) (Cheyne, 2013), and lasts as long as there is a muscle contraction (Erbil and Ungan, 2007; van Wijk et al., 2012). Several studies have reported age-related changes in beta oscillations during movement, such as a greater MRBD in both motor and premotor areas during right-hand finger extensions (Sailer et al., 2000), sequences of finger movements (Heinrichs-Graham et al., 2018; Heinrichs-Graham and Wilson, 2016), cued button presses (Bardouille et al., 2019), bimanual button presses in a go/no-go task (Schmiedt-Fehr et al., 2016), unimanual hand grips (Rossiter et al., 2014), as well as during a right-hand precision grip force modulation task (Hübner et al., 2018a). Interestingly, despite displaying increased MRBD, older adults exhibit higher absolute beta power during muscle contractions compared to younger adults (Heinrichs-Graham and Wilson, 2016). This is mostly due to the fact that older adults exhibit higher resting-state beta activity compared to their younger counterparts (Gómez et al., 2013; Heinrichs-Graham et al., 2018; Heinrichs-Graham and Wilson, 2016; Hübner et al., 2018a; Koyama et al., 1997; Veldhuizen et al., 1993). Pharmacological manipulations of GABA have shown that

increased levels of intracortical GABAergic inhibition lead to higher resting beta power and accentuated MRBD during dynamic contractions (Hall et al., 2011, 2010; Jensen et al., 2005; Muthukumaraswamy et al., 2013). These observations are closely related to the ones observed in aging, which seems to indicate that age-related changes are associated with changes in GABAergic inhibition. Following a motor task, beta oscillations exhibit increased amplitude relative to resting levels, known as post-movement beta rebound (PMBR). PMBR overshoots around 1-2 seconds after the cessation of a motor task and is stronger over the hemisphere contralateral to the moving limb (Fry et al., 2016; Jurkiewicz et al., 2006). Reduced PMBR has been observed in older adults (Bardouille et al., 2019; L. Liu et al., 2017). This suggests that altered brain structures and biochemistry due to aging have consequences on the observed motor-related neural activation patterns.

Steady muscle contractions are maintained by a continuous drive from the motor cortex to spinal motoneurons (Scott, 2012), during which there is a relative increase in beta power compared to dynamic contractions (Baker, 2007; Cassim et al., 2000; Espenhahn et al., 2017; Kilner et al., 2003, 1999; Schoffelen et al., 2008; Spinks et al., 2008; van Wijk et al., 2012). The functional role of this elevation in beta synchrony remains unclear; however, previous studies have suggested that it reflects the integration of afferent information to promote a stable motor output (Androulidakis et al., 2007, 2006; Gilbertson et al., 2005; Omlor et al., 2007). A study from Rossiter and colleagues (Rossiter et al., 2014) examined unimanual sustained handgrips in healthy aging, and found an increased beta suppression with age in the ipsilateral but not in the contralateral primary motor cortex (M1). This may suggest a heterogeneous effect of the aging process in different brain regions. However, the modulation of beta activity during sustained muscle contractions has not yet been formally examined in the context of healthy aging.

The aim of the present study was to examine the modulation of beta oscillations during sustained and dynamic contractions in healthy aging. We used a motor paradigm that included periods of steady handgrips and force modulation, both uni- and bimanual. Exploiting the high spatiotemporal resolution of MEG (Baillet, 2017), we investigated whole-brain age-related changes in spectral dynamics beyond the M1s. We also probed the association between age-induced differences in beta oscillations and motor performance.

Based on previous results, we expected greater resting beta power in older adults in motor areas (Heinrichs-Graham and Wilson, 2016; Rossiter et al., 2014) and hypothesized that age-related increases in resting beta activity would be present beyond the motor cortex since aging is associated with structural alterations in multiple brain regions. We further anticipated that older adults would exhibit increased MRBD during dynamic contractions (Heinrichs-Graham and Wilson, 2016; Hübner et al., 2018a; Sailer et al., 2000; Schmiedt-Fehr et al., 2016). In turn, this would indicate that greater beta desynchronization is required to produce muscle contractions, compensating for elevated resting-state beta power levels in the older population. Finally, we sought to investigate whether the increase in beta synchrony during sustained handgrips would exhibit age-specific differences.

3.4 MATERIALS AND METHODS

3.4.1 Participants

We studied 12 younger (age range 19-28 years) and 12 older (age range 60-74 years) healthy individuals recruited via advertisements. All participants were right-handed according to the Edinburgh Handedness Inventory (Oldfield, 1971). Subject characteristics are detailed in **Table 3-1**. Recruitment criteria included young subjects between 18-30 years and older adults above 60 years, and excluded subjects with a personal history of neurological and psychiatric disorder, as well as MEG exclusion criteria related to presence of ferromagnetic material (e.g. dental braces, metal implants and/or crowns). The study was approved by the McGill University Ethical Advisory Committee. All participants signed a written informed consent and were compensated for their participation. Measurements were carried out using the MEG facility at the McConnell Brain Imaging Centre (BIC) of the Montreal Neurological Institute (MNI), McGill University.

At the beginning of the session, participants completed the following behavioral assessment tests: Nine Hole Peg Test (9HPT) (Mathiowetz et al., 1985b), Box and Blocks Test (BBT) (Mathiowetz et al., 1985a), Purdue Pegboard Test (PPT) (Lindstrom-Hazel and VanderVlies Veenstra, 2015), and Hand Grip Strength (HGS) (Bohannon et al., 2006). All tests were performed using both hands to cover a range of upper limb motor abilities, from manual dexterity to strength. The 9HPT was measured in seconds, reflecting how quickly each participant placed and removed nine pegs into the holes of a board. The BBT was quantified as the number of blocks moved from one compartment of a box to another of equal size within 60 seconds. The HGS was measured in kilograms. The PPT was quantified as the number of pins placed into holes of a board within 30 seconds (dominant, non-dominant and both hands) or the number of assembled pins, collars and washers within 60 seconds (assembly test with both hands). Of note, PPT was not collected for two older subjects. All participants were screened for mental status by means of the mini mental state examination (MMSE) (Folstein et al., 1975). Wilcoxon rank-sum tests were used to determine whether behavioral assessments were significantly different between younger and older adults.

Table 3-1. Subject characteristics and behavioral scores: mean ± SD

		Younger (n=12)	Older (n=12)	*p* value
Age		24.2 ± 2.8	67.7 ± 3.7	
Sex		4 F / 8 M	3 F / 9 M	
Education		16.7 ± 1.9	15.3 ± 2.8	> 0.1
MMSE		29.2 ± 1.0	28.7 ± 1.3	> 0.1
9HPT (sec)	**Right Hand**	17.2 ± 1.8	20.5 ± 2.1	**< 0.0005**
	Left Hand	19.4 ± 2.4	22.7 ± 3.4	**< 0.01**
BBT (blocks)	**Right Hand**	68.3 ± 5.6	57.7 ± 3.9	**< 0.001**
	Left Hand	67.1 ± 6.1	57.4 ± 4.6	**< 0.001**
HGS (kg)	**Right Hand**	48.4 ± 14.6	39.4 ± 9.0	> 0.1
	Left Hand	39.2 ± 9.9	35.3 ± 7.7	> 0.1
PPT (pins)	**Right Hand**	16.9 ± 1.8	13.3 ± 1.6	**< 0.001**
	Left Hand	15.0 ± 1.5	12.7 ± 1.8	**< 0.01**
	Both Hands	12.8 ± 2.0	10.1 ± 1.1	**< 0.005**
	Assembly	42.8 ± 5.1	28.2 ± 5.7	**< 0.0001**

F = female, M = male, MMSE = mini mental state examination, 9HPT = nine hole peg test, BBT = box and blocks test, HGS = hand grip strength, PPT = Purdue pegboard test.

3.4.2 Experimental paradigm

The protocol carried out inside the MEG scanner consisted of two motor tasks alternated by three 5-min resting-state periods (**Figure 3-1a**). During the resting-state periods, subjects were instructed to stare at a white cross displayed on a screen in front of them. They were also instructed not to think of anything in particular and not to manipulate the hand grippers. After the 1st rest period, the maximum voluntary contraction (MVC) was obtained for each participant, using the same hand grippers later employed for the motor tasks. The first motor task consisted of a unimanual isometric right handgrip, during which the subjects had to apply force to track a ramp target as accurately as possible. At the onset of the trial, an orange circle appeared on the screen and the subjects had 2 seconds to increase their force to reach a white target block at 15% of their MVC. This force was held for 3 seconds. Subsequently, participants tracked a linear increase of the force to reach 30% of their MVC over a 3-second period, during which they had to maintain the circle inside the white target block, followed by a 3-second hold at this force (**Figure 3-1b**). A single trial lasted 11 seconds and was repeated 50 times for a total task duration of about 13 minutes. The second motor task consisted of bimanual steady isometric handgrips. At

the onset of the trial, two circles (blue and red) appeared on the screen and the subjects had 2 seconds to increase the force produced by both hands to 15% of their MVC. This force was sustained for 6 seconds (**Figure 3-1c**). A single trial lasted 8 seconds and was repeated 50 times for a total task duration of about 10 minutes. Visual feedback was provided throughout the experiment. For both tasks, the inter-trial interval was jittered between 3-5 seconds, during which subjects stared at a white cross. All subjects practised both motor tasks prior to the MEG acquisition to familiarise themselves with the experiment. Note that the order of the unimanual and bimanual conditions was not counter-balanced.

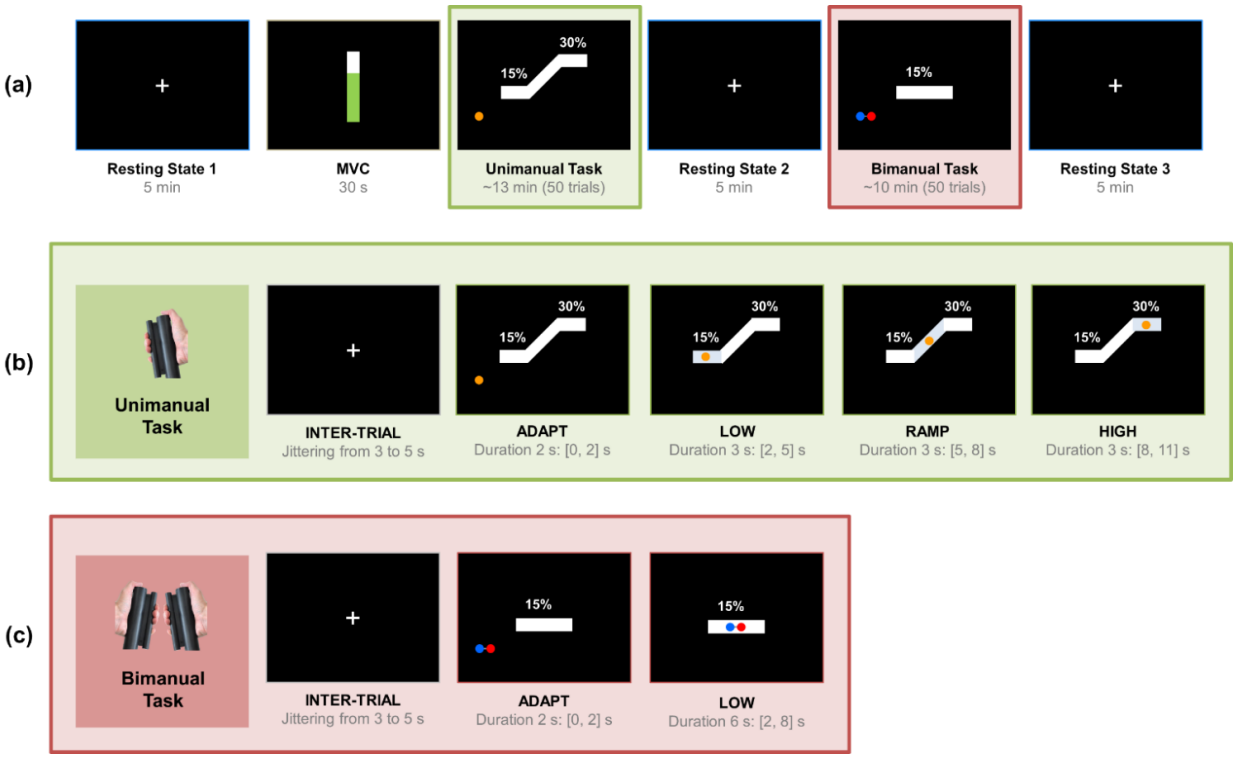

Figure 3-1. (a) Illustration of the protocol. Participants carried out two motor tasks inside the MEG scanner, alternated by three periods of rest, during which subjects fixated on a crosshair for 5 min. After the first rest period, the maximum voluntary contraction (MVC) was obtained for each participant. **(b)** Unimanual task. Participants fixated on a crosshair for a few seconds, for a jittered period lasting between 3 to 5 s. This was followed by the appearance of an orange circle on the screen, where participants had 2 s to apply force to reach 15% of their MVC. A steady grip was then maintained for 3 s, which was followed by a guided ramp period where participants had to apply force to reach 30% of their MVC and sustain this grip strength for another 3 s. **(c)** Bimanual task. Participants fixated on a crosshair for a jittered period lasting between 3 to 5 s. Subsequently, two circles (blue and red) appeared on the screen. Participants had 2 s to apply force to reach 15% of their MVC, which they sustained for 6 s.

3.4.3 Data acquisition and preprocessing

3.4.3.1 Hand grippers: Grip Force Fiber Optic Response Pad

A pair of non-magnetic, non-electronic hand grippers made from plastic to prevent noise in the MEG environment were used (Current Designs Inc, USA). The hand grippers consisted of a machined black enclosure with a protruding force bar that moved in when gripped to produce a linear force measurement output based on the pressure applied. We used a spring with a range of 500N. The dimensions of the force grip were 17.8 × 3.2 cm, with a force bar of 12.7 × 1.3 cm placed 2.5 cm outside the main enclosure. The maximum travel of this bar was 0.127 cm. The grippers were connected to a 932 interface through a 3-m long fiber pigtailed connector, which received the optical signals from the hand grippers in the MEG suite, and converted them into electrical signals that were transferred to a computer.

3.4.3.2 Neuroimaging data acquisition and preprocessing

MEG recordings were acquired with a 275-channel CTF whole-head system. Participants changed into non-magnetic clothes and performed the experiment in a seated position while their arms rested on the armchairs. Bipolar electrocardiogram (ECG) and vertical bipolar electro-oculogram (EOG) were acquired to correct for cardiac artifacts and eye movements. All signals were amplified and digitized at a sampling rate of 2400 Hz, and MEG files were saved after performing third order gradient correction. An empty-room noise recording was collected prior to the acquisition of each session to capture environmental noise conditions and was used in subsequent offline data analyses. The 3-D digitization of the head shape was done with a Polhemus Fastrak device, using around 100 head points distributed uniformly. Individual T1-weighted MRI images were acquired on a 3T MRI scanner (Siemens Prisma; TR=2300 ms; TE=2.32 ms; field of view=240 mm; voxel size=0.9×0.9×0.9 mm). The position of the head localization coils (nasion, left and right pre-auricular) and the head-surface points were used as anatomical references for coregistration between the MEG and MRI coordinate systems.

Offline data were processed using the open-source toolbox Brainstorm (Tadel et al., 2011). Notch filters were applied to remove power line artifacts around 60 Hz and harmonics.

MEG data were band-passed from 1 to 150 Hz. Cardiac and eye movement artifacts were detected using the ECG and EOG signals and corrected using signal-space projection (SSP). Artifacts due to external magnetic fields were removed visually using independent component analysis (ICA). Segments that presented motion artifacts or where subjects moved more than 5mm between head position measurements were discarded from the analysis. MEG signals were down-sampled to a 120-Hz sampling rate.

Resting-state periods. The 5-min recordings were segmented in epochs of 5 s. Epochs that had previously been found to be contaminated by motion artifacts were discarded. The average number of epochs after artifact rejection was 58.6±1.2/57.6±4.6 for younger/older adults (Resting-state 1), 58.3±2.4/56±5.4 for younger/older adults (Resting-state 2), and 56.3±9.3/57.4±2.2 for younger/older adults (Resting-state 3). The difference in the number of epochs between groups was not significant across any of the resting-state periods, as assessed using the Wilcoxon rank-sum test (Resting-state 1: p=0.473; Resting-state 2: p=0.185; Resting-state 3: p=0.679).

Motor tasks. Data from the unimanual task were epoched from -2.5 to +14 s, and data from the bimanual task were epoched from -2.5 to +11 s. Time 0 indicates onset of the visual cue for analysis. The average number of trials after artifact rejection was 40.4±10.4/40.3±9.1 for younger/older adults (Unimanual task), and 44.3±8.4/41.1±8.8 for younger/older adults (Bimanual task). The difference in the number of trials between groups was not significant for any of the tasks, as assessed using the Wilcoxon rank-sum test (Unimanual task: p=0.954; Bimanual task: p=0.277).

3.4.4 Data analysis

3.4.4.1 Behavioral analysis

The force exerted by the subjects was recorded using the calibrated hand grippers. The x and y screen positions of the applied force were also recorded for offline analysis. Task accuracy was quantified as the root mean squared error between the position on the screen and the target profile (defined as the middle of the target ramp), averaged over time and trials. Trials that exceeded 3 standard deviations were considered outliers and therefore not used in the computation of task accuracy. This was the case for two trials of a younger subject, which were also manually rejected in the MEG data.

3.4.4.2 MRI structural analysis

Cortical reconstruction and volumetric segmentation were performed with the FreeSurfer image analysis suite version 5.3.0 (http://surfer.nmr.mgh.harvard.edu/). The technical details of these procedures are described in prior publications (Dale et al., 1999; Dale and Sereno, 1993; Fischl et al., 2004, 2002, 2001, 1999a, 1999b; Fischl and Dale, 2000; Han et al., 2006; Jovicich et al., 2006; Reuter et al., 2012, 2010; Ségonne et al., 2004). Procedures for the measurement of cortical thickness have been validated against histological analysis (Rosas et al., 2002) and manual measurements (Kuperberg et al., 2010; Salat et al., 2004). Thickness measurements were mapped on the inflated surface of each participant's reconstructed brain and projected to the ICBM152 template using Brainstorm (Tadel et al., 2011). Maps were subsequently smoothed using a circularly symmetric Gaussian kernel across the surface with a full-width-half-maximum (FWHM) of 5 mm. Finally, cortical maps were compared between groups using non-parametric permutation tests combined with independent Student's *t*-tests of unequal variance. The null distribution was estimated with 10,000 permutations and results corrected for multiple comparisons using the false discovery rate (FDR) (number of signals 15,000). The structural analysis was done to identify the brain areas that presented differences in cortical thickness between groups. Particularly, we wanted to assess whether age-related differences in cortical thickness could have accounted for the differences observed in MRBD, reported in a previous study within the primary motor cortex (Provencher et al., 2016).

3.4.4.3 MEG source imaging

Lead fields were obtained using an overlapping spheres head model, which computes locally-fitted spheres under each sensor (Huang et al., 1999). Source reconstruction was performed using an extension of the linearly constrained minimum variance (LCMV) beamformer (Van Veen et al., 1997). A set of 15,000 elementary current dipoles distributed over the cortical surface was used, whereby the dipoles were assumed to be perpendicular to the cortical envelope. The empty room recording of a 2-min duration was used to estimate the noise covariance matrix. The data covariance matrix was estimated directly from the MEG recordings. The LCVM regularization parameter applied to the data covariance matrix was set as its median eigenvalue.

Resting-state periods. Normalized source power was computed using Morlet wavelets averaged across the 5 s segments (time resolution=3 s, central frequency=1 Hz) over the entire brain volume for the following frequency bands: alpha (8-12 Hz) and beta (16-28 Hz). The resulting source maps were smoothed with a 5 mm FWHM circularly symmetric Gaussian kernel and projected onto a standard space (ICBM152 template). Grand-averaged surfaces were computed across subjects for each group and frequency band.

Motor tasks. Single trial source waveforms were extracted per subject and decomposed to the time-frequency (TF) domain using Morlet wavelets (time resolution=3 s, central frequency=1 Hz). The evoked response was removed from each trial before computing the TF decomposition, a step that has been recommended for the evaluation of the TF decomposition of neurophysiological signals (Tadel et al., 2011). An average whole-brain TF map across trials was computed and subsequently averaged within the following frequency bands related to sensorimotor rhythms: alpha (8-12 Hz) and beta (16-28 Hz). We selected the 16-28 Hz frequency range to avoid including any power from the contiguous alpha and gamma bands. For both bands, relative power (RP%) was calculated as follows: $\boldsymbol{RP}\% = \frac{\mathbf{P}(t) - \mathbf{B}}{\mathbf{B}} \times \mathbf{100}\%$ (Pfurtscheller and Lopes da Silva, 1999), where P(t) is the absolute power at time t and B is the baseline power. B was defined as the mean power obtained from the 1st resting-state period (see section 3.4.4.7 for the effects of using different baselines). The RP% related to the beta band is denoted as MRBD and PMBR

during and after a muscle contraction, respectively. Subsequently, the *RP*% was averaged across several time windows for each subject. For the unimanual task, *RP*% was averaged within three 3-sec time windows: sustained contraction at 15% MVC (2 to 5 s), guided dynamic contraction from 15% MVC to 30% MVC (5 to 8 s), and sustained contraction at 30% MVC (8 to 11 s). For the bimanual task, the behavioral analysis showed that task accuracy did not reach the desired thresholds until around 4-5s after the onset of the trial, which suggests that subjects were not performing a sustained contraction in the first few seconds of the trial (**Supp. Fig. 3-1b**). Hence, *RP*% for the bimanual task was averaged within two 3-sec time windows: unguided dynamic contraction (2 to 5 s), and sustained contraction at 15% MVC (5 to 8 s). Cortical surfaces were obtained per participant, smoothed with a 5 mm FWHM circularly symmetric Gaussian kernel, and projected onto a standard space (ICBM152 template). Grand-averaged surfaces of each task time window were computed across subjects for each group and frequency band.

Statistics. For both rest and task, permutation testing was used to test for group differences across the whole brain. The test statistic used was the independent Student's *t*-test of unequal variance. For each comparison, 10,000 permutations were computed to build the null distribution. Significance testing was performed with a threshold of 5% using FDR correction for multiple comparisons (number of signals 15,000).

3.4.4.4 Modulation of beta oscillation

We were interested in examining whether the MRBD modulation observed during sustained and dynamic contractions in young subjects was altered in older subjects. To this end, regions of interest (ROIs) were selected for subsequent analysis. The peak MRBD ROIs were identified as the vertices showing the strongest MRBD (top 5%) within the motor cortex. Since dynamic contractions elicit increased MRBD compared to sustained contractions, the windows containing dynamic contractions (Unimanual: 5 to 8 s; Bimanual: 2 to 5 s) were grand-averaged across all subjects and used to define the ROIs related to MRBD. **Supp. Fig. 3-2** displays the peak MRBD ROIs, located within left and right M1, and **Supp. Table 3-1** provides the coordinates of the peak vertex of each MRBD ROI in MNI space. ROI power time-courses were then extracted and averaged across vertices. An ROI was also created from the whole-brain analysis that combined the brain regions identified

to exhibit stronger MRBD in older adults for both unimanual and bimanual tasks, henceforth called "*ageMRBD*". The three ROIs are depicted in the first row of Fig. 5.

The following *Modulation metrics* were used to quantify the depth of variations to which subjects modulated their beta power:

$$\boldsymbol{Modulation\ Unimanual} = abs\left(\beta_{[2,5]} - \beta_{[5,8]}\right) + abs\left(\beta_{[5,8]} - \beta_{[8,11]}\right)$$

$$\boldsymbol{Modulation\ Bimanual} = abs\left(\beta_{[2,5]} - \beta_{[5,8]}\right)$$

where $\beta_{[t_1,t_2]}$ is the averaged beta activity between time-points t_1 and t_2. The beta activity used to compute $\beta_{[t1,t2]}$ was the absolute beta power instead of MRBD and was extracted for all three ROIs (left peak MRBD, right peak MRBD, *ageMRBD*). In this fashion, we can quantify a relative measure of how much beta oscillations were modulated without confounds related to the resting beta power.

Statistics. The *Modulation metrics* were used to test for age-related differences. The data was transformed using the Box-Cox transformation (Box and Cox, 1964) to ensure that the assumption of normality was not violated. We conducted two separate mixed-model ANOVA's for each task, in which "brain region" (left peak MRBD, right peak MRBD, *ageMRBD*) was the within-subjects factor, and "age" (younger, older) was the between-subjects factor. The dependent variable was the modulation metric. A Greenhouse–Geisser correction was applied whenever Mauchly's test indicated a lack of sphericity. *Post hoc* Bonferroni-adjusted *t*-tests were performed whenever a main effect was detected, with an α-level of 0.05.

3.4.4.5 PMBR analysis

We were interested in examining whether PMBR exhibited differences between tasks, hemispheres and/or groups. PMBR is a brain response measure strictly localized in the motor cortex after a motor task, thus we did not perform a whole-brain analysis but focused on ROIs in the motor cortex. Windows starting 1.5 second after each trial and lasting 1 second (Unimanual: 12.5 to 13.5 s; Bimanual: 9.5 to 10.5 s), were grand-averaged across all subjects and used to define the peak ROIs related to PMBR (top 5%). PMBR was localized more anterior than MRBD in both hemispheres (**Supp. Fig. 3-2**), consistent with previous

studies (Fry et al., 2016; Jurkiewicz et al., 2006; Salmelin et al., 1995; Stancák and Pfurtscheller, 1995). **Supp. Table 3-1** provides the coordinates of the peak vertex of each PMBR ROI in MNI space. ROI power time-courses were then extracted and averaged across vertices.

Statistics. PMBR ROI time-courses were averaged within the previously defined 1-sec window for each task. These averaged PMBR values were used to test for power differences. The data was transformed using the Box-Cox transformation (Box and Cox, 1964) to ensure that the assumption of normality was not violated. Note that the data had to be translated prior to applying the transformation since the Box-Cox transformation cannot handle negative values. We conducted two separate mixed-model ANOVA's for each task, in which hemisphere (left, right) was the within-subjects factor, and age (younger, older) was the between-subjects factor. The dependent variable was the averaged PMBR. *Post hoc* Bonferroni-adjusted *t*-tests were performed whenever a main effect was detected, with an α-level of 0.05.

3.4.4.6 Association between beta oscillations and motor performance

To examine the relationship between beta oscillations and motor performance, we carried out separate linear regression analyses, using task accuracy and behavioral scores as the dependent variable respectively. Linear regression was applied separately for each task (unimanual and bimanual); hence in total 4 regressions were performed. The explanatory variables included in all regressions were:

1) Age
2) ***ageMRBD* ROI:** Modulation metric, averaged MRBD (Unimanual: 5 to 8 s, Bimanual: 2 to 5 s), averaged resting-state beta power.
3) **Peak MRBD ROIs (top 5%):** Modulation metric, averaged MRBD (Unimanual: 5 to 8 s, Bimanual: 2 to 5 s), averaged resting-state beta power.
4) **Peak PMBR ROIs (top 5%):** Averaged PMBR (Unimanual: 12.5 to 13.5 s, Bimanual: 9.5 to 10.5 s).

Neural features were extracted from both hemispheres separately. Thus, in total 12 and 8 features were used for the unimanual and bimanual tasks respectively. Principal

component analysis (PCA) was used to summarize the behavioral scores that involved unimanual (9HPT, BBT, PPT (Right hand)) and bimanual movements (PPT (Both hands and assembly)). The first PC was used as the dependent variable in the regression. To investigate whether any individual feature was significantly correlated to motor performance, we first divided the observations into two sets: training (90%) and testing (10%). We then permuted the labels, performed linear regression in the training set, used the linear model to predict the motor performance in the testing set, and calculated the root-mean-squared-error (RMSE) for the testing set. We carried this out 5,000 times to build the null distribution of the testing RMSE. During the second stage of analysis, we repeated the same procedure using the correct labels, and thus obtained the observed testing RMSE. This cross-validation analysis was done for each of the 4 regressions.

3.4.4.7 Effect of baseline on relative power calculation

An important step when examining motor-related oscillatory activity is to express it as a percentage of power change relative to baseline levels. This baseline period is usually defined between 0.5 to 3 s prior to task onset. However, the duration of the PMBR depends on the motor task characteristics and can last several seconds (Fry et al., 2016), which may result in contamination of the baseline if the inter-trial period is not long enough. Careful selection of the baseline is thus a crucial step. Further, it has been shown that older adults exhibit higher absolute beta power during muscle contractions compared to their younger counterparts, despite a larger decrease in beta power relative to baseline (Heinrichs-Graham et al., 2018; Heinrichs-Graham and Wilson, 2016). Therefore, it has been suggested that, to obtain a more holistic understanding of the age-related power changes during a motor task, both absolute and baseline-corrected power should be examined (Hübner et al., 2018a). To this end, we examined three scenarios: 1) Absolute beta power, 2) *RP*% with respect to an inter-trial baseline period (-1 to 0 s), 3) *RP*% with respect to the 1st resting-state period. The latter is the method used for all the subsequent analyses presented in this study.

3.5 RESULTS

3.5.1 Behavioral analysis

Behavioral scores are summarized in Table 1. Finger dexterity measured with 9HPT/PPT and unilateral gross manual dexterity measured with BBT were significantly worse in the older group for both hands. Bimanual finger dexterity coordination measured with PPT was also significantly inferior in older adults.

Regarding the motor tasks carried out inside the MEG scanner, all participants successfully completed both tasks. Differences in task accuracy during the tasks were not significant between age groups (Unimanual task: t_{22} = -0.32, p = 0.752; Bimanual task: t_{22} = 1.54, p = 0.138).

3.5.2 MRI structural analysis

No brain volume differences were found between groups (p = 0.16) (**Supp. Fig. 3-3a**). Cortical thickness was decreased in the older group mainly in frontal and temporal areas (FDR-corrected, p <0.01), as shown in **Supp. Fig. 3-3b**.

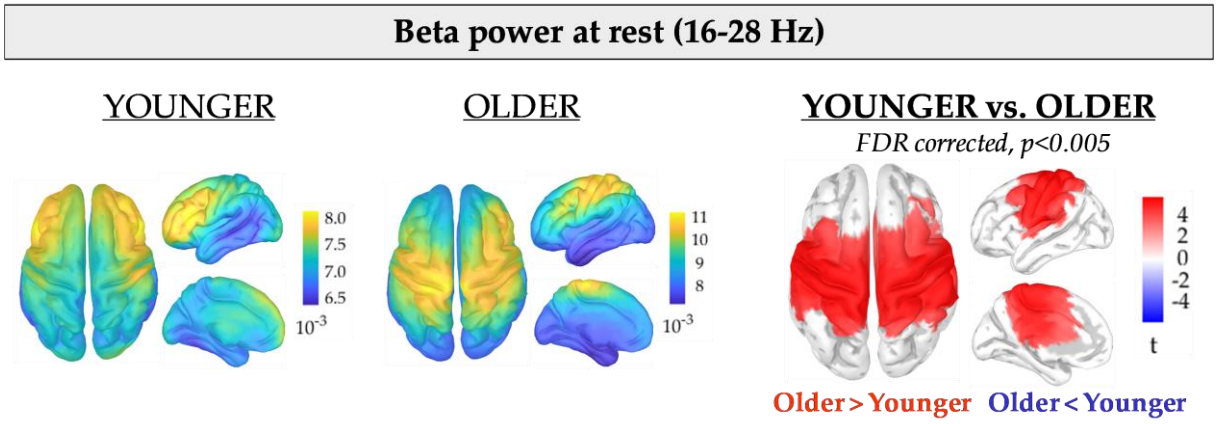

Figure 3-2. Beta power during the 1st resting-state. Left and middle panels: grand-averaged images across younger and older participants, respectively. Right panel: differences in oscillatory power at rest between groups (FDR-corrected, p<0.005). Older adults exhibited greater spontaneous beta power compared to younger adults.

3.5.3 Resting-state oscillatory power

Spontaneous beta power was higher in frontal and parietal areas, particularly in older adults (**Figure 3-2**, left and middle panels), and showed a significant age effect. Older adults exhibited higher beta power compared to their younger counterparts (**Figure 3-2**, right panel). This effect of age on beta power was more pronounced in motor areas, and extended to frontal, parietal and temporal brain areas. These age-related differences in spontaneous beta power were present in all three resting-state recordings. Spontaneous alpha power was greater in visual areas, in both younger and older adults (**Supp. Fig. 3-4**). However, no significant age effects were detected in the alpha band.

3.5.4 Whole-brain MRBD analysis

Unimanual task. Grand-averaged surfaces displaying MRBD are shown in **Figure 3-3b** (upper panel). We found significant differences in MRBD magnitude underlying dynamic force production between the two age groups (**Figure 3-3b**, bottom panel): older adults exhibited increased (i.e. more negative) MRBD during the guided dynamic contraction (5 to 8 s). No significant differences between groups were found during sustained contractions.

Bimanual task. Grand-averaged surfaces showing MRBD are shown in **Figure 3-4b** (upper panel). Similarly to the unimanual task, we found significant differences in MRBD magnitude between the two age groups only at the beginning of the trial (2 to 5s) (**Figure 3-4b**, bottom panel), during which older adults exhibited greater (i.e. more negative) MRBD. This specific time interval corresponds to the period when subjects had not yet accomplished a sustained grip and were thus still performing a dynamic contraction (**Supp. Fig. 3-1b**). The peak location of MRBD (denoted in white in **Figure 3-4b**, top row) did not exhibit significant age-related differences.

Results in the alpha frequency band for the unimanual and bimanual tasks are shown in **Supp. Fig. 3-5** and **Supp. Fig. 3-6**, respectively. Alpha desynchronization did not exhibit significant differences between groups.

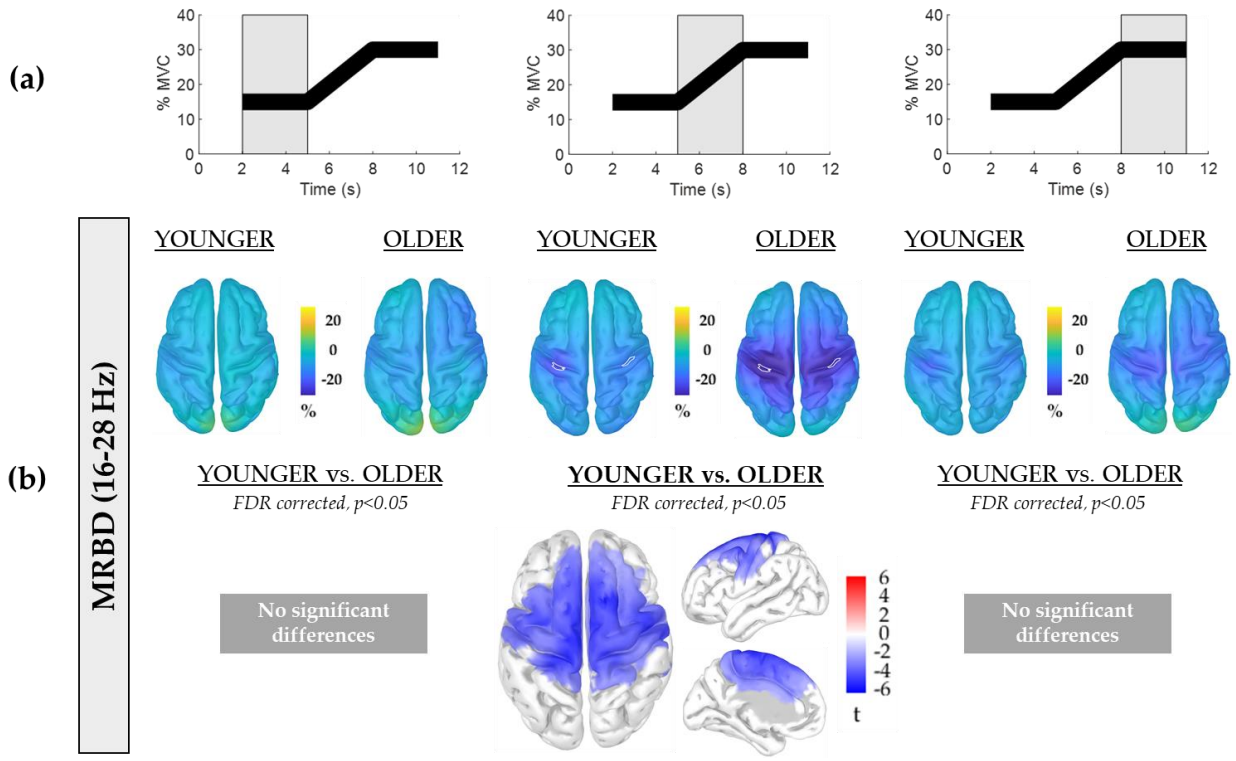

Figure 3-3. Unimanual task: (a) Illustration of the different stages of the task. Grey shaded areas indicate the period displayed in the images on the same column. **(b)** Upper panel: grand-averaged images of MRBD across each group. MRBD ROIs are delineated in white. Lower panel: differences in MRBD between groups (FDR-corrected, $p<0.05$). During the guided dynamic contraction period, older adults exhibited a significantly greater and more widespread MRBD compared to younger adults. During sustained contraction periods, no significant differences in MRBD were found between groups.

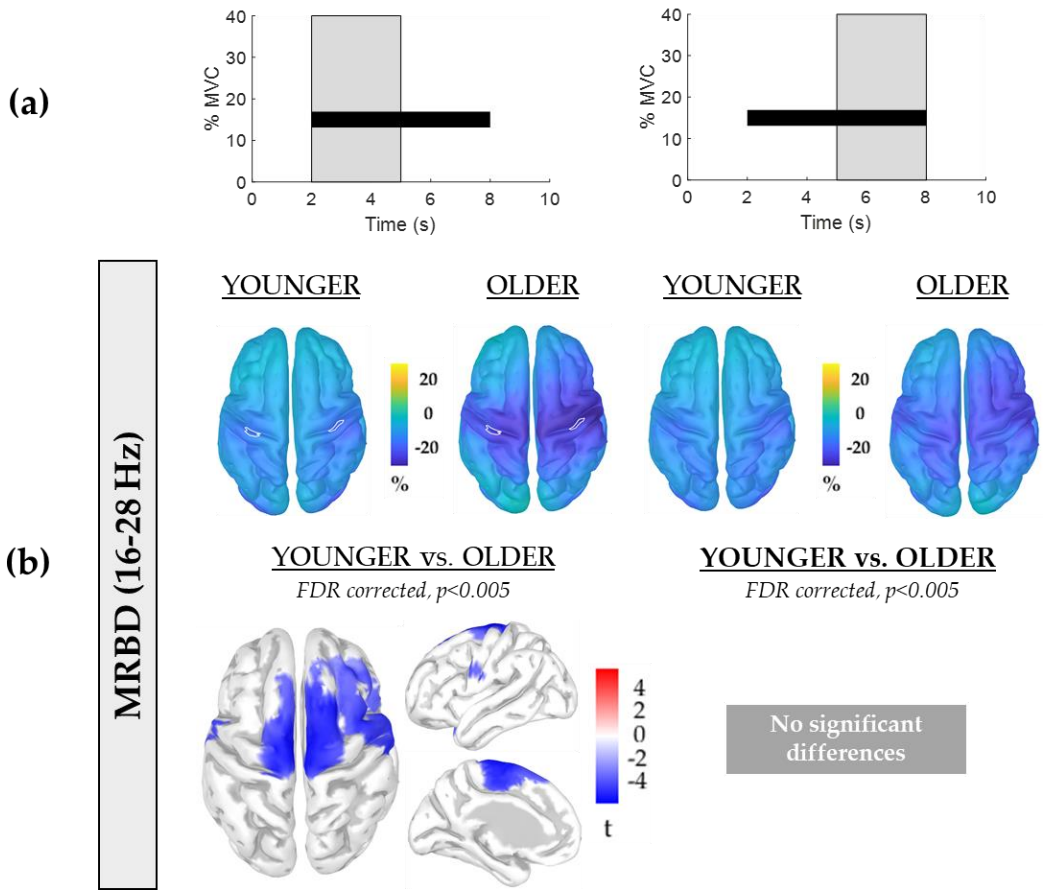

Figure 3-4. Bimanual task: (a) Illustration of the two 3-s subperiods of the task (grey shaded areas). **(b)** Upper panel: grand-averaged images of MRBD across each group. MRBD ROIs are delineated in white. Lower panel: differences in MRBD between groups (FDR-corrected, $p<0.05$). During the first 3-sec period, older adults exhibited a significantly stronger and more widespread MRBD compared to younger adults. During the second 3-sec period, during which subjects achieved the bimanual sustained contraction, no significant differences were found between groups.

3.5.5 Modulation of beta oscillations

To investigate more precisely the modulation of beta oscillations between different brain regions in younger and older adults, we extracted a power modulation metric from all ROIs (depicted in the first row of **Figure 3-5**) for both task paradigms.

Unimanual task. The unimanual task induced modulations in beta power in several brain regions (**Figure 3-5**). The modulations can be observed both in the relative (with respect to resting-state power) and absolute power subfigures. Results of the mixed ANOVA (**Table 3-2**) revealed a significant main effect of "Age", which suggests an overall difference in the amplitude of beta power modulation between groups. *Post-hoc* testing revealed a significantly larger modulation in older compared to younger adults (t_{70} = -3.43, p = 0.001). We also observed a significant main effect of "Brain Region", which suggests that there was an overall difference in beta power modulation between brain regions. *Post-hoc* testing of the "Brain Region" effect showed a significantly greater modulation in the left and right ROIs (peak MRBD, located at the primary motor cortices) compared to the *ageMRBD* ROI (left peak MRBD vs. *ageMRBD*: t_{23} = -2.79, p = 0.010; left peak MRBD vs. *ageMRBD*: t_{23} = -3.68, p = 0.001), but no significant difference between left and right ROIs (t_{23} = -0.02, p = 0.983). Finally, there was no significant interaction between the factors. The statistical analysis quantified through ANOVA can be evaluated qualitatively in **Figure 3-5**.

Bimanual task. The bimanual task induced weaker modulations in MRBD compared to unimanual muscle contractions (**Figure 3-5**). Nonetheless, the mixed ANOVA (**Table 3-2**) revealed the same significant main effects as in the unimanual task. A significant main effect of "Age" was observed, and *post-hoc* testing again showed significantly greater modulation in older adults (t_{70} = -3.56, p <0.001). We also detected a significant main effect of "Brain region", and *post-hoc* testing revealed, as before, a significantly larger modulation in the left and right ROIs (peak MRBD, located at the primary motor cortices) compared to the *ageMRBD* ROI (left peak MRBD vs. *ageMRBD*: t_{23} = -2.65, p = 0.014; left peak MRBD vs. *ageMRBD*: t_{23} = -2.69, p = 0.013), but no significant difference between left and right ROIs (t_{23} = 1.52, p = 0.142). Finally, there was no significant interaction between the factors. The statistical analysis quantified through ANOVA is illustrated qualitatively in **Figure 3-5**.

Table 3-2. Results of the mixed-model ANOVAs for the modulation of beta oscillations – unimanual and bimanual tasks.

	F-statistics				
	SS	***df***	***MS***	***F***	***p* value**
UNIMANUAL					
Age	8.80	1	8.80	6.94	**0.015**
Residuals	27.9	22	1.27		
Brain region	3.82	2	1.91	31.51	**<0.001**
Age:Brain region	0.05	2	0.02	0.38	0.685
Residuals	2.67	44	0.06		
BIMANUAL					
Age	1.65	1	1.65	5.12	**0.034**
Residuals	7.08	22	0.32		
Brain region	0.59	2	0.30	6.22	**0.005**
Age:Brain region	0.03	2	0.02	0.31	0.714
Residuals	2.10	44	0.05		

3.5.6 PMBR analysis

We examined possible differences in PMBR between younger and older adults for both tasks. The ROIs used are depicted in **Supp. Fig. 3-2**.

<u>*Unimanual task*</u>. We found no significant main effect of hemisphere or age; however, there was a significant age-by-hemisphere interaction (**Table 3-3**). This interaction indicates that the effect of hemisphere on PMBR was different in younger compared to older adults. To investigate this interaction, 4 *post-hoc* tests were conducted using paired and independent *t*-tests as appropriate, and a Bonferroni correction was applied (significance at 0.05/4=0.0125). Paired *t*-tests between hemispheres did not reveal any significant difference (Younger: $t_{11} = 2.47$, $p = 0.031$, Older: $t_{11} = -1.35$, $p = 0.204$). Independent *t*-tests yielded a marginally significant greater PMBR in the right hemisphere (ipsilateral) for the older group compared to the younger group ($t_{22} = -2.66$, $p = 0.014$), whereas no significant difference was found in the left hemisphere (contralateral) ($t_{22} = -0.28$, $p = 0.780$).

<u>*Bimanual task*</u>. We did not find a main effect of hemisphere, age, or any age-by-hemisphere interaction (**Table 3-3**).

Table 3-3. Results of the mixed-model ANOVAs for PMBR – unimanual and bimanual tasks.

	F-statistics				
	SS	***df***	***MS***	***F***	***p* value**
UNIMANUAL					
Age	31.5	1	31.5	1.87	0.185
Residuals	370	22	16.8		
Brain region	4.77	1	4.77	2.12	0.159
Age:Brain region	17.8	1	17.8	7.91	**0.010**
Residuals	49.4	22	2.25		
BIMANUAL					
Age	<0.01	1	<0.01	<0.01	0.993
Residuals	2488	22	113		
Brain region	7.09	1	7.09	0.97	0.336
Age:Brain region	6.50	1	6.50	0.89	0.356
Residuals	161	22	7.32		

3.5.7 Associations between beta oscillations and motor performance

We carried out four linear regression analyses between beta oscillations and motor performance scores. The cross-validation analysis is shown in **Supp. Fig. 3-7**. The prediction of task accuracy during the unimanual task was not significantly different compared to using permuted labels, hence no further analysis was done. For the other three cases, the prediction of the dependent variables was significantly better when using the correct labels ($p < 0.05$), hence further analysis was done. For the model predicting task accuracy during the bimanual task, beta desynchronization at the peak locations of MRBD (i.e. left/right M1) was the only identified significant feature. A reduced regression model using only this feature was implemented. **Figure 3-6** displays the correlation between MRBD and task accuracy, which suggests that subjects with stronger (i.e. more negative) MRBD exhibited worse task performance. For the models predicting behavioral scores, a reduced model revealed no significant features beyond age.

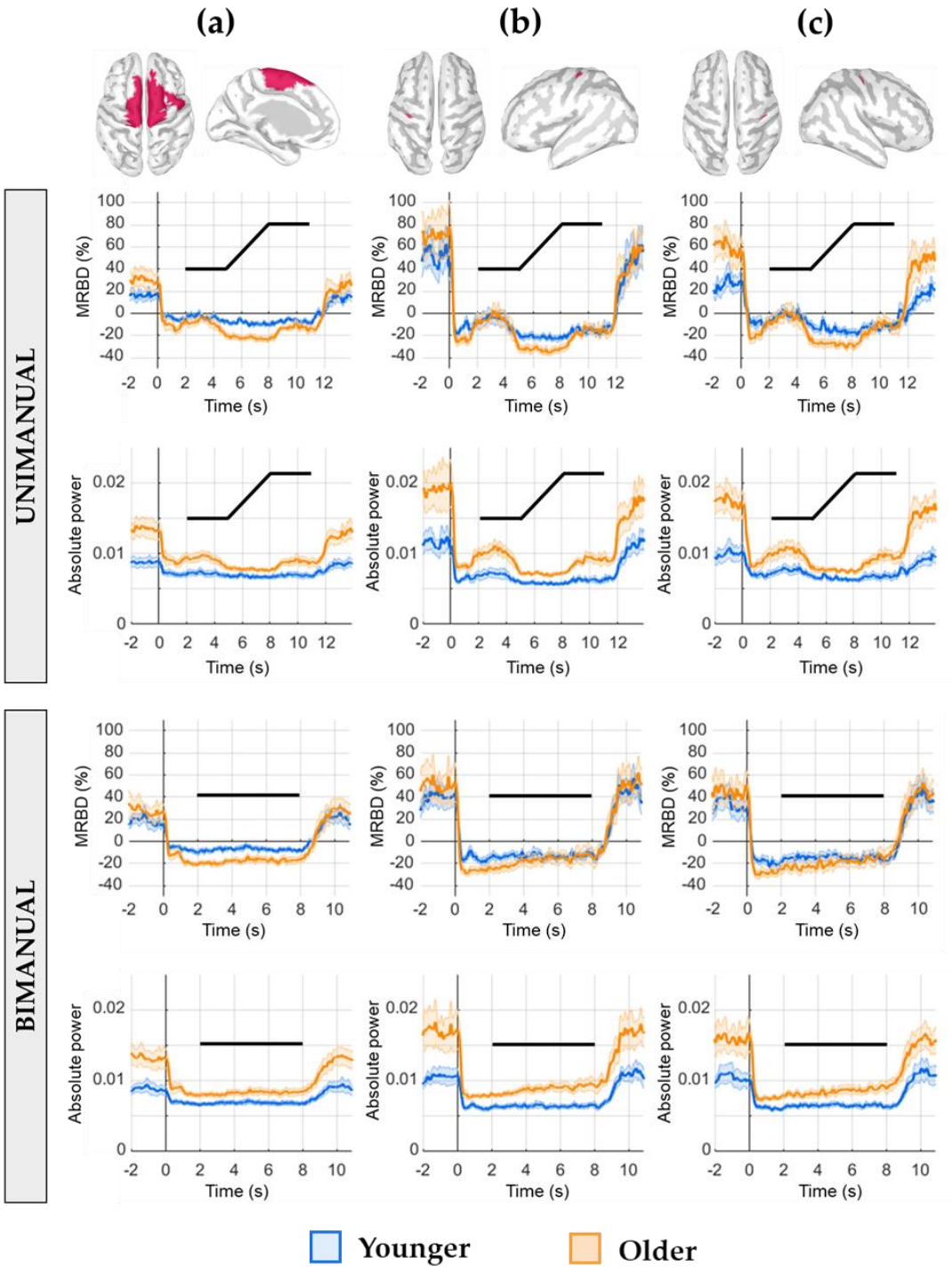

Figure 3-5. Unimanual and Bimanual tasks: Temporal evolution of the MRBD (upper row) and absolute beta power response (lower row) in **(a)** *ageMRBD* ROI, i.e. brain regions identified to exhibit stronger MRBD in older adults, **(b)** peak MRBD ROI (left M1) and **(c)** peak MRBD ROI (right M1). Older adults exhibited higher absolute beta power throughout the entire movement execution for both tasks. During the unimanual task, we observed a greater (more negative) MRBD during the guided dynamic contraction compared to sustained contraction periods (15%MVC and 30%MVC) for both groups. During the bimanual task, older adults exhibited greater (more negative) MRBD at the beginning of the trial compared to their younger counterparts.

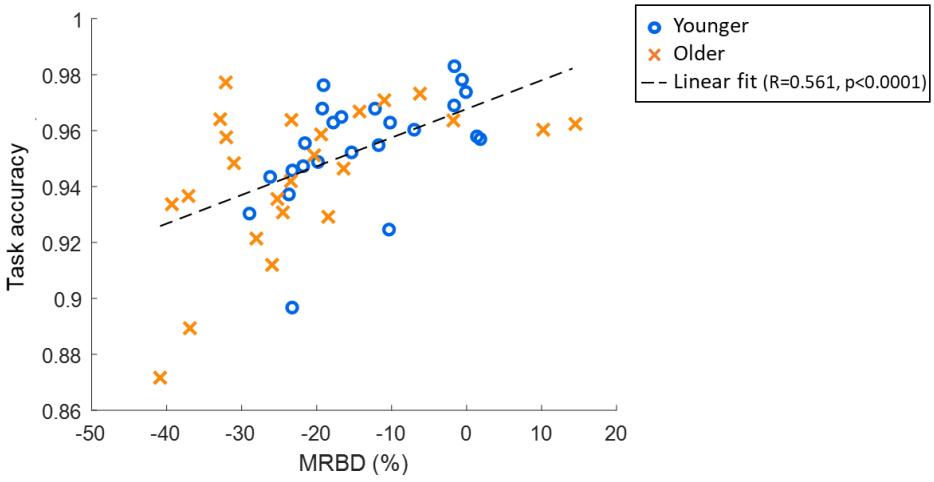

Figure 3-6. Relationship between MRBD at the peak location (primary motor cortex) and task accuracy for the bimanual task. Subjects that exhibited greater (i.e. more negative) MRBD performed worse in the task.

3.5.8 Effect of baseline on relative power calculation

We extracted averaged time-courses from the left and right MRBD ROIs corresponding to absolute beta power, beta *RP*% calculated with respect to an inter-trial baseline, and beta *RP*% calculated with respect to the 1st resting-state. We found that absolute beta power levels were always greater for older participants before and during the motor tasks (**Supp. Fig. 3-8a-b**) compared to their younger counterparts. When inter-trial beta power levels were selected as baseline, we observed that older adults exhibited greater MRBD compared to younger adults across the entire trial (**Supp. Fig. 3-8c-d**). In contrast, when resting beta power levels were selected as baseline, older adults exhibited greater MRBD compared to younger adults only during dynamic contractions (**Supp. Fig. 3-8e-f**).

3.6 DISCUSSION

We examined the influence of healthy aging on motor-related beta oscillations using two motor paradigms: unimanual and bimanual handgrips. Extending previous studies that have focused on M1s, we investigated whether whole-brain age-related differences are present during both sustained and dynamic contractions. Consistent with prior literature, we found greater beta power at rest, as well as increased (i.e. more negative) MRBD in older adults compared to their younger counterparts. Interestingly, although older adults exhibited increased MRBD compared to younger adults during periods of dynamic contraction, the same was not observed during periods of sustained force production. As a result, we showed that older adults exhibit a more pronounced modulation of beta oscillations during dynamic muscle contractions. Furthermore, we found a significant correlation between MRBD during dynamic contractions and behavior. Below we discuss the implications of this work in the context of understanding the functionality of beta oscillations in motor control.

3.6.1 Behavioral analysis

We did not observe differences in terms of task accuracy between groups during the motor tasks performed inside the MEG scanner. This was expected, since the force applied by each subject was the same pre-defined percentage of their MVC, which implies that task-level difficulty was comparable among participants and that differences observed in this study in terms of brain activity patterns are attributable to age rather than other factors, such as increased effort (Aine et al., 2006).

On the other hand, older adults exhibited deteriorated fine motor control in the corresponding behavioral assessments (Table 1), which is in line with the expected motor decline in older adults (Desrosiers et al., 1995; Grice et al., 2003; Lindstrom-Hazel and VanderVlies Veenstra, 2015; Mathiowetz et al., 1985a). Handgrip strength was not significantly different between groups due to high variability between individuals.

3.6.2 Structural analysis

Older adults were characterized by a significant decrease in cortical thickness, particularly in frontal and temporal brain areas (**Supp. Fig. 3-3**). The affected regions are in notable agreement with previous studies that included larger sample sizes (Fjell et al., 2009; Hogstrom et al., 2013; Salat et al., 2004). These brain regions were overall in correspondence with areas that exhibited age-related increases in MRBD (**Figure 3-3, Figure 3-4**); however, the magnitude of MRBD and cortical thickness were not found to be significantly correlated ($R=-0.14$, $p=0.35$), which suggests that the observed age-related functional differences may not be directly associated with this specific neurodegenerative process.

3.6.3 Age-related changes in power at rest

We found that older adults exhibited increased resting beta power compared to younger adults (**Figure 3-2**). We did not find significant differences in resting alpha power between groups. Our results agree with several prior studies regarding age-related differences in power at rest, where it was reported that older adults exhibited similar levels of alpha power (Duffy et al., 1984; Heinrichs-Graham and Wilson, 2016; Koyama et al., 1997; Veldhuizen et al., 1993) and increased beta power (Gómez et al., 2013; Heinrichs-Graham et al., 2018; Heinrichs-Graham and Wilson, 2016; Hübner et al., 2018a; Koyama et al., 1997; Veldhuizen et al., 1993). However, previous studies only evaluated specific brain areas and/or performed the analysis in sensor space. Our whole-brain analysis demonstrated that the motor cortex was the area that showed the most significant differences in spontaneous beta power between younger and older subjects. This aligns with the evidence that beta-band activity is pathologically increased in movement disorders such as Parkinson's disease (Brown et al., 2001; Silberstein et al., 2005), which suggests that increased beta oscillations at rest may be related with a deterioration of flexible behavioral and cognitive control (Engel and Fries, 2010). However, when we probed whether spontaneous beta power was a good predictor of motor performance, we did not find any relationship that linked increased spontaneous beta power with poorer motor performance.

3.6.4 Whole-brain age-related MRBD changes during muscle contractions

The majority of past studies that examined aging effects on motor control have used motor paradigms whereby the subjects performed a dynamic contraction, and they consistently reported age-related increases in MRBD – i.e. more negative desynchronization (Bardouille et al., 2019; Heinrichs-Graham et al., 2018; Heinrichs-Graham and Wilson, 2016; Hübner et al., 2018a; Rossiter et al., 2014). In line with these studies, during periods of dynamic contraction we found a significant increase in MRBD in older adults compared to younger adults. Our whole-brain analysis further revealed a more widespread MRBD in older adults, in contrast with younger adults, for which the desynchronization was mainly located in the M1s (**Figure 3-3b, Figure 3-4b, upper panel**). Specifically, our results suggest a significant age-related increase in MRBD that covered frontal and premotor brain regions (**Figure 3-3b, Figure 3-4b, lower panel**). Moreover, we observed that during periods of steady contractions, no differences were found between groups across the entire brain (**Figure 3-3b, Figure 3-4b, lower panel**). Thus, our results align with the study from Rossiter and colleagues that reported no differences in MRBD in M1 contralateral to the moving hand during steady contractions (Rossiter et al., 2014), however our observations seem to indicate that the ipsilateral primary motor cortex does not show differences in MRBD either, in contrast with the study from Rossiter and colleagues (Rossiter et al., 2014).

3.6.5 Age-related changes in beta power modulation during muscle contractions

Both younger and older adults exhibited the expected modulation of beta oscillations that emerges when sequentially performing sustained and dynamic contractions (Baker, 2007; Cassim et al., 2000; Kilner et al., 2003, 1999; Schoffelen et al., 2008; Spinks et al., 2008; van Wijk et al., 2012). This implies that the motor performance decline observed in healthy aging is not due to an impairment in the capacity to modulate beta oscillations. In fact, we observed a larger modulation in older compared to younger adults (Table 2). The increase in synchronized beta oscillations that emerges when producing a steady muscle contraction has been suggested to provide an efficient processing platform for promoting the maintenance of a steady motor output whilst compromising initiation of new movements

(Androulidakis et al., 2007; Engel and Fries, 2010; Gilbertson et al., 2005; Omlor et al., 2007; Pogosyan et al., 2009). Further, it has been recently suggested that absolute beta power needs to reach a certain threshold level in order to initiate a muscle contraction, regardless of age (Heinrichs-Graham and Wilson, 2016). Beta oscillations at rest are greater in older adults; this suggests that an increased desynchronization is needed for the required threshold to initiate a muscle contraction to be reached. If we only consider the results we obtained during dynamic contractions, our findings align well with this theory, since older adults exhibited increased cortical beta suppression with respect to resting beta levels compared to younger adults. Yet, considering that we baseline-corrected the motor-related beta power using the spontaneous power observed at rest, our results also show that during sustained contractions there were no differences between groups beyond the ones observed at rest. Our findings may suggest that the threshold in terms of absolute beta power for the maintenance of a sustained contraction is shifted in aging, whereas the threshold for executing a dynamic contraction remains the same.

3.6.6 Relationship between MRBD and motor performance

Two main theories have aimed to explain over-recruitment in aging: *compensation* and *dedifferentiation* (Reuter-Lorenz and Park, 2010). The basic idea of *compensation* is that brain reorganization in older adults is a compensatory mechanism to counterbalance impaired function. Alternatively, the *dedifferentiation* hypothesis argues that older adults inefficiently recruit additional brain areas because of less precise brain structure-function interactions. Hence, this over-activation is not seen as a compensation mechanism to achieve better performance, rather as a less selective activation pattern. Several studies have provided evidence of a positive correlation between over-recruitment and performance during a motor task (Mattay et al. 2002; Heuninckx et al. 2008). Other studies have reported that greater brain activity during a cognitive task was correlated to poorer performance (Logan et al. 2002; Stebbins et al. 2002). In another study it was reported that there was no correlation between brain activity and increased difficulty during a motor task (Riecker et al., 2006). These discrepancies suggest that the association between increased activity in a specific brain region and performance in older adults may be task-

specific or dependent on the task demands and the behavioral measure used. Therefore, in an attempt to unravel whether the age-related overactivation of frontal/premotor/motor areas during dynamic contractions and the increased modulation of beta oscillatory power between sustained and dynamic contractions in aging represent a *compensation* or *dedifferentiation* mechanism, we examined its association with motor performance.

Features related to the brain regions that showed significantly increased MRBD in aging (*ageMRBD*) did not reveal any association with behavioral measures. This suggests that they were recruited in a non-selective fashion. Taken together with the fact that these brain regions exhibited decreased cortical thickness in the older participants, the overactivation of these regions in older adults might be indicative of a loss of functional specificity, and therefore supporting the *dedifferentiation* hypothesis. Recent observations that increased prefrontal cortex activity in healthy aging does not contribute to maintain cognitive function (Morcom et al., 2018) would align with these results. Further, the modulation metric that quantified the depth of variations of beta oscillatory power did not show a relation with behaviour in any of the considered regions.

We identified one electrophysiological measure (beta desynchronization at the peak MRBD ROIs) that associated beta oscillations and motor performance, but only during bimanual muscle contractions inside the MEG scanner. An explanation could be that the implemented unimanual task was not sensitive enough for the explanatory values to significantly predict performance. Participants with stronger (i.e. more negative) MRBD at the peak location (M1) exhibited worse task performance. However, these regions did not show significant age-related increases in MRBD (**Figure 3-4b**), thus we cannot interpret this association as a *compensation* or *dedifferentiation* mechanism. This finding is supported by observations that after acute exercise, better performance is coupled with decreased (i.e. less negative) MRBD (Dal Maso et al., 2018; Hübner et al., 2018b). We speculate that, since increased MRBD at the peak location is correlated with greater resting-state beta power (Heinrichs-Graham and Wilson, 2016), the need to attenuate resting beta power to reach the beta threshold for proper motor execution may cause inferior task performance. However, further research is needed to understand the underlying mechanisms that link beta oscillatory activity and behaviour.

3.6.7 Age-related changes in PMBR

Recent studies reported that older adults exhibited reduced PMBR in the contralateral hemisphere to the moving hand during a finger tapping task compared to younger adults (Bardouille et al., 2019; L. Liu et al., 2017). On the other hand, our results suggest that older adults did not exhibit significant differences in PMBR in the contralateral (left) hemisphere to the moving hand during the unimanual task, but rather an increased PMBR in the ipsilateral (right) hemisphere (**Figure 3-5**, **Table 3-3**). Furthermore, during the bimanual task, no significant differences in PMBR were found between groups. It has been proposed that PMBR reflects active inhibition of the motor network (Solis-Escalante et al., 2012) and it has been specifically linked to the inhibitory neurotransmitter γ-aminobutyric acid (GABA) (Gaetz et al., 2011; Jensen et al., 2005). This suggests that PMBR plays a role in preventing the generation of unwanted movements. While speculative, our results may reflect a case of *dedifferentiation*, whereby inhibition of both cortices after a motor task occurs in older adults, in contrast with younger adults for which PMBR occurs only in the contralateral hemisphere to the executing hand. However, the precise mechanism underlying how PMBR is affected by aging remains to be fully elucidated.

3.6.8 Effects of baseline on relative power calculation

In agreement with previous studies, absolute beta power levels were consistently higher in older participants before and during the motor tasks (**Supp. Fig. 3-8a-b**) (Heinrichs-Graham et al., 2018; Heinrichs-Graham and Wilson, 2016; Hübner et al., 2018a). When inter-trial beta power levels were used as baseline, older adults exhibited greater MRBD compared to younger adults across the entire trial (**Supp. Fig. 3-8c-d**). In contrast, when resting beta power levels were used as baseline, older adults exhibited greater MRBD compared to younger adults only during dynamic contraction. The reason for this discrepancy is that beta power levels during the inter-trial period were significantly higher in both groups compared to resting levels (**Supp. Fig. 3-8e-f**), an indication that inter-trial power levels were contaminated by PMBR. This is due to the fact that the rebound effect can last several seconds after the end of a motor task, and has been associated with force output, such that higher force output results in greater PMBR (Fry et al., 2016).

Nevertheless, the inter-trial interval has been traditionally selected as baseline in motor studies focused on MRBD and PMBR. Our results highlight the importance of investigating whether the inter-trial power levels are artificially high due to PMBR contamination by comparing with resting power levels, as also suggested in recent studies (Heinrichs-Graham et al., 2018; Heinrichs-Graham and Wilson, 2016). In cases where the inter-trial is short, resulting in PMBR contamination, the usage of a resting-state recording for baseline normalization is strongly recommended.

3.6.9 Limitations

It has been suggested that resting beta levels and MRBD are modulated by the circadian rhythm (Toth et al., 2007; Wilson et al., 2014). In the present experiment, participants were scanned between 10 a.m. and 6 p.m. (Morning session: 8 younger/6 older; Afternoon session: 4 younger/6 older). Albeit somewhat balanced between groups, we cannot exclude circadian/ultradian effects on the results due to differences in the scanning time.

The inter-trial duration is a crucial parameter to consider when designing protocols to study motor-related beta oscillations. As we exemplify in **Supp. Fig. 3-8**, PMBR levels may contaminate the inter-trial baseline, leading to possibly biased results. In this paper, we used the resting-state beta power levels as baseline to take into account this issue. Still, we cannot exclude the possibility that the MRBD was contaminated by the elevated PMBR, since the inter-trial duration was not long enough for the PMBR to fully return to its baseline levels. Nevertheless, the PMBR is mostly localized within the M1s, whereas we observed most of the age-related differences in premotor and pre-frontal areas. This suggests that the obtained results are not biased by excessive contamination by the elevated PMBR levels.

The force applied during the experiment was based on each subject's own MVC, from 0 to 30% MVC (unimanual) and from 0 to 15% MVC (bimanual), to ensure that the required effort, and consequently the resulting fatigue level, was the same across participants. To investigate whether fatigue modulated the observed age-related differences in MRBD, we repeated our analysis using the initial and final 25 trials corresponding to each task. We subsequently tested for whole-brain differences in MRBD between younger and older

adults for trials in the first and second trial set. For the unimanual task, the analysis revealed age-related differences only during the ramp block and generally in the same brain regions as the results using all trials (**Supp. Fig. 3-9**). These findings suggest that, for the unimanual task, physical fatigue was either non-existent or its effect did not differ between age groups. Specifically, if fatigue did occur, these results suggest that for the resulting fatigue levels, the corresponding cortical adaptions did not differ between age groups. Nevertheless, age-related fatigue modulations were out of the scope of this paper, as we did not expect participants to experience fatigue to a large extent based on the low MVC levels used in our paradigms. However, in future studies the use of the Borg scale to monitor fatigue perception could be a good way to quantify fatigue levels (Borg, 1982). For the bimanual task, age-related differences were obtained during the initial 3s segment of the trial, but only when using the last 25 trials (**Supp. Fig. 3-10**). However, it is not likely that this observation is related to physical fatigue, since the bimanual task required considerably less force (15%MVC) compared to the unimanual task (30%MVC), and its duration was shorter (6 sec/trial) than the unimanual task (9 sec/trial). Therefore, the observation seen in **Supp. Fig. 3-10** is more likely related to low statistical power resulting from splitting the trials in half. However, because the motor tasks were not counterbalanced, we cannot discard the possibility that physical and/or mental fatigue may have had an effect on the results obtained for the bimanual task.

3.7 CONCLUSIONS

Older adults exhibited significantly higher beta oscillations at rest, and our results showed that the motor cortex is the brain area that exhibits the highest increase in resting beta oscillatory activity. The present study confirms that older adults produce a larger MRBD during dynamic muscle contractions compared to younger adults. Our results also suggest that during sustained contractions, there are no differences in beta power between age groups beyond the ones observed at rest. We further probed the relationship between motor performance and age-related differences in beta oscillations during rest and task, but our results suggest that this altered beta activity in aging did not carry additional information.

3.8 ACKNOWLEDGMENTS

We wish to thank Elizabeth Bock for her help during the data acquisition as well as Arna Ghosh for his support in implementing the visual feedback for the experiment. This work was supported by funds from Fonds de la Recherche du Québec – Nature et Technologies (FRQNT; 2016-PR-191780) [MHB, GDM & SB], the Canadian Foundation for Innovation grant numbers 34277 [MHB] and 34362 [GDM], the Natural Sciences and Engineering Research Council of Canada (NSERC 436355-13), the National Institutes of Health (R01 EB026299), the Brain Canada Foundation (PSG15-3755), the Canada Research Chair program [SB], and the Canada First Research Excellence Fund (awarded to McGill University for the Healthy Brains for Healthy Lives (HBHL) initiative). AXP and MK received financial support through funding from McGill University and the Québec Bio-imaging Network (QBIN). GN received financial support through a postdoctorate fellowship from the AXA Research Fund. SL acknowledges funding from FRQ– Santé (FRQS). The funders had no role in study design, data collection and analysis, decision to publish, or preparation of the manuscript. The authors declare no competing financial or non-financial interests.

3.9 SUPPLEMENTARY MATERIAL

Supp. Table 3-1. Coordinates of the ROI peak in MNI space.

		X	*Y*	*Z*
MRBD	**Right Hemisphere**	37.5	-26.3	61.4
	Left Hemisphere	-39.5	-29.1	61.3
PMBR	**Right Hemisphere**	31.9	-25.8	66.7
	Left Hemisphere	-35.5	-29.8	61.2

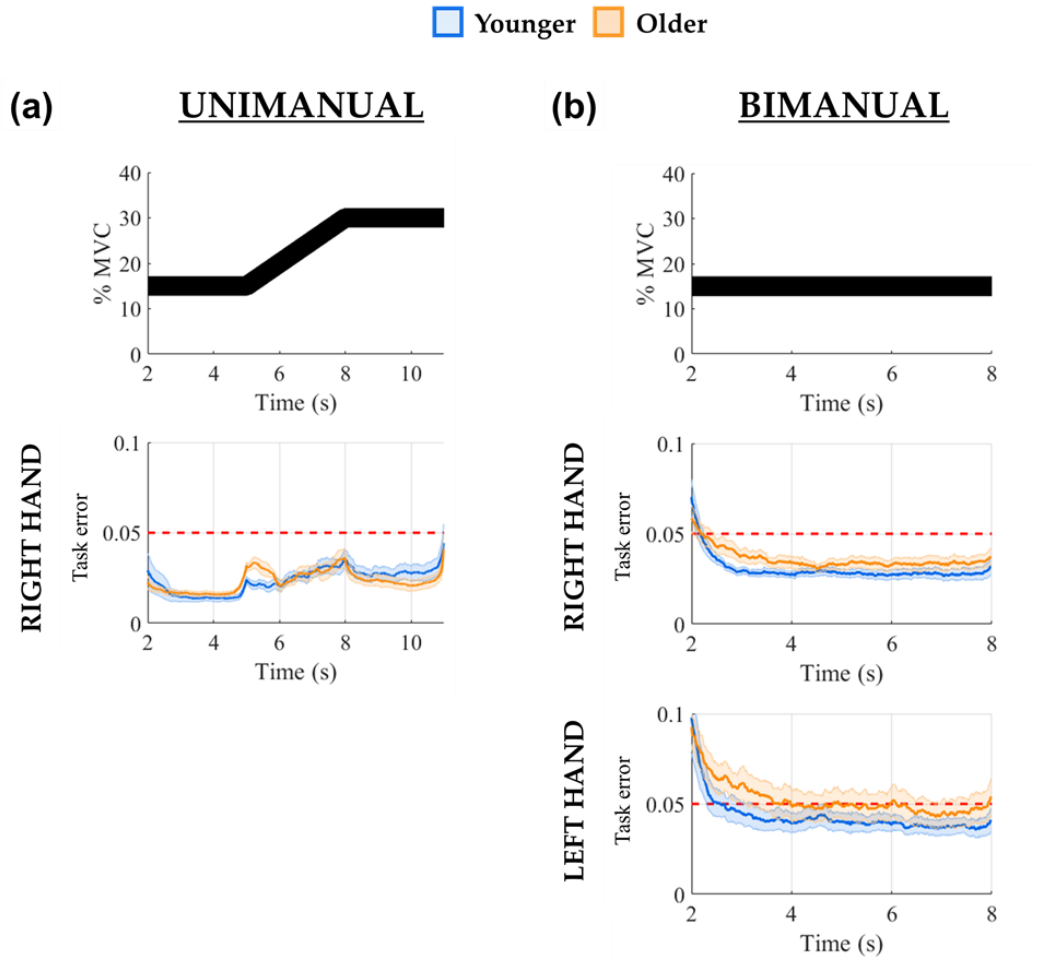

Supp. Fig. 3-1. Temporal evolution of the movement error for the **(a)** unimanual and **(b)** bimanual tasks. The dotted red line indicates the threshold where the circle controlled by the force was inside the boundaries of the target position. During the unimanual task, the movement error was below the threshold for both groups. In contrast, during the bimanual task, the movement error exceeded the threshold, particularly at the beginning of the trial and for the left hand. Is was not until the middle of the trial (around 4s) that the movement error was below the threshold.

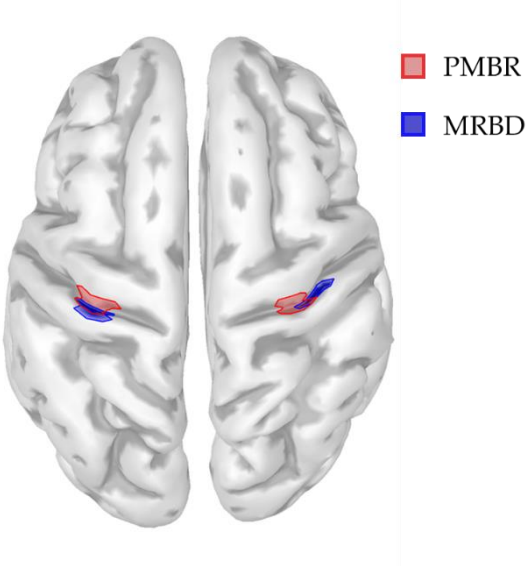

Supp. Fig. 3-2. ROIs for PMBR and MRBD in each hemisphere. The ROIs were defined as the vertices showing highest PMBR and MRBD (top 5%).

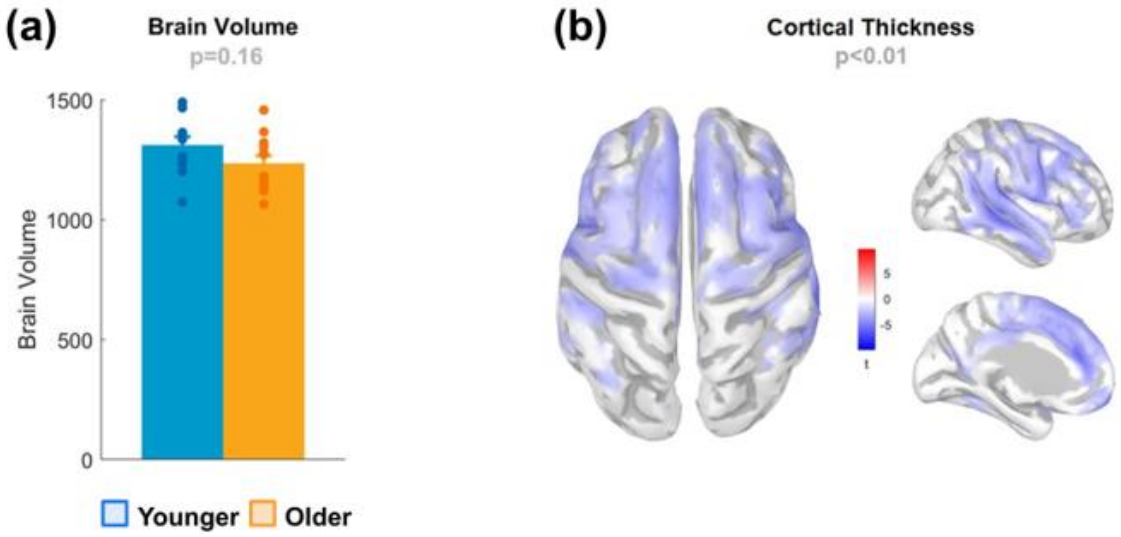

Supp. Fig. 3-3. Structural differences between younger and older participants: **(a)** Brain volume – no significant differences between groups were detected (p=0.16). **(b)** Cortical thickness – older adults exhibited significantly decreased cortical thickness mainly in frontal and temporal areas (FDR-corrected, p<0.01).

Blue = brain areas were older adults displayed decreased cortical thickness compared to younger adults.

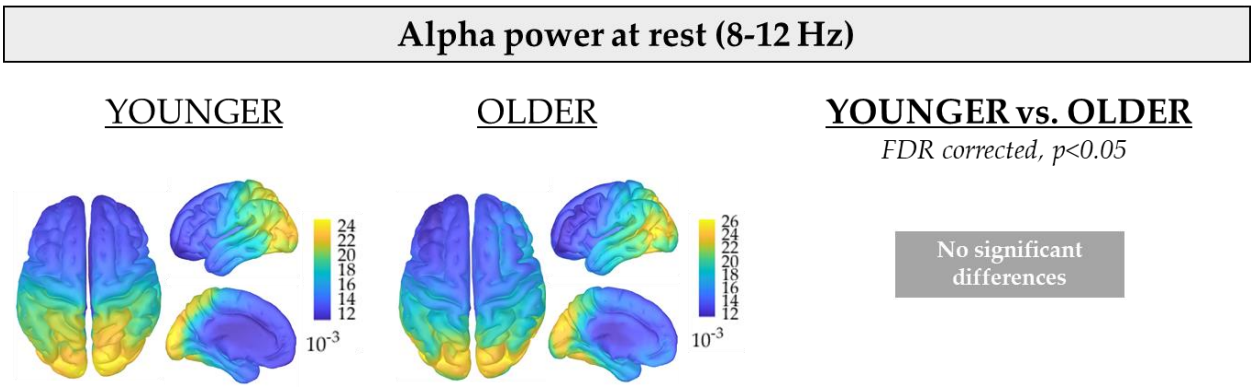

Supp. Fig. 3-4. Alpha power during the 1st resting-state. Left and middle panels: grand-averaged images across younger and older participants, respectively. Right panel: differences in oscillatory power at rest between groups (FDR-corrected, $p<0.05$). Alpha power did not present any significant age-related differences.

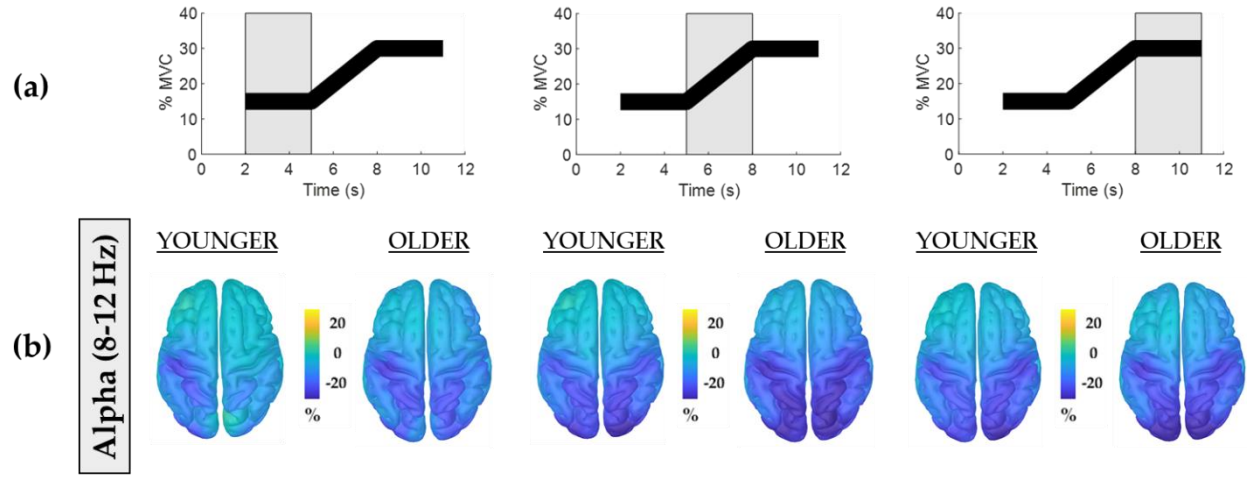

Supp. Fig. 3-5. Unimanual task: (a) Illustration of the different stages of the task. **(b)** Grand-averaged images of alpha relative power across each group. Alpha power did not present any significant age-related differences (FDR-corrected, $p<0.05$).

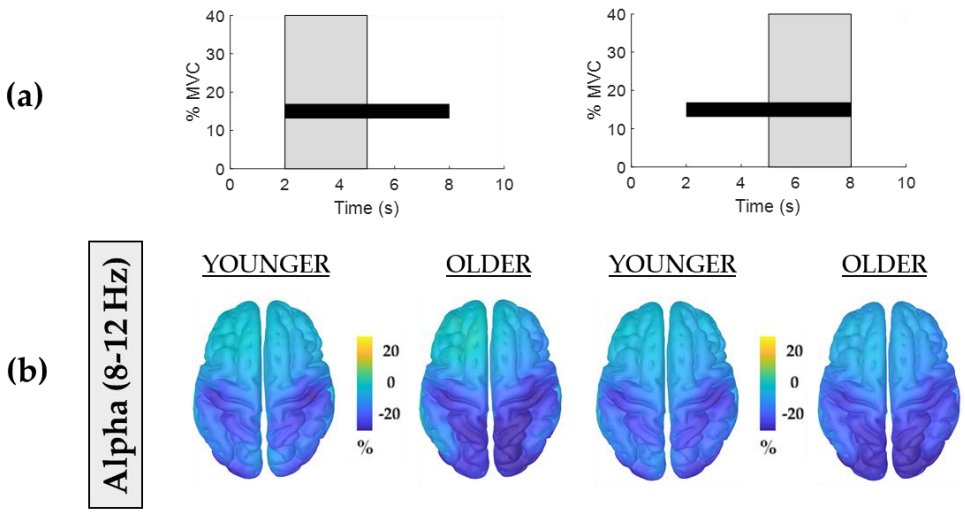

Supp. Fig. 3-6. Bimanual task: (a) Illustration of the two 3-s subperiods of the task (grey shaded areas). **(b)** Grand-averaged images of alpha relative power across each group. Alpha power did not present any significant age-related differences (FDR-corrected, p<0.05).

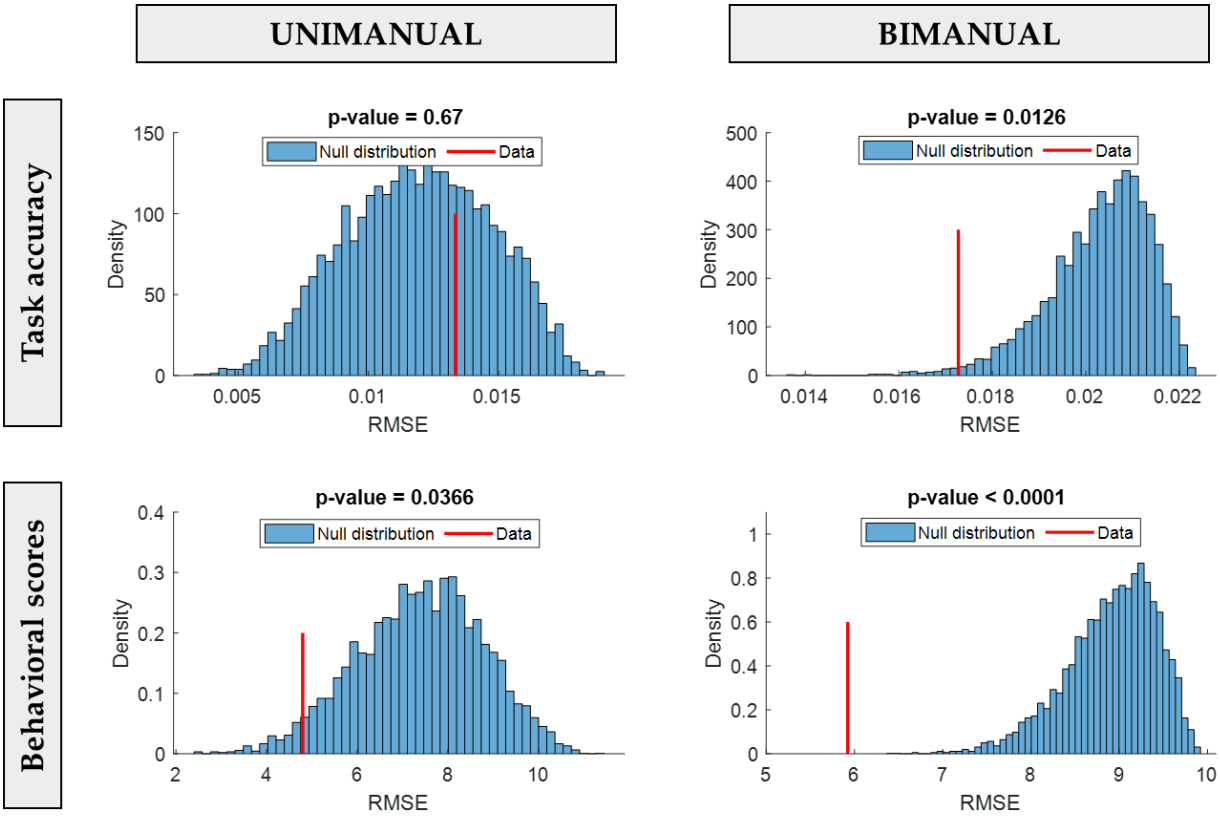

Supp. Fig. 3-7. Null distributions of the RMSE in the test set (blue) and the observed RMSE of the test set (red). Four models were computed: 12 features vs task accuracy during the unimanual task (Top left), 8 features vs task accuracy during the bimanual task (Top right), 12 features vs. unimanual behavioral scores (Bottom left), 8 features vs. bimanual behavioral scores (Bottom right).

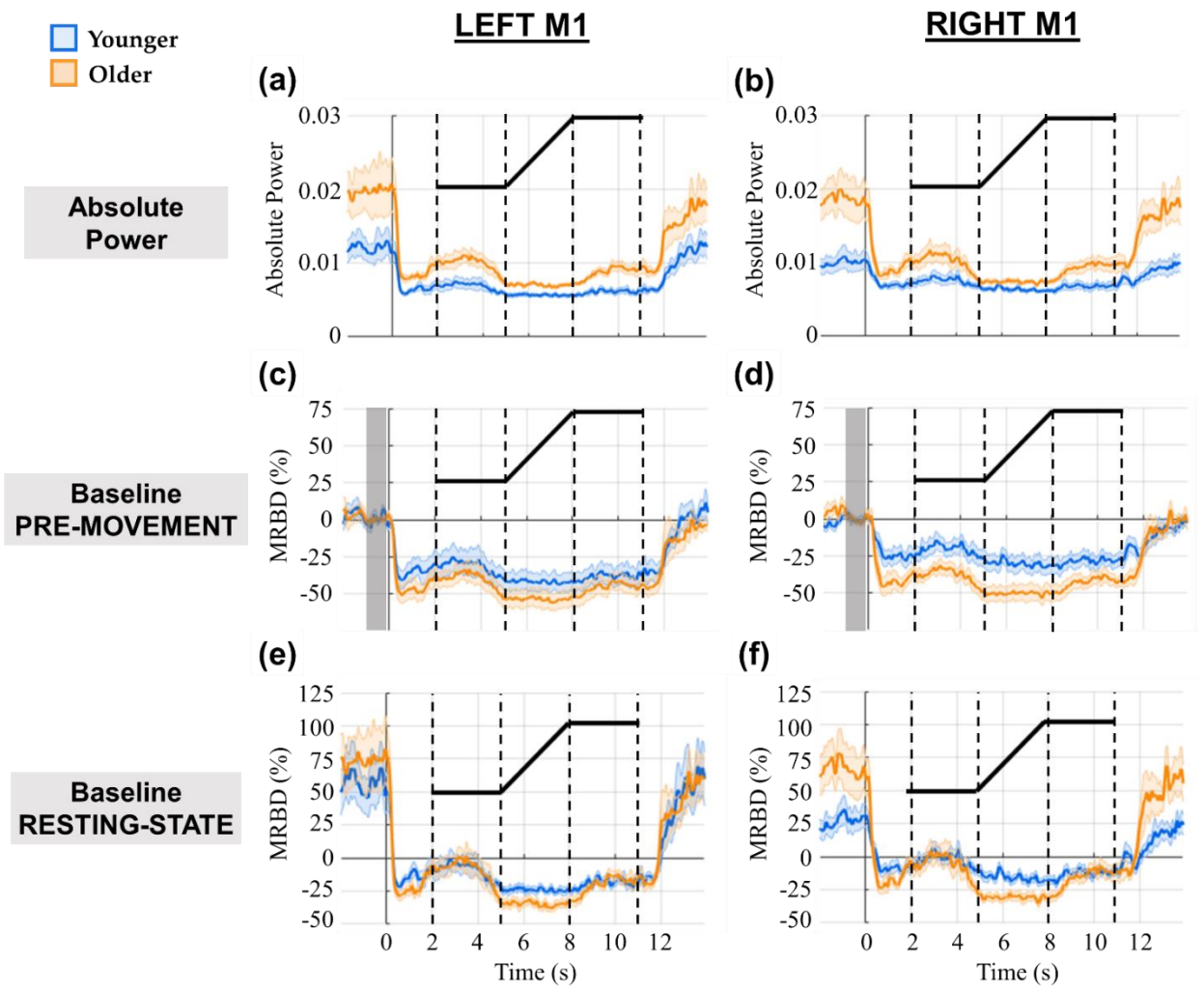

Supp. Fig. 3-8. Temporal evolution of the beta activity during the unimanual task in left and right peak MRBD ROIs (primary motor cortices). **(a)-(b)** Absolute beta power. **(c)-(d)** MRBD relative to pre-movement baseline levels. Gray shaded area indicates the pre-movement period (-1 to 0 s). **(e)-(f)** MRBD relative to resting baseline levels.

Older adults exhibited greater absolute beta power throughout the entire trial. If we baseline-corrected the beta power using the pre-movement period, the results showed a beta suppression present throughout the entire trial. In contrast, if we baseline-corrected the beta power using the resting-state beta values, the results revealed a beta suppression only present during periods of dynamic contractions. This analysis highlights the importance of using baseline periods in which we are certain that the power levels are comparable to resting-state levels.

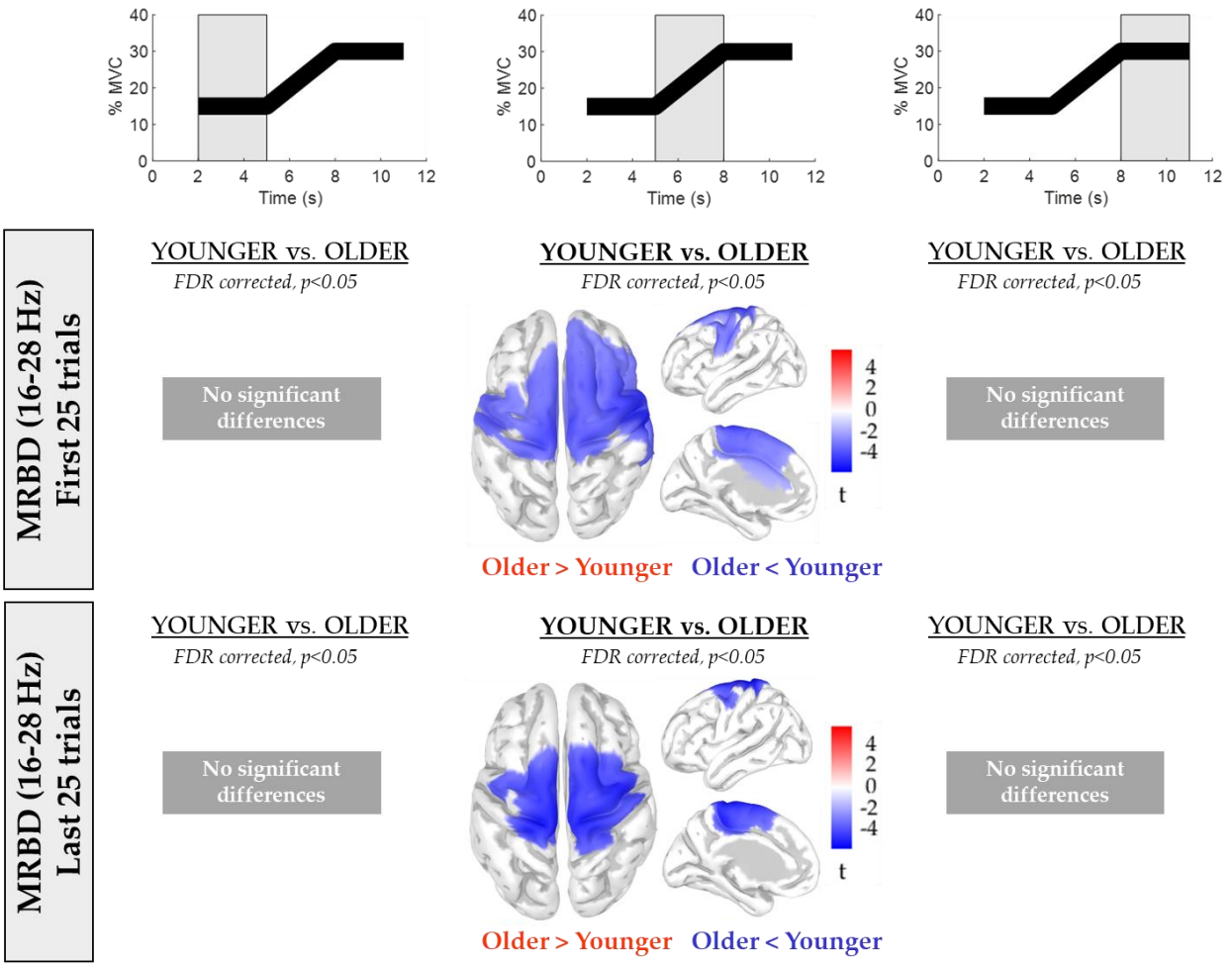

Supp. Fig. 3-9. Unimanual task: Whole-brain age-related differences in MRBD within **(a)** the first 25 trials and **(b)** the last 25 trials.

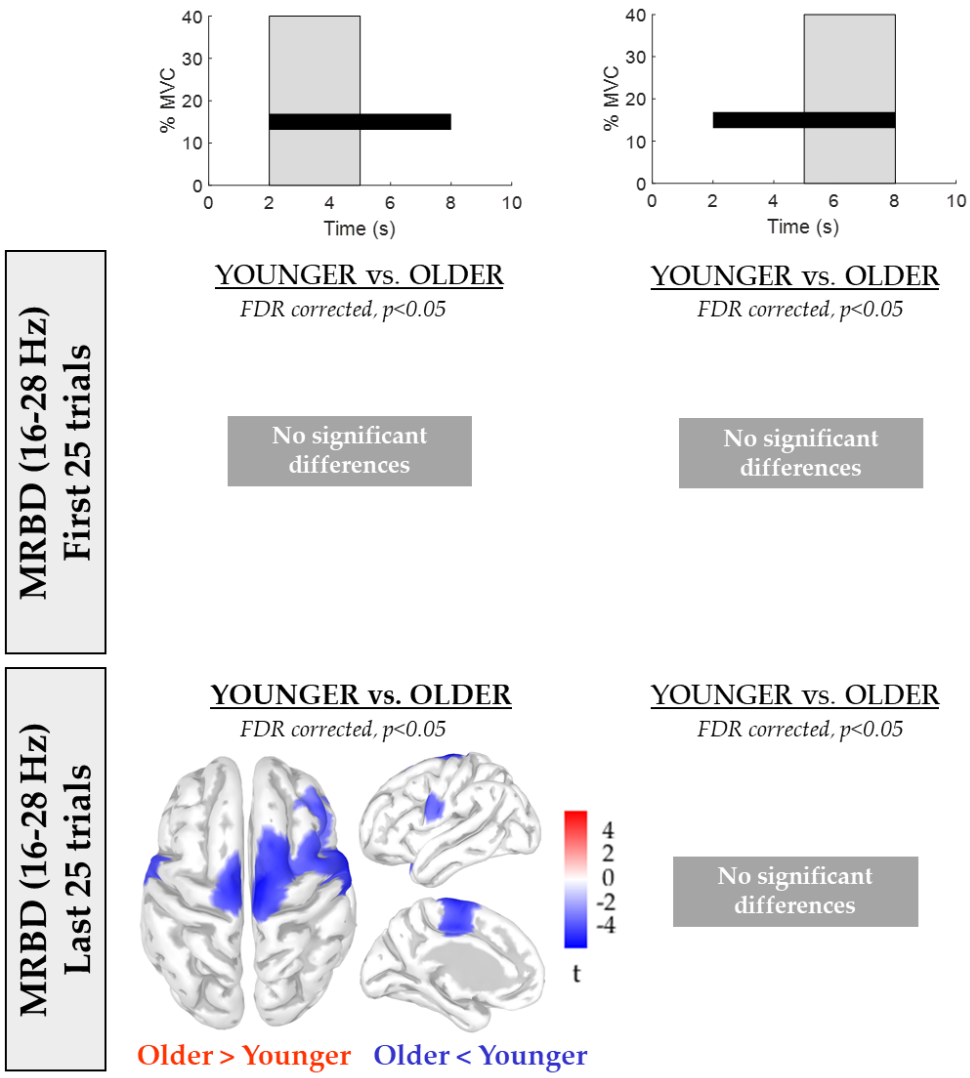

Supp. Fig. 3-10. Bimanual task: Whole-brain age-related differences in MRBD within **(a)** the first 25 trials and **(b)** the last 25 trials.

4

Physiological and head motion signatures in static and time-varying functional connectivity

The following chapter has been submitted for publication in a journal as:

Xifra-Porxas*, A., Kassinopoulos*, M., Mitsis, G.D. (under review). Physiological and head motion signatures in static and time-varying functional connectivity. * equal contribution. *Available as a preprint in bioRxiv*: https://doi.org/10.1101/2020.02.04.934554

CRediT authorship contribution

A. Xifra-Porxas: Conceptualization, Methodology, Software, Formal analysis, Data curation, Project administration, Visualization, Writing - original draft, Writing - review & editing.
M. Kassinopoulos: Conceptualization, Methodology, Data curation, Writing - review & editing.
G. D. Mitsis: Conceptualization, Supervision, Writing - review & editing.

4.1 PREFACE

It is well known that the blood-oxygenation-level-dependent (BOLD) signal measured in functional magnetic resonance imaging (fMRI) is indirectly related to the underlying neural activity; for instance, it is strongly contaminated by head motion and systemic physiological fluctuations. This is a fundamental challenge particularly for task-free paradigms, where the neural signal of interest cannot be readily identified through the temporal structure of the experiment. Furthermore, there is accumulating evidence that these artifacts can give rise to structured artifactual correlations in static functional connectivity (FC) (Jingyuan E. Chen et al., 2020). As a result, head motion and physiological fluctuations can lead to invalid inferences, particularly in resting-state FC studies comparing populations with different tendency for moving during the scan, or different cardiac and breathing rhythms. Moreover, an increasing number of studies have focused on the dynamics of FC within a scan (Lurie et al., 2019), commonly referred as time-varying FC, although it is still an open question whether the fluctuations of FC reflect the dynamics of underlying neural activity or systemic physiological fluctuations (Laumann et al., 2017; Nalci et al., 2019; Nikolaou et al., 2016a). Therefore, the nature of time-varying FC and its disentanglement into its neural and physiological components is still an open question.

To address the aforementioned fundamental questions, the manuscript in this chapter capitalizes on multisession resting-state fMRI data and physiological recordings to identify structured connectome profiles associated with head motion, cardiac pulsatility, breathing motion, and variations in heart rate and breathing patterns. It provides evidence that the examined nuisance processes, except cardiac pulsatility, result in unique structured FC patterns. It further demonstrates that a substantial variance of time-varying FC measures can be attributed to head motion and variations in heart rate and breathing patterns.

A natural question that arises from these results is whether different fMRI preprocessing strategies are able to account for the aforementioned effects, as the validity of inferences in resting-state fMRI studies crucially depends on this ability. In this chapter, we examine several state-of-the-art preprocessing strategies and find that the choice of preprocessing method is crucial and that techniques based on blind source decomposition yield the best

performance. With regards to static FC, these techniques eliminate the effects of physiological processes and lead to a significant reduction of head motion confounds. In contrast, none of the evaluated pipelines are able to successfully remove the effects of head motion and variations in heart rate and breathing patterns on time-varying FC, which highlights the need for developing more effective denoising techniques for the latter.

Finally, recent studies assessing test-retest reliability in resting-state FC have suggested that reproducible intra-individual FC patterns observed across sessions may be partly driven by head motion and physiological confounds (Parkes et al., 2018). However, the extent to which the effects of nuisance processes are subject-specific and whether they could influence connectome-based subject identification (Finn et al., 2015) has not yet been addressed. In this chapter, we show that the connectome profiles associated with the examined sources of noise exhibit above-chance levels of subject specificity. Despite this, our results also demonstrate that the most effective preprocessing strategies with regards to reducing head motion and physiological effects on FC improve connectome-based subject identification accuracy, suggesting that the inter-individual differences in FC patterns that facilitate identification are strongly neural in nature and do not largely stem from physiological processes or head motion.

Overall, this study provides a comprehensive assessment of the effects of nuisance processes in the context of resting-state FC that also answers a basic question about the nature of fMRI-based connectivity, which is be valuable to a wide audience of researchers aiming to characterize the intrinsic organization of the brain. The framework proposed in the present study is of great importance for investigators comparing populations, as it will allow them to control for potential biases in connectivity driven by confounding variables. Furthermore, the methodology developed in this chapter is employed in chapter 5 to disentangle the effects of global signal regression on physiological and neural fluctuations in the context of functional connectivity. Finally, as this framework characterizes nuisance-related FC patterns at the individual level, it will benefit the growing field of individualized (“precision”) fMRI (Gratton et al., 2019b).

4.2 ABSTRACT

Human brain connectivity yields significant potential as a noninvasive biomarker. Several studies have used fMRI-based connectivity fingerprinting to characterize individual patterns of brain activity. However, it is not clear whether these patterns mainly reflect neural activity or the effect of physiological and motion processes. To answer this question, we capitalize on a large data sample from the Human Connectome Project and rigorously investigate the contribution of the aforementioned processes on functional connectivity (FC) and time-varying FC, as well as their contribution to subject identifiability. We find that head motion, as well as heart rate and breathing fluctuations, induce artifactual connectivity within distinct resting-state networks and that they correlate with recurrent patterns in time-varying FC. Even though the spatiotemporal signatures of these processes yield above-chance levels in subject identifiability, removing their effects at the preprocessing stage improves identifiability, suggesting a neural component underpinning the inter-individual differences in connectivity.

4.3 INTRODUCTION

Functional magnetic resonance imaging (fMRI) is based on the blood-oxygenation-level-dependent (BOLD) contrast mechanism (Ogawa et al., 1990), and is widely viewed as the gold standard for studying brain function because of its high spatial resolution and non-invasive nature. The BOLD signal exhibits low frequency (~0.01-0.15 Hz) fluctuations that are synchronized across different regions of the brain, a phenomenon known as functional connectivity (FC). FC has been observed even in the absence of any explicit stimulus or task, giving rise to the so-called resting-state networks (RSNs) (Biswal et al., 1995; Fox and Raichle, 2007; Stephen M Smith et al., 2009). Initially, FC was viewed as a stationary phenomenon (static FC) and was commonly measured as the correlation between brain regions over an entire scan. However, several researchers challenged this assumption (Chang and Glover, 2010; Sakoglu et al., 2010), and recent studies have been focusing on FC dynamics, quantified over shorter time scales than the scan duration (time-varying FC) (Hutchison et al., 2013; Lurie et al., 2019).

Although the neurophysiological basis of resting-state FC measured with fMRI is not yet fully understood, many studies have provided evidence to support its neuronal origin. For instance, in animal models, a strong association between spontaneous BOLD fluctuations and neural activity, in particular band-limited local field potentials and firing rates, has been reported (Logothetis et al., 2001; Schölvinck et al., 2010; Shmuel and Leopold, 2008; Thompson et al., 2013b). Furthermore, a recent study suggested a close correspondence between windowed FC calculated from simultaneously recorded hemodynamic signals and calcium transients (Matsui et al., 2018). In human studies, direct measurements of macroscale neural activity have revealed a spatial correlation structure similar to that of spontaneous BOLD fluctuations (Brookes et al., 2011; Hacker et al., 2017; He et al., 2008; Hipp et al., 2012; Kucyi et al., 2018), even during transient (50-200 ms) events (A. P. Baker et al., 2014; Hunyadi et al., 2019; Vidaurre et al., 2018). Therefore, it is widely assumed that resting-state FC measured using BOLD fMRI reflects spontaneous co-fluctuations of the underlying neuronal networks.

However, BOLD signals rely on changes in local cerebral blood flow (CBF) to infer underlying changes in neuronal activity, and according to a recent study, at least 50% of the spontaneous hemodynamic signal is unrelated to ongoing neural activity (Winder et al., 2017). For instance, systemic physiological functions can induce variations in global and local CBF, which in turn result in BOLD signal fluctuations. In particular, low frequency variations in breathing activity (Birn et al., 2008b, 2006; Power et al., 2017b), arterial blood pressure (Whittaker et al., 2019), arterial CO_2 concentration (Prokopiou et al., 2019; Wise et al., 2004), and heart rate (Chang et al., 2009; Shmueli et al., 2007) are known to account for a considerable fraction of variance of the BOLD signal, presumably through changes in CBF. In addition, the BOLD signal intensity is distorted by high-frequency physiological fluctuations, such as cardiovascular pulsation and breathing, through displacement of the brain tissues and perturbations of the B_0 magnetic field (Dagli et al., 1999; Glover et al., 2000). Further, head motion is well-known to have a substantial impact on fMRI through partial volume, magnetic inhomogeneity and spin-history effects (Friston et al., 1996; Power et al., 2012). These non-neuronal factors may introduce common variance components in signals recorded from different brain regions and subsequently induce spurious correlations between these areas (Jingyuan E Chen et al., 2020). Therefore, to account for motion-related and physiological confounds, nuisance regressors are typically obtained using model-based and data-driven techniques, and regressed out from the fMRI data before further analysis (Caballero-Gaudes and Reynolds, 2017).

Static and time-varying resting-state FC have shown promise for providing concise descriptions of how the brain changes across the lifespan (Battaglia et al., 2017; Chan et al., 2014; Ferreira et al., 2016; Geerligs et al., 2015; Sala-Llonch et al., 2015; Xia et al., 2019), and to assay neural differences that are associated with disease (J. T. Baker et al., 2014; Chen et al., 2017; Damaraju et al., 2014; Demirtaş et al., 2016; Drysdale et al., 2017; Du et al., 2016; Gratton et al., 2019a; Hahamy et al., 2015; Mash et al., 2019; Morgan et al., 2017; Xia et al., 2018). However, recent studies assessing the performance of a large range of preprocessing strategies found that there is always a trade-off between adequately removing confounds from fMRI data and preserving the signal of interest (Ciric et al., 2017; Kassinopoulos and Mitsis, 2019a; Parkes et al., 2018). Importantly, these studies found that

widely used techniques for the preprocessing of fMRI data may not efficiently remove physiological and motion artifacts. The latter raises a concern, as it is still not clear how nuisance fluctuations may impact the outcome of FC studies.

Several studies have examined whether physiological fluctuations across the brain could give rise to structured spatial patterns that resemble common RSNs, based on the evidence that vascular responses following systemic changes are spatially heterogenous (Chang et al., 2009; Pinto et al., 2017), or account for the observed time-varying interactions between RSNs. For instance, (Bright and Murphy, 2015) applied independent component analysis (ICA) to the fraction of the fMRI data explained by nuisance regressors related to head motion and physiological variability and revealed a characteristic network structure similar to previously reported RSNs. Similarly, (Tong et al., 2013; Tong and Frederick, 2014) found significant contributions of systemic fluctuations on ICA time courses related to the visual, sensorimotor and auditory networks. Recently, (Jingyuan E Chen et al., 2020) generated BOLD data containing only slow respiratory-related dynamics and showed that respiratory variation can give rise to apparent neurally-related connectivity patterns. Further, recent investigations have shown that physiological confounds can modulate time-varying FC measures (Chang et al., 2013; Nalci et al., 2019; Nikolaou et al., 2016b). These results suggest that changes in brain physiology, breathing patterns, heart rhythms and head motion across sessions, within-subject or across populations, may introduce artifactual inter-individual and group-related differences in FC independent of any underlying differences in neural activity. For instance, cardiac autonomic dysregulation has been associated to a variety of psychiatric disorders (Alvares et al., 2016; Benjamin et al., 2020), which could in principle lead to group differences in connectivity patterns between patients and controls if the effects of heart rate are not accounted for. Therefore, the disentanglement of the neural and physiological correlates of resting-state FC is crucial for maximizing its clinical impact.

While the previous findings provide evidence for the dual-nature of RSNs in both static and time-varying scenarios, only specific physiological processes and/or particular brain networks were evaluated in each of the aforementioned studies. A more holistic assessment of the impact of these non-neural processes on FC measures is needed to better understand

whether and how systemic fluctuations, as well as head or breathing motion affect inter-individual and group differences. Importantly, the wide range of possible preprocessing strategies needs to be reassessed taking into consideration the effects of several non-neural processes on FC measures rather than accounting only for the effects of a specific process (e.g. head motion).

The varying efficiency of different preprocessing pipelines with respect to removing the effect of physiological fluctuations and motion has also implications for studies investigating properties of FC at the individual level. Recent studies have shown that connectivity profiles vary substantially between individuals, acting as an identifying fingerprint (Finn et al., 2015; Mira-Dominguez et al., 2014) that is stable over long periods of time (Horien et al., 2019). However, the high subject discriminability of connectivity profiles may arise partly as a result of physiological processes (Batchvarov et al., 2002; Golestani et al., 2015; Malik et al., 2008; Pinna et al., 2007; Pitzalis et al., 1996; Power et al., 2020; Reland et al., 2005) and head motion (van Dijk et al., 2012; Zeng et al., 2014) being highly subject-specific. Evidence supporting this hypothesis comes from studies showing that the mean of intraclass correlation values of functional connections, associated to test-retest reliability across sessions, is reduced when a relatively aggressive pipeline is used (Birn et al., 2014; Kassinopoulos and Mitsis, 2019a; Parkes et al., 2018), suggesting that artifacts exhibit high subject specificity. However, the relation between subject discrimination and inter-individual differences in physiological processes and head motion has yet to be addressed.

In the present work, we capitalize on 3T resting-state fMRI data from the Human Connectome Project (HCP) to uncover the whole-brain connectome profiles of systemic low-frequency oscillations (SLFOs) associated with heart rate and breathing patterns, cardiac pulsatility, breathing motion and head motion on estimates of static and time-varying FC. To quantify the contributions of physiological processes and head motion on FC, we employ model-based techniques with externally recorded physiological measurements, and subsequently generate nuisance datasets that only contain non-neural fluctuations. Using these datasets, we provide a comprehensive examination of the regional variability of the impact of the considered nuisance processes on the BOLD signal, as well

as an investigation of the group consistency and inter-individual differences of their characteristic signatures on FC. We further evaluate several fMRI preprocessing strategies to assess the extent to which different techniques remove the physiological and motion FC signatures from the fMRI data. Finally, we investigate the potential effect of physiological processes and head motion on individual discriminability in the context of connectome fingerprinting.

Using the proposed approach, we show that SLFOs and head motion have a larger impact on FC measures compared to breathing motion and cardiac pulsatility, and we highlight the functional connections that are more prone to exhibiting biases. Furthermore, our findings suggest that the recurrent whole-brain connectivity patterns observed in time-varying FC can be partly attributed to SLFOs and head motion. Finally, we show that connectome fingerprinting accuracies are higher when non-neural confounds are reduced, suggesting a neural component underpinning the individual nature of FC patterns.

The codes that were employed to carry out the analyses described in the present study are publicly available and can be found on github.com/axifra/Nuisance_signatures_FC.

4.4 RESULTS

4.4.1 Contributions of nuisance processes on the BOLD signal

We examined regional differences in the influence of physiological processes and head motion on the BOLD signal. The physiological processes evaluated here were breathing motion, cardiac pulsatility, and SLFOs associated with changes in heart rate and breathing patterns. Scans with LR and RL phase encoding were examined separately as it has been suggested that breathing motion artifacts vary across scans with different phase encoding directions (Raj et al., 2001), and thus we aimed to examine whether other processes such as head motion demonstrate a similar dependence. The contributions of each nuisance process on BOLD signal fluctuations were quantified as the correlation between the nuisance fluctuations of the process in question, modelled using externally recorded physiological measurements, and the BOLD fluctuations "cleaned" of all other nuisance fluctuations (denoted as r_{nuis} in the Materials and methods section – Isolation of nuisance fluctuations from fMRI data, see also **Figure 4-7**). We computed these contributions for each scan and then tested for the presence of consistent patterns across scans with the same phase encoding direction (significance testing using inter-subject surrogates, two-sample t-test, p<0.05, Bonferroni corrected).

The results showed distinct regional patterns for each of the nuisance processes. SLFOs mostly affected sensory regions, including the visual and somatosensory cortices (particularly of the face) (**Figure 4-1A**). Phase encoding was not found to modulate the magnitude of the SLFOs contributions on the BOLD signal (**Figure 4-1A**). Head motion exhibited the largest effect in the somatosensory and visual cortices (**Figure 4-1B**). Intriguingly, the effect in the visual cortex was highest in the right hemisphere for LR phase encoding, but highest in the left hemisphere for RL phase encoding (**Figure 4-1B**). Breathing motion effects were more pronounced in prefrontal, parietal and temporal brain regions (**Figure 4-1C**). Further, breathing motion had a much larger impact on the left hemisphere when the phase encoding was LR, whereas the reverse pattern was observed for RL phase encoding (**Figure 4-1C**). Cardiac pulsatility was highest in regions such as the visual and auditory cortices, as well as the insular cortex (**Figure 4-1D**).

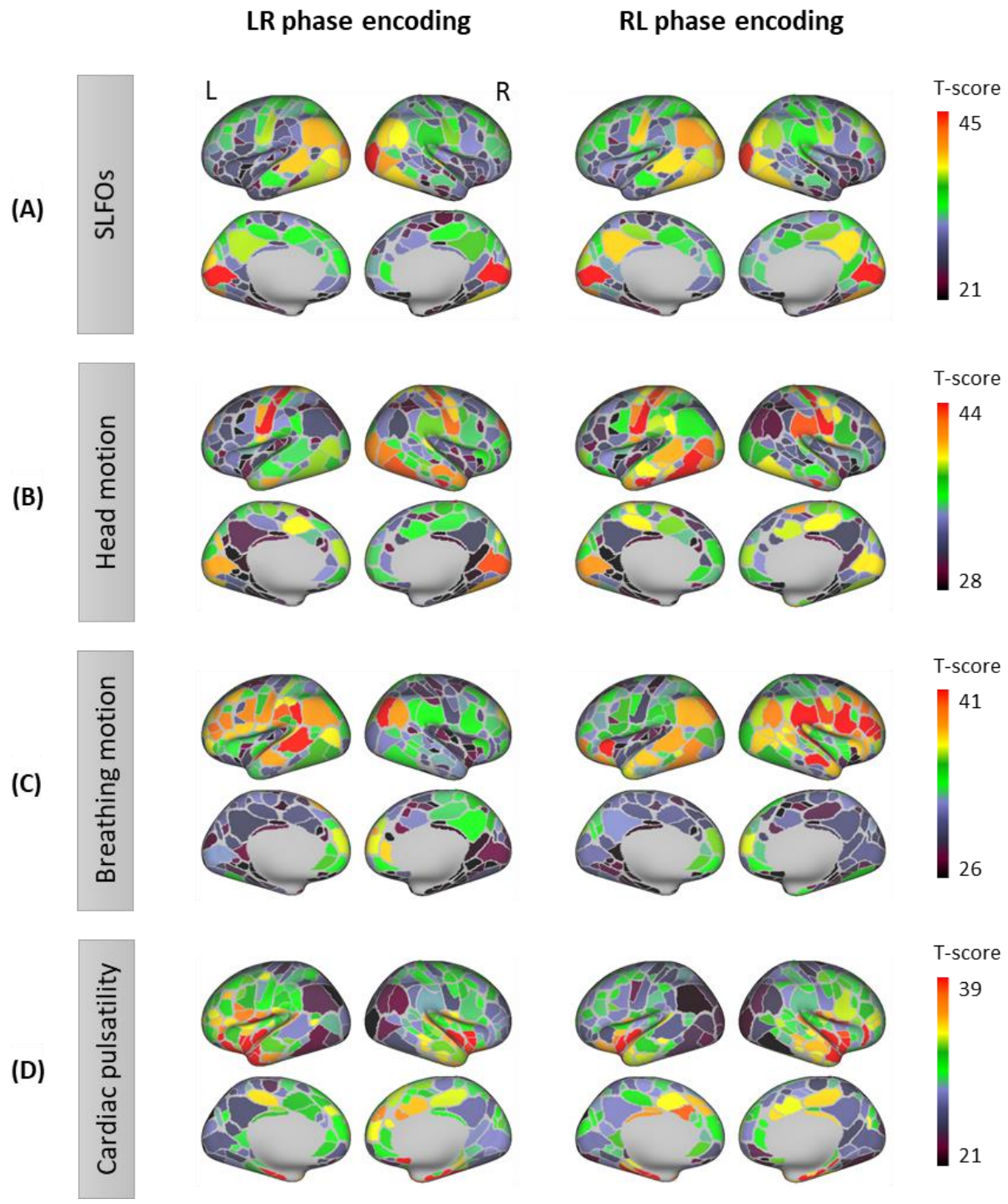

Figure 4-1. Contributions of nuisance processes on the resting-state BOLD signal. T-score maps of the correlation between each nuisance process and BOLD fMRI fluctuations (raw data) for **(A)** SLFOs, **(B)** head motion, **(C)** breathing motion, and **(D)** cardiac pulsatility, computed within each parcel of the Gordon atlas (two-sample t-test against the surrogate data, $p<0.05$, Bonferroni corrected). The t-tests were calculated for each phase encoding separately. The physiological fluctuations were obtained from simultaneous external recordings. These results illustrate the cortical regions most affected by each nuisance process.

4.4.2 Physiological and head motion signatures in static FC

To examine the effect of physiological fluctuations and head motion in static FC, we developed a framework that quantifies the extent to which functional connections are influenced by a nuisance process at the individual scan level. Briefly, synthetic datasets were generated for each scan based on the contributions of the examined nuisance processes within each ROI (see Materials and methods – Isolation of nuisance fluctuations from fMRI data). These datasets retained the variance explained by nuisance fluctuations and replaced the remaining variance (often considered as the "neural" variance) with uncorrelated random signals. This framework allowed us to compute FC matrices that illustrate the whole-brain connectome profiles arising from the nuisance processes of interest (see Materials and methods – Estimation of static and time-varying functional connectivity).

The group-averaged static FC matrices across all 1,568 scans revealed consistent whole-brain connectome patterns for SLFOs, head motion and breathing motion (**Figure 4-2**,**A-C**). SLFO-based connectivity profiles exhibited strong positive correlations for all edges of the FC matrix, particularly for edges within the visual network, as well as between the visual network and the rest of the brain (**Figure 4-2A**). Head motion mainly influenced functional connections within the visual and sensorimotor networks, as well as edges within the DMN (**Figure 4-2B**). Note that even though areas in both the visual and sensorimotor networks were influenced by motion artifacts (**Figure 4-1B**), we did not observe strong correlations between the two aforementioned networks. This is not entirely surprising, as two brain areas may be associated with a different linear combination of head motion nuisance regressors and, thus, the correlation between the region-specific motion-induced fluctuations can in principle be around zero. Breathing motion exhibited an intriguing chess-like pattern, with both positive and negative correlations (**Figure 4-2C**, lower triangular matrix). Based on this observation, we subsequently reordered the ROIs with respect to their hemisphere, which revealed that positive correlations were mostly confined between ROIs of the same hemisphere, whereas correlations between hemispheres were close to zero or even negative (**Figure 4-2C**, upper triangular matrix). Even when scans with LR and RL phase encoding were averaged separately, both

hemispheres exhibited increased within-hemisphere connectivity (**Supp. Fig. 4-1C**). Nonetheless, the connectome profile of breathing motion exhibited clear differences between phase encoding directions, whereas all other nuisance processes did not exhibit perceivable differences (**Supp. Fig. 4-1**). Finally, cardiac pulsatility did not exhibit a characteristic spatial pattern and the group-averaged correlation values were low, suggesting that it does not affect static FC in a systematic manner across subjects (**Figure 4-2D**).

Figure 4-2. (next page) Whole-brain connectome patterns induced by nuisance processes and effect of preprocessing strategies. (A-D) Group averaged nuisance FC matrices across all 1,568 scans for **(A)** SLFOs, **(B)** head motion, **(C)** breathing motion, and **(D)** cardiac pulsatility. These results demonstrate that nuisance fluctuations induce heterogeneous whole-brain connectivity profiles which, if unaccounted for, can result in biased estimates functional connectivity. **(E-H)** Distribution of Pearson correlation coefficients across all 1,568 scans between the "neural" FC matrix for different preprocessing strategies and nuisance FC matrices associated to **(E)** SLFOs, **(F)** head motion, **(G)** breathing motion, and **(H)** cardiac pulsatility. Correlation values were Fisher z transformed. SLFOs, head motion and breathing motion were found to confound the FC matrices more severely **(E-G)**. GSR effectively removed the effects of SLFOs, while more aggressive preprocessing pipelines mitigated the effects of head motion, breathing motion and cardiac pulsatility.

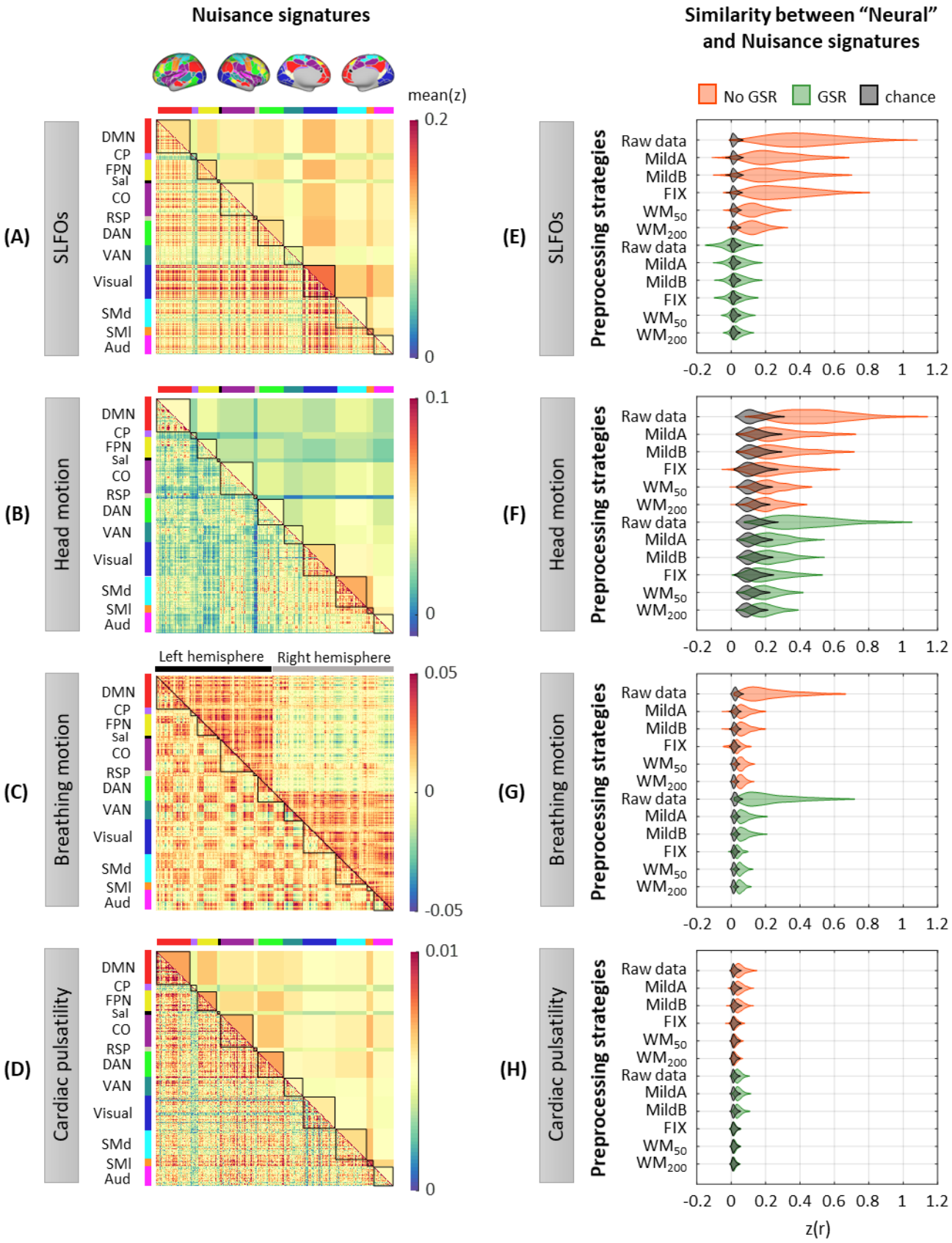
Nuisance signatures
Similarity between "Neural" and Nuisance signatures
mean(z)
No GSR
GSR
chance
(A)
SLFOs
(B)
Head motion
(C)
Breathing motion
(D)
Cardiac pulsatility
DMN
CP
FPN
Sal
CO
RSP
DAN
VAN
Visual
SMd
SMl
Aud
Left hemisphere
Right hemisphere
0.2
0
0.1
0
0.05
0
-0.05
0.01
0
(E)
(F)
(G)
(H)
Preprocessing strategies
Raw data
MildA
MildB
FIX
WM50
WM200
-0.2
0
0.2
0.4
0.6
0.8
1
1.2
z(r)

4.4.3 Capability of preprocessing strategies to remove the nuisance signatures on static FC at the individual level

To examine the capability of various preprocessing strategies to reduce the effects introduced by physiological processes and head motion on static FC, we computed for each scan the similarity of the connectome profile that arises from a nuisance process with the connectome profile calculated from preprocessed fMRI data (considered as the "neural" profile). This similarity reflects the extent to which the "neural" connectome profile extracted after a specific denoising strategy is confounded by physiological and head motion artifacts. A distribution of the similarity values across scans, in this case Pearson's correlation coefficients, is shown in **Figure 4-2 E-H** for each preprocessing strategy and nuisance process. We found that SLFOs, head motion and breathing motion had the strongest influence on static FC, based on the similarity of their connectome profiles with the "neural" connectome profiles from the raw data (**Figure 4-2**,**E-H**).

The signature induced by SLFOs remained after the MildA, MildB and FIX pipelines were applied, but was greatly reduced by the WM_{50} and WM_{200} strategies (**Figure 4-2E**). The observation that FIX, which is a rather aggressive preprocessing strategy, was unable to remove most of the SLFOs is consistent with recent studies showing that global artifactual fluctuations are still prominent after FIX denoising (Burgess et al., 2016a; Glasser et al., 2018; Kassinopoulos and Mitsis, 2019b; Power et al., 2018, 2017b). Notably, GSR seemed to be an effective technique for removing the physiological signature from SLFOs on static FC, albeit for some scans it appeared to introduce a negative correlation between the SLFOs and "neural" FC matrices (**Figure 4-2E**). This effect was greater when the global signal was computed across the whole brain in volumetric space, compared to across vertices in surface space (**Supp. Fig. 4-2A**). The effect of the signature related to head motion was reduced with more aggressive preprocessing strategies, but none of the examined approaches completely eradicated the head motion effects in static FC (**Figure 4-2F**). GSR slightly reduced the similarity between the head motion and "neural" connectome profiles. The signature induced by breathing motion was greatly reduced by all preprocessing strategies, and particularly by FIX denoising, which yielded almost chance level (**Figure 4-2G**). Still, none of the preprocessing strategies entirely eliminated the breathing motion

signature in static FC. The confounds introduced by cardiac pulsatility were overall small and effectively removed by the FIX, WM_{50} and WM_{200} strategies (**Figure 4-2H**). GSR did not have any effect on the removal of breathing motion and cardiac pulsatility connectome profiles.

Finally, we evaluated the addition of model-based nuisance regressors to the preprocessing strategies. Specifically, we added the physiological regressors used to model SLFOs (Kassinopoulos and Mitsis, 2019b), cardiac pulsatility and breathing motion (Glover et al., 2000). We found that including the regressor that models SLFOs reduces their effect on static FC for all preprocessing strategies apart from WM_{50} and WM_{200}, but, in contrast to GSR, the similarity remains well above chance levels (**Supp. Fig. 4-3A**). Including the RETROICOR regressors related to breathing motion considerably reduced the breathing motion signature in the raw data; however, none of the preprocessing strategies benefited from including these regressors (**Supp. Fig. 4-3C**). On the contrary, including the RETROICOR regressors related to cardiac pulsatility completely removed the effect of the latter for the raw data and the MildA and MildB strategies (**Supp. Fig. 4-3D**), suggesting that conservative preprocessing strategies greatly benefit by adding the model-based regressors for cardiac pulsatility.

4.4.4 Connectome-based identification of individual subjects

We next investigated the extent to which FC matrices associated to physiological processes and head motion can identify an individual subject, and whether the accuracy of connectome-based fingerprinting is inflated by the examined nuisance processes (see Materials and methods – Connectome-based identification of individual subjects).

We initially considered all the edges of the FC matrices for subject identification (Gordon atlas: 40,755 edges). Accuracy was above chance for all database-target combinations for the nuisance processes, with rates up to 40% (**Figure 4-3A**). Breathing motion exhibited an intriguing bimodal distribution: database-target pairs that had the same phase encoding yielded much higher identification rates than database-target pairs with different phase encodings, even if the latter were acquired on the same day. This effect was also observed, although to a lesser extent, for cardiac pulsatility and head motion.

Identification accuracy was much higher for the "neural" datasets compared to the nuisance datasets, with rates ranging from 52% to 99% (**Figure 4-3B**). The MildA, MildB and FIX techniques considerably improved the accuracy compared to the raw data, and the WM_{50} and WM_{200} techniques significantly outperformed all other preprocessing strategies. GSR considerably improved identification accuracy for the MildA, MildB and FIX strategies. Furthermore, we observed that for the raw data, database-target pairs from different days with the same phase encoding showed identification rates as high as the ones from the same day but different phase encoding. In contrast, for all other preprocessing strategies the database-target pairs from the same day were always higher.

We subsequently tested identification accuracy on the basis of within and between edges of specific functional networks to examine whether certain functional connections had a more pronounced contribution to individual subject discriminability. Results for the nuisance datasets are shown in **Figure 4-4A**, where it can be seen that nuisance processes yielded a markedly lower identification accuracy when using specific edges compared to using all edges (**Figure 4-3A**). Furthermore, functional connections between networks seemed to contribute more to the subject discriminability of SLFOs compared to connections within brain networks ($p<0.001$, Wilcoxon rank-sum).

Regarding the "neural" datasets, we focused on the most aggressive strategies, namely FIX and WM_{200}. Networks of "top-down" control (FPN, CO, DAN, VAN), as well as the DMN, yielded higher identification accuracy compared to sensorimotor processing networks (Visual, SMd, Aud) for all preprocessing strategies (**Figure 4-4B**). These results indicate that FC patterns in higher-order association cortices ("top-down" control networks) tend to be distinctive for each individual, whereas primary sensory and motor regions (processing networks) tend to exhibit similar patterns across individuals, consistent with previous studies (Finn et al., 2015; Gratton et al., 2018; Horien et al., 2019). We then tested for differences in identification accuracy between the raw data vs. FIX and WM_{200} data (**Figure 4-4C**, $p<0.05$, Bonferroni corrected, Wilcoxon rank-sum). FIX denoising significantly increased the subject discriminability of connections within and between several top-down control networks, but significantly decreased the subject discriminability of connections between the FPN and SMd, as well as the FPN and Aud networks. Conversely,

WM_{200} denoising significantly increased the subject discriminability of connections within and between all top-down control networks, connections within the Visual and SMd networks, and connections of the DAN with the Visual and SMd network.

Figure 4-3. (next page) Connectome fingerprinting results. (A) Fingerprinting accuracy obtained using the static FC matrices from the generated nuisance datasets whereby non-neural fluctuations were isolated from the BOLD data. Above-chance level accuracy values were obtained for all nuisance processes, suggesting some degree of subject specificity in whole-brain connectivity profiles arises from nuisance fluctuations. **(B)** Fingerprinting accuracy obtained using the static FC matrices generated from each of the preprocessing strategies evaluated. The pairs of resting-state scans are indicated with different symbols, depending on whether they belong to the same or different day session, as well as whether they have the same phase encoding. Higher fingerprinting accuracy values were observed for white matter denoising approaches (WM_{50}, WM_{200}) compared to milder pipelines and FIX denoising. Both mild and more aggressive pipelines yielded higher subject discriminability for pairs of scans acquired on the same day. GSR increased the fingerprinting accuracy of milder strategies and FIX denoising.

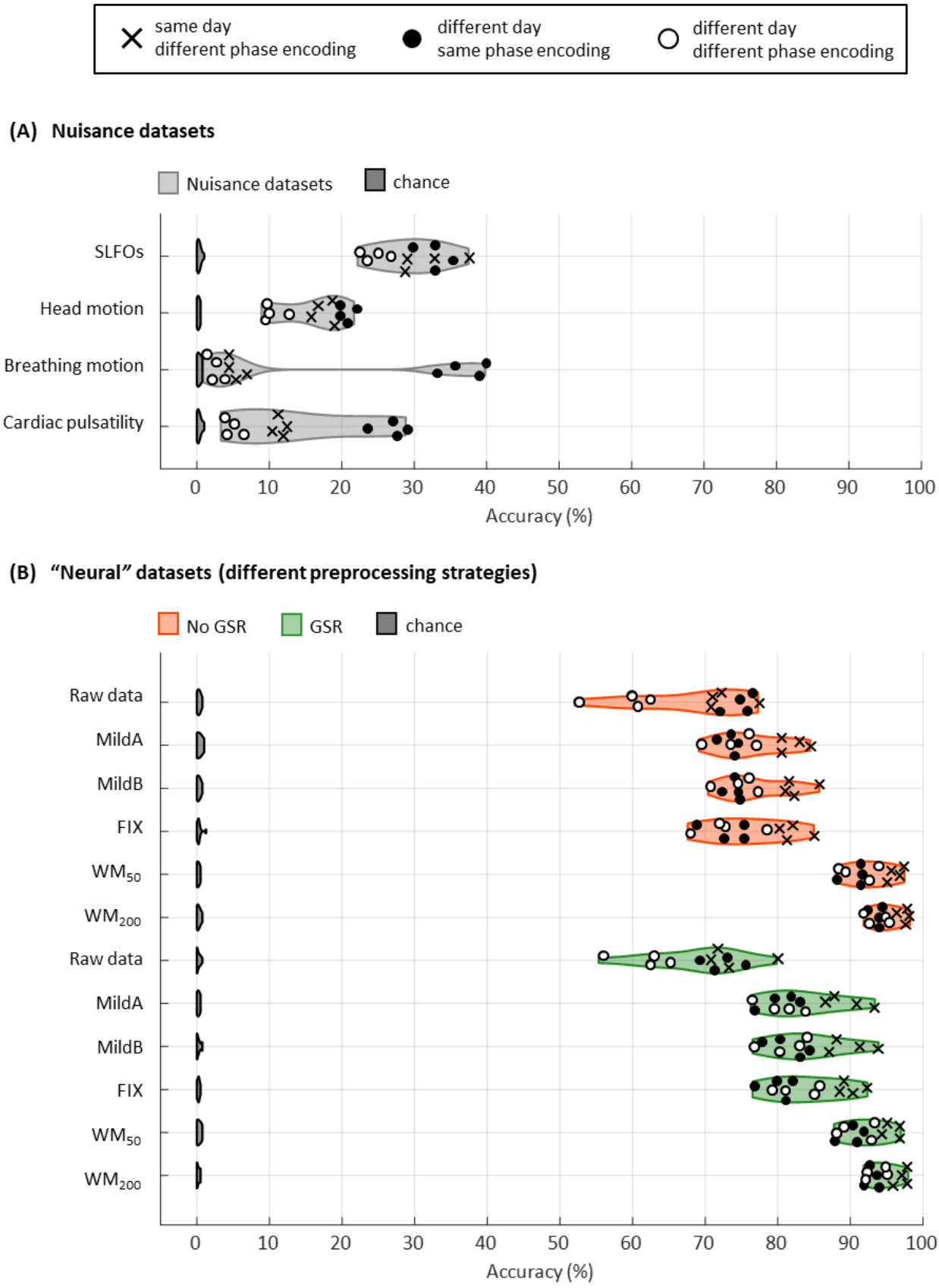
same day
different phase encoding
different day
same phase encoding
different day
different phase encoding
(A) Nuisance datasets
Nuisance datasets
chance
SLFOs
Head motion
Breathing motion
Cardiac pulsatility
0
10
20
30
40
50
60
70
80
90
100
Accuracy (%)
(B) "Neural" datasets (different preprocessing strategies)
No GSR
GSR
chance
Raw data
MildA
MildB
FIX
WM50
WM200
Raw data
MildA
MildB
FIX
WM50
WM200
0
10
20
30
40
50
60
70
80
90
100
Accuracy (%)

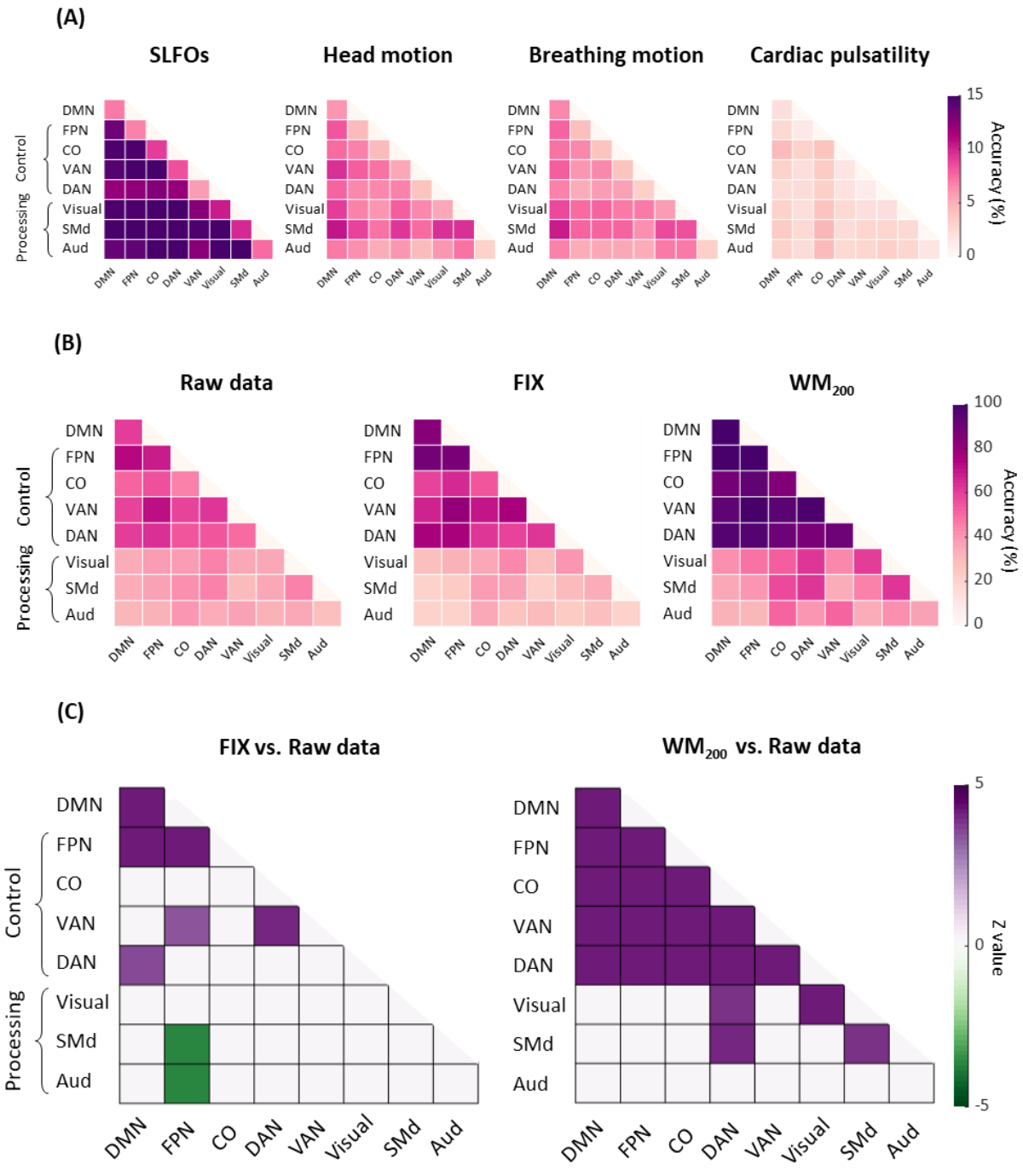

Figure 4-4. Connectome fingerprinting results using edges within and between networks.
(A) Fingerprinting accuracy for SLFOs, head motion, breathing motion and cardiac pulsatility, averaged across all database-target pairs. **(B)** Fingerprinting accuracy for the raw data, FIX and WM200 pipelines, averaged across all database-target pairs. **(C)** Significant differences in fingerprinting accuracy obtained when using the FIX and WM200 pipelines as compared to the raw data ($p<0.05$, Bonferroni corrected, Wilcoxon rank-sum). Connectivity profiles within and between top-down control networks (FPN, CO, VAN, DAN) and DMN yielded higher identification accuracy compared to connectivity profiles within and between sensorimotor processing networks (Visual, SMd, Aud).

4.4.5 Physiological and head motion signatures in time-varying FC and the effect of preprocessing strategies

To examine the effect of physiological processes and head motion on time-varying FC estimates, we computed functional connectivity dynamics (FCD) matrices (Hansen et al., 2015) using the generated nuisance and "neural" datasets from each scan, whereby each FCD matrix captures the temporal evolution of FC patterns within a scan. We subsequently computed the similarity of the nuisance and "neural" FCD matrices at the individual level to examine the capability of various preprocessing strategies to reduce the confounds introduced by physiological processes and head motion on time-varying FC. A distribution of the similarity values, in this case Pearson's correlation coefficients, is shown in **Figure 4-5** for each preprocessing strategy and nuisance process. We observed that the temporal evolution of FC patterns from SLFOs and head motion were similar to the ones observed in the raw data. An illustration of this similarity is shown in **Figure 4-6** for six subjects. On the other hand, breathing motion and cardiac pulsatility FCD matrices did not show similarities with the FCD matrices obtained from "neural" datasets (**Figure 4-5**).

None of the preprocessing pipelines was able to vanish the effects of SLFOs and head motion. However, these effects were considerably reduced by the WM_{50} and WM_{200} strategies (**Figure 4-5,A-B**; **Figure 4-6**). FIX denoising was the least successful strategy in terms of reducing the SLFOs' signature (**Figure 4-5A**, **Figure 4-6**), similarly to static FC (**Figure 4-2E**), and only achieved the same levels of performance as other strategies after GSR. However, even after GSR none of the strategies reached chance levels (**Figure 4-5A**), in contrast with the static FC results (**Figure 4-2E**). GSR led also to a slight reduction in the similarity between the head motion and "neural" FCD matrices (**Figure 4-5B**), as in the case of static FC (**Figure 4-2F**).

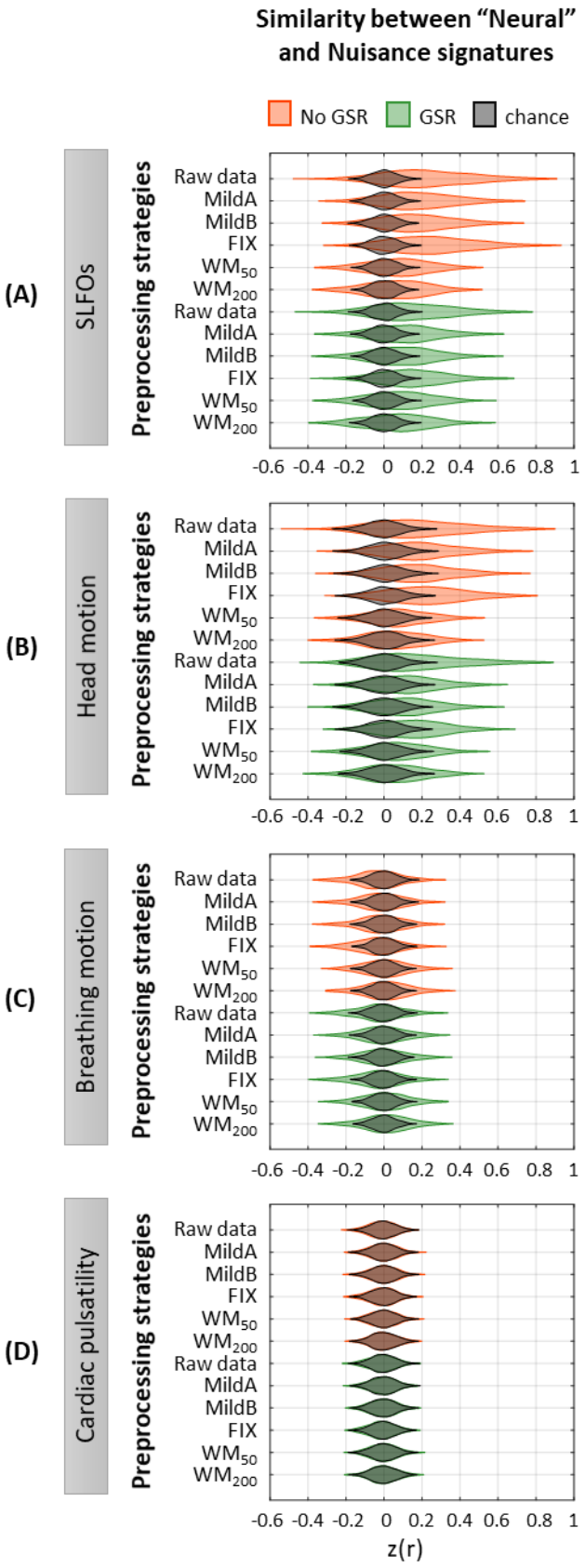

Figure 4-5. Effectiveness of preprocessing strategies in reducing functional connectivity dynamics (FCD) profiles induced by physiological and motion processes.
Distribution of Pearson correlation coefficients across all 1,568 scans between the "neural" functional connectivity dynamics (FCD) matrix after each preprocessing pipeline and nuisance FCD matrices associated to **(A)** SLFOs, **(B)** head motion, **(C)** breathing motion, and **(D)** cardiac pulsatility. Correlation values were Fisher z transformed. Results shown in the top row of each subpanel (raw data) suggest that SLFOs and head motion most severely confound the FC matrices, whereas breathing motion and cardiac pulsatility do not induce artifactual dynamics. None of the examined strategies completely eliminated these effects.

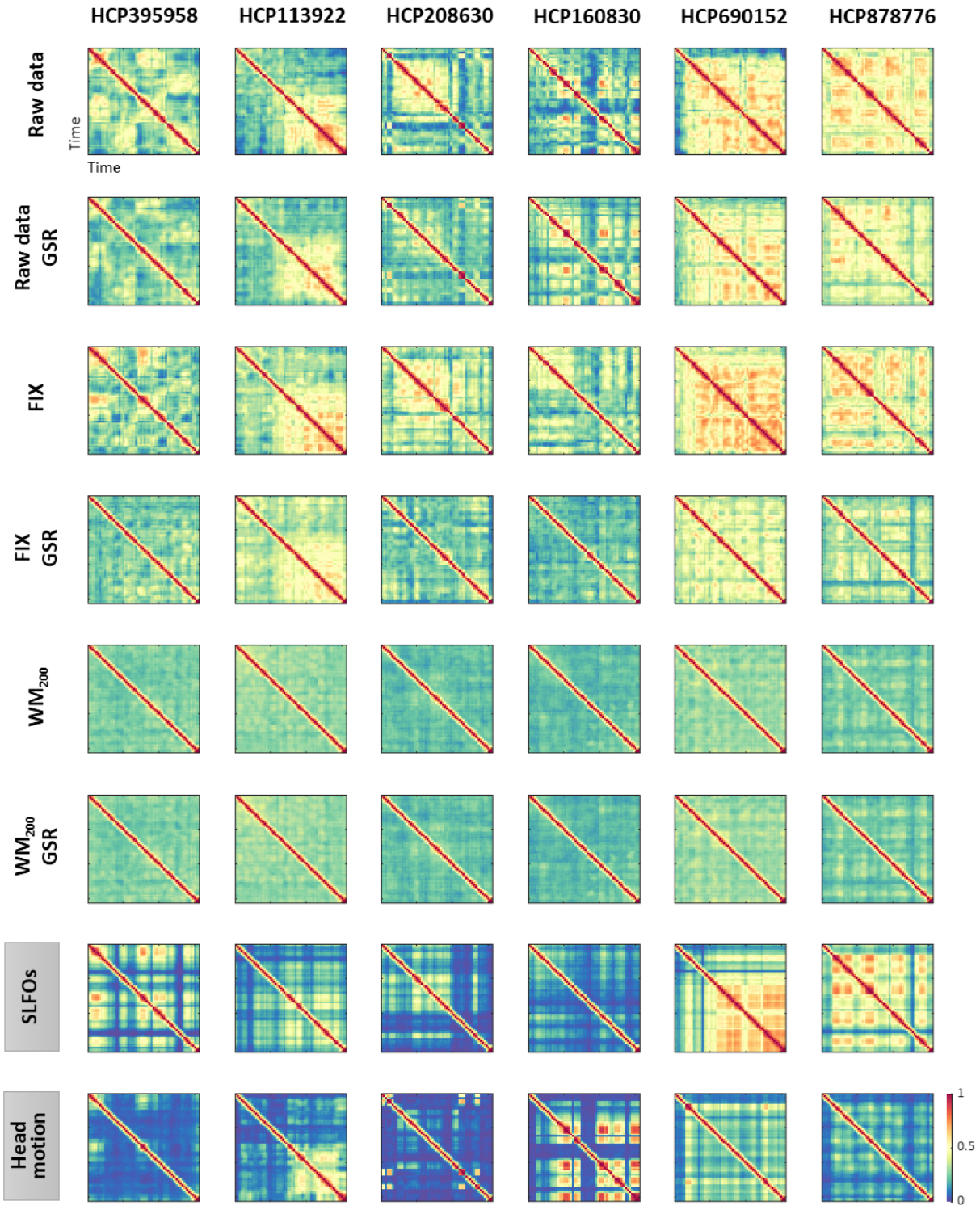

Figure 4-6. Functional connectivity dynamics (FCD) profiles associated with SLFOs and head motion resemble patterns commonly attributed to neural processes. Illustrative examples of FCD matrices from specific HCP subjects as obtained from the fMRI data for several pre-processing pipelines (rows 1-6), as well as from SLFOs and head motion (rows 7 and 8, respectively). All the examples are from the HCP scan Rest1_LR. These examples show a clear resemblance between FCD matrices computed from the "neural" datasets and the nuisance processes (SLFOs and head motion).

4.5 DISCUSSION

In this work, we characterized the effects of physiological processes and head motion on static and time-varying estimates of functional connectivity measured with BOLD fMRI. While the BOLD signal is considered a proxy of neural activity via changes in local blood oxygenation, physiological processes and motion artifacts can also induce variations in the BOLD signal, which can in turn lead to confounds in estimates of functional connectivity. Here, we developed an innovative framework to characterize the spatial signature of head motion and physiological processes (cardiac and breathing activity) on estimates of functional connectivity. Our results demonstrated that functional connectivity measures can be influenced by non-neural processes. Specifically, we identified stereotyped whole-brain functional connectivity profiles for SLFOs, head motion and breathing motion (**Figure 4-2**,**A-C**), suggesting that these processes introduce a systematic bias in estimates of functional connectivity if they are not properly accounted for. Furthermore, we provided evidence that recurring patterns in time-varying FC can be attributed, to some extent, to SLFOs and head motion (**Figure 4-5**, **Figure 4-6**). We also assessed the performance of several state-of-the-art preprocessing strategies in mitigating the effects of nuisance processes, and showed that more aggressive preprocessing strategies such as FIX (Salimi-Khorshidi et al., 2014) and WM denoising (Kassinopoulos and Mitsis, 2019a) combined with GSR were the most effective with regards to removing the effects of non-neural processes for both static and time-varying FC analyses (**Figure 4-2**,**E-H**, **Figure 4-5**, **Figure 4-6**). Finally, we evaluated the potential subject specificity of the connectivity profiles associated with physiological and motion confounds, along with their role as hypothetical contributors to connectome fingerprinting accuracy. Interestingly, we found that these non-neural functional connectivity patterns are to some extent subject specific (**Figure 4-3A**); however, fMRI data corrected for these confounds increased identification accuracy in connectome fingerprinting (**Figure 4-3B**), suggesting that the inter-individual differences in FC that facilitate subject identification are strongly neural and do not largely stem from physiological processes or head motion.

4.5.1 Spatially heterogeneous contributions of nuisance processes to the BOLD signal

It is well established that head and breathing motion affect areas at the edges of the brain (Jo et al., 2010; Patriat et al., 2015; Satterthwaite et al., 2013), whereas cardiac pulsatility affects areas near the large cerebral arteries just above the neck (Glover et al., 2000; Kassinopoulos and Mitsis, 2020). These observations are based on studies that typically examine the brain regions affected by the aforementioned sources of noise on a voxel-wise basis. However, at the voxel level we cannot easily assess whether the average fMRI signal from atlas-based ROIs includes significant contributions from these nuisance processes. In principle, it could be the case that the dynamics of artifacts associated with a specific nuisance process demonstrate significant variability across voxels, and as a result their effects cancel out when averaging voxels within an ROI. In the present study, we assessed the impact and regional variation of these nuisance processes in the Gordon parcellation (Gordon et al., 2016), a widely used atlas in the literature.

SLFOs related to changes in heart rate and breathing patterns were found to affect mostly sensory regions including the visual and somatosensory cortices (particularly of the face) (**Figure 4-1A**), which correspond to regions with a high density of veins (Bernier et al., 2018; Huck et al., 2019). The spatial pattern of SLFOs is very similar to statistical maps reported in prior works, which have highlighted brain regions highly correlated with the global signal (Billings and Keilholz, 2018; Glasser et al., 2016; Li et al., 2019a; Power et al., 2017b; Tong et al., 2013; Zhang et al., 2019). This is not surprising, since the global signal is strongly driven by fluctuations in heart rate and breathing patterns (Birn et al., 2006; Chang and Glover, 2009a; Falahpour et al., 2013; Kassinopoulos and Mitsis, 2019b; Shmueli et al., 2007). Moreover, we show evidence that SLFOs and cardiac pulsatility do not affect the same brain regions, consistent with (Chen et al., 2019; Kassinopoulos and Mitsis, 2019b; Tong and Frederick, 2014). Specifically, cardiac pulsatility was more dominant in regions such as the insular and auditory cortices, which align with cortical branches of the middle cerebral artery (**Figure 4-1D**) and are the regions with highest arterial density (Bernier et al., 2018).

Regarding head motion, previous studies found that its effect was more pronounced in prefrontal, sensorimotor and visual brain regions (Satterthwaite et al., 2013; Yan et al., 2013). However, these studies did not remove breathing artifacts from the realignment parameters, which are present even in single-band datasets (Gratton et al., 2020), and thus were unable to disentangle whether a specific type of motion affected particular brain regions. In the present work, we regressed out breathing motion from the realignment parameters, and observed that sensorimotor and visual areas were strongly affected by head motion (**Figure 4-1B**), whereas breathing motion artifacts were more pronounced in the prefrontal cortex and brain regions in the parietal and temporal cortices (**Figure 4-1C**). Furthermore, Yan et al. showed that framewise displacement was positively correlated with sensory regions and negatively correlated with prefrontal regions. Collectively, these findings suggest that most regions exhibit an increase in the BOLD signal due to head and breathing motion, whereas the prefrontal cortex may exhibit a decrease in the BOLD signal likely due to breathing-related chest movements.

4.5.2 Physiological and head motion signatures in static FC

Head motion is considered the biggest source of confound for FC fMRI studies and there is a significant effort from the neuroimaging community towards developing and evaluating preprocessing strategies that mitigate its effects (Ciric et al., 2017; Parkes et al., 2018; Power et al., 2015). On the other hand, while it has been shown that SLFOs affect the default-mode network (Birn et al., 2014, 2008a; Chang and Glover, 2009a), and high frequency cardiac and breathing artifacts influence the BOLD signal (Glover et al., 2000; Power et al., 2019), a systematic investigation of the effects of physiological processes in the context of whole-brain FC is lacking in the literature. In the present study, we evaluated collectively the impact of the aforementioned sources of noise on whole-brain fMRI resting-state FC.

Our results revealed that all four nuisance datasets exhibited mainly positive correlations between ROIs (**Figure 4-2**,**A-D**), suggesting that the presence of nuisance fluctuations in a conventional fMRI dataset typically leads to a shift of correlation values towards more positive numbers. In other words, in the case of an fMRI dataset that has not been corrected

for nuisance fluctuations, two ROIs for which neural-related fluctuations are negatively correlated could be found to be positively correlated due to the presence of similar nuisance fluctuations in the ROIs. Furthermore, we observed that SLFOs and head motion confounded FC to a larger degree compared to breathing motion and cardiac pulsatility (**Figure 4-2**,**E-H**).

Our results suggest that SLFOs due to spontaneous changes in heart rate or breathing patterns inflate connectivity (towards more positive values) across the whole brain but particularly for edges within the visual network, as well as edges between the visual and the rest of the networks (**Figure 4-2A**). It is well known that the visual cortex is characterized by the highest venous density (Bernier et al., 2018), possibly due to its functional importance (Collins et al., 2010). In addition, it has been shown that brain regions with higher vascular density exhibit larger amplitude of spontaneous BOLD fluctuations (Vigneau-Roy et al., 2014). Therefore, it is likely that the structure of the SLFOs' connectome profile may largely reflect the underlying vascular architecture. The effect of SLFOs on static FC was considerably reduced after WM denoising, while additionally performing GSR almost removed this effect (Fig. 4E). Notably, FIX denoising without GSR was unable to remove the confounds introduced by SLFOs, which is consistent with recent studies showing that global artifactual fluctuations are still prominent after FIX denoising (Burgess et al., 2016a; Glasser et al., 2018; Kassinopoulos and Mitsis, 2019b; Power et al., 2018, 2017b).

Head motion was found to influence the connectivity within the visual and sensorimotor networks (**Figure 4-2B**), in line with previous studies (Power et al., 2012; Satterthwaite et al., 2012; van Dijk et al., 2012). Our results showed that only regressing out the realignment parameters and average WM/CSF signals (with or without expansion terms) is not sufficient to remove the effects of head motion (**Figure 4-2F**, MildA and MildB pipelines), which is consistent with findings in (Parkes et al., 2018). Among all preprocessing strategies, WM denoising yielded the largest reduction of motion effects (**Figure 4-2F**). The two pipelines WM_{50} and WM_{200} refer to the removal of 50 and 200 white matter regressors from the data (i.e. principal components obtained from the white matter compartment). In our previous study we showed that while both pipelines yielded high large-scale network

identifiability compared to other pipelines, the more aggressive WM_{200} resulted in a larger reduction of motion artifacts compared to WM_{50} (Kassinopoulos and Mitsis, 2019a). The results of the current study also show a stronger reduction of head motion effects for the former compared to the latter (**Figure 4-2F**), which may explain the higher accuracy in connectome fingerprinting observed for the pipeline WM_{200} compared to WM_{50} (**Figure 4-3B**).

A natural concern regarding the head motion connectome profile is that it may reflect motor-related activity (Yan et al., 2013). Even though motor-related neural activity would be expected to lag the instantaneous motion traces due to the sluggishness of the hemodynamic response, we cannot exclude the scenario that the head motion connectome profile reflects the neural correlates of the executed movements and eye adjustments to fixate on the cross. Nonetheless, even if preprocessing strategies remove neural activity associated with spontaneous head movements, this source of neural activity is typically of no interest in resting-state fMRI studies.

Furthermore, we provide evidence that head and breathing motion do not affect functional connectivity in the same manner. Specifically, breathing motion was found to inflate within-hemisphere connectivity (**Figure 4-2C**). This bias seems to arise as a result of factitious motion rather than real motion of the head, since it is related to the LR/RL phase encoding direction (see section 4.4 for more details). All preprocessing strategies yielded a substantial reduction of artifacts related to breathing motion, with FIX denoising being the most effective (**Figure 4-2G**).

In our dataset, cardiac pulsatility did not seem to have a large effect on FC, neither in cortical nor subcortical regions (**Figure 4-2D**, **Supp. Fig. 4-5D**), and its effect was entirely removed with more aggressive pipelines such as FIX and WM denoising (**Figure 4-2H**), as well as with model-based techniques (**Supp. Fig. 4-3D**). However, it has been recently reported that the 3T HCP dataset has poor temporal signal-to-noise ratio in the subcortex (Ji et al., 2018; Seitzman et al., 2020). Therefore, it is possible that we may have underestimated the effect of cardiac pulsatility in functional connections involving subcortical regions.

It is important to note that our proposed methodology assumes that the stereotyped nuisance connectome profiles do not resemble the true neural connectome profiles. However, in principle, nuisance fluctuations could give rise to similar spatial patterns as neurally-driven fluctuations. A recent study by (Bright et al., 2018) provided evidence that physiological fluctuations (end-tidal CO_2) give rise to networks that spatially resemble neurally-driven networks linked to working memory and visual stimuli. The authors suggested that this phenomenon may be due to the vasculature adapting to the neural network architecture, as vascular and neuronal growth processes evolve concurrently during development (Quaegebeur et al., 2011). These findings suggest a possible caveat of our methodology when assessing pre-processing strategies, as pipelines that yield the lowest similarity between nuisance and "neural" FC matrices might also remove some signal of interest. Nonetheless, the pre-processing strategies that were found in this study to reduce the nuisance effects the most (i.e. FIX and WM denoising combined with GSR) have been shown to demonstrate the highest improvement in large-scale network identifiability in an earlier study (Kassinopoulos and Mitsis, 2019a). In addition, these pipelines were found to exhibit the highest accuracy in connectome fingerprinting (**Figure 4-3B**). These results suggest that they are able to adequately remove the effects of nuisance processes while also preserving the signal of interest.

4.5.3 Physiological and head motion signatures on time-varying FC

The investigation of neural dynamics using resting-state fMRI is a promising avenue of research that has gained increasing attention lately (Hutchison et al., 2013; Lurie et al., 2019). Yet, there is skepticism regarding its validity and underlying origins. For instance, variations in FC over shorter time-scales (i.e. minutes) could largely be explained by sampling error, acquisition artifacts and subject arousal (Hindriks et al., 2016; Laumann et al., 2017; Savva et al., 2019), as well as head motion and physiological processes (Nalci et al., 2019; Nikolaou et al., 2016b).

In the present study, we sought to evaluate whether non-neural fluctuations could partly explain the recurrent connectivity patterns observed in fMRI studies. To this end, we computed time-resolved FC dynamics (Hansen et al., 2015) for all four nuisance datasets,

and assessed their similarity with time-resolved FC dynamics obtained from fMRI data preprocessed employing widely used denoising strategies ("neural" datasets). The FC dynamics of head motion and SLFOs datasets were markedly similar to the FC dynamics observed in preprocessed fMRI data (**Figure 4-5**,**A-B**), albeit the similarity was smaller compared to static FC (**Figure 4-2,E-F**). When observing the time-resolved FC matrices (**Figure 4-6**), it becomes apparent that a large component of variability in FC patterns is due to non-neural processes, and that these patterns remain after implementing popular preprocessing pipelines such as MildA, MildB and FIX. These results are aligned with the observation that even after regressing out nuisance processes from the BOLD signal, correlations between time-varying FC measures and nuisance fluctuations remain (Nalci et al., 2019). WM denoising was found to be the most efficient strategy in terms of mitigating the influence of nuisance processes on time-varying FC (**Figure 4-5**,**A-B**).

After WM denoising, variability in FC patterns was greatly diminished (**Figure 4-6**), even when those patterns could not be directly associated with any nuisance process (**Supp. Fig. 4-4**). These results can be interpreted in two ways that are not mutually exclusive: (1) A significant fraction of the variability in FC patterns is a result of non-neural confounds and WM denoising is able to remove most of these confounds. This is supported by the fact that many other nuisance processes, which we did not examine here (e.g. arterial blood pressure, CO_2 concentration, scanner instabilities), can influence the BOLD signal and time-varying FC patterns (Nikolaou et al., 2016b; Whittaker et al., 2019; Wise et al., 2004). (2) WM denoising removes a considerable fraction of variance of neural origin. Future work with concurrent direct measurements of neuronal activity (e.g. electroencephalography, calcium imaging) and additional physiological recordings would be instrumental for resolving to which extent time-varying FC is the result of underlying neural dynamics.

While head motion and SLFOs were found to be strongly associated to recurrent connectivity patterns, breathing motion and cardiac pulsatility do not seem to be a main concern for time-varying FC studies (**Figure 4-5**,**C-D**). Likely, the effects of breathing motion and cardiac pulsatility do not influence time-varying FC, because their effect on the BOLD signal does not change from window to window, possibly due to their quasi-periodic nature. In contrast, the levels of head motion vary across time windows, which can

modulate time-varying FC patterns. Heart rate and breathing patterns can be relatively constant during some time periods, whereby SLFOs are not expected to influence the BOLD signal and, in turn, the FC measures across time windows. On the other hand, in other instances heart rate and breathing patterns may change considerably over time, whereby SLFOs are expected to influence the BOLD signal and thus modulate the FC measures across time windows. In other words, ROIs sensitive to head motion and SLFOs are likely to exhibit a time-varying signal-to-noise ratio depending on the presence of these sources of noise, which eventually leads to confounds in time-varying FC measures.

Importantly, none of the evaluated pipelines were able to completely remove these confounds. It was only recently that researchers have started to examine the performance of pre-processing pipelines in the context of time-varying FC (Lydon-Staley et al., 2019), albeit with a focus on motion effects, thus more work is needed to identify effective data cleaning strategies for resting-state time-varying FC studies.

4.5.4 Global signal regression

The practice of removing the GS from fMRI data (i.e. GSR) has been adopted by many fMRI investigators as it has been linked to head motion artifacts and fluctuations in heart rate and breathing patterns (Birn et al., 2006; Byrge and Kennedy, 2018; Chang and Glover, 2009a; Falahpour et al., 2013; Kassinopoulos and Mitsis, 2019b; Power et al., 2018, 2014a; Shmueli et al., 2007). Further, GSR has been shown to increase the neuronal-hemodynamic correspondence of FC measures extracted from BOLD signals and electrophysiological high gamma recordings (Keller et al., 2013), as well as strengthen the association between FC and behaviour (Li et al., 2019b). On the other hand, studies capitalizing on EEG-fMRI data have reported an association between the GS amplitude and vigilance measures (C. K. Wong et al., 2016; Wong et al., 2013) and individual differences in the global signal topography have been related to behavior and cognition (Li et al., 2019a). Thus, as there is evidence that GSR may remove neuronal-related activity in addition to nuisance-related fluctuations, GSR still remains a controversial pre-processing step (T. T. Liu et al., 2017; Murphy et al., 2009; Murphy and Fox, 2017).

Our results provide evidence that, in the context of static FC, GSR removes physiological fluctuations related to SLFOs and to a lesser extent head motion artifacts (**Figure 4-2**,**E-F**). Note that GSR does not account for breathing motion artifacts (**Figure 4-2G**) but rather changes in breathing patterns and deep breaths, which are related to SLFOs and possibly the head motion component at ~0.12 Hz (Power et al., 2019). Furthermore, GSR improved connectome fingerprinting accuracy (**Figure 4-3B**), which suggests that by removing nuisance fluctuations due to SLFOs and head motion, GSR enhances the individual specificity of connectivity profiles. Overall, our results suggest that the strong reduction in the effects of SLFOs and head motion achieved by GSR outweighs the possible loss of neuronal-driven fluctuations when examining FC patterns. GSR is particularly important when using ICA-based noise correction techniques such as FIX and AROMA (Pruim et al., 2015; Salimi-Khorshidi et al., 2014), since ICA components related to SLFOs frequently exhibit similar spatial patterns and frequency profile to neural components and thus are classified as non-artifactual and remain in the data after denoising.

Regarding time-varying FC, GSR did not reduce the effect of nuisance processes equally well compared to static FC (**Figure 4-2**,**E-F** vs. **Figure 4-5**,**A-B**). Nonetheless, a recent study evaluating preprocessing strategies in the context of time-varying FC showed that incorporating GSR in the preprocessing improved the identification of modularity in functional networks (Lydon-Staley et al., 2019). This may indicate that GSR was able to remove nuisance processes that we did not evaluate in the current study. These processes may be related to scanner instabilities, CO_2 concentration (Power et al., 2017b; Wise et al., 2004) and finger skin vascular tone (Kassinopoulos and Mitsis, 2020; Özbay et al., 2019), which are known to be reflected on the GS.

Despite the effectiveness of GSR in reducing nuisance confounds from the data, we cannot exclude the possibility of removing some neuronal-related fluctuations. Alternatives to GSR that have been proposed to remove global artifacts include time delay analysis using "rapidtide" (Tong et al., 2019), removal of the first principal component from the fMRI data (Carbonell et al., 2011), removal of fluctuations associated to large clusters of coherent voxels (Aquino et al., 2020), and the use of temporal ICA (Glasser et al., 2018), albeit the latter is only applicable to datasets with a large number of subjects such as the HCP.

4.5.5 The effect of phase encoding direction in connectivity

Earlier studies have demonstrated that chest wall movements due to breathing perturb the B_0 field (Raj et al., 2001, 2000; Van de Moortele et al., 2002), which has consequences on EPI fMRI data. While this phenomenon is not fully understood, it seems to have two main effects that are observable along the phase encoding direction: (1) Breathing causes factitious motion of the fMRI volumes in the phase encoding direction (Raj et al., 2001, 2000). This effect has sparkled attention recently, since it has been recognised that it may have critical implications for motion correction when performing censoring (i.e. removal of motion-contaminated fMRI volumes) in multi-band (Fair et al., 2019; Power et al., 2019) and single-band (Gratton et al., 2020) data. (2) Breathing induces artifacts on voxel timeseries that depend on the location of those voxels along the phase encoding direction (Raj et al., 2001, 2000). Our results provide further evidence in support of the latter effect. Specifically, we found that depending on the phase encoding direction (LR or RL), breathing motion artifacts were more pronounced in the left or right hemisphere respectively (**Figure 4-1C**). Moreover, we observed that breathing motion increased within-hemisphere connectivity for both phase encoding scan types (**Figure 4-2C**, **Supp. Fig. 4-1C**), which implies that breathing induces artifactual fluctuations that are to a certain extent different between hemispheres. However, note that the connectome profile of breathing motion exhibited some differences between the two phase encoding directions (**Supp. Fig. 4-1C**), which explains the higher connectome fingerprinting accuracy in the breathing motion dataset when examining pairs of scans with the same phase encoding direction, compared to scans with different phase encoding direction (**Figure 4-3A**).

Our results point to a systematic effect of breathing on static FC through variations in the B_0 magnetic field. Importantly, this systematic bias is contingent on the phase encoding direction, which seems to indicate that factitious rather than real motion is the predominant source of respiration-related motion artifacts in fMRI, as has been previously suggested (Brosch et al., 2002; Raj et al., 2001). Even though common preprocessing pipelines greatly reduce these effects, they do not eliminate them **Figure 4-2G**). Thus, studies that consider datasets with different phase encodings, should be aware of the effect

of phase encoding on FC, especially if data from different groups have been acquired with different phase encodings.

4.5.6 Individual discriminability

Test-retest reliability is important for establishing the stability of inter-individual variation in fMRI FC across time. However, apart from neural processes, nuisance processes can also have an impact on test-retest reliability, given the subject-specific nature of physiological processes (Batchvarov et al., 2002; Golestani et al., 2015; Malik et al., 2008; Pinna et al., 2007; Pitzalis et al., 1996; Power et al., 2020; Reland et al., 2005) and head motion (van Dijk et al., 2012; Zeng et al., 2014). This leads to the concerning notion that nuisance processes may be artifactually driving the reports of high reliability in FC measures. For instance, it has been reported that the median of intraclass correlation values across functional connections, which is a metric of test-retest reliability, is reduced when a relatively aggressive pipeline is used (Birn et al., 2014; Parkes et al., 2018). Furthermore, motion can classify subjects at above-chance levels (Horien et al., 2019), and breathing motion is more prominent in older individuals and those with a higher body mass index (Gratton et al., 2020). In the present study, we examined the potential effect of nuisance processes on subject discriminability using connectome fingerprinting.

4.5.6.1 Whole-brain identification

To assess the individual discriminability of nuisance processes, we performed connectome fingerprinting analysis using the generated nuisance datasets. All nuisance processes exhibited identification accuracy above chance level (**Figure 4-3A**). Pairs of scans with the same phase encoding yielded higher identification accuracy than pairs of scans with different phase encoding (**Figure 4-3A**). This effect is particularly evident for breathing motion, and to a lesser extent cardiac pulsatility and head motion. This observation suggests that not only these confounds exert a distinctive artifactual spatial pattern that is dependent on the phase encoding direction, which can be also observed upon careful examination of **Figure 4-1B-D**, but also that this artifactual pattern is to a certain degree subject-specific. On the other hand, the subject discriminability of SLFOs is not modulated by phase encoding (**Figure 4-3A**). Given the nature of SLFOs (i.e. they affect the BOLD

signal through changes in CBF), the high subject discriminability of SLFOs suggests a certain degree of idiosyncrasy that is possibly related to the vascular architecture of an individual. Overall, our results suggest that there is some degree of subject discriminability in nuisance processes.

Identification accuracies of "neural" datasets were very high for all preprocessing strategies (**Figure 4-3B**), in line with previous studies (Finn et al., 2015; Horien et al., 2019). WM denoising, which was found to be the most effective strategy for reducing confounds due to head motion and physiological fluctuations (**Figure 4-2**,**E-H**), yielded also the highest accuracy in connectome fingerprinting (**Figure 4-3B**), suggesting that the high subject discriminability observed in the HCP data is not due to the presence of confounds. Interestingly, the increased accuracy observed in the nuisance datasets for scans with the same phase encoding (**Figure 4-3A**) was also observed in the case of the raw data (**Figure 4-3B**). In contrast, for the rest of the pipelines the difference in accuracy between pairs of scans from different days with the same or different phase encoding direction vanishes (**Figure 4-3B**). This is likely because of the reduction of nuisance effects, mainly breathing motion artifacts. Note also that for both mild and aggressive pipelines, pairs of scans from the same day exhibited higher accuracies compared to pairs of scans from different days, which cannot be attributed to potential residuals of nuisance fluctuations (**Figure 4-3A**). Possible explanations for this finding are that the functional connectome of a subject reflects some aspects of their vigilance levels (Tagliazucchi and Laufs, 2014; Thompson et al., 2013a; Wang et al., 2016), mind-wandering (Gonzalez-Castillo et al., 2019; Gorgolewski et al., 2014; Kucyi, 2018; Kucyi and Davis, 2014), or the effect of time of day (Hodkinson et al., 2014; Jiang et al., 2016; Orban et al., 2020; Shannon et al., 2013), which can differ across sessions. Overall, the high connectome-based identification accuracies reported in the literature do not appear to be driven by nuisance confounds, suggesting a neural origin underpinning the inter-individual differences in connectivity. Nonetheless, it is worth pointing out that subject variability in the magnitude of functional connections has been shown to arise as a result of spatial topographical variability in the location of functional regions across individuals (Bijsterbosch et al., 2018), which could also explain the high subject discriminability observed in fMRI-based connectomes.

4.5.6.2 Network-based identification

We observed that edges within association cortices (e.g. parts of the frontoparietal, default mode, and cinguloopercular systems) exhibited the highest subject specificity (**Figure 4-4B**), consistent with previous studies (Finn et al., 2015; Gratton et al., 2018; Horien et al., 2019; Mueller et al., 2013; Seitzman et al., 2019; Vanderwal et al., 2017). The fact that association cortices are the most evolutionarily recent (Zilles et al., 1988) and are thought to be involved in higher-level functions (Cole et al., 2014, 2013; Dosenbach et al., 2007; Gratton et al., 2017; Raichle, 2015) has been posited as a possible reason for the high identification accuracy yielded by these networks. On the other hand, it has also been speculated that medial frontal and frontoparietal networks exhibit the highest identification accuracy as a result of being less prone to distortions from susceptibility artifacts (Horien et al., 2019; Noble et al., 2017). If the latter was the case, we would expect to see decreased accuracy for these networks when probing the nuisance datasets. However, we did not observe such a tendency for any of the nuisance processes evaluated (**Figure 4-4A**), and preprocessing strategies that successfully removed nuisance processes yielded enhanced subject discriminability of control networks and the DMN (**Figure 4-4C**). These results seem to indicate that the basis of the high identification rates for association cortices is of neural origin, and thus that resting-state fMRI-based connectome fingerprinting can capture idiosyncratic aspects of cognition reflected on the resting-state functional characteristics of the association cortex.

4.6 CONCLUSIONS

The current study introduces a novel framework for assessing the effects of the main fMRI confounds on static and time-varying FC. Our results suggest that head motion and systemic BOLD fluctuations associated to changes in heart rate and breathing patterns cause systematic biases in static FC and result in recurrent patterns in time-varying FC. Data-driven techniques based on decomposing the data into principal or independent components (PCA, ICA), combined with GSR, lead to the strongest reduction of the aforementioned effects. Importantly, these preprocessing strategies also improve connectome-based subject identification, indicating that the high subject discriminability reported in the literature is not attributable to nuisance processes.

4.7 Materials and Methods

4.7.1 Human Connectome Project (HCP) dataset

The resting-state fMRI data analysed in this study are from the S1200 release of the 3T HCP dataset (Smith et al., 2013; Van Essen et al., 2013), which consists of young, healthy twins and siblings (age range: 22-36 years). The HCP dataset includes, among others, resting-state data acquired on two different days, during which subjects were instructed to keep their eyes open and fixated on a cross-hair. Each day included two consecutive 15-min resting-state runs, acquired with left-to-right (LR) and right-to-left (RL) phase encoding direction. During each fMRI run, 1200 frames were acquired using a gradient-echo echo-planar imaging (EPI) sequence with a multiband factor of 8, spatial resolution of 2 mm isotropic voxels, and a TR of 0.72 s. Further details of the data acquisition parameters can be found in previous publications (Smith et al., 2013; Van Essen et al., 2012). Concurrently with fMRI images, cardiac and respiratory signals were measured using a standard Siemens pulse oximeter placed on the fingertip and a breathing belt placed around the chest, with a 400 Hz sampling rate.

We only considered subjects who had available data from all 4 runs, and excluded subjects based on the quality of the physiological recordings (see section 4.7.2.1 below for details). Pulse oximeter and respiratory belt signals from ~1000 subjects were first visually inspected to determine their quality, since their traces are often not of sufficient quality for reliable peak detection (Power, 2019). The selection process resulted in a final dataset with 392 subjects (ID numbers provided in Supp. Material).

4.7.2 Preprocessing

4.7.2.1 Preprocessing of physiological recordings

After selecting subjects with good quality traces, the pulse wave was processed to automatically detect beat-to-beat intervals (RR), and the heart rate signal was further computed as the inverse of the time differences between pairs of adjacent peaks and converted to units of beats-per-minute (bpm). Heart rate traces were visually checked to

ensure that outliers and abnormalities were not present. An outlier replacement filter was used to eliminate spurious changes in heart rate when these changes were found to be due to sporadic noisy cardiac measurements (for more details see Supp. Figs. 1 and 2 from (Kassinopoulos and Mitsis, 2019b)). We also excluded subjects with a heart rate of exactly 48 bpm and lack of heartbeat interval variability, as they have been pointed out as outliers in recent studies (Orban et al., 2020; Valenza et al., 2019). The signal from the breathing belt was detrended linearly, visually inspected and corrected for outliers using a replacement filter. Subsequently, it was low-pass filtered at 5 Hz and *Z*-scored. The respiratory flow, proposed in (Kassinopoulos and Mitsis, 2019b) as a robust measure of the absolute flow of inhalation and exhalation of a subject at each time point, was subsequently extracted by applying further smoothing on the breathing signal (moving average filter of 1.5 sec window) and, subsequently, computing the square of the derivative of the smoothed breathing signal. Finally, heart rate and respiratory flow time-series were re-sampled at 10 Hz.

An example code (Preprocess_Phys.m) showing the detailed specifications of the algorithms used during the preprocessing of the physiological signals is available on github.com/mkassinopoulos/PRF_estimation/.

4.7.2.2 Preprocessing of fMRI data: assessing the impact of denoising strategies

From the HCP database we downloaded the minimally preprocessed data described in (Glasser et al., 2013) and the FIX-denoised data, both in volume and surface space. Briefly, the minimal preprocessing pipeline included removal of spatial distortion, motion correction via volume re-alignment, registration to the structural image, bias-field correction, 4D image intensity normalization by a global mean, brain masking, and non-linear registration to MNI space. Further steps to obtain surface data were volume to surface projection, multimodal inter-subject alignment of the cortical surface data (Robinson et al., 2014), and 2 mm (FWHM) surface-constrained smoothing. Additional steps following minimal preprocessing to obtain the FIX-denoised data were de-trending using a mild high-pass filter (2000 s), head motion correction via 24 parameter regression, and denoising via spatial ICA followed by an automated component classifier (FMRIB's ICA-based X-noiseifier, FIX) (Griffanti et al., 2014; Salimi-Khorshidi et al., 2014). Minimal spatial

smoothing (FWHM = 4 mm) was applied to the downloaded minimally preprocessed and FIX-denoised volumetric data. Both minimally preprocessed and FIX-denoised data were parcellated employing the Gordon atlas across 333 regions of interest (ROIs) (Gordon et al., 2016) and the Seitzman atlas across 300 ROIs (Seitzman et al., 2020), using the surface and volume space data, respectively. ROIs that did not belong to a brain network were disregarded, hence a total of 286 ROIs (Gordon atlas) and 285 ROIs (Seitzman atlas) were retained for further analyses. The main differences between these two brain parcellations, apart from being computed on the surface and volume space respectively, are that the ROIs in the Gordon atlas do not have the same size, whereas in the Seitzman atlas the ROIs are all spheres of 8 mm diameter, and that the Gordon atlas only includes cortical regions, whereas the Seitzman atlas includes cortical and subcortical regions. The results from the Gordon atlas are presented in the main manuscript whereas the results from the Seitzman atlas can be found in the Supplementary Material (**Supp. Fig. 4-5**, **Supp. Fig. 4-6**, **Supp. Fig. 4-7**). Further, the parcellated data were high-pass filtered at 0.01 Hz.

In addition to the FIX-denoising strategy, several other data-driven preprocessing techniques were evaluated to assess the extent to which they were able to remove physiological and motion-driven confounds (**Table 4-1**). We chose pipelines that had been used in the landmark FC studies of (Finn et al., 2015) and (Laumann et al., 2017). These were denoted as "mild" pipelines, since they regress out considerably fewer components compared to FIX. Further, we also included two more aggressive pipelines that were found to outperform previously proposed techniques in terms of network identifiability (Kassinopoulos and Mitsis, 2019a). Nuisance regression was performed after the minimally preprocessed data had been parcellated to reduce computational time. All preprocessing strategies were evaluated with and without global signal regression (GSR), since the latter is still somewhat controversial (T. T. Liu et al., 2017; Murphy et al., 2009; Murphy and Fox, 2017). To facilitate the comparison between preprocessing strategies, the minimally preprocessed data were also evaluated, yielding in total 12 preprocessing strategies. Given that the minimal preprocessing pipeline consists of only the initial steps for fMRI denoising, for simplicity in the results we refer to these data as raw data. The regressors included in each preprocessing strategy can be found in **Table 4-1**. Note that for the pipeline from

(Laumann et al., 2017) the derivative of the global signal was also regressed out. The global signal for the surface and volumetric data was computed as the average fMRI timeseries across vertices and the whole brain respectively.

Table 4-1. Preprocessing strategies examined. All strategies were evaluated with and without global signal regression (GSR).

Preprocessing strategy	Acronym	Regressors included
Minimally preprocessed HCP data	Minprep	-
FIX-denoised HCP data	FIX	-
Pipeline used in Finn et al. (2015), *Nature Neuroscience*	MildA	Mean time-series of the white matter and CSF voxels (2); realignment parameters and their first derivatives (12)
Pipeline used in Laumann et al. (2017), *Cerebral Cortex*	MildB	Mean time-series of the white matter and CSF voxels and their derivatives (4); realignment parameters and their first derivatives, quadratic terms, and squares of derivatives (24)
Pipeline proposed by Kassinopoulos & Mitsis (2019b), *bioRxiv*	WM_{50}	50 PCA components from white matter voxels
	WM_{200}	200 PCA components from white matter voxels

4.7.3 Nuisance processes evaluated

The following four nuisance processes were considered (**Table 4-2**):

a. **Systemic low frequency oscillations (SLFOs):** SLFOs refer to non-neuronal global BOLD fluctuations. Major sources of SLFOs are spontaneous fluctuations in the rate or depth of breathing (Birn et al., 2006) and fluctuations in heart rate (Chang et al., 2009; Shmueli et al., 2007). The former mainly exert their effects via changing the concentration of arterial CO_2, which is a potent vasodilator, altering CBF and thus the BOLD fMRI signal (Birn et al., 2008a, 2008b; Chang and Glover, 2009b; Prokopiou et al., 2019; Wise et al., 2004), Importantly, there is evidence that SLFOs are a more substantial source of physiological noise in BOLD fMRI compared to high frequency cardiac pulsatility and breathing motion artifacts (Tong et al., 2019; Tong and Frederick, 2014). In this study, SLFOs were modelled following a framework proposed in our previous work (Kassinopoulos and Mitsis, 2019a; scripts available on github.com/mkassinopoulos/PRF_estimation/). Briefly, the extracted heart rate and

respiratory flow signals were fed into an algorithm that estimated scan-specific physiological response functions (PRFs). This algorithm estimates PRF curves that maximize the correlation between their convolution with heart rate and respiratory flow and the global signal of the same scan, while ensuring that the shapes of the PRF curves are physiologically plausible. The heart rate and respiratory flow signals were subsequently convolved with their respective PRFs and added to each other, yielding time-series that reflect the total effect of SLFOs (**Supp. Fig. 4-8**). These time-series were used in the current study as the physiological regressor related to SLFOs.

b. Cardiac pulsatility: Pulsatility of blood flow in the brain can cause pronounced modulations of the BOLD signal (Noll and Schneider, 1994), which tend to be localized along the vertebrobasilar arterial system and the sigmoid transverse and superior sagittal sinuses (Dagli et al., 1999; Kassinopoulos and Mitsis, 2019b). We modelled fluctuations induced by cardiac pulsatility using 6 regressors obtained with 3rd order RETROICOR (Glover et al., 2000), based on the pulse oximeter signal of each scan.

c. Breathing Motion: Chest movements during the breathing cycle generate head motion in the form of head nodding by mechanical linkage through the neck, but also factitious motion (also known as pseudomotion) through small perturbations of the B_0 magnetic field caused by changes in abdominal volume when air enters the lungs (Power et al., 2019; Raj et al., 2001; Van de Moortele et al., 2002). We modelled breathing-induced fluctuations using 6 regressors obtained with 3rd order RETROICOR (Glover et al., 2000), based on the respiratory signal of each scan.

d. **Head motion:** Subject motion produces substantial signal disruptions in fMRI studies (Friston et al., 1996; Power et al., 2012) and is a major confound when evaluating connectivity differences between groups with dissimilar tendencies for motion (Makowski et al., 2019; Satterthwaite et al., 2012; van Dijk et al., 2012). We quantified head motion using the six realignment parameters as well as their temporal first derivatives provided by the HCP. The six physiological regressors related to breathing motion were regressed out from the realignment parameters and their derivatives, since true and factitious motion due to breathing is reflected on the realignment parameters (Fair et al., 2019).

Table 4-2. Nuisance processes examined.

	SLFOs	Cardiac pulsatility	Breathing motion	Head motion
Recordings	Pulse oximeter, breathing belt, fMRI global signal	Pulse oximeter	Breathing belt	fMRI
Signals employed	Heart rate, respiratory flow, global signal	Cardiac cycle	Breathing cycle	Realignment parameters and derivatives
Model	Kassinopoulos & Mitsis (2019a), *NeuroImage*	3rd order RETROICOR Glover et al. (2000), *NeuroImage*	3rd order RETROICOR Glover et al. (2000), *NeuroImage*	-
Number of regressors	1	6	6	12

All nuisance regressors were high-pass filtered at 0.01 Hz to ensure similar spectral content with the fMRI data and thus avoid reintroduction of nuisance-related variation (Bright et al., 2017; Hallquist et al., 2013). The regressors were then normalized to zero mean and unit variance. **Supp. Fig. 4-9** demonstrates the spectral content of each nuisance process, as well as the effect of regressing out breathing motion from the realignment parameters.

4.7.4 Isolation of nuisance fluctuations from fMRI data

We propose a framework to isolate nuisance fluctuations for each of the aforementioned processes, which reflects the physiologically-driven fluctuations and head motion artifacts observed in the fMRI data (**Figure 4-7**). A similar methodology was used in (Bright and Murphy, 2015) to investigate whether preprocessing strategies remove variance associated to resting-state networks.

Initially, the contribution of each nuisance process on the ROI time-series was quantified using a generalised linear model, formulated as:

$$y(t) = \beta_0 + \beta_{SLFOs} x_{SLFOs}(t) + \mathbf{\beta}_{CP}\mathbf{x}_{CP}(t) + \mathbf{\beta}_{BM}\mathbf{x}_{BM}(t) + \mathbf{\beta}_{HM}\mathbf{x}_{HM}(t) + \varepsilon(t) \quad (4.1)$$

$$\mathbf{\beta}_{CP} = [\beta_{CP}^1 \quad \cdots \quad \beta_{CP}^6],\ \mathbf{\beta}_{BM} = [\beta_{BM}^1 \quad \cdots \quad \beta_{BM}^6],\ \mathbf{\beta}_{HM} = [\beta_{HM}^1 \quad \cdots \quad \beta_{HM}^{12}]$$

$$\mathbf{x}_{CP}(t) = \begin{bmatrix} x_{CP}^1(t) \\ \vdots \\ x_{CP}^6(t) \end{bmatrix},\ \mathbf{x}_{BM}(t) = \begin{bmatrix} x_{BM}^1(t) \\ \vdots \\ x_{BM}^6(t) \end{bmatrix},\ \mathbf{x}_{HM}(t) = \begin{bmatrix} x_{HM}^1(t) \\ \vdots \\ x_{HM}^{12}(t) \end{bmatrix}$$

where y are ROI time-series from the minimally preprocessed data, x_{SLFOs} is the physiological regressor modeling SLFOs, $\mathbf{x}_{CP}(t)$ are the 6 physiological regressors modeling cardiac pulsatility, $\mathbf{x}_{BM}(t)$ are the 6 physiological regressors modeling breathing motion, $\mathbf{x}_{HM}(t)$ are the 12 regressors modeling head motion, $\{\beta_0, \beta_{SLFOs}, \boldsymbol{\beta}_{CP}, \boldsymbol{\beta}_{BM}, \boldsymbol{\beta}_{HM}\}$ denote the parameters to be estimated, and ε is the error (or residual). As can be seen, all four nuisance processes (25 regressors in total) were included simultaneously in the regression to model the BOLD signal fluctuations in a specific ROI.

For each nuisance process, the estimated values $\widehat{\boldsymbol{\beta}}$ were multiplied by their corresponding regressors and added together to obtain the fluctuations of the nuisance process of interest ($\hat{y}_{NPI}(t)$) within a specific ROI, and a "clean" time-series was calculated via removal of all other nuisance processes ($\hat{y}_{NPI+Neur}(t)$), as follows:

SLFOs:

$$\hat{y}_{NPI}(t) = \hat{\beta}_{SLFOs} x_{SLFOs}(t) \tag{4.2}$$

$$\hat{y}_{NPI+Neur}(t) = y(t) - \hat{\beta}_0 - \widehat{\boldsymbol{\beta}}_{CP}\mathbf{x}_{CP}(t) - \widehat{\boldsymbol{\beta}}_{BM}\mathbf{x}_{BM}(t) - \widehat{\boldsymbol{\beta}}_{HM}\mathbf{x}_{HM}(t) \tag{4.3}$$

Cardiac pulsatility:

$$\hat{y}_{NPI}(t) = \widehat{\boldsymbol{\beta}}_{CP}\mathbf{x}_{CP}(t) \tag{4.4}$$

$$\hat{y}_{NPI+Neur}(t) = y(t) - \hat{\beta}_0 - \hat{\beta}_{SLFOs} x_{SLFOs}(t) - \widehat{\boldsymbol{\beta}}_{BM}\mathbf{x}_{BM}(t) - \widehat{\boldsymbol{\beta}}_{HM}\mathbf{x}_{HM}(t) \tag{4.5}$$

Breathing motion:

$$\hat{y}_{NPI}(t) = \widehat{\boldsymbol{\beta}}_{BM}\mathbf{x}_{BM}(t) \tag{4.6}$$

$$\hat{y}_{NPI+Neur}(t) = y(t) - \hat{\beta}_0 - \hat{\beta}_{SLFOs} x_{SLFOs}(t) - \widehat{\boldsymbol{\beta}}_{CP}\mathbf{x}_{CP}(t) - \widehat{\boldsymbol{\beta}}_{HM}\mathbf{x}_{HM}(t) \tag{4.7}$$

Head motion:

$$\hat{y}_{NPI}(t) = \widehat{\boldsymbol{\beta}}_{HM}\mathbf{x}_{HM}(t) \tag{4.8}$$

$$\hat{y}_{NPI+Neur}(t) = y(t) - \hat{\beta}_0 - \hat{\beta}_{SLFOs} x_{SLFOs}(t) - \widehat{\boldsymbol{\beta}}_{CP}\mathbf{x}_{CP}(t) - \widehat{\boldsymbol{\beta}}_{BM}\mathbf{x}_{BM}(t) \tag{4.9}$$

In this manner, we generated "cleaned" ROI time-series ($\hat{y}_{NPI+Neur}(t)$) in which all considered noisy fluctuations were removed except the ones corresponding to the specific nuisance process being evaluated. The next step was to quantify the contribution of the latter to the remaining fluctuations within each ROI. To achieve this, the estimated nuisance signal was correlated to the "clean" ROI time-series:

$$r_{nuis} = corr(\hat{y}_{NPI}(t), \hat{y}_{NPI+Neur}(t)) \tag{4.10}$$

Subsequently, the estimated nuisance signal was subtracted from the "clean" ROI time-series to obtain what is typically considered the "neural" time-series. These time-series were correlated to the "clean" time-series to quantify the contribution of the "neural" variations to the total ROI signal fluctuations:

$$\hat{y}_{Neur}(t) = \hat{y}_{NPI+Neur}(t) - \hat{y}_{NPI}(t) \tag{4.11}$$

$$r_{neur} = corr(\hat{y}_{Neur}(t), \hat{y}_{NPI+Neur}(t)) \tag{4.12}$$

Afterwards, nuisance datasets for each process were created by scaling the estimated nuisance signal within each ROI with its corresponding correlation coefficient r_{nuis} and adding Gaussian random signals ($\xi(t)$) scaled with r_{neur}. This is expressed as:

$$y_{Nuis}(t) = r_{nuis}\, Z[\hat{y}_{NPI}(t)] + r_{neur}\, Z[\xi(t)] \tag{4.13}$$

where $Z[\cdot]$ denotes normalization to zero mean and unit variance.

Thus, this framework generated four synthetic nuisance datasets that contained the isolated fluctuations from each of the nuisance processes evaluated. In a sense, the ROI time-series in each nuisance dataset are equivalent to the term $\hat{y}_{NPI+Neur}(t)$, with the "neural" fluctuations replaced by random signals. These time-series were used to characterize the connectome profile of the nuisance processes without the presence of neurally-related signals, while maintaining the noise-to-signal ratio between physiological/motion-related noise and "neural" signal intact. Note that if the nuisance datasets consisted solely of artifactual fluctuations without the random signals added, this would result in an overestimation of the correlation fraction attributed to the nuisance processes that was present in the experimental fMRI data. This can be easily understood in the case of two ROI time-series that are weakly driven by SLFOs. As the contribution of this nuisance process to the aggregate ROI time-series would be small, the parameter $\hat{\beta}_{SLFOs}$ in Eq. 2 for both ROIs would be relatively small as well. However, without the addition of random signals, the correlation of the time-series $\hat{y}_{NPI}$ associated with these two ROIs would be 1.00 (or -1.00 depending on the signs of the corresponding beta parameters) as Pearson's correlation is a metric that is blind to the variance of the signals, thereby overestimating the contribution of SLFOs to the FC between those ROIs.

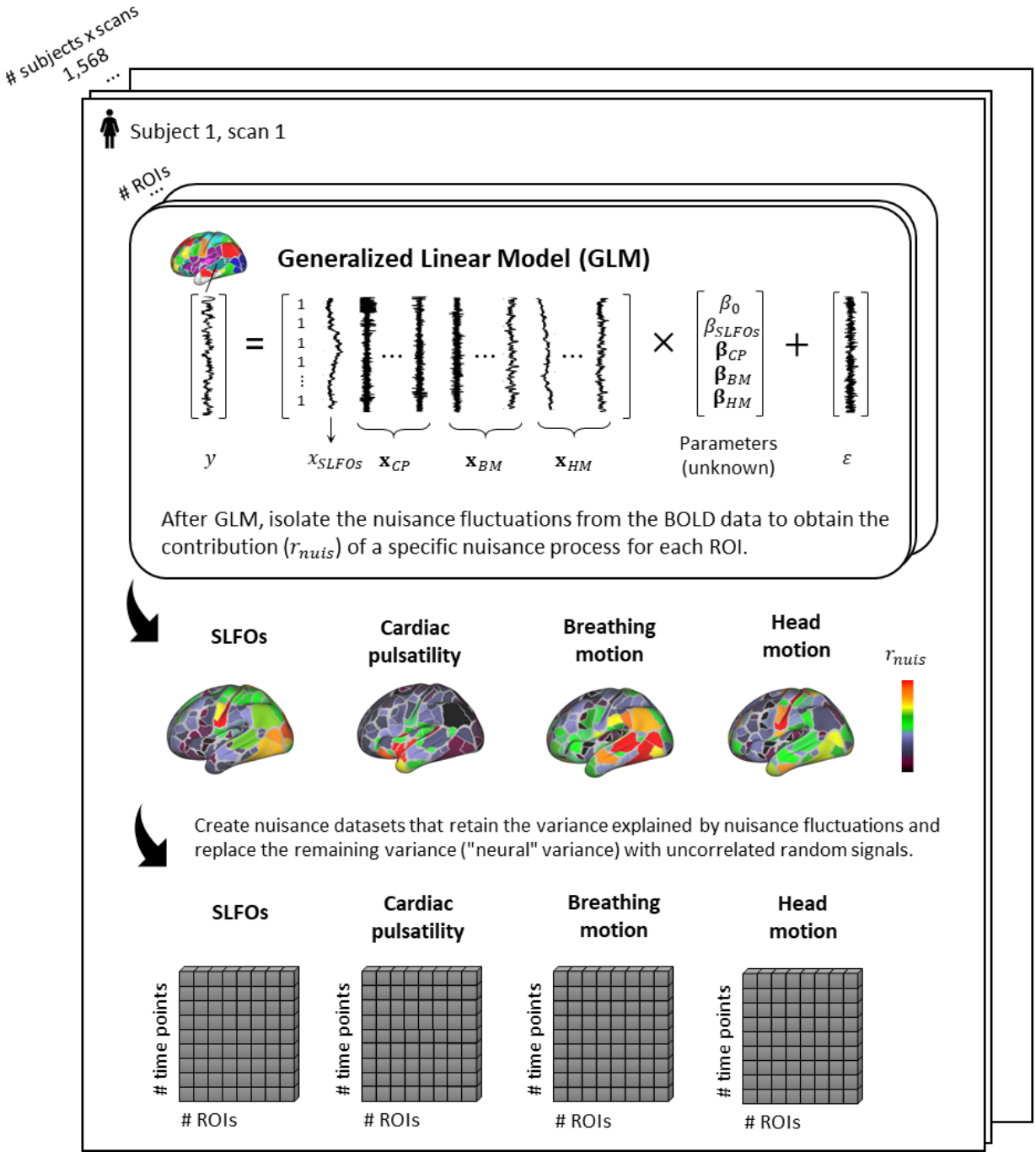

Figure 4-7. Graphical summary of the proposed framework for isolating the fluctuations for each physiological process. For each scan, the ROI time-series are modeled using the regressors related to systemic low frequency oscillations (SLFOs), cardiac pulsatility (CP), breathing motion (BM), and head motion (HM). Subsequently, the fraction of BOLD variance explained by each nuisance process is isolated and employed to generate synthetic datasets that only contain nuisance fluctuations.

4.7.5 Estimation of static and time-varying functional connectivity (FC)

Using the pre-processed fMRI data from each of the 12 pipelines (see section 4.7.2.2), henceforth called "neural" datasets, and the 4 nuisance datasets, we performed Pearson correlation analyses between brain regions over the whole scan (static FC) and within sliding windows (time-varying FC). To quantify time-varying FC, the entire scan was split up into 62 sliding windows of 43.2 sec (60 samples) duration, with 70% overlap in time. Subsequently, for each scan, we computed the functional connectivity dynamics (FCD) matrix (Hansen et al., 2015), which is a symmetric matrix in which the entries (i, j) correspond to the Pearson correlations between the upper triangular elements of the FC matrices in windows i and j. The size of the FCD matrix was $W \times W$, where W is the number of windows (62). Thus, while the static FC matrix characterizes the spatial structure of resting activity, the FCD matrix captures the temporal evolution of connectome correlations.

The analyses resulted in 32 matrices for each subject (**Figure 4-8**): 4 static FC and 4 FCD nuisance matrices (one for each physiological process considered), as well as 12 static FC and 12 FCD "neural" matrices (one for each preprocessing strategy evaluated). To quantify the influence of the nuisance processes on static FC and FCD for each preprocessing strategy, similarities between pairs of nuisance and "neural" matrices were evaluated by correlating their upper triangular values. Note that for the FCD matrices, upper triangular elements corresponding to the correlation between overlapping windows were disregarded because of high correlation by design (see block diagonal in **Figure 4-8**). All correlation values were Fisher z transformed.

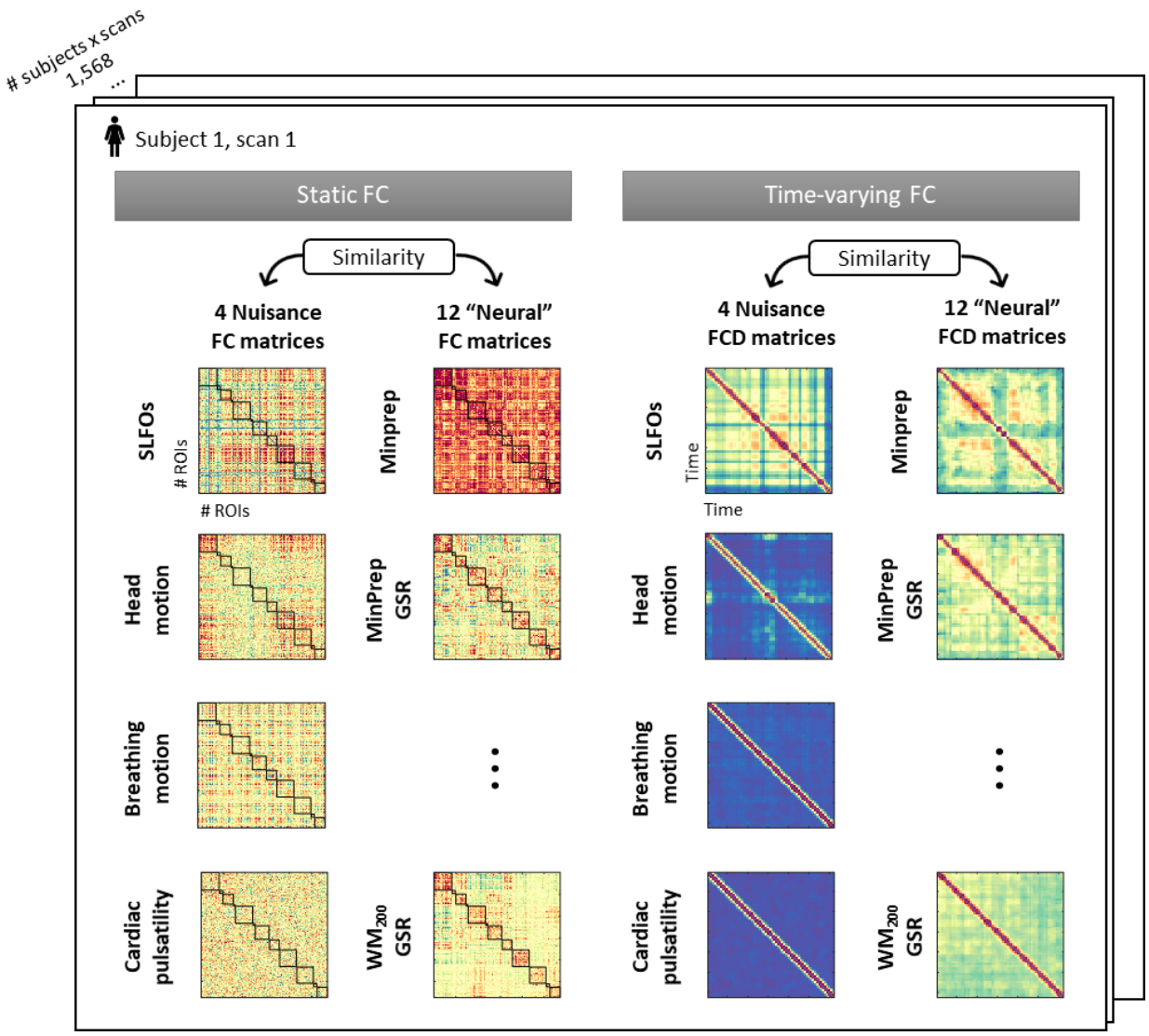

Figure 4-8. Illustration of the 32 connectivity matrices computed per scan. For both static and time-varying FC analyses, 4 nuisance connectivity matrices were computed using the generated nuisance datasets, as well as 12 "neural" connectivity matrices corresponding to the 12 pre-processing strategies evaluated (note that each of the 6 strategies listed in Table 1 was assessed with and without GSR). Static FC matrices were computed as the correlation across brain regions using the whole scan. Time-varying FC analysis constructed time-resolved connectivity matrices as the correlation between static FC matrices within sliding windows, known as functional connectivity dynamics (FCD) matrices (Hansen et al. 2015).

4.7.6 Connectome-based identification of individual subjects

We implemented a connectome-based identification of individual subjects using the static FC matrices to investigate the potential effect of "nuisance fingerprints" on the degree of subject specificity in individual FC metrics. The identification procedure, known as connectome fingerprinting, has been described in detail previously (Finn et al., 2015). Briefly, a database was first created consisting of all subjects' FC matrices from a particular resting-state scan (**Supp. Fig. 4-10B**). An FC matrix from a specific subject and different resting-state scan was then selected and denoted as the target ($Subj_x$). Pearson correlation coefficients ($r_1, \dots, r_N$) were computed between the upper triangular values of the target FC matrix and all the FC matrices in the database. If the highest correlation coefficient corresponded to a pair of FC matrices from the same subject, a successful identification was indicated ($ID_{Subj_x} = 1$); otherwise, it was marked as an incorrect identification ($ID_{Subj_x} = 0$). The identification test was repeated such that each subject serves as the target subject once, and then the ID values were averaged across subjects to obtain the identification accuracy of the database-target pair. This process was repeated until tests between all scanning sessions were performed. In total, 12 database-target combinations were computed (**Supp. Fig. 4-10A**). Identification was performed using the whole brain connectivity matrix, as well as based on edges from within and between networks. In the latter case, networks containing less than 10 ROIs were excluded from the analysis.

The connectome fingerprinting analysis was performed independently for each physiological process, as well as for each preprocessing strategy, using the generated FC matrices (**Figure 4-8**). This analysis was only performed on static FC matrices and not time-varying FC matrices because recurrent patterns of connectivity observed in the FCD matrices are not expected to occur at similar time instances between scans.

4.7.7 Statistics

To assess the significance of the results, surrogate nuisance datasets were generated via inter-subject surrogates (Lancaster *et al.*, 2018), using fMRI data recorded from one subject's scan and physiological signals recorded from a different subject's scan (in the case of the head motion dataset, volume realignment parameters were employed). This

procedure was performed for all 1,568 scans, creating a surrogate dataset for each of the four examined physiological processes with the same dimensions as the evaluated datasets. Note that when creating each surrogate dataset, only the nuisance process being examined is replaced by signals from a different subject, whereas all other nuisance regressors remain the same. The same analyses described before were repeated using these surrogate datasets, generating a chance distribution against which the results were compared. Thus, the significance of the contributions of each nuisance process to the BOLD signal fluctuations were tested against the contributions found using the surrogate data (two-sample t-test, $p < 0.05$, Bonferroni corrected), and the similarity between the nuisance and "neural" FC matrices was compared against the similarity obtained using surrogate nuisance FC matrices. Note that for visualization purposes, similarity values identified as outliers (> 3 SD) are not displayed in **Figure 4-2** and **Figure 4-5**.

To assess the significance of the fingerprinting analysis, we performed nonparametric permutation testing as in (Finn et al., 2015). Briefly, the described fingerprinting analysis was repeated for all scans and database-target combinations, but for the identification test, the subject identity in the database set was permuted. In this way, a "successful" identification was designated when the highest correlation coefficient was between the FC matrices of two different subjects. As expected, for all the nuisance and "neural" datasets, the identification accuracy estimated with nonparametric permutation testing was around 0.3%, which corresponds to the probability of selecting a specific subject from a group of 392 subjects when the subject is selected at random.

4.8 ACKNOWLEDGMENTS

This work was supported by the Natural Sciences and Engineering Research Council of Canada (Discovery Grant 34362 awarded to GDM), the Fonds de la Recherche du Quebec - Nature et Technologies (FRQNT; Team Grant PR191780-2016 awarded to GDM) and the Canada First Research Excellence Fund (awarded to McGill University for the Healthy Brains for Healthy Lives initiative). AXP and MK acknowledge funding from Québec Bio-imaging Network (QBIN). Data were provided by the Human Connectome Project, WU-Minn Consortium (Principal Investigators: David Van Essen and Kamil Ugurbil; 1U54MH091657) funded by the 16 NIH Institutes and Centers that support the NIH Blueprint for Neuroscience Research; and by the McDonnell Center for Systems Neuroscience at Washington University. We are extremely grateful to all Human Connectome Project study participants, who generously donated their time to make this resource possible.

4.9 SUPPLEMENTARY MATERIAL

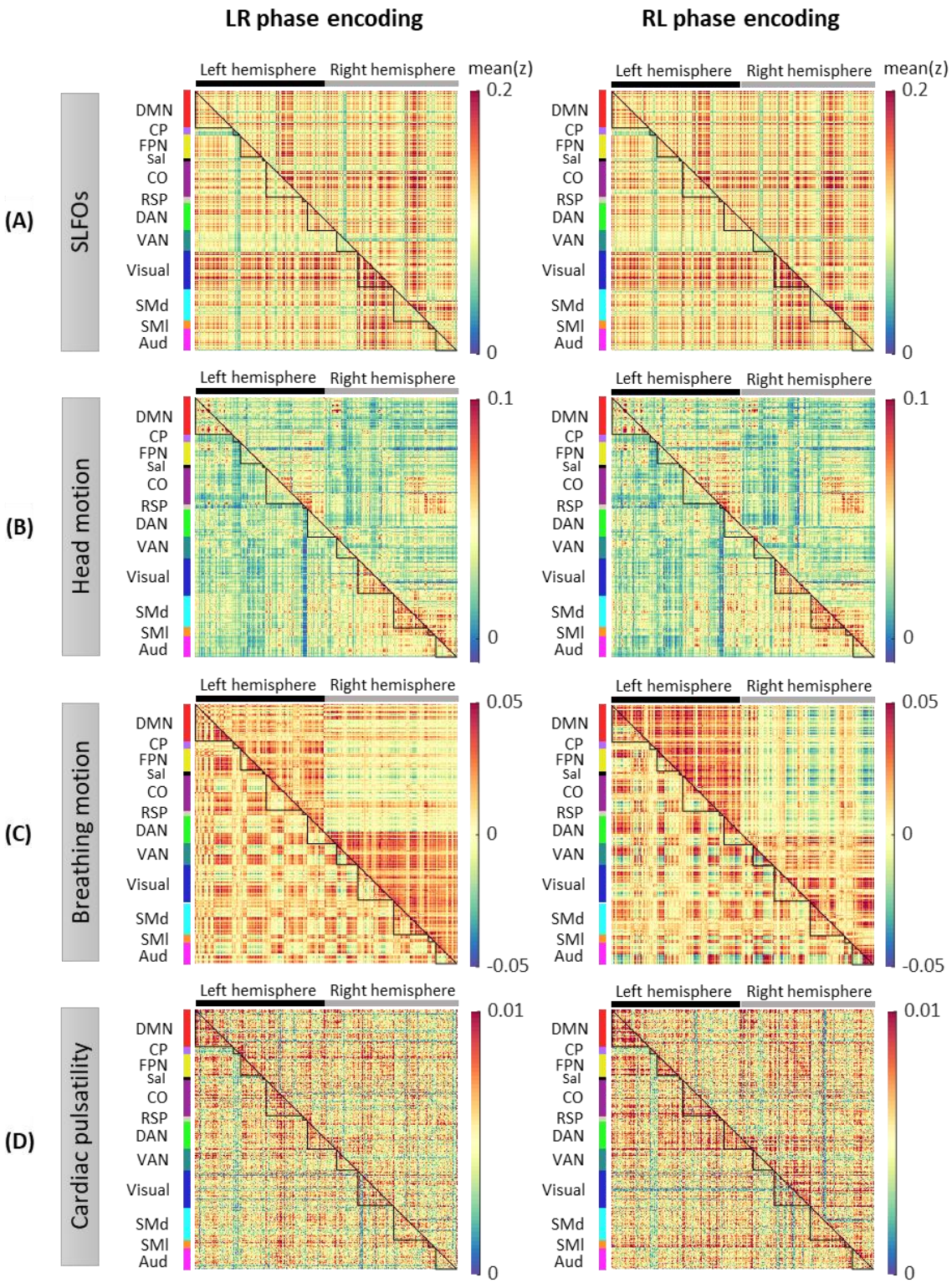

Supp. Fig. 4-1. Whole-brain connectome patterns induced by nuisance processes, separately for scans with LR and RL phase encoding. Group averaged nuisance FC matrices across 784 scans based on their LR and RL phase encoding direction for **(A)** SLFOs, **(B)** head motion, **(C)** breathing motion, and **(D)** cardiac pulsatility.

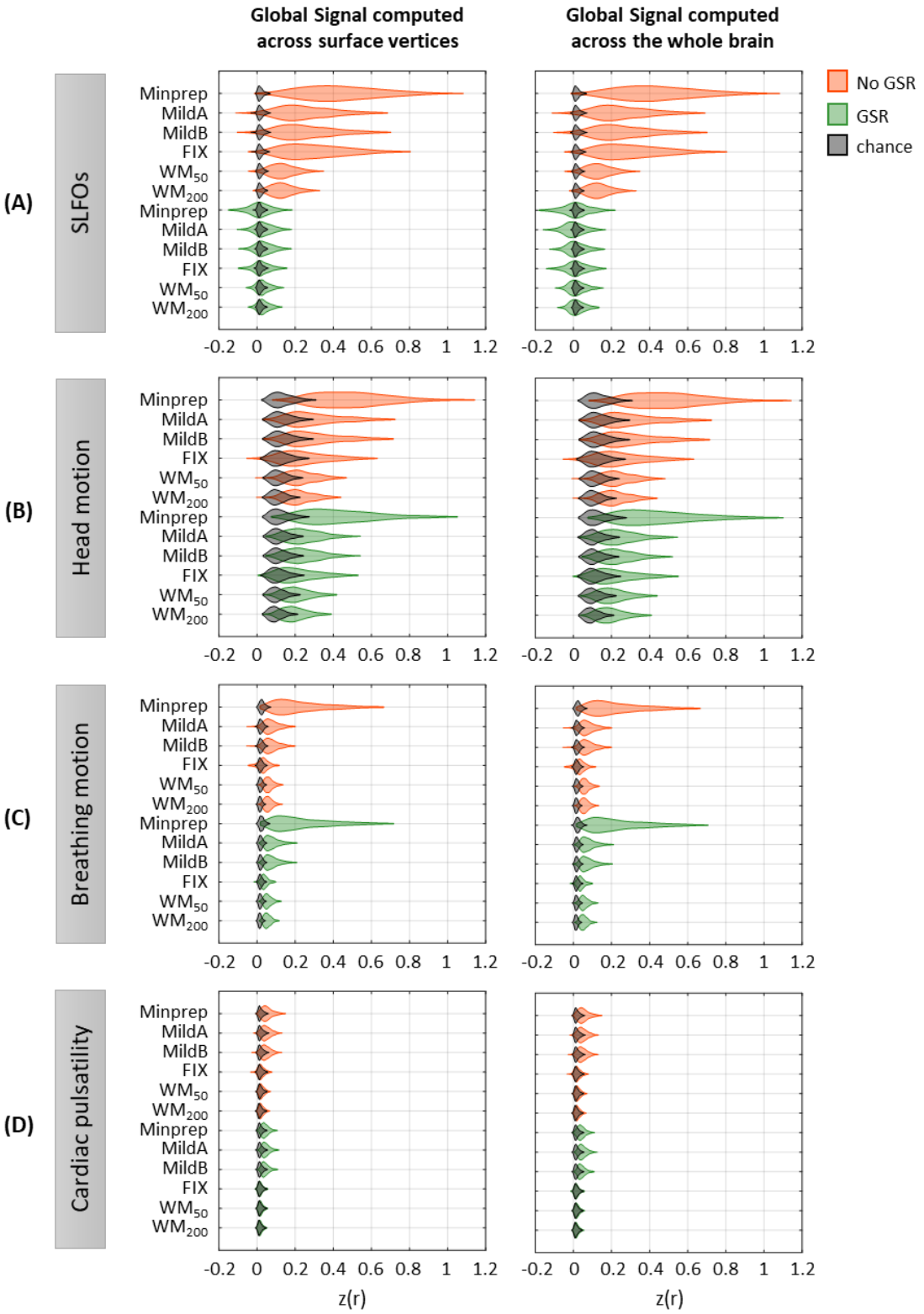

Supp. Fig. 4-2. Effectiveness of preprocessing strategies in reducing the whole-brain connectivity profiles effects of each nuisance process for two different global signal calculation methods. Distribution of Pearson correlation coefficients across all 1,568 scans between the "neural" FC matrix after each preprocessing pipeline and nuisance FC matrices associated to **(A)** SLFOs, **(B)** head motion, **(C)** breathing motion, and **(D)** cardiac pulsatility, both when the global signal was computed across vertices in surface space (left column), and when the global signal was computed across the whole brain in volumetric space (right column). Correlation values were Fisher z transformed.

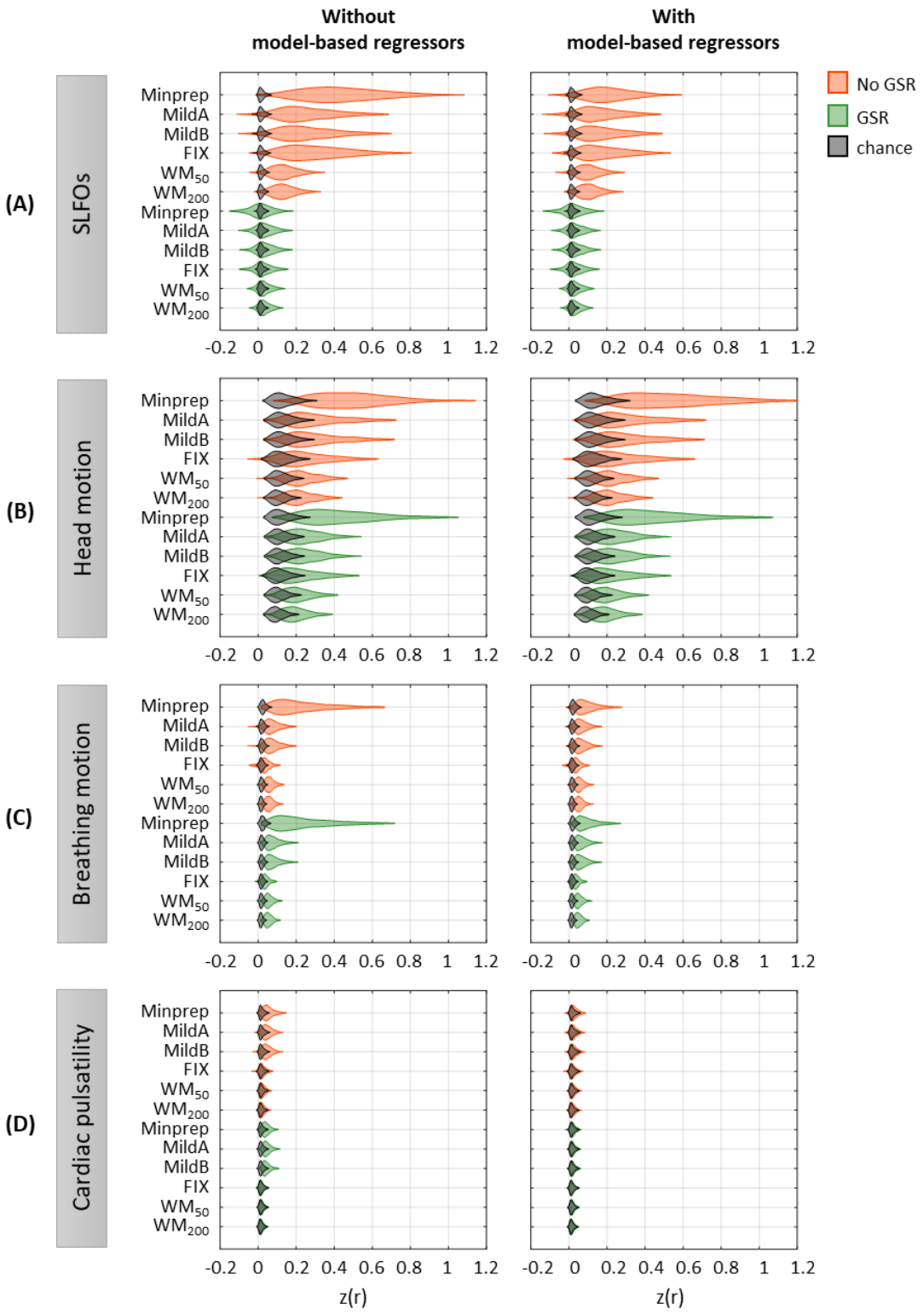

Supp. Fig. 4-3. Effectiveness of preprocessing strategies in reducing the whole-brain connectivity effect of each nuisance process, with and without including model-based regressors. Distribution of Pearson correlation coefficients across all 1,568 runs between the "neural" FC matrix after each preprocessing pipeline and nuisance FC matrices associated to **(A)** SLFOs, **(B)** head motion, **(C)** breathing motion, and **(D)** cardiac pulsatility, when physiological regressors obtained from model-based techniques were included (right column) or not (left column) as nuisance regressors in the preprocessing strategies. Correlation values were Fisher z transformed.

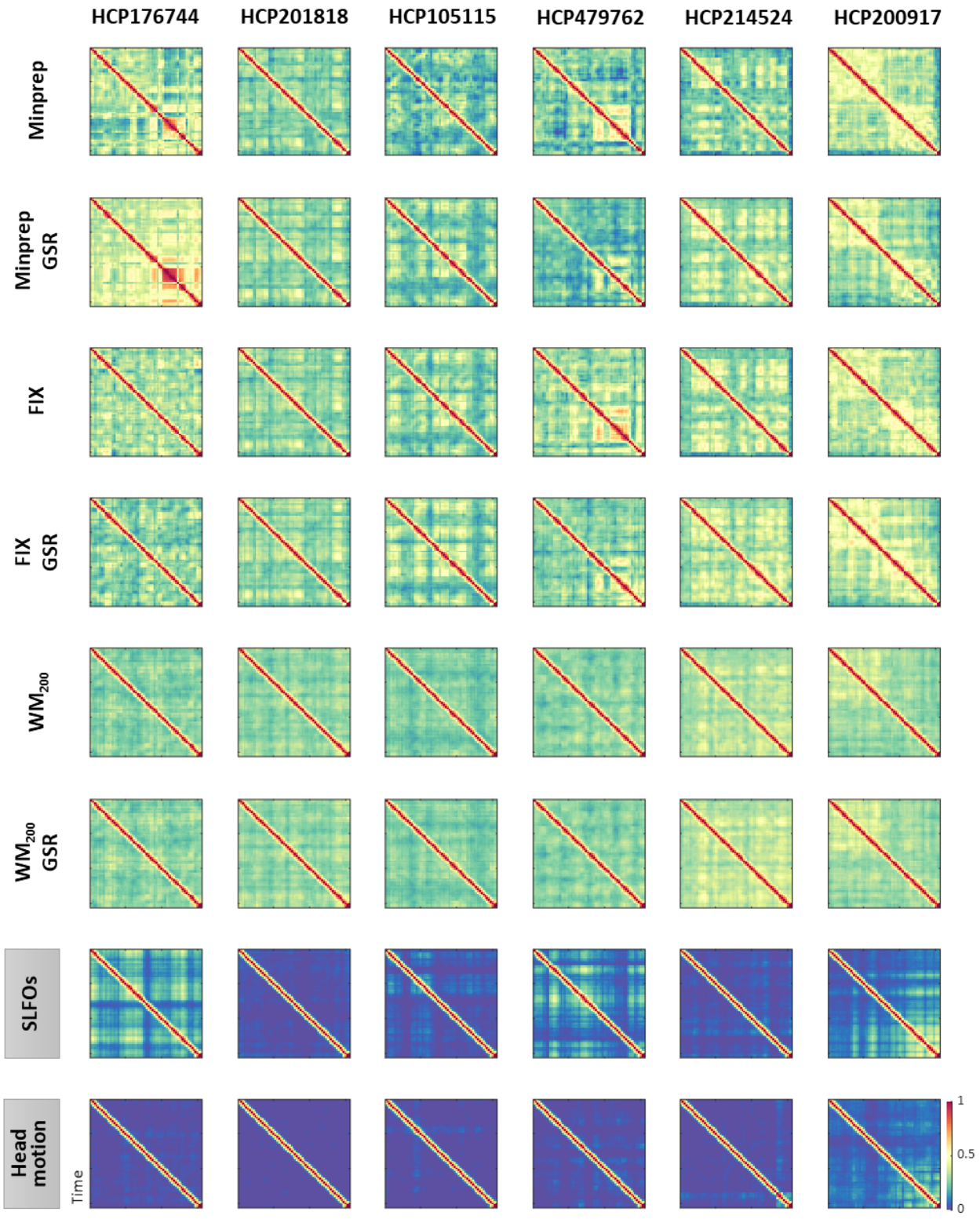

Supp. Fig. 4-4. Examples of functional connectivity dynamics (FCD) profiles. Illustrative examples of FCD matrices from specific HCP subjects for several pre-processing pipelines (rows 1-6), SLFOs and head motion (rows 7 and 8, respectively). All the examples are from the HCP scan Rest1_LR. These subjects did not exhibit a large resemblance between FCD matrices computed from the "neural" datasets and FCD matrices computed from the nuisance datasets of SLFOs and head motion. Note that the WM_{200} preprocessing strategy substantially diminished the recurrent FC patterns.

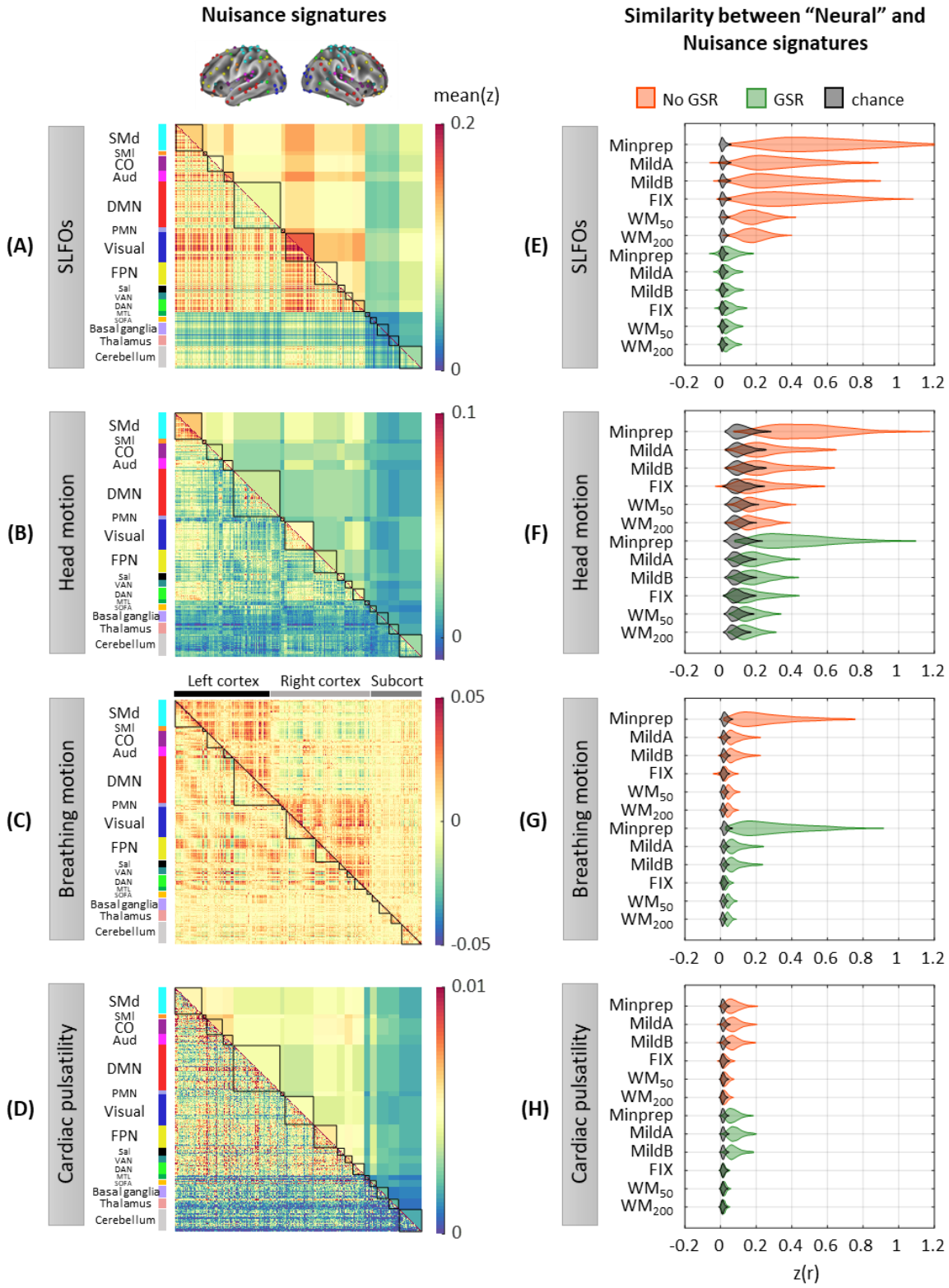

Supp. Fig. 4-5. Whole-brain connectome patterns induced by nuisance processes and effect of preprocessing strategies, using the Seitzman atlas. (A-D) Group averaged "physiological" FC across all 1,568 scans for **(A)** SLFOs, **(B)** head motion, **(C)** breathing motion, and **(D)** cardiac pulsatility. **(E-H)** Distribution of Pearson correlation coefficients across all 1,568 scans between the "neural" FC matrix after each preprocessing pipeline and nuisance FC matrices associated to **(E)** SLFOs, **(F)** head motion, **(G)** breathing motion, and **(H)** cardiac pulsatility. Correlation values were Fisher z transformed.

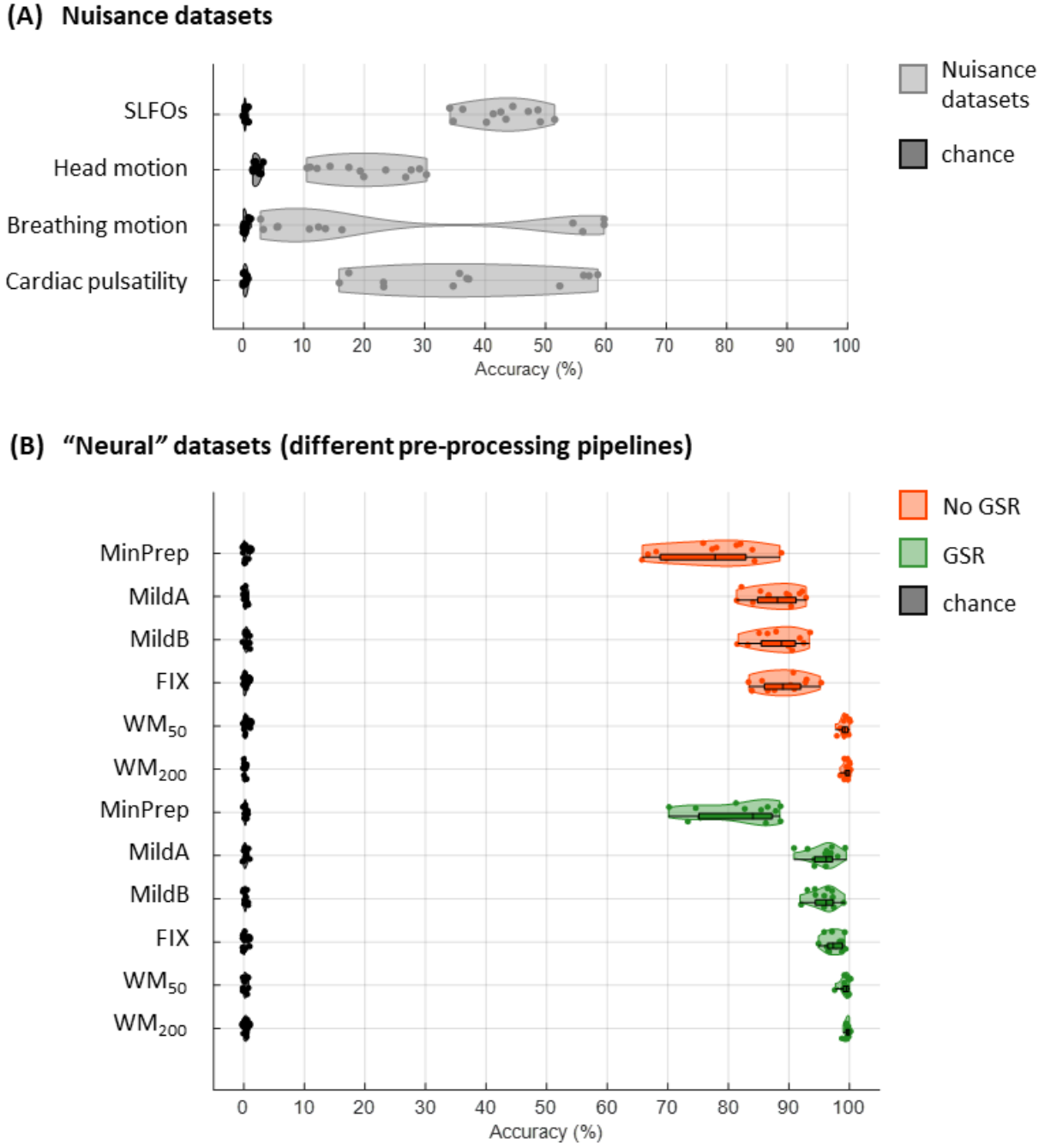

Supp. Fig. 4-6. Connectome fingerprinting results for the Seitzman atlas. (A) Fingerprinting accuracy obtained using the static FC matrices from the generated nuisance datasets where non-neural fluctuations were isolated from the BOLD data. **(B)** Fingerprinting accuracy obtained using the static FC matrices generated from each of the preprocessing strategies evaluated.

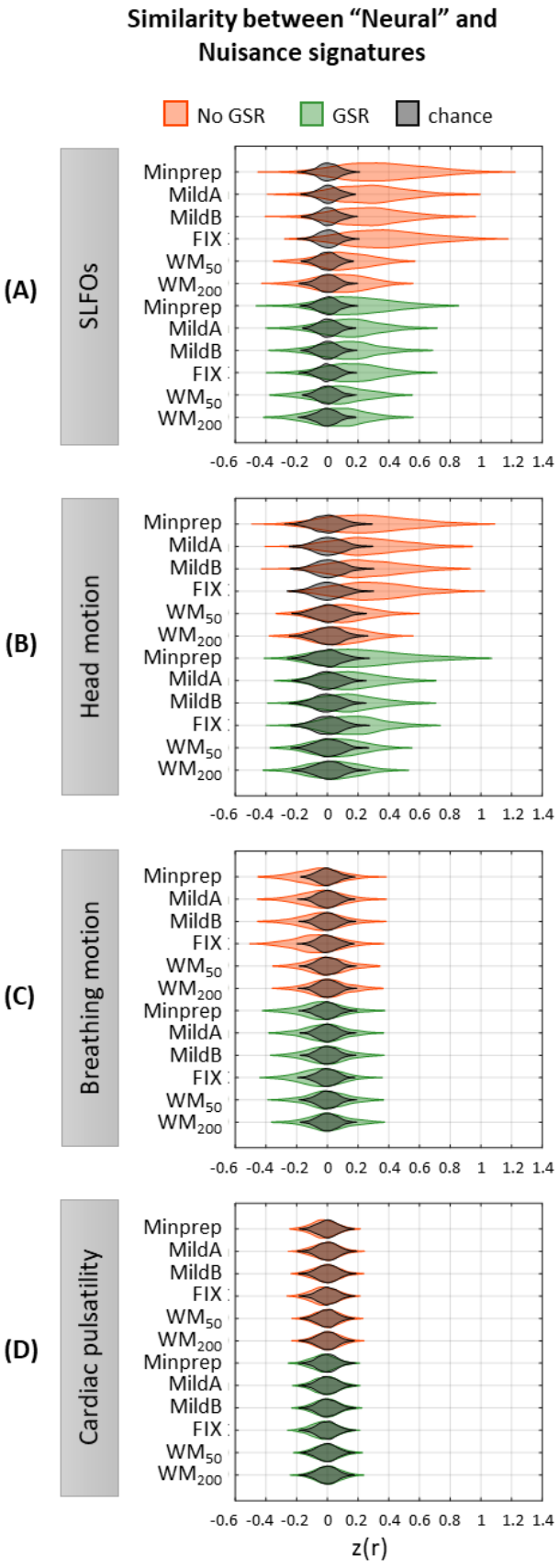

Supp. Fig. 4-7. Effectiveness of preprocessing strategies in reducing functional connectivity dynamics (FCD) profiles induced by physiological and motion processes, using the Seitzman atlas.

Distribution of Pearson correlation coefficients across all 1,568 scans between the "neural" FCD matrix after each preprocessing pipeline and nuisance FCD matrices associated to **(A)** SLFOs, **(B)** head motion, **(C)** breathing motion, and **(D)** cardiac pulsatility. Correlation values were Fisher z transformed.

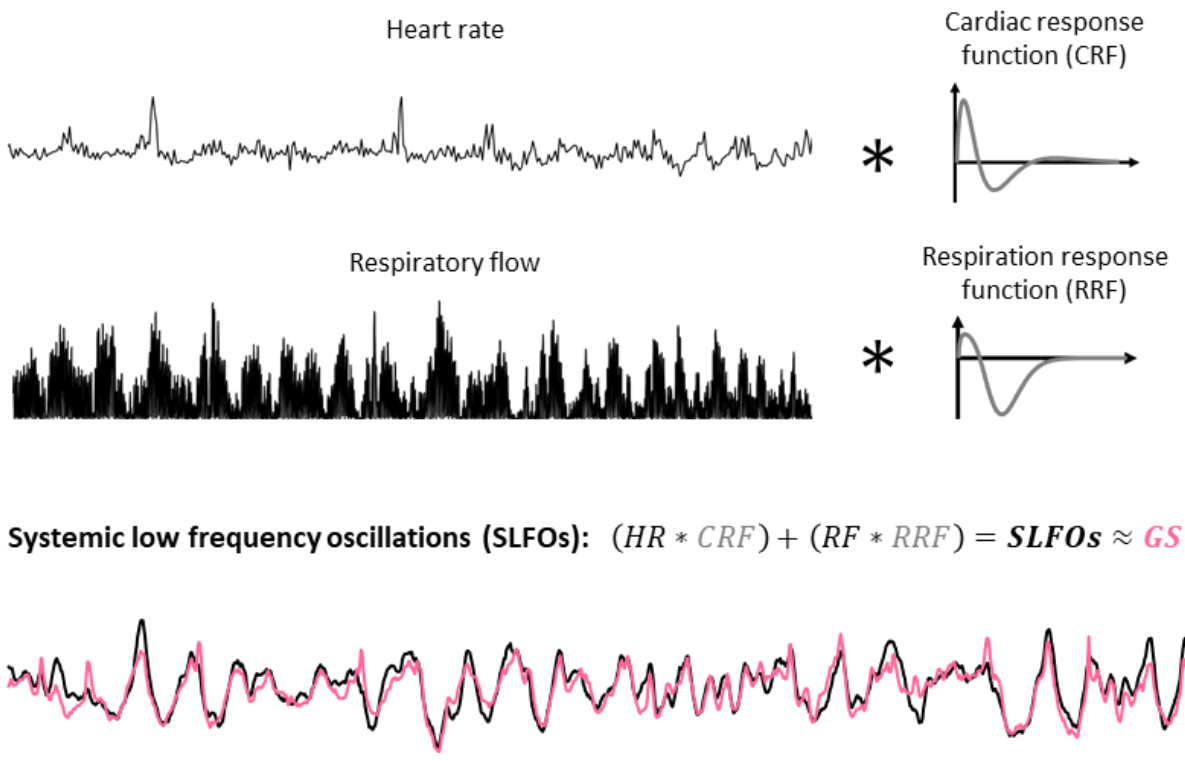

Supp. Fig. 4-8. Illustration of methodology for modeling systemic low frequency oscillations (SLFOs) using the traces of heart rate and breathing activity. The respiratory flow was defined as the square of the derivative of the breathing signal. The cardiac and respiration response functions were estimated separately for each scan, using the methodology proposed in (Kassinopoulos and Mitsis, 2019a). Heart rate and respiratory flow were convolved with the cardiac and respiration response functions, respectively, in order to obtain the fluctuations of SLFOs. As can be seen in the example, SLFOs exhibit high correlation with the global signal (GS; the average correlation is 0.65 across all scans considered in this study).

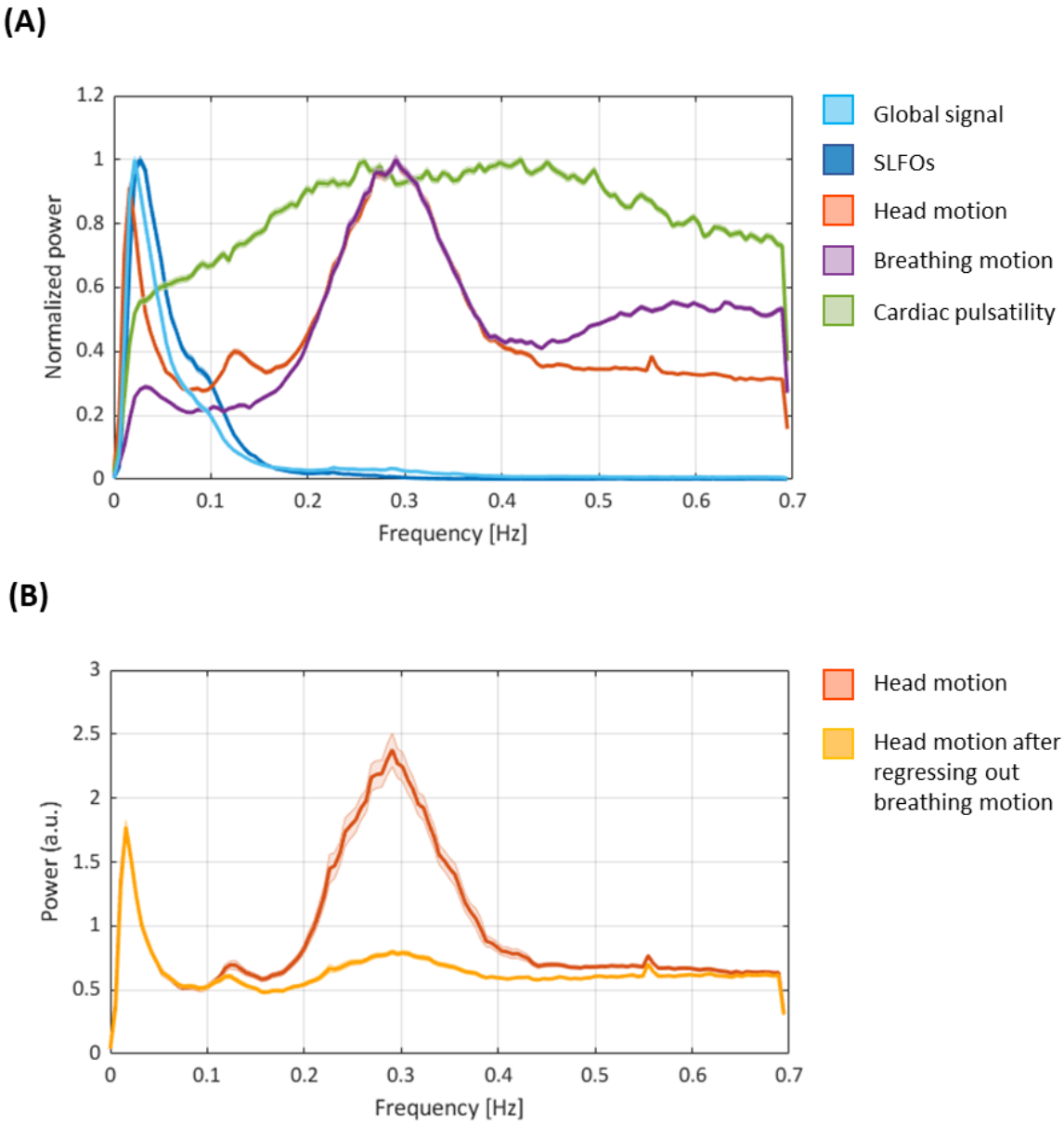

Supp. Fig. 4-9. (A) Power spectral densities of the nuisance processes evaluated in the present study (as well as the global signal for reference). SLFOs mostly exhibit low-frequency fluctuations (<0.15 Hz). Breathing motion exhibits a peak at ~0.3 Hz, consistent with the average breathing rate across subjects. Head motion exhibits the same 0.3 Hz peak, underscoring the observation that realignment parameters are contaminated by breathing. We also observe a peak in head motion at ~0.12 Hz, recently attributed to deep breaths (Power et al. 2019), and a very narrow peak at 0.55 Hz that is likely due to scanner artifacts. The fMRI data is not sampled fast enough to capture cardiac pulsatility (~1 Hz), hence the effect of cardiac activity is aliased within a range of lower frequencies. Thus, any variation in heart rate during a scan as well as across subjects is likely to spread cardiac pulsatility artifacts across different frequencies, broadening the main spectral peak. **(B) Power spectral density of head motion before and after regressing out breathing motion.** Note the substantial decrease in power around 0.3 Hz after removing the effect of breathing motion. Both figures show the mean and standard error across subjects for scan Rest1_LR (similar results were observed for all other scans).

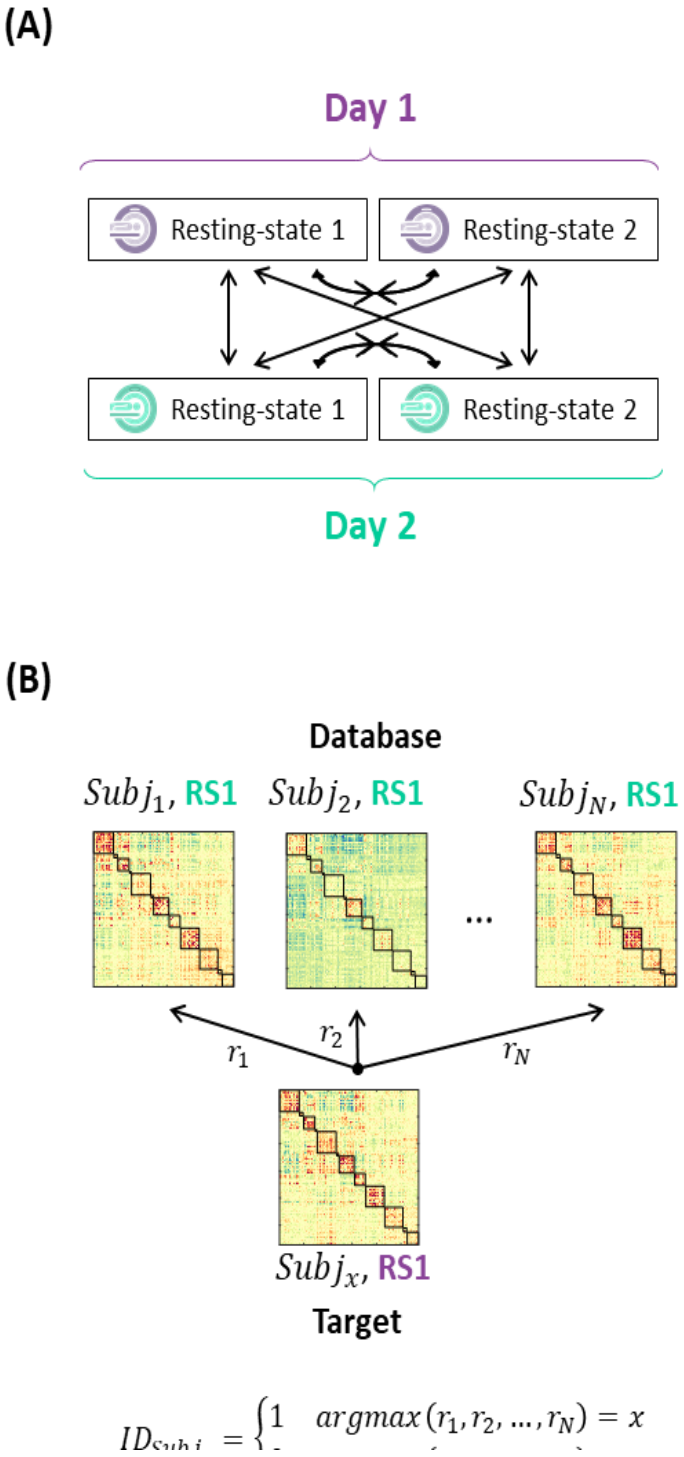

Supp. Fig. 4-10. Connectome fingerprinting. (A) Diagram of the target-database combinations between resting-state scans. **(B)** Example on how to compute the identification accuracy for a target-database pair. Figure based on Finn et al. (2015).

5

Does global signal regression alter fMRI connectivity patterns related to EEG activity?

An EEG-fMRI study in humans

The following chapter will be soon submitted in a journal as:

Xifra-Porxas, A., Kassinopoulos, M., Prokopiou, P., Boudrias, MH., Mitsis, G.D.
(in preparation). Does global signal regression alter fMRI connectivity patterns related to EEG activity? An EEG-fMRI study in humans

CRediT authorship contribution

A. Xifra-Porxas: Conceptualization, Methodology, Software, Investigation, Formal analysis, Data curation, Project administration, Visualization, Writing - original draft, Writing - review & editing. **M. Kassinopoulos:** Conceptualization, Software, Investigation, Data curation, Writing - review & editing. **P. Prokopiou:** Investigation, Data curation, Writing - review & editing. **MH. Boudrias:** Funding acquisition, Writing - review & editing. **G. D. Mitsis:** Conceptualization, Funding acquisition, Supervision, Writing - review & editing.

5.1 PREFACE

The previous chapter provided evidence that regressing out the mean time-series across all voxels in the brain from the fMRI data (i.e. GSR) seems to be the best preprocessing method to successfully remove the global fluctuations associated with heart rate and breathing patterns. However, the dataset used in the previous chapter did not include concurrent direct measurements of neural activity, thus we could not exclude the possibility that GSR is removing signal of interest as well as physiological noise. To answer this question, the manuscript in this chapter describes an investigation of the underpinnings of the global fMRI signal using simultaneous EEG-fMRI data as well as concurrent physiological recordings. Furthermore, in this chapter we use the methodology developed in chapter 4 to investigate the effects of GSR on fMRI functional connectivity patterns related to physiological and EEG activity. The results of this chapter provide further evidence that GSR successfully reduces physiological noise and suggest that the potential loss of signal of interest through GSR may be negligible for functional connectivity fMRI studies.

5.2 ABSTRACT

Functional brain connectivity has generated wide interest as a potential noninvasive biomarker, with resting-state fMRI having been used in several connectivity fingerprinting studies. In this context, one of the most controversial preprocessing strategies is global signal regression (GSR). While it has been shown that a considerable fraction of global signal variations is associated to physiological and motion sources, GSR may also result in removing global neural activity. Here, we examine the fundamental sources of resting global signal fluctuations using simultaneous EEG-fMRI data combined with cardiac and breathing recordings. We find that systemic physiological fluctuations account for a significantly larger fraction of global signal variance compared to electrophysiological fluctuations. Furthermore, we show that GSR reduces the artifactual connectivity due to heart rate and breathing fluctuations but preserves connectivity patterns associated with electrophysiological activity within the alpha and beta frequency ranges. Overall, these results provide evidence in favor of performing GSR in resting-state connectivity studies.

5.3 INTRODUCTION

The study of the brain at rest has become a powerful tool towards revealing intrinsic characteristics of the functional brain organization. Even in the absence of overt behaviour, brain activity fluctuates in an organized fashion in the form of large-scale brain networks that resemble those observed during behavioral tasks (Biswal et al., 1995; Fox and Raichle, 2007; Gratton et al., 2018; S. M. Smith et al., 2009). Functional magnetic resonance imaging (fMRI) is widely used to study resting-state activity of temporally correlated and spatially distributed brain regions. However, only a fraction of the recorded fMRI signal is of neural origin, with the remainder of the variance being thermal noise and artifacts. Furthermore, even this neurally driven fraction is not a direct measurement of neural activity, but an indirect measurement of the latter determined by neurovascular coupling mechanisms (Iadecola, 2017; Logothetis et al., 2001; Nikos K. Logothetis, 2008). Specifically, fMRI relies on changes in local cerebral blood flow (CBF) to detect neural activity, which suggests an important caveat as there are other processes that can also induce fluctuations in CBF. For instance, changes in heart rate and breathing patterns (Birn et al., 2006; Shmueli et al., 2007), variations in CO_2 (Prokopiou et al., 2019; Wise et al., 2004), and arterial blood pressure (Whittaker et al., 2019) can induce significant fluctuations in CBF as well. The complexity of the fMRI signal renders the removal of non-neural components a crucial and challenging task, which is particularly exacerbated in resting-state studies where there is no a priori assumption for the temporal pattern of the underlying neural activity. Although there have been many advances on resting-state fMRI denoising (Caballero-Gaudes and Reynolds, 2017; Ciric et al., 2018), there is still no gold standard for resting-state fMRI preprocessing.

Global signal regression (GSR), which typically involves regressing out the average fMRI signal across the whole brain (i.e. global signal) from every voxel, has been proposed as a technique to remove the often present fMRI global fluctuations (Aguirre et al., 1998; Fox et al., 2009; Macey et al., 2004). Yet, as the processes underpinning the global signal are still poorly understood, GSR has turned out to be one of the most contentious preprocessing steps in fMRI denoising (T. T. Liu et al., 2017; Murphy and Fox, 2017; Power et al., 2017a). The rationale behind GSR is that the global signal mostly encompasses non-neuronal

processes arising from physiological sources, head motion and scanner artifacts (Power et al., 2017b), and is therefore a highly effective data-driven approach to remove these global fluctuations that can also lead to artifactual functional connectivity (Burgess et al., 2016b; Ciric et al., 2017; Parkes et al., 2018; Xifra-Porxas et al., 2020). Indeed, GSR has been shown to increase the similarity of functional connectivity estimates across modalities (Keller et al., 2013). In addition, recent studies found that GSR improves the identifiability of well-established resting-state networks (Kassinopoulos and Mitsis, 2019a), as well as the association between resting-state functional connectivity and behavioral measures (Li et al., 2019b), which suggests that GSR can lead to fMRI data quality improvement.

However, there is converging evidence from simultaneous electrophysiological-fMRI studies that neural activity is also strongly linked to the global signal. Early investigations, albeit not directly examining the global signal, showed that fluctuations in local field potentials exhibited fairly widespread correlations with fMRI activity over the macaque brain (Scholvinck et al., 2010). More recently, fluctuations of the global signal have been linked to electrophysiological indices of arousal (C. W. Wong et al., 2016; Wong et al., 2013) and glucose metabolism (Thompson et al., 2016). Furthermore, global resting-state fluctuations were found to at least partially stem from the basal forebrain (Liu et al., 2018; Turchi et al., 2018). Recently, Gutierrez-Barragan and colleagues showed that brain states occur at specific phases of global signal fluctuations in the mouse brain (Gutierrez-Barragan et al., 2019). In addition, individual variation in global signal topography has been associated with behavioral measures (Li et al., 2019a). All these reports suggest that GSR may potentially remove neuronal-related fluctuations that may be of interest in functional connectivity studies.

Until now, most studies investigating the processes underpinning the global signal either probed its physiological or neural origin. The neurally-related fraction of the global signal seems to be associated to fluctuations in arousal and vigilance, likely regulated by the autonomic nervous system (Oken et al., 2006; Olbrich et al., 2011). However, these apparent neural fluctuations could be also associated with systemic changes such as heart rate and breathing variations, which would in turn be reflected on the fMRI signal. Hence, there is potentially a closed loop path through which neural autonomic activity could indirectly be

contributing to the global signal through changes in physiological signals. Therefore, both physiological and neural processes must be simultaneously taken into consideration to understand whether they explain similar variations of the global signal or they are two separate processes contributing to the global signal.

While GSR is a more prevalent technique in resting-state studies, it was originally developed for task-based studies (Zarahn et al., 1997), and it is still frequently applied to fMRI task-based scans (e.g. (Finn et al., 2015; Marek et al., 2018)). Given that neuronal contributions in the global signal likely stem from fluctuations in arousal and vigilance (Chang et al., 2016; Falahpour et al., 2018; C. K. Wong et al., 2016; Wong et al., 2013), these contributions could be larger in the absence of an engaging task (i.e. resting-state conditions), as retaining a constant level of vigilance is more challenging. However, (Glasser et al., 2018) found that application of GSR to task fMRI data led to reduced statistical sensitivity for detecting activations, suggesting the possibility that the global signal, in task-based studies, may also contain relevant neural signal. As previous simultaneous electrophysiological-fMRI investigations of the global signal only examined resting-state conditions, the contributions of neurally-related fluctuations in the global signal during behavioral tasks have not yet been elucidated.

In this study, we used simultaneously acquired EEG-fMRI data, as well as physiological recordings, to quantify the unique and shared contributions of physiological and neural processes on the global signal, both at rest and during a motor task. Furthermore, we generated synthetic fMRI datasets that consisted of either systemic or electrophysiological fluctuations, and evaluated the similarity between connectivity estimates extracted from the synthetic and experimental fMRI datasets. This allowed us to examine the effects of GSR on connectivity estimates, and address explicitly whether eliminating the bias introduced by physiological processes inadvertently also removes the connectivity patterns related to electrophysiological activity.

5.4 MATERIALS AND METHODS

5.4.1 Participants

A total of 12 healthy volunteers (25.1 ± 2.9 years; 4 female) participated in the study. All subjects were right-handed according to the Edinburgh Handedness Inventory (Oldfield, 1971) and had no history of neurological or psychiatric disorders. The study was approved by the McGill University Ethical Advisory Committee. All participants signed a written informed consent and were compensated for their participation.

5.4.2 Experimental paradigm

The protocol carried out inside the MR scanner consisted of two 15-min resting-state runs, alternated by a motor task (**Figure 5-1a**). During the resting-state periods, subjects were instructed to stare at a white fixation cross displayed on a dark background and not to think of anything in particular. After the first rest period, the maximum voluntary contraction (MVC) was obtained for each participant, using the same hand gripper later employed for the motor task. The motor task was a unimanual isometric right handgrip, during which the subjects had to apply force to track a ramp target as accurately as possible. At the onset of the trial, an orange circle appeared on the screen and the subjects had 2 s to increase their force to reach a white target block at 15% of their MVC. This force was held for 3 s. Subsequently, participants tracked a linear increase of the force to reach 30% of their MVC over a 3-s period, during which they had to maintain the circle inside the white target block, followed by a 3-s hold at 30% of their MVC (**Figure 5-1b**). A single trial lasted 11 s and the inter-trial interval was jittered between 3 and 5 s, during which subjects stared at a white cross. The task consisted of 50 trials, resulting in a total duration of about 13 min. Visual feedback was provided throughout the task.

5.4.3 Data acquisition: EEG-fMRI data and physiological recordings

All experiments were conducted at the McConnell Brain Imaging Centre (BIC) of the Montreal Neurological Institute (MNI), McGill University, using a 3T Siemens MAGNETOM Prisma fit MRI scanner (Siemens AG, Germany). A 32-channel head coil was used to acquire

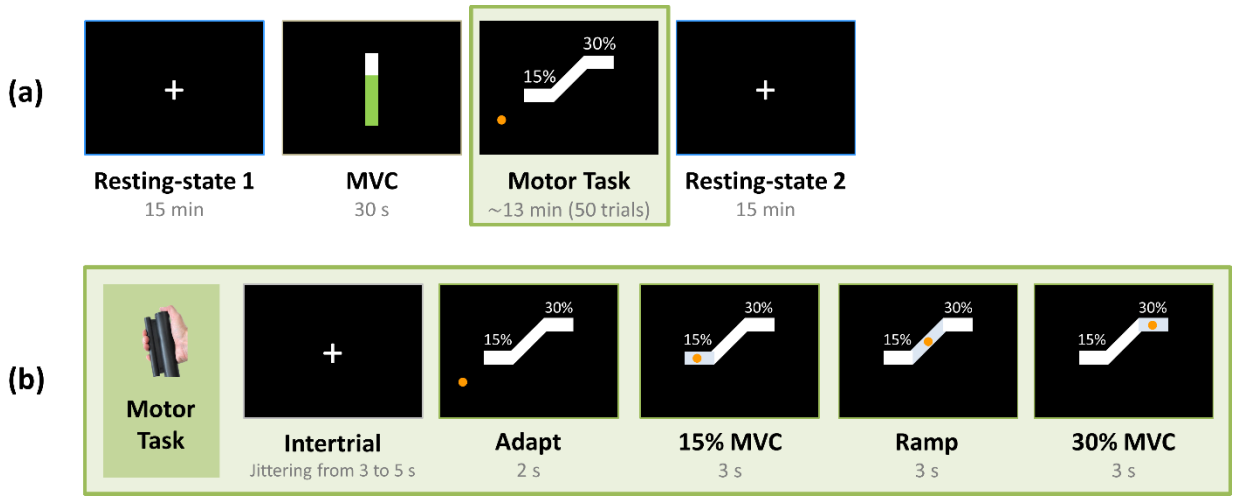

Figure 5-1. (a) Experimental paradigm. Participants underwent two resting-state scans with eyes open, alternated by a motor task. The maximum voluntary contraction (MVC) of each participant was obtained before performing the motor task. **(b) Motor task.** Participants performed a unimanual right handgrip task. In each trial, they fixated on a crosshair for a few seconds. This was followed by the appearance of an orange circle on the screen, where participants had 2 s to apply force to reach 15% of their MVC. A steady grip was then maintained for 3 s, which was followed by a guided ramp period where participants had to apply force to reach 30% of their MVC and sustain this grip strength for another 3 s.

whole-brain T2*-weighted functional gradient echo planar (EPI) data (3×3×4 mm^3 voxels, TR=2120 ms, TE=30 ms, flip angle=90°, FOV=192×192 mm^2, anterior-posterior phase encoding direction). Volumes were recorded in 35 transverse slices in descending order. A high-resolution structural volume was also acquired using a T1-weighted magnetization-prepared rapid acquisition gradient echo (MPRAGE) sequence (TR=2300 ms, TE=2.32 ms, flip angle=8°, FOV=240×240 mm^2, 0.9 mm^3 isotropic voxels).

EEG data were simultaneously recorded with an MR-compatible 64-channel system with Ag/AgCl ring-type electrodes (BrainAmp MR, Brain Products GmbH, Germany), sampled at 5000 Hz. Electrode impedances were maintained below 20 kΩ. An equidistant electrode layout was used with AFz and Cz as ground and online recording reference, respectively. The EEG acquisition clock was synchronised with the MR scanner clock through a device that sent triggers to the EEG recording system every time an fMRI volume was acquired (TriggerBox, Brain Products GmbH, Germany). The electrodes were precisely localized using a 3-D electromagnetic digitizer (Polhemus Isotrack, USA).

Subject's cardiac and breathing measurements were continuously recorded throughout the experiment using a pulse oximeter and respiratory belt (BIOPAC Systems, Inc., USA). An MR-compatible hand clench dynamometer (BIOPAC Systems, Inc., USA) was used to measure the subjects' hand grip strength during the motor paradigm. The pulse oximeter, respiratory belt and dynamometer were connected to an MP150 data acquisition system (BIOPAC Systems, Inc., USA) from which the signals were transferred to a computer, sampled at 1000 Hz.

5.4.4 Preprocessing

5.4.4.1 fMRI data

The fMRI data were preprocessed using FSL (Jenkinson et al., 2012). More specifically, we performed automated brain extraction using BET, motion correction via volume realignment using MCFLIRT, spatial smoothing (5mm FWHM Gaussian kernel) and high-pass temporal filtering (100 s cutoff). Additional preprocessing included motion censoring based on the frame-wise displacement (FD) and root mean square intensity change of BOLD signal across the whole brain (DVARS) measures (Power et al., 2012). Motion censoring was applied by discarding volumes with FD>0.25 mm or when DVARS exceeded its median absolute deviation by a factor of 3, as well as their adjacent volumes. Volumes with subthreshold values of FD and DVARS were also discarded if they were preceded and followed by flagged volumes. All scans from one participant were excluded from the analysis since more than 40% of volumes were identified as being contaminated by motion. Therefore, results from a total of 11 subjects are presented below. The censored fMRI data were coregistered to each subject's structural image and normalized to MNI space (2 mm). Subsequently, preprocessed data were parcellated into 300 regions of interest (ROIs) based on the Seitzman atlas (Seitzman et al., 2020). ROIs that were unassigned to a specific brain network were disregarded, hence a total of 285 ROIs were used for further analyses. To account for other sources of noise, we applied white matter denoising using principal component analysis (PCA) to the parcellated data (Kassinopoulos and Mitsis, 2019a). Specifically, 10 white matter PCA components were removed from the data, as this number was found to maximize the functional connectivity contrast (FCC) (Kassinopoulos and

Mitsis, 2019a), which quantifies the difference in correlation values among edges within- and between-networks (**Figure 5-2**). Finally, note that when assessing the effects of GSR, we regressed out the PCA components and the global signal simultaneously.

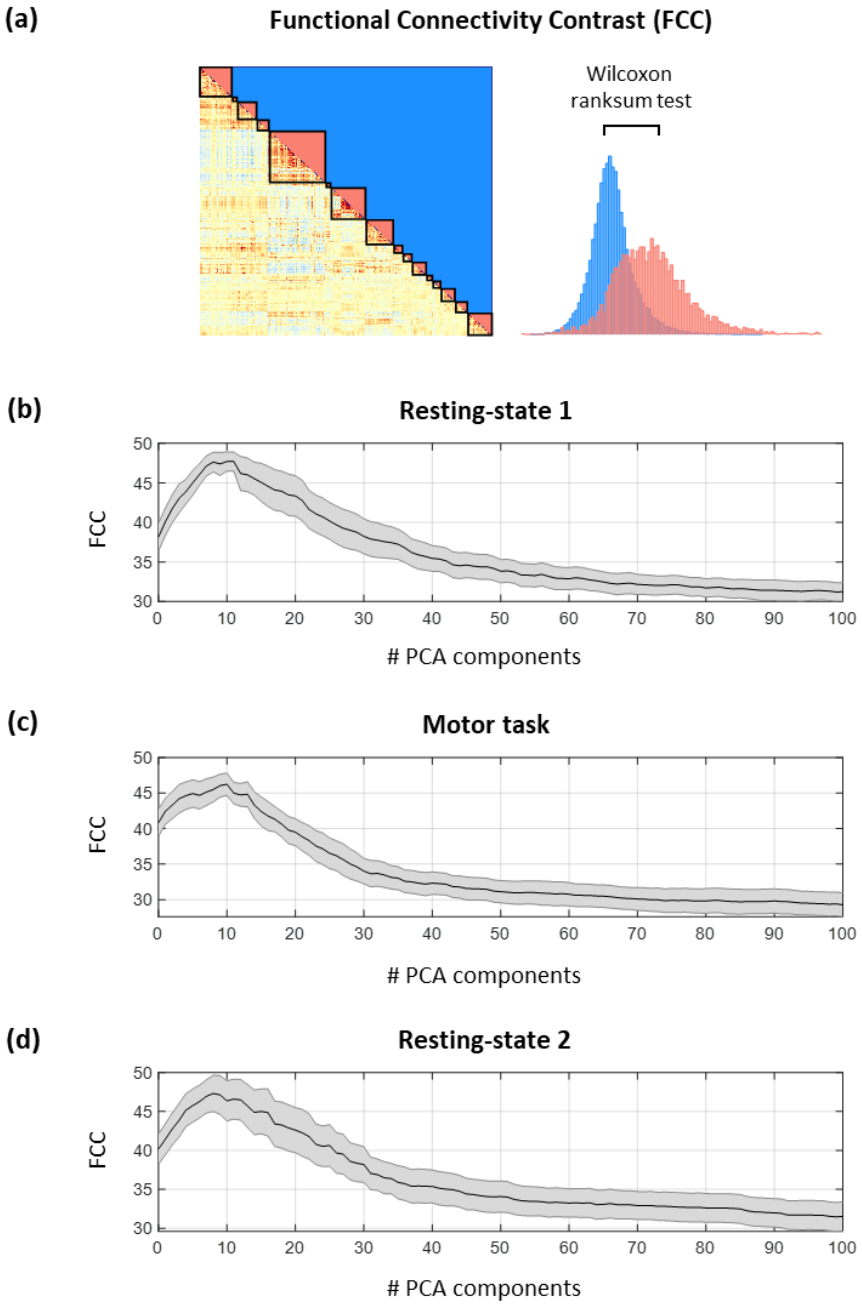

Figure 5-2. Selection of the number of PCA white matter components for fMRI denoising. (a) Illustration on how the calculation of the FCC measure was performed. **(b-d)** Group-averaged FCC measure as a function of the number of white matter PCA components used for denoising for **(b)** resting-state 1, **(c)** motor task, and **(d)** resting-state 2. The black line denotes mean across subjects and the shaded area denotes standard error. Based on these traces 10 PCA components were considered as the optimal number for denoising.

5.4.4.2 EEG data

EEG data were corrected offline for gradient and ballistocardiogram (BCG) artifacts using sliding average template subtraction in BrainVision Analyzer 2 (Brain Products GmbH, Germany). Data were subsequently downsampled to 200 Hz and further processed with independent component analysis to remove remaining non-neural components such as ocular and muscle artifacts, as well as gradient and BCG residuals. The preprocessed data were re-referenced using the average of all channels.

Time-frequency spectrograms were calculated for each EEG channel using Morlet wavelets and a global spectrogram was obtained by taking the root mean square of all spectra across all channels. Then, we extracted the instantaneous power time-series through averaging of the global spectrogram within the following frequency bands: delta (1.5-4 Hz), theta (4-8 Hz), alpha (8-15 Hz) and beta (15-26 Hz). These global EEG power time-series were subsequently convolved with a canonical double-gamma haemodynamic response function and downsampled to the frequency of image volume sampling (TR=2.12 s). The censored frames flagged during fMRI preprocessing were removed from the convolved EEG power time-series.

5.4.4.3 Physiological recordings

Beat-to-beat intervals were detected from the pulse oximeter signal, and the heart rate signal was computed as the inverse of the time differences between pairs of adjacent peaks and scaled to beats-per-minute (bpm). Heart rate traces were visually examined to identify outliers, and an outlier replacement filter was used to eliminate spurious changes in heart rate. The breathing signal from the respiratory belt was detrended linearly, visually inspected and corrected for outliers using a replacement filter, low-pass filtered at 5 Hz, and z-scored. The respiratory flow, proposed in (Kassinopoulos and Mitsis, 2019a) as a robust measure of the absolute flow of inhalation and exhalation of a subject at each time point, was extracted by further smoothing the breathing signal (moving average filter using a 1.5 sec window) and, subsequently, computing the square of the derivative of the smoothed breathing signal. Both heart rate and respiratory flow signals were resampled to 10 Hz.

Following this, we modelled systemic low-frequency oscillations (SLFOs) associated with heart rate and breathing patterns using a recently developed method that computes scan-specific physiological response functions (PRFs) (Kassinopoulos and Mitsis, 2019b, scripts available on https://github.com/mkassinopoulos/PRF_estimation/). Briefly, this algorithm estimates PRF curves so that the convolution between heart rate and respiratory flow with their corresponding PRFs optimizes the fit on the global signal of the same scan, while ensuring that the shapes of the PRF curves are physiologically plausible. The heart rate and respiratory flow were convolved with their respective PRFs and added to obtain a time-series that reflects the effect of SLFOs.

5.4.5 Data analyses

We initially quantified the variance explained by SLFOs and EEG power in the fMRI global signal using partial correlation. Specifically, the contribution of SLFOs to the global signal was computed controlling for the EEG power time-series, and the contribution of each EEG power was computed controlling for SLFOs. To assess the significance of these contributions to the global signal, surrogate data were generated via inter-subject surrogates (Lancaster et al., 2018), using physiological and EEG power time-series from different subjects. The observed contributions were tested against the contributions found using the surrogate data through the Wilcoxon rank-sum test. The significance level was set to 0.05, and the p-values for the EEG bands were adjusted for multiple comparisons using the false discovery rate (FDR) method.

Subsequently, we quantified the contributions of SLFOs and EEG power time-series within each fMRI ROI using multiple linear regression, as follows:

$$y(t) = \beta_0 + \beta_{SLFOs} x_{SLFOs}(t) + \boldsymbol{\beta}_{EEG}\mathbf{x}_{EEG}(t) + \boldsymbol{\beta}_{PCA\_WM}\mathbf{x}_{PCA\_WM}(t) + \varepsilon(t) \quad (5.1)$$

$$\boldsymbol{\beta}_{EEG} = [\beta_{delta} \quad \beta_{theta} \quad \beta_{alpha} \quad \beta_{beta}],\ \boldsymbol{\beta}_{PCA\_WM} = [\beta_{pca1} \quad \cdots \quad \beta_{pca10}]$$

$$\mathbf{x}_{EEG}(t) = \begin{bmatrix} x_{delta}(t) \\ x_{theta}(t) \\ x_{alpha}(t) \\ x_{beta}(t) \end{bmatrix},\ \mathbf{x}_{PCA\_WM}(t) = \begin{bmatrix} x_{pca1}(t) \\ \vdots \\ x_{pca10}(t) \end{bmatrix}$$

where y is an fMRI ROI time-series, $x_{SLFOs}(t)$ is the physiological regressor related to low frequency fluctuations in heart rate and breathing patterns, $\mathbf{x}_{EEG}(t)$ are the four EEG power time-series, $\mathbf{x}_{PCA\_WM}(t)$ are the 10 PCA components from white matter, the values $\{\beta_0, \beta_{SLFOs}, \boldsymbol{\beta}_{EEG}, \boldsymbol{\beta}_{PCA\_WM}\}$ represent the parameters to be estimated, and ε is the error.

Synthetic fMRI datasets were generated for each subject based on the SLFOs and EEG contributions, following the same methodology as in (Xifra-Porxas et al., 2020). Briefly, each synthetic dataset was constructed so that the variance explained by SLFOs, as well as EEG alpha and beta power for each ROI was retained and the remaining variance was replaced with uncorrelated random signals. We only considered the alpha and beta power bands because these were the only EEG bands that significantly contributed to the global signal (**Figure 5-3**). We then computed the correlation between ROIs across the entire scan (i.e. static functional connectivity matrices) for the following datasets: raw experimental fMRI, preprocessed experimental fMRI without GSR, preprocessed experimental fMRI with GSR, SLFOs synthetic fMRI, alpha power synthetic fMRI, and beta power synthetic fMRI. To quantify the similarity between the SLFOs, alpha power and beta power connectivity matrices with respect to the fMRI connectivity matrices at different preprocessing stages, we calculated the correlations between their upper triangular values. The goal was to assess the effect of GSR on the similarity between SLFOs and fMRI connectivity, as well as EEG power and fMRI connectivity.

5.5 RESULTS

5.5.1 Association of SLFOs and EEG power with the fMRI global signal

In line with previous studies (Birn et al., 2006; Kassinopoulos and Mitsis, 2019b; Power et al., 2017a; Shmueli et al., 2007), SLFOs were significantly correlated with the global signal, both at rest and during the motor task (**Figure 5-3**). Regarding the EEG bands, alpha power was negatively correlated with the global signal both at rest and during the motor task (**Figure 5-3**), and beta power was negatively correlated with the global signal during the motor task (**Figure 5-3b**). It is worth noting that the correlation strength of alpha and beta fluctuations with the global signal, albeit significant, was much weaker compared to the correlation between SLFOs and the global signal. Furthermore, the mean correlation across subjects for the full model containing both SLFOs and significant EEG power bands was equal to 0.64 ± 0.12 (resting-state 1), 0.64 ± 0.09 (motor task), and 0.59 ± 0.09 (resting-state 2). Moreover, alpha power was found to be negatively correlated with SLFOs ($R = -0.09, p = 0.02$) during resting-state 1. This correlation vanished when alpha and SLFOs were controlled for global signal fluctuations (R=0.02, p=0.84), which may suggest a common component between those two variables that is reflected on the global signal, possibly

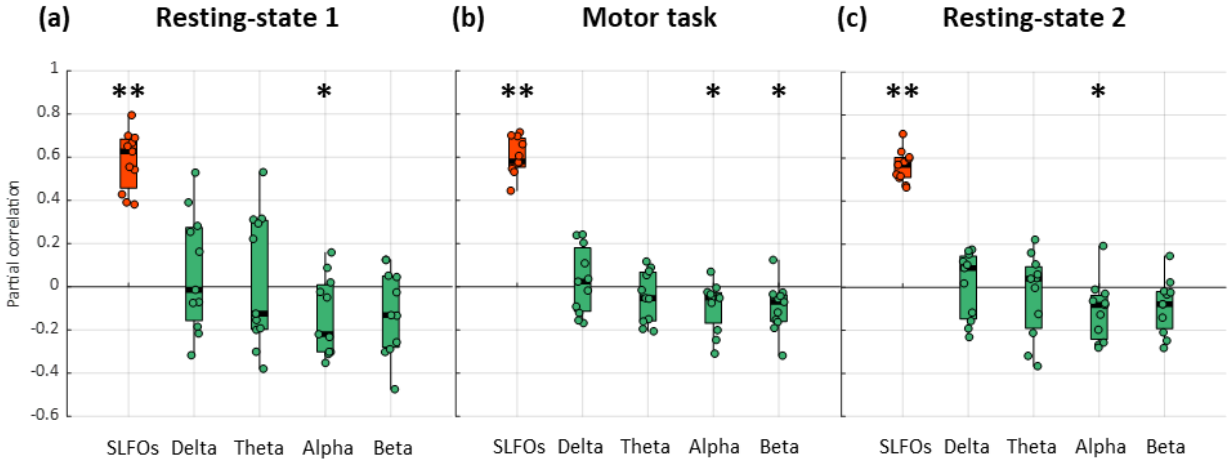

Figure 5-3. Partial correlation of SLFOs and EEG power time-series with the fMRI global signal across subjects for (a) resting-state 1, (b) motor task, and (c) resting-state 2. Significance testing against surrogate data (Wilcoxon rank-sum test, * $p < 0.05$, ** $p < 0.001$). The p-values for the four EEG bands were corrected for multiple comparisons using FDR. SLFOs were highly correlated with the global signal, whereas alpha and beta power fluctuations were weakly correlated with global signal variations.

reflecting a direct or indirect effect of autonomic activity. Yet, we were unable to replicate this result during the motor task or resting-state 2 (i.e. alpha power was not significantly correlated with SLFOs). Finally, delta and theta power did not yield a consistent contribution to the global signal across subjects for any of the scans.

5.5.2 GSR effects on fMRI-based connectivity estimates related to EEG activity

For each subject and scan, connectivity matrices were derived using the synthetic dataset generated from SLFOs, which highlighted the connectivity edges more prone to exhibit artifactual connectivity attributable to SLFOs. We found that fluctuations due to SLFOs artifactually increased the connectivity across most brain networks and particularly within the visual network, as well as between the visual network and other brain networks (**Figure 5-4a**), consistent with previous observations using a larger number of subjects (Xifra-Porxas et al., 2020). Furthermore, the effect of SLFOs on the visual network were found to be spatially homogenous at rest, whereas during the motor task specific edges were more affected than others (**Figure 5-4a**). Consistent with our earlier study (Xifra-Porxas et al., 2020), GSR reduced the similarity between the SLFOs' and the fMRI connectivity matrices both at rest and during the motor task (**Figure 5-4b**). This result supports the extensive evidence that, at least with respect to mitigating nuisance processes, GSR is effective.

To determine whether applying GSR also removed substantial EEG power fluctuations, we derived connectivity matrices using the fMRI synthetic datasets generated based on the fraction of BOLD variance attributed to alpha and beta power, thus highlighting the edges underpinning connectivity of neural origin. At rest, alpha power variations mostly contributed to connectivity within the visual network and dorsal attention network as well as between these two networks (**Figure 5-5a**). On the other hand, during the motor task, alpha power variations mostly contributed to connectivity within the default mode network (**Figure 5-5a**), whereas beta power variations mainly contributed to connectivity within some edges of the visual network (**Figure 5-5c**). Subsequently, we evaluated whether performing GSR on the preprocessed fMRI data significantly removed the connectivity signature of these neural processes. As we can see in **Figure 5-5b** & **Figure 5-5d**, GSR did

not have any significant effect on the similarity between the EEG-related signatures and fMRI connectivity matrices, either for alpha or beta power variations.

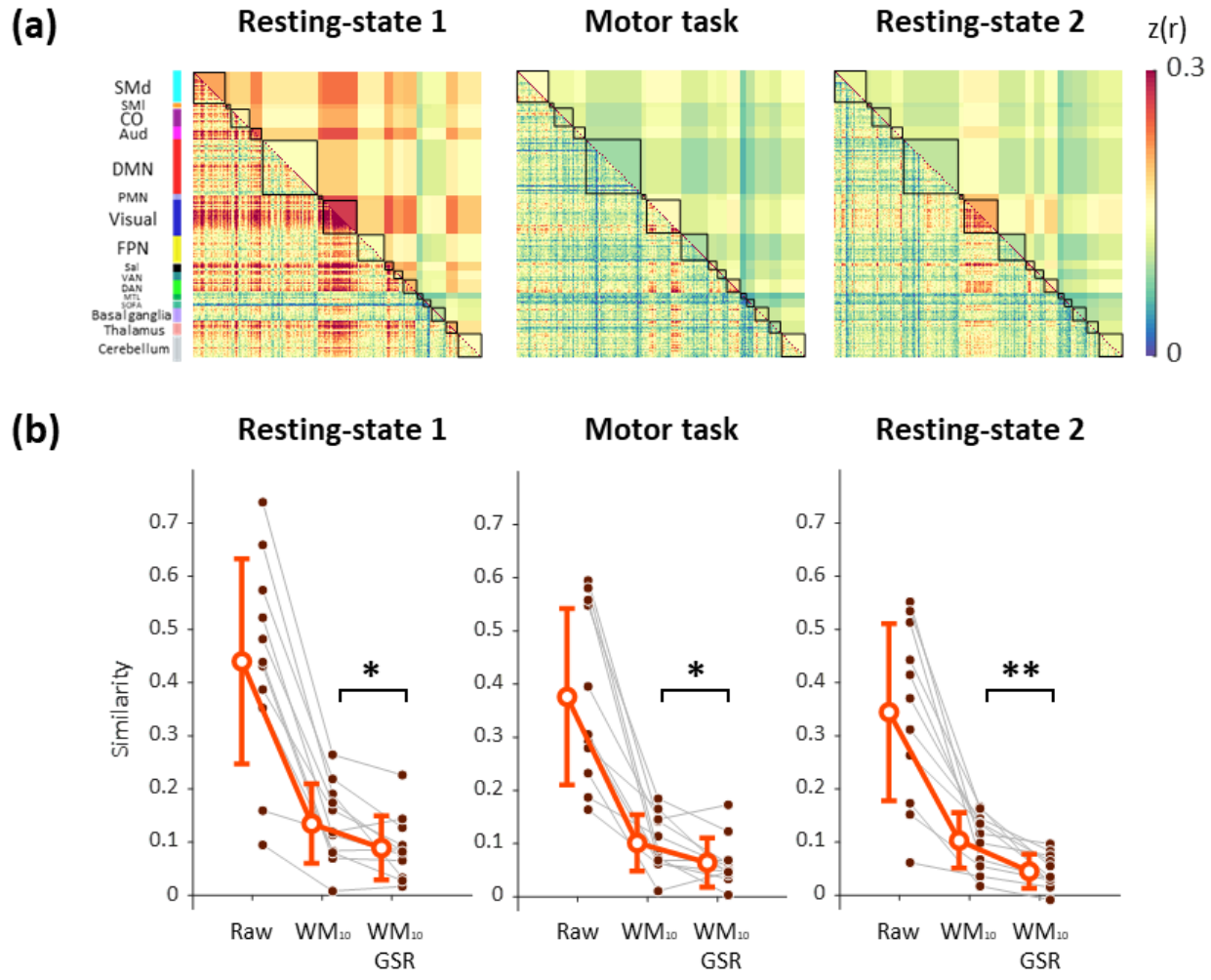

Figure 5-4. Effect of GSR on connectome patterns induced by SLFOs. (a) Group averaged FC matrices computed using the synthetic dataset based on the contributions of systemic low frequency fluctuations (SLFOs) to each fMRI parcel time-series, for each scan. **(b)** Similarity between the SLFOs' FC matrices and the FC matrices extracted from the raw data, the preprocessed data (i.e. fMRI data after regressing out 10 PCA white matter components; WM_{10}), and the preprocessed data after global signal regression (GSR). GSR significantly reduced the bias in connectivity introduced by SLFOs (Wilcoxon rank-sum test, * $p < 0.05$, ** $p < 0.005$). Error bars denote standard deviation.

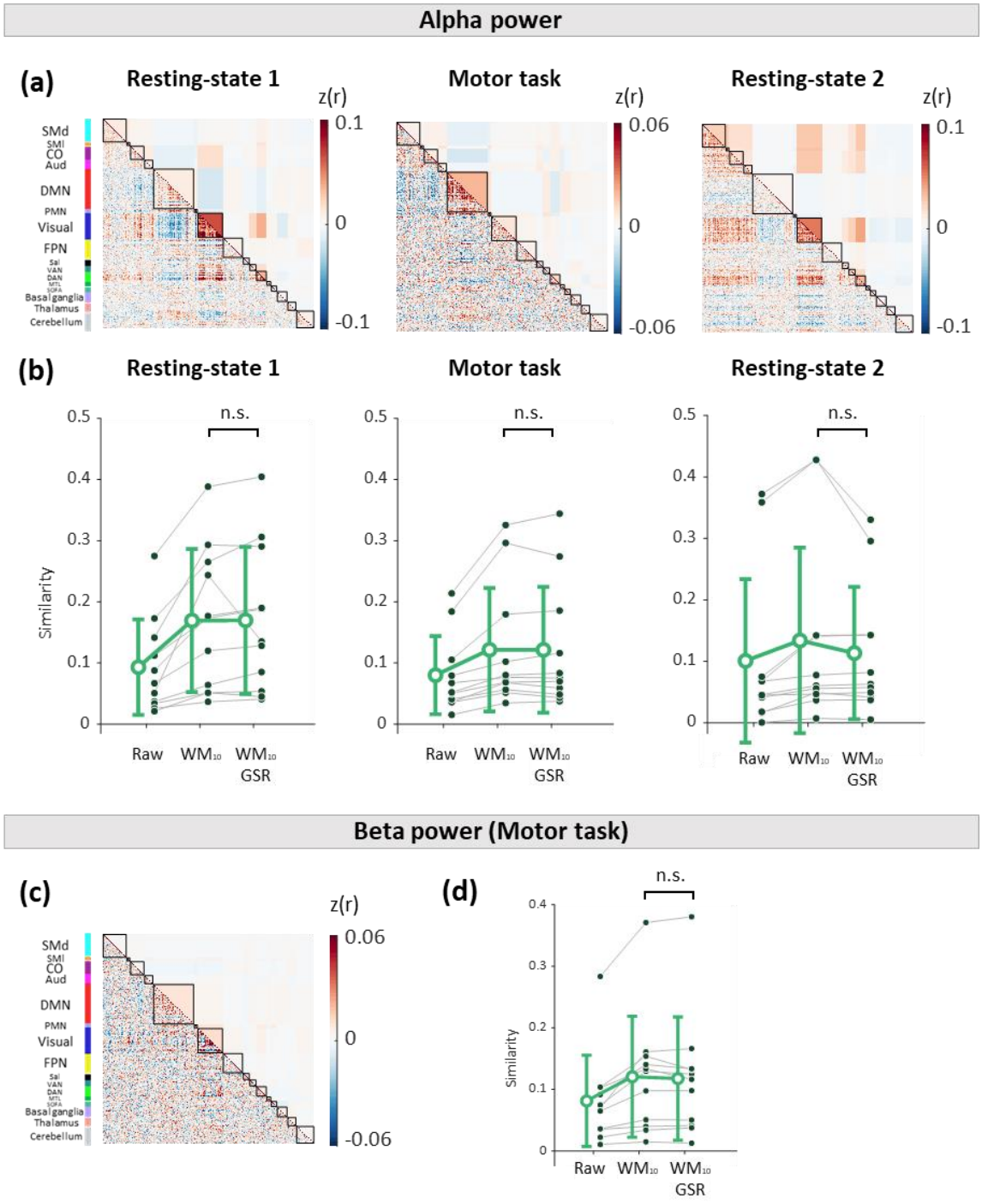

Figure 5-5. Effect of GSR on connectome patterns associated with EEG power. (a) Group averaged FC matrices computed using the fMRI synthetic dataset associated with fluctuations in alpha power, for each scan. **(b)** Similarity between the alpha band EEG-based FC matrices and the FC matrices extracted from the raw data, the preprocessed data (i.e. fMRI data after regressing out 10 PCA white matter components; WM_{10}), and the preprocessed data after global signal regression (GSR). **(c)** Group averaged FC matrices computed using the fMRI synthetic dataset associated with fluctuations beta power, for the motor task. **(d)** Similarity between the beta band EEG-based FC matrices and the FC matrices extracted from the raw data, the preprocessed data (WM_{10}), and the preprocessed data after GSR. GSR did not significantly reduce the connectivity related to EEG activity (Wilcoxon rank-sum test). In all subplots, error bars denote standard deviation. n.s. = not significant.

5.6 DISCUSSION

GSR is a widely used preprocessing step to remove global artifacts (mostly heart rate, respiratory effects; SLFOs) from fMRI data (Ciric et al., 2017; Parkes et al., 2018; Power et al., 2018, 2017b), but remains highly controversial because it may also discard neural signals (T. T. Liu et al., 2017; Murphy and Fox, 2017). Up to date, the vast majority of studies investigating the origins of the global signal and evaluating the potential effects of GSR have examined fMRI data concurrently with either physiological or electrophysiological recordings, but not both. In the present study, we used simultaneous EEG-fMRI data, as well as cardiac and breathing recordings, to examine the processes underpinning the global signal and the impact of GSR on measures of brain activity and connectivity related to systemic and neural fluctuations. Our results show that the global signal is strongly associated with physiological processes ($R \sim 0.6$) and only weakly associated with EEG power fluctuations ($R \sim -0.1$). We further demonstrate that GSR effectively removes the structured connectome patterns induced by physiological processes, while preserving the connectome patterns associated with EEG power bands. These results provide evidence that, in the context of connectivity analyses, GSR improves the denoising of fMRI data and does not seem to alter the connectivity profiles associated with electrophysiological activity.

5.6.1 Association of SLFOs and EEG power with the fMRI global signal

We first evaluated the unique contributions of SLFOs and EEG activity to the global signal. SLFOs was found to explain a large fraction of global signal variance at rest (**Figure 5-3a**, **Figure 5-3c**), consistent with several earlier studies (Birn et al., 2006; Chang and Glover, 2009a; Erdoğan et al., 2016; Kassinopoulos and Mitsis, 2019b; Power et al., 2017b), as well as during the motor task (**Figure 5-3b**). Alpha power was found to be negatively correlated with the global signal for all scans (**Figure 5-3**,**a-c**), consistent with earlier work (T. T. Liu et al., 2017), and beta power was found to be negatively correlated with the global signal during the motor task (**Figure 5-3b**). Our results suggest that contributions of electrophysiological origin to the global signal, albeit significant, are substantially smaller than physiological contributions.

A possible explanation for this is that the correlation sign between fMRI fluctuations and EEG activity may vary across brain regions and, thus, when averaging fMRI signals across the whole brain, these electrophysiological fluctuations, to some extent, cancel out. Several studies have reported that, during resting conditions, alpha activity is negatively correlated with sensorimotor areas but positively correlated with default-mode regions (D Mantini et al., 2007; Mayhew and Bagshaw, 2017; Scheeringa et al., 2012). These trends were also observed in our data, resulting in the presence of both positively and negatively correlated activity in **Figure 5-5a**. Therefore, it is indeed likely that the weak relationship between global signal and EEG activity may be due to differences in polarity of associated fMRI activity across regions.

5.6.2 Association between SLFOs and alpha power

Furthermore, we observed that alpha power and SLFOs were negatively correlated during resting-state 1, albeit weakly. This finding was not replicated during the motor task and resting-state 2. The weak association between SLFOs and alpha activity may be due to that subjects had their eyes open, which is in agreement to previous work that has demonstrated an association between respiration and alpha power during an eyes closed condition but not during eyes open (Yuan et al., 2013). Independent of this, shared contributions from SLFOs and alpha activity to the global signal, which would potentially reflect a direct or indirect effect of autonomic activity, were not consistently observed in our data. Therefore, our results seem to indicate that the major contributor to the global signal is physiological in origin.

5.6.3 Effect of GSR on connectome patterns associated with SLFOs and EEG power

We initially assessed the systematic effect of SLFOs on estimates of functional connectivity. The grand-averaged functional connectivity matrices calculated from the SLFOs synthetic datasets exhibited a heterogeneous pattern, characterized by stronger correlations within and between sensory cortices, including the visual cortex, somatosensory cortex and auditory cortex, as well as subcortical regions such as the thalamus and cerebellum (**Figure**

5-4a). This heterogeneity among brain regions is not surprising as it has been reported that global signal fluctuations are non-uniformly distributed across the brain (Fox et al., 2009; Kassinopoulos and Mitsis, 2019b; Power et al., 2017b). Furthermore, the artifactual connectivity patterns due to SLFOs observed here were similar to these reported in our recent study where a large number of healthy subjects from the Human Connectome Project (HCP) dataset was used (Xifra-Porxas et al., 2020). Specifically, we were able to replicate our previous results in cortical regions, and further showed artifactual connectivity within and between subcortical regions such as the thalamus and cerebellum, which we were unable to observe in the HCP dataset, likely due to poor signal-to-noise ratio in the subcortex (Ji et al., 2018; Seitzman et al., 2020). Moreover, we observed a task-related effect on the SLFOs connectivity pattern (**Figure 5-4a**), whereby contributions of SLFOs on the fMRI data were weaker during the motor task and the second resting-state period. This observation may seem paradoxical as the contribution of SLFOs to the global signal did not significantly decrease across scans (**Figure 5-3**), but may be explained by the fact that global signal fluctuations were found to be reduced during the motor task and the second resting-state period compared to the first resting-state period (**Supp. Fig. 5-1**). This observation may also indicate that subjects were more alert during and after the motor task (Wong et al., 2013; Yeo et al., 2015), but it could reflect the effect of circadian/ultradian physiological fluctuation effects, given that scanning started at 6pm for all subjects and it has been reported that global signal fluctuation decreases as the day progresses (Orban et al., 2020).

The grand-averaged functional connectivity matrices calculated from the fraction of BOLD variance explained by alpha and beta power fluctuations revealed structured patterns (**Figure 5-5a**, **Figure 5-5c**). At rest, fluctuations in alpha power were associated with positively correlated fMRI connectivity mostly within and between visual and dorsal attention networks (**Figure 5-5a**). Fluctuations in alpha power were also associated with anticorrelations of visual and dorsal attention networks with the default mode network and several subcortical regions. These results are consistent with earlier work reporting a positive association of alpha power fluctuations with fMRI activity in the default mode network as well as several subcortical regions, and a negative association between alpha

power and fMRI activity in sensory regions (Bowman et al., 2017; Jann et al., 2009; D Mantini et al., 2007; Mayhew and Bagshaw, 2017; Mo et al., 2013; Moosmann et al., 2003; Scheeringa et al., 2012). During the motor task, we found that alpha power was associated with fMRI connectivity within the default mode network (**Figure 5-5a**), which has been suggested to arise as a result of alpha patterns of synchronization/desynchronization during a task being analogous to the default mode fluctuations of activation/deactivation (Mayhew et al., 2013; Mo et al., 2013). Furthermore, fluctuations in beta power were mostly associated with positively and negatively correlated activity within the visual and default mode networks (**Figure 5-5c**).

Regarding the effect of GSR on the estimates of functional connectivity, our recent work (Xifra-Porxas et al., 2020) provided evidence that GSR seems to be most effective method for removing systematic biases on measures of functional connectivity that arise due to SLFOs. However, since we did not have electrophysiological recordings, we were unable to assess whether GSR also removed signal of interest. In the present study, we sought to answer this question. First, we showed that, as expected, GSR significantly reduced the connectivity patterns attributed to SLFOs, both at rest and during the motor task (**Figure 5-4b**). It is worth noting that even though we used a relatively aggressive preprocessing pipeline (i.e. 10 PCA components from white matter) (Kassinopoulos and Mitsis, 2019a), performing GSR was still found to be beneficial. Considering that in a large number of fMRI studies only the average signals from white matter and cerebrospinal fluid compartments are regressed out, our results suggest that the effectiveness of GSR with respect to artifact removal would have been even more pronounced for such a mild preprocessing pipeline. Second, we found that GSR did not have any effect on the fMRI connectivity patterns attributed to alpha (**Figure 5-5b**) and beta (**Figure 5-5d**) electrophysiological power, neither at rest nor during the motor task. These results suggest that, even though we found significant correlations between EEG power bands and the global signal (**Figure 5-3**), the observed associations are not strong enough to significantly alter the connectivity patterns associated with EEG activity after GSR. This is to some extent supported by the findings reported in a recent study involving macaque monkeys, where it was shown that, while inactivation of the basal forebrain led to selective suppression of ipsilateral global

components, resting-state brain networks preserved their distinctive topography (Turchi et al., 2018). Overall, the current results align with the view that the benefits of GSR in terms of fMRI denoising outweigh the small loss of neural information (Li et al., 2019a, 2019b).

5.6.4 Limitations

Despite the large fraction of the global signal variance that was explained by SLFOs, and to a lesser extent EEG power (**Figure 5-3**), there was still variance unaccounted for. The EEG signal is not a perfect reflection of neural activity and is known to be considerably noisy in the MR environment, as well as blind to deep sources. Therefore, there may be additional neural activity in the global signal that we were unable to detect. Likewise, there are other physiological factors not considered here that are known to give rise to SLFOs and are reflected on the global signal, such as finger skin vascular tone (Özbay et al., 2019) and arterial CO2 changes (Prokopiou et al., 2019; Wise et al., 2004). Future studies using more direct surrogates of neuronal activity (e.g. intracranial EEG) are needed to confirm whether crucial neural information is being removed through GSR.

Furthermore, in this study we examined resting conditions and a motor task, but results could be different during other conditions, such as sleep (Duyn et al., 2020) or when investigating diurnal variations in large-scale spontaneous brain activity (Orban et al., 2020).

5.7 Conclusions

Our results demonstrate that the global signal has a stronger association with SLFOs rather than neural activity and provide further evidence that GSR effectively removes confounds in functional connectivity induced by SLFOs. While we also found a reproducible association between alpha and beta EEG activity and the global signal, our results suggested that GSR did not seem to disrupt the functional connectivity patterns attributed to alpha and beta activity.

5.8 Acknowledgements

We would like to thank the MRI technicians at the Montreal Neurological Institute for their patience and assistance collecting the data. This work was supported by funds from Fonds de la Recherche du Québec – Nature et Technologies (FRQNT; 2016-PR-191780) [MHB & GDM], the Canadian Foundation for Innovation grant numbers 34277 [MHB] and 34362 [GDM], and the Canada First Research Excellence Fund (awarded to McGill University for the Healthy Brains for Healthy Lives (HBHL) initiative). AXP and MK received financial support through funding from McGill University and the Québec Bio-imaging Network (QBIN).

5.9 SUPPLEMENTARY MATERIAL

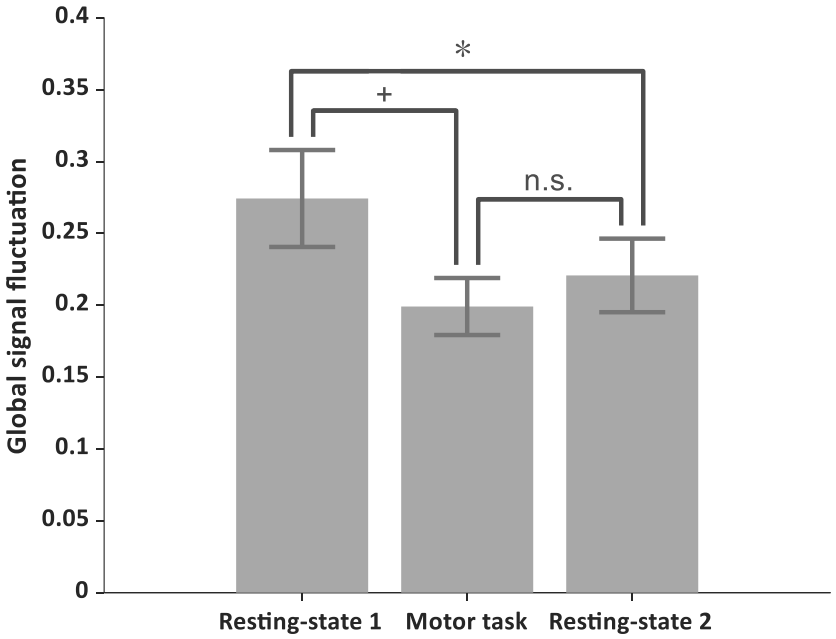

Supp. Fig. 5-1. Mean global signal fluctuation (standard deviation of the global signal) across participants for each scan. Error bars denote standard error of the mean. Significance testing using the sign-rank test (* p <0.05, $^{+}$ p <0.1).

6

General discussion

6.1 SUMMARY OF FINDINGS AND DISCUSSIONS

The work presented in this thesis has contributed to the field of neuroimaging in two main aspects. First, it has enhanced our understanding of motor-related brain oscillations in the context of healthy aging. Second, it has shed novel insights into the neural and physiological sources of static and time-varying fMRI-based functional connectivity by developing a new methodology to assess preprocessing strategies and applying it to fMRI and simultaneous fMRI-EEG data.

In Chapter 3, we investigated the effects of aging on the modulation of beta oscillations during handgrip contractions. Our results complemented previous research showing an increased beta desynchronization during dynamic contractions in older relative to younger adults (Heinrichs-Graham and Wilson, 2016; Hübner et al., 2018a; Schmiedt-Fehr et al., 2016), and demonstrated that this larger beta desynchronization extended beyond the primary motor cortices to frontal and premotor brain regions. Conversely, during sustained contractions, we provided new evidence showing similar levels of beta desynchronization (with respect to resting beta levels) between age groups. Altogether, these results indicate that older adults exhibit a larger modulation of beta power compared to their younger counterparts during a sequence of sustained and dynamic contractions, both during uni- and bimanual handgrips.

In Chapter 4, we developed a framework for characterizing the whole-brain functional connectivity profiles of the main confounds of fMRI variability. These include global confounds that arise from fluctuations in heart rate and breathing patterns (i.e. SLFOs), head motion, breathing motion, and cardiac pulsatility. We quantified the functional connectivity signatures of these confounds at the individual level and then examined their consistency at the group level. Our results revealed that the connectivity profiles of SLFOs, head motion and breathing motion exhibit a structured pattern, suggesting that these processes introduce a systematic bias on estimates of functional connectivity, if they are not properly accounted for. Specifically, SLFOs induce increased positive correlations across the whole brain, particularly within and between the visual network. Head motion introduces artifactual connectivity within the sensorimotor and visual networks; and breathing motion increases within-hemisphere connectivity, which we demonstrated is attributable to the phase encoding direction. We then examined the potential subject specificity of these nuisance functional connectivity profiles and found that their individual variability was quite reliable across scans, particularly for SLFOs. Furthermore, we evaluated the capability of several state-of-the-art preprocessing strategies in mitigating the effects of the considered nuisance processes. We showed that data-driven techniques based on decomposing the data into principal or independent components (PCA, ICA), combined with global signal regression (GSR), were more successful in reducing the effects introduced by physiological and head motion confounds. Finally, we examined whether the identification of subjects based on their functional connectivity profiles (connectome fingerprinting) is reduced when applying denoising strategies that successfully remove these confounds, given that the observed subject specificity of some of these nuisance processes could be contributing to subject identification. Encouragingly, our results showed that the best preprocessing strategies also yielded the highest subject identification accuracy, suggesting that the inter-individual differences in functional connectivity that facilitate identification are strongly neural in nature and do not largely stem from physiological processes or head motion.

In Chapter 5, we sought to shed light on the controversy with regards to regression of the global fMRI signal (Murphy and Fox, 2017). Using a dataset comprising simultaneous EEG-fMRI and physiological recordings, we first examined the physiological and neural basis of

the global fMRI signal. We found that physiological fluctuations explained a larger fraction of the global signal variance compared to EEG activity. Nonetheless, albeit small, we found consistent associations of EEG activity with global signal fluctuations, which were reliably detected at rest and during a motor task. We subsequently examined whether performing GSR had any impact on estimates of functional connectivity linked to neural activity. Using the framework developed in Chapter 4, we extracted the whole-brain functional connectivity profiles associated with alpha and beta activity, as well as physiological global fluctuations (i.e. SLFOs). We first showed that GSR significantly reduced the artifactual connectivity profiles induced by SLFOs, replicating our results in Chapter 4. Finally, we showed that GSR did not significantly alter the fMRI connectivity profiles related to alpha or beta activity. Our results suggest that the amount of neural-related explained variance in the global signal is not strong enough to alter the connectivity profiles emerging from the EEG activity.

6.2 FUTURE RESEARCH

6.2.1 Future directions with respect to chapter 3

Chapter 3 contributed knowledge to the age-related neural correlates of motor control. Given the prevalence of motor control impairments in older adults, it is crucial to characterize the motor-related neural correlates of healthy aging if measures such as MRBD and PMBR are to become clinical markers of disease. For instance, it has been reported that MRBD is diminished in Parkinson's disease (Heinrichs-Graham et al., 2014), whereas a delayed PMBR and larger MRBD was found in patients with amyotrophic lateral sclerosis (Proudfoot et al., 2017). However, these investigations mainly focused on dynamic contractions. Future research examining sustained contractions in clinical populations might provide new insights into the neuropathology of motor disorders.

Furthermore, our results yield promise for identifying novel targets to design therapeutic interventions using non-invasive brain stimulation techniques (Cespón et al., 2018; Tatti et al., 2016). Even though the regions that exhibited increased MRBD in older adults did not exhibit an association with performance, we identified a link with behavior beyond age on

the primary motor cortices, whereby smaller (i.e. less negative) MRBD was associated with better task performance. These findings are in agreement with previous investigations reporting decreases in MRBD after motor learning (Espenhahn et al., 2019) or acute exercise (Dal Maso et al., 2018; Hübner et al., 2018b). Related to this, future research could aim entraining beta oscillations while subjects perform a motor task to improve their performance. However, it should be taken into consideration that exceeding the resting-state beta levels could induce the opposite effect, as application of transcranial alternating current stimulation within the beta frequency band has been shown to slow movements (Joundi et al., 2012; Pogosyan et al., 2009). Another possible avenue would be to entrain beta oscillations on the contralateral primary motor cortex during the intertrial periods of a task, as recent investigations have shown an association between contralateral PMBR and motor learning (Espenhahn et al., 2020, 2019).

6.2.2 Future directions with respect to chapter 4

The framework developed in Chapter 4 opens many avenues to extend the current study. For instance, it would be interesting to explore whether similar nuisance functional connectivity profiles arise when participants are engaged in a behavioral task, considering recently observed ordered physiological modulations of fMRI signals during an auditory paradigm (Chang et al., 2019). The HCP dataset contains a wide-ranging selection of 3T task-evoked fMRI scans engaging a broad range of neural systems (Van Essen et al., 2012); therefore, it is well suited to pursue this avenue of research. Furthermore, a subset of 200 subjects were also scanned using a 7T scanner, which could be used to investigate the influence of field strength on the connectivity profiles of nuisance processes, given that the influence of physiological sources increases at ultra-high field fMRI (Triantafyllou et al., 2011, 2005).

Moreover, a recent study using the HCP dataset showed that global signal variation during the day did not follow the chronotype characteristic of arousal levels (higher at late morning and early evening than in mid-afternoon). Instead, it exhibited a steady decrease during the day (Orban et al., 2020), possibly related to cerebral blood flow increases from morning to evening (Braun et al., 1997; Elvsåshagen et al., 2019). Therefore, it would be interesting to examine whether nuisance functional connectivity patterns exhibit any change with respect

to time of day, particularly those associated with SLFOs, and potentially provide a time window that is less prone to nuisance biases in functional connectivity.

Looking ahead, the developed framework could be applied to fMRI studies comparing populations, particularly those in which differences in heart rhythms, breathing, or motion are expected. For instance, a large-scale dataset that would be worth examining in this context is the HCP Aging (Bookheimer et al., 2019). Older adults demonstrate vascular differences compared to young adults (Tsvetanov et al., 2019, 2015), as well as lower HR variability (O'Brien et al., 1986). Further, differences in motion between young and older participants are known to bias functional connectivity analyses (van Dijk et al., 2012). A better characterization of the nuisance connectivity profiles in aging could help distinguish the age effects on physiological processes and head motion versus neural function.

Moreover, an exciting new avenue is to leverage the physiologically-driven variations of the fMRI signal to characterize vascular physiology, instead of discarding them as confounds. In such instances, the "nuisance" connectivity profiles discussed in Chapter 4 may provide meaningful insights into impairments in cerebral blood flow regulation (e.g. stroke, Moyamoya disease). This emerging field of "physiological MRI" holds great potential in establishing clinical biomarkers of cerebrovascular diseases and neurodegenerative diseases associated with vascular dysfunction (Lu, 2019).

Additionally, future work could examine the effects of other sources of noise that are known to influence fMRI signals, such as blood pressure fluctuations (Whittaker et al., 2019) and levels of CO_2 (Prokopiou et al., 2019; Wise et al., 2004), through data collection of targeted fMRI recordings with concurrent measurements of blood pressure and/or end-tidal CO_2 concentration. This line of research could help validate the notion that data-driven approaches correct for these confounds.

6.2.3 Future directions with respect to chapter 5

Chapter 5 examined the contributions of systemic and neural signals on global fMRI fluctuations, as well as the effect of GSR on whole-brain functional connectivity profiles related to EEG activity. Specifically, we examined electrophysiological activity associated

with delta, theta, alpha and beta power fluctuations. Alpha activity was particularly relevant to the study as it is related to arousal (Cantero Lorente et al., 1999) and global signal variations have been attributed to changes in vigilance levels (C. W. Wong et al., 2016; Wong et al., 2013). Nonetheless, it would be worth exploring whether more direct measures of arousal (e.g. electrodermal activity, eye tracking) could provide a better insight into the contributions of arousal on global fMRI fluctuations, following landmark work in macaque monkeys (Chang et al., 2016). Furthermore, additional physiological measures that are known to explain a fraction of the global fMRI signal should be taken into consideration in future studies, such as finger skin vascular tone based on PPG amplitude (Özbay et al., 2019).

Moreover, the proposed framework could be used to assess the effects of GSR in the context of other behavioral tasks (e.g. auditory), in order to inform future studies about the validity of applying GSR when studying a different neural substrate than the one evaluated in the present work (i.e. a motor paradigm).

Finally, we used a canonical HRF to model neurovascular coupling. However, the dynamics of the HRF may be different during resting-state conditions, as recent investigations seem to point towards a faster HRF at rest (Chen and Glover, 2015). Future research could entail constructing scan- and/or task-specific HRFs to model the link between neural activity and the BOLD signal, and test whether this would lead to a larger contribution of neural activity on global fMRI fluctuations.

List of publications

A full list of my journal, conference and abstract publications during my PhD studies is provided below:

Journal publications

- Botvinik-Nezer, R., Holzmeister, F., Camerer, C. F. [and 194 others, including Xifra-Porxas, A.] (2020). Variability in the analysis of a single neuroimaging dataset by many groups. Nature. https://doi.org/10.1038/s41586-020-2314-9
- Xifra-Porxas, A., Niso, G., Larivière, S., Kassinopoulos, M., Baillet, S., Mitsis, G.D., Boudrias, MH. (2019). Older adults exhibit a more pronounced modulation of beta oscillations when performing sustained and dynamic handgrips. NeuroImage 201, 116037. https://doi.org/10.1016/j.neuroimage.2019.116037
- Larivière, S., Xifra-Porxas, A., Kassinopoulos, M., Niso, G., Baillet, S., Mitsis, G.D., Boudrias, MH. (2019). Functional and effective reorganization of the aging brain during unimanual and bimanual hand movements. Human Brain Mapping 40, 3027–3040. https://doi.org/10.1002/hbm.24578

Preprints, under review, in preparation:

- Xifra-Porxas*, A., Kassinopoulos*, M., Mitsis, G.D. (under review). Physiological and head motion signatures in static and time-varying functional connectivity and their subject discriminability. * equal contribution. *Available in bioRxiv*: https://doi.org/10.1101/2020.02.04.934554
- Xifra-Porxas*, A., Ghosh*, A., Mitsis, G.D., Boudrias, MH. (under review). Biological brain age prediction using structural MRI and MEG recordings: Insights from dimensionality reduction techniques. * equal contribution. *Available in bioRxiv*: https://doi.org/10.1101/859660
- Xifra-Porxas, A., Kassinopoulos, M., Prokopiou, P., Boudrias, MH., Mitsis, G.D. (in preparation). Does global signal regression alter fMRI connectivity patterns related to EEG activity? A simultaneous EEG-fMRI study in humans.
- Prokopiou, P., Xifra-Porxas, A., Kassinopoulos, M., Boudrias, MH., Mitsis, G.D. (under review). Modeling the hemodynamic response function using EEG-fMRI data during eyes-open resting-state conditions and motor task execution. *Available in bioRxiv*: https://doi.org/10.1101/2020.06.29.178483

- Prokopiou, P., Kassinopoulos, M., Xifra-Porxas, A., Boudrias, MH., Mitsis, G.D. (in preparation). Modeling the hemodynamic response function using simultaneous EEG-fMRI data and convolutional sparse coding analysis with rank-1 constraints.

Conference publications

- Xifra-Porxas, A., Kostoglou, K., Larivière, S., Niso, G., Kassinopoulos, M., Boudrias, MH., Mitsis, G.D. (2018). Identification of time-varying cortico-cortical and cortico-muscular coherence during motor tasks with multivariate autoregressive models. IEEE EMBC. https://doi.org/10.1109/EMBC.2018.8512475

Conference abstracts

OHBM – Organization for Human Brain Mapping
ISMRM – International Society for Magnetic Resonance in Medicine

- Xifra-Porxas, A., Kassinopoulos, M., Mitsis, G.D. (2020). Physiological and motion signatures in functional connectivity and their subject discriminability. OHBM
- Xifra-Porxas, A., Kassinopoulos, M., Prokopiou, P., Boudrias, MH., Mitsis, G.D. (2020). Does global signal regression remove alpha power fluctuations? An EEG-fMRI study in humans at rest. OHBM
- Kassinopoulos, M., Xifra-Porxas, A., Mitsis, G.D. (2020). Transient increases in heart rate during resting-state fMRI and their association to peaks in DVARS. OHBM
- Prokopiou, P., Kassinopoulos, M., Xifra-Porxas, A., Boudrias, MH., Mitsis, G.D. (2020). Lower amplitude BOLD signal peaks drive resting-state functional connectivity. OHBM
- Xifra-Porxas, A., Kassinopoulos, M., Mitsis, G.D. (2019). Association between physiological processes and time-varying resting-state functional connectivity. OHBM
- Ghosh, A., Xifra-Porxas, A., Mitsis, G.D., Boudrias, MH. (2019). Combining structural MRI images and MEG recordings for biological brain age prediction. OHBM
- Prokopiou, P., Xifra-Porxas, A., Kassinopoulos, M., Boudrias, MH., Mitsis, G.D. (2019). Estimating hemodynamic response functions using motor task and resting-state EEG-fMRI data acquired during wakefulness with eyes open. ISMRM
- Ghosh, A., Xifra-Porxas, A., Mitsis, G.D., Boudrias, MH. (2019). Biological brain age prediction using structural MRI: Insights from dimensionality reduction techniques. ISMRM
- Kassinopoulos, M., Xifra-Porxas, A., Prokopiou, P., Boudrias, MH., Mitsis, G.D. (2018). Physiological noise correction improves the reproducibility of the DMN spatial pattern. Resting State and Brain Connectivity

- Prokopiou, P., Kassinopoulos, M., Xifra-Porxas, A., Boudrias, MH., Mitsis, G.D. (2018). Estimating hemodynamic response functions using resting-state EEG-fMRI data acquired during wakefulness with eyes open. Resting State and Brain Connectivity
- Larivière, S., Xifra-Porxas, A., Niso, G., Kassinopoulos, M., Mitsis, G.D., Boudrias, MH. (2017). Motor-Task Induced Changes in Resting-State MEG Networks in Healthy Aging. OHBM
- Xifra-Porxas, A., Larivière, S., Kostoglou, K., Kassinopoulos, M., Niso, G., Boudrias, MH., Mitsis, G.D. (2017). Cortico-cortical and Cortico-muscular Coherence using Time-varying Multivariate Autoregressive Models. OHBM

Bibliography

Aguirre, G.K., Zarahn, E., Esposito, M.D., 1998. The Inferential Impact of Global Signal Covariates in Functional Neuroimaging Analyses. Neuroimage 306, 1–5.

Ahlfors, S.P., Han, J., Lin, F.H., Witzel, T., Belliveau, J.W., Hämäläinen, M.S., Halgren, E., 2010. Cancellation of EEG and MEG signals generated by extended and distributed sources. Hum. Brain Mapp. 31, 140–149. https://doi.org/10.1002/hbm.20851

Aine, C.J., Woodruff, C.C., Knoefel, J.E., Adair, J.C., Hudson, D., Qualls, C., Bockholt, J., Best, E., Kovacevic, S., Cobb, W., Padilla, D., Hart, B., Stephen, J.M., 2006. Aging: Compensation or maturation? Neuroimage 32, 1891–1904. https://doi.org/10.1016/j.neuroimage.2006.05.005

Alegre, M., De Gurtubay, I.G., Labarga, A., Iriarte, J., Malanda, A., Artieda, J., 2004. Alpha and beta oscillatory activity during a sequence of two movements. Clin. Neurophysiol. 115, 124–130. https://doi.org/10.1016/S1388-2457(03)00311-0

Alegre, M., Gurtubay, I.G., Labarga, A., Iriarte, J., Malanda, A., Artieda, J., 2003. Alpha and beta oscillatory changes during stimulus-induced movement paradigms: effect of stimulus predictability. Neuroreport 14, 381–5. https://doi.org/10.1097/01.wnr.0000059624.96928.c0

Allen, E.A., Damaraju, E., Plis, S.M., Erhardt, E.B., Eichele, T., Calhoun, V.D., 2014. Tracking whole-brain connectivity dynamics in the resting state. Cereb. Cortex 24, 663–676. https://doi.org/10.1093/cercor/bhs352

Allen, P.J., Polizzi, G., Krakow, K., Fish, D.R., Lemieux, L., 1998. Identification of EEG events in the MR scanner: The problem of pulse artifact and a method for its subtraction. Neuroimage 8, 229–239. https://doi.org/10.1006/nimg.1998.0361

Alvares, G.A., Quintana, D.S., Hickie, I.B., Guastella, A.J., 2016. Autonomic nervous system dysfunction in psychiatric disorders and the impact of psychotropic medications: A systematic review and meta-analysis. J. Psychiatry Neurosci. 41, 89–104. https://doi.org/10.1503/jpn.140217

Andersen, L.M., Jerbi, K., Dalal, S.S., 2020. Can EEG and MEG detect signals from the human cerebellum? Neuroimage 215, 116817. https://doi.org/10.1016/j.neuroimage.2020.116817

Androulidakis, A.G., Doyle, L.M.F., Gilbertson, T.P., Brown, P., 2006. Corrective movements in response to displacements in visual feedback are more effective during periods of 13-35 Hz oscillatory synchrony in the human corticospinal system. Eur. J. Neurosci. 24, 3299–3304. https://doi.org/10.1111/j.1460-9568.2006.05201.x

Androulidakis, A.G., Doyle, L.M.F., Yarrow, K., Litvak, V., Gilbertson, T.P., Brown, P., 2007. Anticipatory changes in beta synchrony in the human corticospinal system and associated improvements in task performance. Eur. J. Neurosci. 25, 3758–3765. https://doi.org/10.1111/j.1460-9568.2007.05620.x

Aquino, K.M., Fulcher, B.D., Parkes, L., Sabaroedin, K., Fornito, A., 2020. Identifying and removing widespread signal deflections from fMRI data: Rethinking the global signal regression problem. Neuroimage 212, 116614. https://doi.org/10.1016/j.neuroimage.2020.116614

Babiloni, F., Astolfi, L., 2014. Social neuroscience and hyperscanning techniques: Past, present and future. Neurosci. Biobehav. Rev. 44, 76–93. https://doi.org/10.1016/j.neubiorev.2012.07.006

Baillet, S., 2017. Magnetoencephalography for brain electrophysiology and imaging. Nat. Neurosci. 20, 327–339. https://doi.org/10.1038/nn.4504

Baillet, S., 2015. Forward and Inverse Problems of MEG-EEG. Encycl. Comput. Neurosci.

Baillet, S., Mosher, J.C., Leahy, R.M., 2001. Electromagnetic brain mapping. IEEE Signal Process. Mag.

Baker, A.P., Brookes, M.J., Rezek, I.A., Smith, S.M., Behrens, T., Smith, P.J.P., Woolrich, M., 2014. Fast transient networks in spontaneous human brain activity. Elife 2014, 1–18. https://doi.org/10.7554/eLife.01867

Baker, J.T., Holmes, A.J., Masters, G.A., Yeo, B.T.T., Krienen, F., Buckner, R.L., Ongür, D., 2014. Disruption of cortical association networks in schizophrenia and psychotic bipolar disorder. JAMA Psychiatry 71, 109–118. https://doi.org/10.1001/jamapsychiatry.2013.3469

Baker, S.N., 2007. Oscillatory interactions between sensorimotor cortex and the periphery. Curr. Opin. Neurobiol. 17, 649–655. https://doi.org/10.1016/j.conb.2008.01.007

Bandettini, P.A., Wong, E.C., Hinks, R.S., Tikofsky, R.S., Hyde, J.S., 1992. Time course EPI during task activation. Magn Res Med 25, 390–397.

Bardouille, T., Bailey, L., CamCAN Group, 2019. Evidence for age-related changes in sensorimotor neuromagnetic responses during cued button pressing in a large open-access dataset. Neuroimage 193, 25–34. https://doi.org/10.1016/j.neuroimage.2019.02.065

Batchvarov, V.N., Ghuran, A., Smetana, P., Hnatkova, K., Harries, M., Dilaveris, P., Camm, A.J., Malik, M., 2002. QT-RR relationship in healthy subjects exhibits substantial intersubject variability and high intrasubject stability. Am. J. Physiol. - Hear. Circ. Physiol. 282, 2356–2363. https://doi.org/10.1152/ajpheart.00860.2001

Battaglia, D., Thomas, B., Hansen, E.C., Chettouf, S., Daffertshofer, A., McIntosh, A.R., Zimmermann, J., Ritter, P., Jirsa, V., 2017. Functional Connectivity Dynamics of the Resting State across the Human Adult Lifespan. bioRxiv 107243. https://doi.org/10.1101/107243

Behzadi, Y., Restom, K., Liau, J., Liu, T.T., 2007. A component based noise correction method (CompCor) for BOLD and perfusion based fMRI. Neuroimage 37, 90–101. https://doi.org/10.1016/j.neuroimage.2007.04.042

Benjamin, B.R., Valstad, M., Elvsåshagen, T., Jönsson, E.G., Moberget, T., Winterton, A., Haram, M., Høegh, M.C., Lagerberg, T. V., Steen, N.E., Larsen, L., Andreassen, O.A., Westlye, L.T., Quintana, D.S., 2020. Reduced heart rate variability is associated with disease severity in psychosis spectrum disorders. OSF Prepr. https://doi.org/10.31219/osf.io/upj3f

Berger, H., 1929. Über das elektrenkephalogramm des menschen. Eur. Arch. Psychiatry Clin. Neurosci. 87, 527–570.

Bernier, M., Cunnane, S.C., Whittingstall, K., 2018. The morphology of the human cerebrovascular system. Hum. Brain Mapp. 1–14. https://doi.org/10.1002/hbm.24337

Bijsterbosch, J.D., Woolrich, M.W., Glasser, M.F., Robinson, E.C., Beckmann, C.F., Van Essen, D.C., Harrison, S.J., Smith, S.M., 2018. The relationship between spatial configuration and functional connectivity of brain regions. Elife 7, 1–27. https://doi.org/10.7554/eLife.32992

Billings, J.C.W., Keilholz, S.D., 2018. The Not-So-Global BOLD Signal. Brain Connect. 8, brain.2017.0517. https://doi.org/10.1089/brain.2017.0517

Birn, R.M., Cornejo, M.D. aniel., Molloy, E.K., Patriat, R., Meier, T.B., Kirk, G.R., Nair, V.A., Meyerand, M.E., Prabhakaran, V., 2014. The influence of physiological noise correction on test-retest reliability of resting-state functional connectivity. Brain Connect. 4, 511–522. https://doi.org/10.1089/brain.2014.0284

Birn, R.M., Diamond, J.B., Smith, M.A., Bandettini, P.A., 2006. Separating respiratory-variation-related fluctuations from neuronal-activity-related fluctuations in fMRI. Neuroimage 31, 1536–1548. https://doi.org/10.1016/j.neuroimage.2006.02.048

Birn, R.M., Murphy, K., Bandettini, P.A., 2008a. The effect of respiration variations on independent component analysis results of resting state functional connectivity. Hum. Brain Mapp. 29, 740–750. https://doi.org/10.1002/hbm.20577

Birn, R.M., Smith, M.A., Jones, T.B., Bandettini, P.A., 2008b. The respiration response function: The temporal dynamics of fMRI signal fluctuations related to changes in respiration. Neuroimage 40, 644–654. https://doi.org/10.1016/j.neuroimage.2007.11.059

Biswal, B., Yetkin, F.Z., Haughton, V.M., Hyde, J.S., 1995. Functional connectivity in the motor cortex of resting human brain using echo-planar MRI. Magn. Reson. Med. https://doi.org/10.1002/mrm.1910340409

Bohannon, R.W., Peolsson, A., Massy-Westropp, N., Desrosiers, J., Bear-Lehman, J., 2006. Reference values for adult grip strength measured with a Jamar dynamometer: a descriptive meta-analysis. Physiotherapy 92, 11–15. https://doi.org/10.1016/j.physio.2005.05.003

Bonaiuto, J.J., Meyer, S.S., Little, S., Rossiter, H., Callaghan, M.F., Dick, F., Barnes, G.R., Bestmann, S., 2018. Laminar-specific cortical dynamics in human visual and sensorimotor cortices. Elife 226274. https://doi.org/10.1101/226274

Bonnet, M.H., Arand, D.L., 1997. Heart rate variability: Sleep stage, time of night, and arousal influences. Electroencephalogr. Clin. Neurophysiol. 102, 390–396. https://doi.org/10.1016/S0921-884X(96)96070-1

Bookheimer, S.Y., Salat, D.H., Terpstra, M., Ances, B.M., Barch, D.M., Buckner, R.L., Burgess, G.C., Curtiss, S.W., Diaz-Santos, M., Elam, J.S., Fischl, B., Greve, D.N., Hagy, H.A., Harms, M.P., Hatch, O.M., Hedden, T., Hodge, C., Japardi, K.C., Kuhn, T.P., Ly, T.K., Smith, S.M., Somerville, L.H., Uğurbil, K., van der Kouwe, A., Van Essen, D., Woods, R.P., Yacoub, E., 2019. The Lifespan Human Connectome Project in Aging: An overview. Neuroimage 185, 335–348. https://doi.org/10.1016/j.neuroimage.2018.10.009

Borg, G.., 1982. Psychophysical bases of perceived exertion. Med. Sci. Sports Exerc. 14, 377–381. https://doi.org/10.1249/00005768-198205000-00012

Bowman, A.D., Griffis, J.C., Visscher, K.M., Dobbins, A.C., Gawne, T.J., DiFrancesco, M.W., Szaflarski, J.P., 2017. Relationship Between Alpha Rhythm and the Default Mode Network. J. Clin. Neurophysiol. 34, 527–533. https://doi.org/10.1097/WNP.0000000000000411

Box, G.E.P., Cox, D.R., 1964. An Analysis of Transformations. J. R. Stat. Soc. Ser. B 26, 211–256.

Braitenberg, V., 1974. Thoughts on the cerebral cortex. J. Theor. Biol. 46, 421–447. https://doi.org/10.1016/0022-5193(74)90007-1

Braun, A.R., Balkin, T.J., Wesensten, N.J., Carson, R.E., Varga, M., Baldwin, P., Selbie, S., Belenky, G., Herscovitch, P., 1997. Regional cerebral blood flow throughout the sleep-wake cycle. An H215O PET study. Brain 120, 1173–1197. https://doi.org/10.1093/brain/120.7.1173

Brennan, B.P., Wang, D., Li, M., Perriello, C., Ren, J., Elias, J.A., Van Kirk, N.P., Krompinger, J.W., Pope, H.G., Haber, S.N., Rauch, S.L., Baker, J.T., Liu, H., 2019. Use of an Individual-Level Approach to Identify Cortical Connectivity Biomarkers in Obsessive-Compulsive Disorder. Biol. Psychiatry Cogn. Neurosci. Neuroimaging 4, 27–38. https://doi.org/10.1016/j.bpsc.2018.07.014

Bright, M.G., Murphy, K., 2015. Is fMRI "noise" really noise? Resting state nuisance regressors remove variance with network structure. Neuroimage 114, 158–169. https://doi.org/10.1016/j.neuroimage.2015.03.070

Bright, M.G., Tench, C.R., Murphy, K., 2017. Potential pitfalls when denoising resting state fMRI data using nuisance regression. Neuroimage 154, 159–168. https://doi.org/10.1016/j.neuroimage.2016.12.027

Bright, M.G., Whittaker, J.R., Driver, I.D., Murphy, K., 2018. Vascular physiology drives functional brain networks. bioRxiv 475491. https://doi.org/10.1101/475491

Brookes, M.J., Hale, J.R., Zumer, J.M., Stevenson, C.M., Francis, S.T., Barnes, G.R., Owen, J.P., Morris, P.G., Nagarajan, S.S., 2011. Measuring functional connectivity using MEG: Methodology and comparison with fcMRI. Neuroimage 56, 1082–1104. https://doi.org/10.1016/j.neuroimage.2011.02.054

Brosch, J.R., Talavage, T.M., Ulmer, J.L., Nyenhuis, J.A., 2002. Simulation of human respiration in fMRI with a

mechanical model. IEEE Trans. Biomed. Eng. 49, 700–707. https://doi.org/10.1109/TBME.2002.1010854

Brown, P., Oliviero, A., Mazzone, P., Insola, A., Tonali, P., Di Lazzaro, V., 2001. Dopamine dependency of oscillations between subthalamic nucleus and pallidum in Parkinson's disease. J. Neurosci. 21, 1033–1038. https://doi.org/21/3/1033 [pii]

Burgess, G.C., Kandala, S., Nolan, D., Laumann, T.O., Power, J.D., Adeyemo, B., Harms, M.P., Petersen, S.E., Barch, D.M., 2016a. Evaluation of Denoising Strategies to Address Motion-Correlated Artifacts in Resting-State Functional Magnetic Resonance Imaging Data from the Human Connectome Project. Brain Connect. 6, 669–680. https://doi.org/10.1089/brain.2016.0435

Burgess, G.C., Kandala, S., Nolan, D., Laumann, T.O., Power, J.D., Adeyemo, B., Harms, M.P., Petersen, S.E., Barch, D.M., 2016b. Evaluation of Denoising Strategies to Address Motion-Correlated Artifacts in Resting-State Functional Magnetic Resonance Imaging Data from the Human Connectome Project. Brain Connect. 6, 669–680. https://doi.org/10.1089/brain.2016.0435

Butler, R., Bernier, P.-M., Lefebvre, J., Gilbert, G., Whittingstall, K., 2017. Decorrelated Input Dissociates Narrow Band γ Power and BOLD in Human Visual Cortex. J. Neurosci. 37, 5408–5418. https://doi.org/10.1523/JNEUROSCI.3938-16.2017

Buzsáki, G., Anastassiou, C.A., Koch, C., 2012. The origin of extracellular fields and currents-EEG, ECoG, LFP and spikes. Nat. Rev. Neurosci. 13, 407–420. https://doi.org/10.1038/nrn3241

Byrge, L., Kennedy, D.P., 2018. Identifying and characterizing systematic temporally-lagged BOLD artifacts. Neuroimage 171, 376–392. https://doi.org/10.1016/j.neuroimage.2017.12.082

Caballero-Gaudes, C., Reynolds, R.C., 2017. Methods for cleaning the BOLD fMRI signal. Neuroimage 154, 128–149. https://doi.org/10.1016/j.neuroimage.2016.12.018

Cantero Lorente, J.L., Atienza, M., Gómez, C.M., Salas, R.M., 1999. Spectral structure and brain mapping of human alpha activities in different arousal states. Neuropsychobiology 39, 110–116. https://doi.org/10.1159/000026569

Carbonell, F., Bellec, P., Shmuel, A., 2011. Global and System-Specific Resting-State fMRI Fluctuations Are Uncorrelated: Principal Component Analysis Reveals Anti-Correlated Networks. Brain Connect. 1, 496–510. https://doi.org/10.1089/brain.2011.0065

Cassim, F., Szurhaj, W., Sediri, H., Devos, D., Bourriez, J.L., Poirot, I., Derambure, P., Defebvre, L., Guieu, J.D., 2000. Brief and sustained movements: Differences in event-related (de)synchronization (ERD/ERS) patterns. Clin. Neurophysiol. 111, 2032–2039. https://doi.org/10.1016/S1388-2457(00)00455-7

Caton, R., 1875. The electric currents of the brain. Br Med J 2, 278. https://doi.org/10.1136/bmj.2.762.155

Cespón, J., Miniussi, C., Pellicciari, M.C., 2018. Interventional programmes to improve cognition during healthy and pathological ageing: Cortical modulations and evidence for brain plasticity. Ageing Res. Rev. 43, 81–98. https://doi.org/10.1016/j.arr.2018.03.001

Chan, M.Y., Park, D.C., Savalia, N.K., Petersen, S.E., Wig, G.S., 2014. Decreased segregation of brain systems across the healthy adult lifespan. Proc. Natl. Acad. Sci. 111, E4997–E5006. https://doi.org/10.1073/pnas.1415122111

Chang, C., Cunningham, J.P., Glover, G.H., 2009. Influence of heart rate on the BOLD signal: The cardiac response function. Neuroimage 44, 857–869. https://doi.org/10.1016/j.neuroimage.2008.09.029

Chang, C., Glover, G.H., 2010. Time-frequency dynamics of resting-state brain connectivity measured with fMRI. Neuroimage 50, 81–98. https://doi.org/10.1016/j.neuroimage.2009.12.011

Chang, C., Glover, G.H., 2009a. Effects of model-based physiological noise correction on default mode network anti-correlations and correlations. Neuroimage 47, 1448–1459.

https://doi.org/10.1016/j.neuroimage.2009.05.012

Chang, C., Glover, G.H., 2009b. Relationship between respiration, end-tidal CO2, and BOLD signals in resting-state fMRI. Neuroimage 47, 1381–1393. https://doi.org/10.1016/j.neuroimage.2009.04.048

Chang, C., Leopold, D.A., Schölvinck, M.L., Mandelkow, H., Picchioni, D., Liu, X., Ye, F.Q., Turchi, J.N., Duyn, J.H., 2016. Tracking brain arousal fluctuations with fMRI. Proc. Natl. Acad. Sci. 113, 4518–4523. https://doi.org/10.1073/pnas.1520613113

Chang, C., Metzger, C.D., Glover, G.H., Duyn, J.H., Heinze, H.J., Walter, M., 2013. Association between heart rate variability and fluctuations in resting-state functional connectivity. Neuroimage 68, 93–104. https://doi.org/10.1016/j.neuroimage.2012.11.038

Chang, C., Özbay, P.S., Zwart, J. de, Duyn, J.H., 2019. FMRI correlates of stimulus-triggered changes in systemic physiology. Annu. Meet. Organ. Hum. Brain Mapp. 1901.

Chatrian, G.E., Petersen, M.C., Lazarte, J.A., 1959. The blocking of the rolandic wicket rhythm and some central changes related to movement. Electroencephalogr. Clin. Neurophysiol. 11, 497–510. https://doi.org/10.1016/0013-4694(59)90048-3

Chen, Heng, Nomi, J.S., Uddin, L.Q., Duan, X., Chen, Huafu, 2017. Intrinsic functional connectivity variance and state-specific under-connectivity in autism. Hum. Brain Mapp. 38, 5740–5755. https://doi.org/10.1002/hbm.23764

Chen, J.E., Glover, G.H., 2015. BOLD fractional contribution to resting-state functional connectivity above 0.1Hz. Neuroimage 107, 207–218. https://doi.org/10.1016/j.neuroimage.2014.12.012

Chen, Jingyuan E., Lewis, L.D., Chang, C., Tian, Q., Fultz, N.E., Ohringer, N.A., Rosen, B.R., Polimeni, J.R., 2020. Resting-state "physiological networks." Neuroimage 213, 116707. https://doi.org/10.1016/j.neuroimage.2020.116707

Chen, Jingyuan E, Lewis, L.D., Chang, C., Tian, Q., Fultz, N.E., Ohringer, N.A., Rosen, B.R., Polimeni, J.R., 2020. Resting-state "physiological networks." Neuroimage 213, 116707. https://doi.org/10.1016/j.neuroimage.2020.116707

Chen, J.E., Polimeni, J.R., Bollmann, S., Glover, G.H., 2019. On the analysis of rapidly sampled fMRI data. Neuroimage 188, 807–820. https://doi.org/10.1016/j.neuroimage.2019.02.008

Cheyne, D.O., 2013. MEG studies of sensorimotor rhythms: A review. Exp. Neurol. 245, 27–39. https://doi.org/10.1016/j.expneurol.2012.08.030

Ciric, R., Rosen, A.F.G., Erus, G., Cieslak, M., Adebimpe, A., Cook, P.A., Bassett, D.S., Davatzikos, C., Wolf, D.H., Satterthwaite, T.D., 2018. Mitigating head motion artifact in functional connectivity MRI. Nat. Protoc. 13, 2801–2826. https://doi.org/10.1038/s41596-018-0065-y

Ciric, R., Wolf, D.H., Power, J.D., Roalf, D.R., Baum, G.L., Ruparel, K., Shinohara, R.T., Elliott, M.A., Eickho, S.B., Davatzikos, C., Gur, R.C., Gur, R.E., Bassett, D.S., 2017. Benchmarking of participant-level confound regression strategies for the control of motion artifact in studies of functional connectivity. Neuroimage 154, 174–187. https://doi.org/10.1016/j.neuroimage.2017.03.020

Cohen, D., 1972. Magnetoencephalography: Detection of the Brain's Electrical Activity with a Superconducting Magnetometer. Science (80-.). 175, 664–666.

Cohen, D., 1968. Magnetoencephalography: Evidence of Magnetic Fields Produced by Alpha-Rhythm Currents. Science (80-.). 161, 784–786.

Cole, M.W., Repovš, G., Anticevic, A., 2014. The frontoparietal control system: A central role in mental health. Neuroscientist 20, 652–664. https://doi.org/10.1177/1073858414525995

Cole, M.W., Reynolds, J.R., Power, J.D., Repovs, G., Anticevic, A., Braver, T.S., 2013. Multi-task connectivity

reveals flexible hubs for adaptive task control. Nat. Neurosci. 16, 1348–1355. https://doi.org/10.1038/nn.3470

Collins, C.E., Airey, D.C., Young, N.A., Leitch, D.B., Kaas, J.H., 2010. Neuron densities vary across and within cortical areas in primates. Proc. Natl. Acad. Sci. U. S. A. 107, 15927–15932. https://doi.org/10.1073/pnas.1010356107

Crowell, A.L., Ryapolova-Webb, E.S., Ostrem, J.L., Galifianakis, N.B., Shimamoto, S., Lim, D.A., Starr, P.A., 2012. Oscillations in sensorimotor cortex in movement disorders: An electrocorticography study. Brain 135, 615–630. https://doi.org/10.1093/brain/awr332

Dagli, M.S., Ingeholm, J.E., Haxby, J. V., 1999. Localization of cardiac-induced signal change in fMRI. Neuroimage 9, 407–415. https://doi.org/10.1006/nimg.1998.0424

Dal Maso, F., Desormeau, B., Boudrias, M.H., Roig, M., 2018. Acute cardiovascular exercise promotes functional changes in cortico-motor networks during the early stages of motor memory consolidation. Neuroimage 174, 380–392. https://doi.org/10.1016/j.neuroimage.2018.03.029

Dale, A.M., Fischl, B., Sereno, M.I., 1999. Cortical surface-based analysis: I. Segmentation and surface reconstruction. Neuroimage 9, 179–194. https://doi.org/10.1006/nimg.1998.0395

Dale, A.M., Sereno, M.I., 1993. Improved Localizadon of Cortical Activity by Combining EEG and MEG with MRI Cortical Surface Reconstruction: A Linear Approach. J. Cogn. Neurosci. 5, 162–176. https://doi.org/10.1162/jocn.1993.5.2.162

Damaraju, E., Allen, E.A., Belger, A., Ford, J.M., McEwen, S., Mathalon, D.H., Mueller, B.A., Pearlson, G.D., Potkin, S.G., Preda, A., Turner, J.A., Vaidya, J.G., Van Erp, T.G., Calhoun, V.D., 2014. Dynamic functional connectivity analysis reveals transient states of dysconnectivity in schizophrenia. NeuroImage Clin. 5, 298–308. https://doi.org/10.1016/j.nicl.2014.07.003

Demirtaş, M., Tornador, C., Falcón, C., López-Solà, M., Hernández-Ribas, R., Pujol, J., Menchón, J.M., Ritter, P., Cardoner, N., Soriano-Mas, C., Deco, G., 2016. Dynamic functional connectivity reveals altered variability in functional connectivity among patients with major depressive disorder. Hum. Brain Mapp. 37, 2918–2930. https://doi.org/10.1002/hbm.23215

Desrosiers, J., Hébert, R., Bravo, G., Dutil, E., 1995. The purdue pegboard test: Normative data for people aged 60 and Over. Disabil. Rehabil. 17, 217–224. https://doi.org/10.3109/09638289509166638

Dosenbach, N.U.F., Fair, D.A., Miezin, F.M., Cohen, A.L., Wenger, K.K., Dosenbach, R.A.T., Fox, M.D., Snyder, A.Z., Vincent, J.L., Raichle, M.E., Schlaggar, B.L., Petersen, S.E., 2007. Distinct brain networks for adaptive and stable task control in humans. Proc. Natl. Acad. Sci. 104, 11073–11078. https://doi.org/10.1073/pnas.0704320104

Drysdale, A.T., Grosenick, L., Downar, J., Dunlop, K., Mansouri, F., Meng, Y., Fetcho, R.N., Zebley, B., Oathes, D.J., Etkin, A., Schatzberg, A.F., Sudheimer, K., Keller, J., Mayberg, H.S., Gunning, F.M., Alexopoulos, G.S., Fox, M.D., Pascual-Leone, A., Voss, H.U., Casey, B.J., Dubin, M.J., Liston, C., 2017. Resting-state connectivity biomarkers define neurophysiological subtypes of depression. Nat. Med. 23, 28–38. https://doi.org/10.1038/nm.4246

Du, Y., Pearlson, G.D., Yu, Q., He, H., Lin, D., Sui, J., Wu, L., Calhoun, V.D., 2016. Interaction among subsystems within default mode network diminished in schizophrenia patients: A dynamic connectivity approach. Schizophr. Res. 170, 55–65. https://doi.org/10.1016/j.schres.2015.11.021

Duffy, F.H., Albert, M.S., McAnulty, G., Garvey, A.J., 1984. Age-related differences in brain electrical activity of healthy subjects. Ann. Neurol. 16, 430–438. https://doi.org/10.1002/ana.410160403

Duyn, J.H., Ozbay, P.S., Chang, C., Picchioni, D., 2020. Physiological changes in sleep that affect fMRI inference. Curr. Opin. Behav. Sci. 33, 42–50. https://doi.org/10.1016/j.cobeha.2019.12.007

Elvsåshagen, T., Mutsaerts, H.J., Zak, N., Norbom, L.B., Quraishi, S.H., Pedersen, P., Malt, U.F., Westlye, L.T., van

Someren, E.J., Bjørnerud, A., Groote, I.R., 2019. Cerebral blood flow changes after a day of wake, sleep, and sleep deprivation. Neuroimage 186, 497–509. https://doi.org/10.1016/j.neuroimage.2018.11.032

Engel, A.K., Fries, P., 2010. Beta-band oscillations-signalling the status quo? Curr. Opin. Neurobiol. 20, 156–165. https://doi.org/10.1016/j.conb.2010.02.015

Erbil, N., Ungan, P., 2007. Changes in the alpha and beta amplitudes of the central EEG during the onset, continuation, and offset of long-duration repetitive hand movements. Brain Res. 1169, 44–56. https://doi.org/10.1016/j.brainres.2007.07.014

Erdoğan, S.B., Tong, Y., Hocke, L.M., Lindsey, K.P., deB Frederick, B., 2016. Correcting for blood arrival time in global mean regression enhances functional connectivity analysis of resting state fMRI-BOLD signals. Front. Hum. Neurosci. 10, 1–22. https://doi.org/10.3389/fnhum.2016.00311

Espenhahn, S., de Berker, A.O., van Wijk, B.C.M., Rossiter, H.E., Ward, S., 2017. Movement-related beta oscillations show high intra-individual reliability. Neuroimage 147, 175–185. https://doi.org/10.1016/j.neuroimage.2016.12.025

Espenhahn, S., Rossiter, H.E., van Wijk, B.C., Redman, N., Rondina, J.M., Diedrichsen, J., Ward, N.S., 2020. Motor cortex beta oscillations reflect motor skill learning ability after stroke. medRxiv 1.

Espenhahn, S., van Wijk, B.C.M., Rossiter, H.E., de Berker, A.O., Redman, N.D., Rondina, J., Diedrichsen, J., Ward, N.S., 2019. Cortical beta oscillations are associated with motor performance following visuomotor learning. Neuroimage. https://doi.org/10.1016/j.neuroimage.2019.03.079

Espy, M., Matlashov, A., Volegov, P., 2013. SQUID-detected ultra-low field MRI. J. Magn. Reson. 229, 127–141. https://doi.org/10.1016/j.jmr.2013.02.009

Fair, D.A., Miranda-Dominguez, O., Snyder, A.Z., Perrone, A., Earl, E.A., Van, A.N., Koller, J.M., Feczko, E., Tisdall, M.D., van der Kouwe, A., Klein, R.L., Mirro, A.E., Hampton, J.M., Adeyemo, B., Laumann, T.O., Gratton, C., Greene, D.J., Schlaggar, B.L., Hagler, D., Watts, R., Garavan, H., Barch, D.M., Nigg, J.T., Petersen, S.E., Dale, A.M., Feldstein-Ewing, S.W., Nagel, B.J., Dosenbach, N.U.F., 2019. Correction of respiratory artifacts in MRI head motion estimates. Neuroimage 116400. https://doi.org/10.1016/j.neuroimage.2019.116400

Falahpour, M., Chang, C., Wong, C.W., Liu, T.T., 2018. Template-based prediction of vigilance fluctuations in resting-state fMRI. Neuroimage 174, 317–327. https://doi.org/10.1016/j.neuroimage.2018.03.012

Falahpour, M., Refai, H., Bodurka, J., 2013. Subject specific BOLD fMRI respiratory and cardiac response functions obtained from global signal. Neuroimage 72, 252–264. https://doi.org/10.1016/j.neuroimage.2013.01.050

Ferreira, L.K., Carolina, A., Regina, B., Kovacevic, N., Morais, G., Santos, P.P., Carneiro, C.D.G., Kerr, D.S., Jr, E.A., Mcintosh, A.R., Busatto, G.F., 2016. Aging Effects on Whole-Brain Functional Connectivity in Adults Free of Cognitive and Psychiatric Disorders. Cereb. Cortex 3851–3865. https://doi.org/10.1093/cercor/bhv190

Finn, E.S., Shen, X., Scheinost, D., Rosenberg, M.D., Huang, J., Chun, M.M., Papademetris, X., Constable, R.T., 2015. Functional connectome fingerprinting: Identifying individuals using patterns of brain connectivity. Nat. Neurosci. 18, 1664–1671. https://doi.org/10.1038/nn.4135

Fischl, B., Dale, A.M., 2000. Measuring the thickness of the human cerebral cortex from magnetic resonance images. Proc. Natl. Acad. Sci. 97, 11050–11055. https://doi.org/10.1073/pnas.200033797

Fischl, B., Liu, A., Dale, A.M., 2001. Automated manifold surgery: Constructing geometrically accurate and topologically correct models of the human cerebral cortex. IEEE Trans. Med. Imaging 20, 70–80. https://doi.org/10.1109/42.906426

Fischl, B., Salat, D.H., Busa, E., Albert, M., Dieterich, M., Haselgrove, C., Van Der Kouwe, A., Killiany, R., Kennedy, D., Klaveness, S., Montillo, A., Makris, N., Rosen, B., Dale, A.M., 2002. Whole brain segmentation: Automated labeling of neuroanatomical structures in the human brain. Neuron 33, 341–355.

https://doi.org/10.1016/S0896-6273(02)00569-X

Fischl, B., Sereno, M.I., Dale, A.M., 1999a. Cortical surface-based analysis: II. Inflation, flattening, and a surface-based coordinate system. Neuroimage 9, 195–207. https://doi.org/10.1006/nimg.1998.0396

Fischl, B., Sereno, M.I., Tootell, R.B.H., Dale, A.M., 1999b. High-resolution inter-subject averaging and a surface-based coordinate system. Hum. Brain Mapp. 8, 272–284. https://doi.org/10.1002/(SICI)1097-0193(1999)8

Fischl, B., Van Der Kouwe, A., Destrieux, C., Halgren, E., Ségonne, F., Salat, D.H., Busa, E., Seidman, L.J., Goldstein, J., Kennedy, D., Caviness, V., Makris, N., Rosen, B., Dale, A.M., 2004. Automatically Parcellating the Human Cerebral Cortex. Cereb. Cortex 14, 11–22. https://doi.org/10.1093/cercor/bhg087

Fjell, A.M., Westlye, L.T., Amlien, I., Espeseth, T., Reinvang, I., Raz, N., Agartz, I., Salat, D.H., Greve, D.N., Fischl, B., Dale, A.M., Walhovd, K.B., 2009. High consistency of regional cortical thinning in aging across multiple samples. Cereb. Cortex 19, 2001–2012. https://doi.org/10.1093/cercor/bhn232

Folstein, M.F., Folstein, S.E., McHugh, P.R., 1975. "Mini-mental state". A practical method for grading the cognitive state of patients for the clinician. J. psychiat. Res. 12, 189–198. https://doi.org/10.1016/0022-3956(75)90026-6

Fox, M.D., Raichle, M.E., 2007. Spontaneous fluctuations in brain activity observed with functional magnetic resonance imaging. Nat Rev Neurosci 8, 700–711. https://doi.org/10.1038/nrn2201

Fox, M.D., Snyder, A.Z., Vincent, J.L., Corbetta, M., Van Essen, D.C., Raichle, M.E., 2005. The human brain is intrinsically organized into dynamic, anticorrelated functional networks. Proc. Natl. Acad. Sci. U. S. A. 102, 9673–8. https://doi.org/10.1073/pnas.0504136102

Fox, M.D., Zhang, D., Snyder, A.Z., Raichle, M.E., 2009. The global signal and observed anticorrelated resting state brain networks. J. Neurophysiol. 101, 3270–83. https://doi.org/10.1152/jn.90777.2008

Friston, K.J., Williams, S., Howard, R., Frackowiak, R.S.J., Turner, R., 1996. Movement-related effects in fMRI time-series. Magn. Reson. Med. 35, 346–355. https://doi.org/10.1002/mrm.1910350312

Fry, A., Mullinger, K.J., O'Neill, G.C., Barratt, E.L., Morris, P.G., Bauer, M., Folland, J.P., Brookes, M.J., 2016. Modulation of post-movement beta rebound by contraction force and rate of force development. Hum. Brain Mapp. 37, 2493–2511. https://doi.org/10.1002/hbm.23189

Gaetz, W., Edgar, J.C., Wang, D.J., Roberts, T.P.L., 2011. Relating MEG measured motor cortical oscillations to resting γ-Aminobutyric acid (GABA) concentration. Neuroimage 55, 616–621. https://doi.org/10.1016/j.neuroimage.2010.12.077

Gaetz, W., MacDonald, M., Cheyne, D., Snead, O.C., 2010. Neuromagnetic imaging of movement-related cortical oscillations in children and adults: Age predicts post-movement beta rebound. Neuroimage 51, 792–807. https://doi.org/10.1016/j.neuroimage.2010.01.077

Geerligs, L., Renken, R.J., Saliasi, E., Maurits, N.M., Lorist, M.M., 2015. A Brain-Wide Study of Age-Related Changes in Functional Connectivity. Cereb. Cortex 25, 1987–1999. https://doi.org/10.1093/cercor/bhu012

Gilbertson, T., Lalo, E., Doyle, L., Di Lazzaro, V., Cioni, B., Brown, P., 2005. Existing Motor State Is Favored at the Expense of New Movement during 13-35 Hz Oscillatory Synchrony in the Human Corticospinal System. J. Neurosci. 25, 7771–7779. https://doi.org/10.1523/JNEUROSCI.1762-05.2005

Glasser, M.F., Coalson, T.S., Bijsterbosch, J.D., Harrison, S.J., Harms, M.P., Anticevic, A., Van Essen, D.C., Smith, S.M., 2018. Using temporal ICA to selectively remove global noise while preserving global signal in functional MRI data. Neuroimage 181, 692–717. https://doi.org/10.1016/j.neuroimage.2018.04.076

Glasser, M.F., Smith, S.M., Marcus, D.S., Andersson, J.L.R., Auerbach, E.J., Behrens, T.E.J., Coalson, T.S., Harms, M.P., Jenkinson, M., Moeller, S., Robinson, E.C., Sotiropoulos, S.N., Xu, J., Yacoub, E., Ugurbil, K., Van Essen,

D.C., 2016. The Human Connectome Project's neuroimaging approach. Nat. Neurosci. 19, 1175–87. https://doi.org/10.1038/nn.4361

Glasser, M.F., Sotiropoulos, S.N., Wilson, J.A., Coalson, T.S., Fischl, B., Andersson, J.L., Xu, J., Jbabdi, S., Webster, M., Polimeni, J.R., Van Essen, D.C., Jenkinson, M., 2013. The minimal preprocessing pipelines for the Human Connectome Project. Neuroimage 80, 105–124. https://doi.org/10.1016/j.neuroimage.2013.04.127

Glover, G.H., 2011. Overview of functional magnetic resonance imaging. Neurosurg. Clin. N. Am. 22, 133–139. https://doi.org/10.1016/j.nec.2010.11.001

Glover, G.H., Li, T., Ress, D., 2000. Image-Based Method for Retrospective Correction of Physiological Motion Effects in fMRI: RETROICOR. Magn. Reson. Med. 44, 162–167. https://doi.org/10.1002/1522-2594(200007)44:1<162::AID-MRM23>3.0.CO;2-E

Golestani, A.M., Chang, C., Kwinta, J.B., Khatamian, Y.B., Jean Chen, J., 2015. Mapping the end-tidal CO2 response function in the resting-state BOLD fMRI signal: Spatial specificity, test-retest reliability and effect of fMRI sampling rate. Neuroimage 104, 266–277. https://doi.org/10.1016/j.neuroimage.2014.10.031

Gómez, C., M Pérez-Macías, J., Poza, J., Fernández, A., Hornero, R., 2013. Spectral changes in spontaneous MEG activity across the lifespan. J. Neural Eng. 10. https://doi.org/10.1088/1741-2560/10/6/066006

Gonzalez-Castillo, J., Caballero-Gaudes, C., Topolski, N., Handwerker, D.A., Pereira, F., Bandettini, P.A., 2019. Imaging the spontaneous flow of thought: Distinct periods of cognition contribute to dynamic functional connectivity during rest. Neuroimage 202, 116129. https://doi.org/10.1016/j.neuroimage.2019.116129

Gordon, E.M., Laumann, T.O., Adeyemo, B., Huckins, J.F., Kelley, W.M., Petersen, S.E., 2016. Generation and Evaluation of a Cortical Area Parcellation from Resting-State Correlations. Cereb. Cortex 26, 288–303. https://doi.org/10.1093/cercor/bhu239

Gorgolewski, K.J., Lurie, D., Urchs, S., Kipping, J.A., Craddock, R.C., Milham, M.P., Margulies, D.S., Smallwood, J., 2014. A correspondence between individual differences in the brain's intrinsic functional architecture and the content and form of self-generated thoughts. PLoS One 9. https://doi.org/10.1371/journal.pone.0097176

Gotman, J., Kobayashi, E., Bagshaw, A.P., Bénar, C.G., Dubeau, F., 2006. Combining EEG and fMRI: A multimodal tool for epilepsy research. J. Magn. Reson. Imaging 23, 906–920. https://doi.org/10.1002/jmri.20577

Grady, C., 2012. The cognitive neuroscience of ageing. Nat. Rev. Neurosci. 13, 491–505. https://doi.org/10.1038/nrn3256

Gratton, C., Dworetsky, A., Coalson, R.S., Adeyemo, B., Laumann, T.O., Wig, G.S., Kong, T.S., Gratton, G., Fabiani, M., Barch, D.M., Tranel, D., Dominguez, O.M.-, Fair, D.A., Dosenbach, N.U.F., Snyder, A.Z., Perlmutter, J.S., Petersen, S.E., Campbell, M.C., 2020. Removal of high frequency contamination from motion estimates in single-band fMRI saves data without biasing functional connectivity. Neuroimage 116866. https://doi.org/10.1016/j.neuroimage.2020.116866

Gratton, C., Koller, J.M., Shannon, W., Greene, D.J., Maiti, B., Snyder, A.Z., Petersen, S.E., Perlmutter, J.S., Campbell, M.C., 2019a. Emergent Functional Network Effects in Parkinson Disease. Cereb. Cortex 29, 2509–2523. https://doi.org/10.1093/cercor/bhy121

Gratton, C., Kraus, B.T., Greene, D.J., Gordon, E.M., Laumann, T.O., Nelson, S.M., Dosenbach, N.U.F., Petersen, S.E., 2019b. Defining Individual-Specific Functional Neuroanatomy for Precision Psychiatry. Biol. Psychiatry. https://doi.org/10.1016/J.BIOPSYCH.2019.10.026

Gratton, C., Laumann, T.O., Nielsen, A.N., Greene, D.J., Gordon, E.M., Gilmore, A.W., Nelson, S.M., Coalson, R.S., Snyder, A.Z., Schlaggar, B.L., Dosenbach, N.U.F., Petersen, S.E., 2018. Functional Brain Networks Are Dominated by Stable Group and Individual Factors, Not Cognitive or Daily Variation. Neuron 439–452.

https://doi.org/10.1016/j.neuron.2018.03.035

Gratton, C., Neta, M., Sun, H., Ploran, E.J., Schlaggar, B.L., Wheeler, M.E., Petersen, S.E., Nelson, S.M., 2017. Distinct Stages of Moment-to-Moment Processing in the Cinguloopercular and Frontoparietal Networks. Cereb. Cortex 27, 2403–2417. https://doi.org/10.1093/cercor/bhw092

Grice, K.O., Vogel, K.A., Le, V., Mitchell, A., Muniz, S., Vollmer, M.A., 2003. Adult norms for a commercially available nine hole peg test for finger dexterity. Am. J. Occup. Ther. 57, 570–573. https://doi.org/10.5014/ajot.57.5.570

Griffanti, L., Salimi-Khorshidi, G., Beckmann, C.F., Auerbach, E.J., Douaud, G., Sexton, C.E., Zsoldos, E., Ebmeier, K.P., Filippini, N., Mackay, C.E., Moeller, S., Xu, J., Yacoub, E., Baselli, G., Ugurbil, K., Miller, K.L., Smith, S.M., 2014. ICA-based artefact removal and accelerated fMRI acquisition for improved resting state network imaging. Neuroimage 95, 232–247. https://doi.org/10.1016/j.neuroimage.2014.03.034

Gross, J., 2019. Magnetoencephalography in Cognitive Neuroscience: A Primer. Neuron 104, 189–204. https://doi.org/10.1016/j.neuron.2019.07.001

Gutierrez-Barragan, D., Basson, M.A., Panzeri, S., Gozzi, A., 2019. Infraslow State Fluctuations Govern Spontaneous fMRI Network Dynamics. Curr. Biol. 29, 2295-2306.e5. https://doi.org/10.1016/j.cub.2019.06.017

Hacker, C.D., Snyder, A.Z., Pahwa, M., Corbetta, M., Leuthardt, E.C., 2017. Frequency-specific electrophysiologic correlates of resting state fMRI networks. Neuroimage 149, 446–457. https://doi.org/10.1016/j.neuroimage.2017.01.054

Hahamy, A., Behrmann, M., Malach, R., 2015. The idiosyncratic brain: Distortion of spontaneous connectivity patterns in autism spectrum disorder. Nat. Neurosci. 18, 302–309. https://doi.org/10.1038/nn.3919

Hall, S.D., Barnes, G.R., Furlong, P.L., Seri, S., Hillebrand, A., 2010. Neuronal network pharmacodynamics of GABAergic modulation in the human cortex determined using pharmaco-magnetoencephalography. Hum. Brain Mapp. 31, 581–594. https://doi.org/10.1002/hbm.20889

Hall, S.D., Stanford, I.M., Yamawaki, N., McAllister, C.J., Rönnqvist, K.C., Woodhall, G.L., Furlong, P.L., 2011. The role of GABAergic modulation in motor function related neuronal network activity. Neuroimage 56, 1506–1510. https://doi.org/10.1016/j.neuroimage.2011.02.025

Hallquist, M.N., Hwang, K., Luna, B., 2013. The nuisance of nuisance regression: Spectral misspecification in a common approach to resting-state fMRI preprocessing reintroduces noise and obscures functional connectivity. Neuroimage 82, 208–225. https://doi.org/10.1016/j.neuroimage.2013.05.116

Hamalainen, M., Hari, R., Ilmoniemi, R.J., Knuutila, J., Lounasmaa, O. V., 1993. Magnetoencephalography theory, instrumentation, to noninvasive studies of the working human brain. Rev. Mod. Phys. 65, 413–497.

Han, X., Jovicich, J., Salat, D., van der Kouwe, A., Quinn, B., Czanner, S., Busa, E., Pacheco, J., Albert, M., Killiany, R., Maguire, P., Rosas, D., Makris, N., Dale, A., Dickerson, B., Fischl, B., 2006. Reliability of MRI-derived measurements of human cerebral cortical thickness: The effects of field strength, scanner upgrade and manufacturer. Neuroimage 32, 180–194. https://doi.org/10.1016/j.neuroimage.2006.02.051

Hansen, E.C.A., Battaglia, D., Spiegler, A., Deco, G., Jirsa, V.K., 2015. Functional connectivity dynamics: Modeling the switching behavior of the resting state. Neuroimage 105, 525–535. https://doi.org/10.1016/j.neuroimage.2014.11.001

Hari, R., Puce, A., 2017. MEG-EEG Primer. Oxford University Press.

He, B.J., Snyder, A.Z., Zempel, J.M., Smyth, M.D., Raichle, M.E., 2008. Electrophysiological correlates of the brain's intrinsic large-scale functional architecture. Proc. Natl. Acad. Sci. 105, 16039–16044. https://doi.org/10.1073/pnas.0807010105

Heinrichs-Graham, E., McDermott, T.J., Mills, M.S., Wiesman, A.I., Wang, Y.-P., Stephen, J.M., Calhoun, V.D.,

Wilson, T.W., 2018. The lifespan trajectory of neural oscillatory activity in the motor system. Dev. Cogn. Neurosci. 30, 159–168. https://doi.org/10.1016/j.dcn.2018.02.013

Heinrichs-Graham, E., Wilson, T.W., 2016. Is an absolute level of cortical beta suppression required for proper movement? Magnetoencephalographic evidence from healthy aging. Neuroimage 134, 514–521. https://doi.org/10.1016/j.neuroimage.2016.04.032

Heinrichs-Graham, E., Wilson, T.W., Santamaria, P.M., Heithoff, S.K., Torres-russotto, D., Hutter-saunders, J.A.L., Estes, K.A., Meza, J.L., Mosley, R.L., Gendelman, H.E., 2014. Neuromagnetic Evidence of Abnormal Movement-Related Beta Desynchronization in Parkinson' s Disease. Cereb. Cortex 24, 2669–2678. https://doi.org/10.1093/cercor/bht121

Heuninckx, S., Wenderoth, N., Swinnen, S.P., 2008. Systems Neuroplasticity in the Aging Brain: Recruiting Additional Neural Resources for Successful Motor Performance in Elderly Persons. J. Neurosci. 28, 91–99. https://doi.org/10.1523/JNEUROSCI.3300-07.2008

Hindriks, R., Adhikari, M.H., Murayama, Y., Ganzetti, M., Mantini, D., Logothetis, N.K., Deco, G., 2016. Can sliding-window correlations reveal dynamic functional connectivity in resting-state fMRI? Neuroimage 127, 242–256. https://doi.org/10.1016/j.neuroimage.2015.11.055

Hipp, J.F., Hawellek, D.J., Corbetta, M., Siegel, M., Engel, A.K., 2012. Large-scale cortical correlation structure of spontaneous oscillatory activity. Nat. Neurosci.

Hodkinson, D.J., O'Daly, O., Zunszain, P.A., Pariante, C.M., Lazurenko, V., Zelaya, F.O., Howard, M.A., Williams, S.C.R., 2014. Circadian and homeostatic modulation of functional connectivity and regional cerebral blood flow in humans under normal entrained conditions. J. Cereb. Blood Flow Metab. 34, 1493–1499. https://doi.org/10.1038/jcbfm.2014.109

Hogstrom, L.J., Westlye, L.T., Walhovd, K.B., Fjell, A.M., 2013. The structure of the cerebral cortex across adult life: Age-related patterns of surface area, thickness, and gyrification. Cereb. Cortex 23, 2521–2530. https://doi.org/10.1093/cercor/bhs231

Horien, C., Shen, X., Scheinost, D., Constable, R.T., 2019. The individual functional connectome is unique and stable over months to years. Neuroimage 189, 676–687. https://doi.org/10.1016/j.neuroimage.2019.02.002

Huang, M.X., Mosher, J.C., Leahy, R.M., 1999. A sensor-weighted overlapping-sphere head model and exhaustive head model comparison for MEG. Phys. Med. Biol. 44, 423–440. https://doi.org/10.1088/0031-9155/44/2/010

Hübner, L., Godde, B., Voelcker-Rehage, C., 2018a. Older adults reveal enhanced task-related beta power decreases during a force modulation task. Behav. Brain Res. 345, 104–113. https://doi.org/10.1016/j.bbr.2018.02.028

Hübner, L., Godde, B., Voelcker-Rehage, C., 2018b. Acute Exercise as an Intervention to Trigger Motor Performance and EEG Beta Activity in Older Adults. Neural Plast. 2018, 4756785. https://doi.org/10.1155/2018/4756785

Huck, J., Wanner, Y., Fan, A.P., Jäger, A.T., Grahl, S., Schneider, U., Villringer, A., Steele, C.J., Tardif, C.L., Bazin, P.L., Gauthier, C.J., 2019. High resolution atlas of the venous brain vasculature from 7 T quantitative susceptibility maps. Brain Struct. Funct. 224, 2467–2485. https://doi.org/10.1007/s00429-019-01919-4

Huettel, S.A., Song, A.W., McCarthy, G., 2014. Functional Magnetic Resonance Imaging, Third. ed. Oxford University Press.

Hunyadi, B., Woolrich, M.W., Quinn, A.J., Vidaurre, D., De Vos, M., 2019. A dynamic system of brain networks revealed by fast transient EEG fluctuations and their fMRI correlates. Neuroimage 185, 72–82. https://doi.org/10.1016/j.neuroimage.2018.09.082

Hutchison, R.M., Womelsdorf, T., Allen, E.A., Bandettini, P.A., Calhoun, V.D., Corbetta, M., Della Penna, S., Duyn, J.H., Glover, G.H., Gonzalez-Castillo, J., Handwerker, D.A., Keilholz, S., Kiviniemi, V., Leopold, D.A., de Pasquale, F., Sporns, O., Walter, M., Chang, C., 2013. Dynamic functional connectivity: Promise, issues, and interpretations. Neuroimage 80, 360–378. https://doi.org/10.1016/j.neuroimage.2013.05.079

Iadecola, C., 2017. The Neurovascular Unit Coming of Age: A Journey through Neurovascular Coupling in Health and Disease. Neuron 96, 17–42. https://doi.org/10.1016/j.neuron.2017.07.030

Jann, K., Dierks, T., Boesch, C., Kottlow, M., Strik, W., Koenig, T., 2009. BOLD correlates of EEG alpha phase-locking and the fMRI default mode network. Neuroimage 45, 903–916. https://doi.org/10.1016/j.neuroimage.2009.01.001

Jasper, H., Penfield, W., 1949. Electrocorticograms in man: Effect of voluntary movement upon the electrical activity of the precentral gyrus. Arch. Psychiatr. Nervenkr. 183, 163–174. https://doi.org/10.1007/BF01062488

Jenkinson, M., Beckmann, C.F., Behrens, T.E.J., Woolrich, M.W., Smith, S.M., 2012. FSL. Neuroimage 62, 782–790. https://doi.org/10.1016/j.neuroimage.2011.09.015

Jensen, O., Goel, P., Kopell, N., Pohja, M., Hari, R., Ermentrout, B., 2005. On the human sensorimotor-cortex beta rhythm : Sources and modeling. Neuroimage 26, 347–355. https://doi.org/10.1016/j.neuroimage.2005.02.008

Ji, J.L., Kulkarni, K., Repovš, G., Spronk, M., Cole, M.W., Anticevic, A., 2018. Mapping the human brain's cortical-subcortical functional network organization. Neuroimage 185, 35–57. https://doi.org/10.1016/j.neuroimage.2018.10.006

Jiang, C., Yi, L., Su, S., Shi, C., Long, X., Xie, G., Zhang, L., 2016. Diurnal variations in neural activity of healthy human brain decoded with resting-state blood oxygen level dependent fMRI. Front. Hum. Neurosci. 10, 1–9. https://doi.org/10.3389/fnhum.2016.00634

Jo, H.J., Saad, Z.S., Simmons, W.K., Milbury, L.A., Cox, R.W., 2010. Mapping sources of correlation in resting state FMRI, with artifact detection and removal. Neuroimage 52, 571–582. https://doi.org/10.1016/j.neuroimage.2010.04.246

Joundi, R.A., Jenkinson, N., Brittain, J.S., Aziz, T.Z., Brown, P., 2012. Driving oscillatory activity in the human cortex enhances motor performance. Curr. Biol. 22, 403–407. https://doi.org/10.1016/j.cub.2012.01.024

Jovicich, J., Czanner, S., Greve, D., Haley, E., Van Der Kouwe, A., Gollub, R., Kennedy, D., Schmitt, F., Brown, G., MacFall, J., Fischl, B., Dale, A., 2006. Reliability in multi-site structural MRI studies: Effects of gradient non-linearity correction on phantom and human data. Neuroimage 30, 436–443. https://doi.org/10.1016/j.neuroimage.2005.09.046

Jurkiewicz, M.T., Gaetz, W.C., Bostan, A.C., Cheyne, D., 2006. Post-movement beta rebound is generated in motor cortex: Evidence from neuromagnetic recordings. Neuroimage 32, 1281–1289. https://doi.org/10.1016/j.neuroimage.2006.06.005

Kassinopoulos, M., Mitsis, G.D., 2020. Physiological noise modeling in fMRI based on the pulsatile component of photoplethysmograph. bioRxiv. https://doi.org/10.1101/2020.06.01.128306

Kassinopoulos, M., Mitsis, G.D., 2019a. White Matter Denoising Improves the Identifiability of Large-Scale Networks and Reduces the Effects of Motion in fMRI Functional Connectivity. bioRxiv.

Kassinopoulos, M., Mitsis, G.D., 2019b. Identification of physiological response functions to correct for fluctuations in resting-state fMRI related to heart rate and respiration. Neuroimage 202. https://doi.org/10.1101/512855

Keller, C.J., Bickel, S., Honey, C.J., Groppe, D.M., Entz, L., Craddock, R.C., Lado, F.A., Kelly, C., Milham, M., Mehta, A.D., 2013. Neurophysiological investigation of spontaneous correlated and anticorrelated fluctuations

of the BOLD signal. J. Neurosci. 33, 6333–6342. https://doi.org/10.1523/JNEUROSCI.4837-12.2013

Kilavik, B.E., Zaepffel, M., Brovelli, A., MacKay, W.A., Riehle, A., 2013. The ups and downs of beta oscillations in sensorimotor cortex. Exp. Neurol. 245, 15–26. https://doi.org/10.1016/j.expneurol.2012.09.014

Kilner, J.M., Baker, S.N., Salenius, S., Jousmäki, V., Hari, R., Lemon, R.N., 1999. Task-dependent modulation of 15-30 Hz coherence between rectified EMGs from human hand and forearm muscles. J. Physiol. 516, 559–570. https://doi.org/10.1111/j.1469-7793.1999.0559v.x

Kilner, J.M., Salenius, S., Baker, S.N., Jackson, A., Hari, R., Lemon, R.N., 2003. Task-Dependent Modulations of Cortical Oscillatory Activity in Human Subjects during a Bimanual Precision Grip Task. Neuroimage 18, 67–73. https://doi.org/10.1006/nimg.2002.1322

Kondylis, E.D., Randazzo, M.J., Alhourani, A., Lipski, W.J., Wozny, T.A., Pandya, Y., Ghuman, A.S., Turner, R.S., Crammond, D.J., Richardson, R.M., 2016. Movement-related dynamics of cortical oscillations in Parkinson's disease and essential tremor. Brain 139, 2211–2223. https://doi.org/10.1093/brain/aww144

Koyama, K., Hirasawa, H., Okubo, Y., Karasawa, A., 1997. Quantitative EEG correlates of normal aging in the elderly. Clin Electroencephalogr 28, 160–165.

Krakow, K., Woermann, F.G., Symms, M.R., Allen, P.J., Lemieux, L., Barker, G.J., Duncan, J.S., Fish, D.R., 1999. EEG-triggered functional MRI of interictal epileptiform activity in patients with partial seizures. Brain 122, 1679–1688. https://doi.org/10.1093/brain/122.9.1679

Kucyi, A., 2018. Just a thought: How mind-wandering is represented in dynamic brain connectivity. Neuroimage 180, 505–514. https://doi.org/10.1016/j.neuroimage.2017.07.001

Kucyi, A., Davis, K.D., 2014. Dynamic functional connectivity of the default mode network tracks daydreaming. Neuroimage 100, 471–480. https://doi.org/10.1016/j.neuroimage.2014.06.044

Kucyi, A., Schrouff, J., Bickel, S., Foster, B.L., Shine, J.M., Parvizi, J., 2018. Intracranial electrophysiology reveals reproducible intrinsic functional connectivity within human brain networks. J. Neurosci. 38, 4230–4242. https://doi.org/10.1523/JNEUROSCI.0217-18.2018

Kuperberg, G.R., Broome, M.R., McGuire, P.K., David, A.S., Eddy, M., Ozawa, F., Goff, D., West, W.C., Williams, S.C.R., Kouwe, A.J.W. van der, Salat, D.H., Dale, A.M., Fischl, B., 2010. Regionally Localized Thinning of the Cerebral Cortex in Schizophrenia. Schizophrenia 60.

Lancaster, G., Iatsenko, D., Pidde, A., Ticcinelli, V., Stefanovska, A., 2018. Surrogate data for hypothesis testing of physical systems. Phys. Rep. 748, 1–60. https://doi.org/10.1016/j.physrep.2018.06.001

Laumann, T.O., Snyder, A.Z., Mitra, A., Gordon, E.M., Gratton, C., Adeyemo, B., Gilmore, A.W., Nelson, S.M., Berg, J.J., Greene, D.J., McCarthy, J.E., Tagliazucchi, E., Laufs, H., Schlaggar, B.L., Dosenbach, N.U.F., Petersen, S.E., 2017. On the Stability of BOLD fMRI Correlations. Cereb. Cortex 27, 4719–4732. https://doi.org/10.1093/cercor/bhw265

Lemieux, L., Salek-Haddadi, A., Lund, T.E., Laufs, H., Carmichael, D., 2007. Modelling large motion events in fMRI studies of patients with epilepsy. Magn. Reson. Imaging 25, 894–901. https://doi.org/10.1016/j.mri.2007.03.009

Li, J., Bolt, T., Bzdok, D., Nomi, J., Yeo, B.T.., Spreng, R.N., Uddin, L.Q., 2019a. Topography and behavioral relevance of the global signal in the human brain. Sci. Rep. 10, 1–5. https://doi.org/10.1038/s41598-019-50750-8

Li, J., Kong, R., Liégeois, R., Orban, C., Tan, Y., Sun, N., Holmes, A.J., Sabuncu, M.R., Ge, T., Yeo, B.T.T., 2019b. Global signal regression strengthens association between resting-state functional connectivity and behavior. Neuroimage 196, 126–141. https://doi.org/10.1016/j.neuroimage.2019.04.016

Lindstrom-Hazel, D.K., VanderVlies Veenstra, N., 2015. Examining the Purdue Pegboard Test for Occupational

Therapy Practice. Open J. Occup. Ther. 3. https://doi.org/10.15453/2168-6408.1178

Liu, L., Rosjat, N., Popovych, S., Wang, B.A., Yeldesbay, A., Toth, T.I., Viswanathan, S., Grefkes, C.B., Fink, G.R., Daun, S., 2017. Age-related changes in oscillatory power affect motor action. PLoS One 12, 1–19. https://doi.org/10.1371/journal.pone.0187911

Liu, T.T., Nalci, A., Falahpour, M., 2017. The global signal in fMRI: Nuisance or Information? Neuroimage 150, 213–229. https://doi.org/10.1016/j.neuroimage.2017.02.036

Liu, X., De Zwart, J.A., Schölvinck, M.L., Chang, C., Ye, F.Q., Leopold, D.A., Duyn, J.H., 2018. Subcortical evidence for a contribution of arousal to fMRI studies of brain activity. Nat. Commun. 9, 1–10. https://doi.org/10.1038/s41467-017-02815-3

Logan, J.M., Sanders, A.L., Snyder, A.Z., Morris, J.C., Buckner, R.L., 2002. Under-recruitment and nonselective recruitment: Dissociable neural mechanisms associated with aging. Neuron 33, 827–840. https://doi.org/10.1016/S0896-6273(02)00612-8

Logothetis, Nikos K, 2008. What we can do and what we cannot do with fMRI. Nature 453, 869–78. https://doi.org/10.1038/nature06976

Logothetis, Nikos K., 2008. What we can do and what we cannot do with fMRI. Nature 453, 869–878.

Logothetis, N.K., Pauls, J., Augath, M., Trinath, T., Oeltermann, A., 2001. Neurophysiological investigation of the basis of the fMRI signal. Nature 412, 150–157. https://doi.org/10.1038/35084005

Lopes da Silva, F., 2013. EEG and MEG: Relevance to neuroscience. Neuron 80, 1112–1128. https://doi.org/10.1016/j.neuron.2013.10.017

Lu, H., 2019. Physiological MRI of the brain: Emerging techniques and clinical applications. Neuroimage 187, 1–2. https://doi.org/10.1016/j.neuroimage.2018.08.047

Lurie, D.J., Kessler, D., Bassett, D.S., Betzel, R.F., Breakspear, M., Keilholz, S., Kucyi, A., Liégeois, R., Lindquist, M.A., McIntosh, A.R., Poldrack, R.A., Shine, J.M., Thompson, W.H., Bielczyk, N.Z., Douw20, L., Kraft, D., Miller, R.L., Muthuraman, M., Pasquini, L., Razi, A., Vidaurre, D., Xie, H., Calhoun, V.D., 2019. Questions and controversies in the study of time-varying functional connectivity in resting fMRI. Netw. Neurosci. https://doi.org/https://doi.org/10.1162/netn_a_00116

Lydon-Staley, D.M., Ciric, R., Satterthwaite, T.D., Basset, D.S., 2019. Evaluation of confound regression strategies for the mitigation of micromovement artifact in studies of dynamic resting-state functional connectivity and multilayer network modularity. Netw. Neurosci. 3, 427–454. https://doi.org/10.1162/netn

Macey, P.M., Macey, K.E., Kumar, R., Harper, R.M., 2004. A method for removal of global effects from fMRI time series. Neuroimage 22, 360–366. https://doi.org/10.1016/j.neuroimage.2003.12.042

Maes, C., Gooijers, J., Orban de Xivry, J.J., Swinnen, S.P., Boisgontier, M.P., 2017. Two hands, one brain, and aging. Neurosci. Biobehav. Rev. 75, 234–256. https://doi.org/10.1016/j.neubiorev.2017.01.052

Makowski, C., Lepage, M., Evans, A.C., 2019. Head motion: The dirty little secret of neuroimaging in psychiatry. J. Psychiatry Neurosci. 44, 62–68. https://doi.org/10.1503/jpn.180022

Malik, M., Hnatkova, K., Sisakova, M., Schmidt, G., 2008. Subject-specific heart rate dependency of electrocardiographic QT, PQ, and QRS intervals. J. Electrocardiol. 41, 491–497. https://doi.org/10.1016/j.jelectrocard.2008.06.022

Mantini, D., Perrucci, M.G., Cugini, S., Ferretti, A., Romani, G.L., Del Gratta, C., 2007. Complete artifact removal for EEG recorded during continuous fMRI using independent component analysis. Neuroimage 34, 598–607. https://doi.org/10.1016/j.neuroimage.2006.09.037

Mantini, D, Perrucci, M.G., Gratta, D., C., R., G.l, Corbetta, M., Del Gratta, C., Romani, G., 2007.

Electrophysiological signatures of resting state networks in the human brain. Proc. Natl. Acad. Sci. 104, 13170.

Marek, S., Siegel, J.S., Gordon, E.M., Raut, R. V., Gratton, C., Newbold, D.J., Ortega, M., Laumann, T.O., Miller, D.B., Zheng, A., Lopez, K.C., Berg, J.J., Coalson, R.S., Nguyen, A.L., Dierker, D., Van, A.N., Hoyt, C.R., McDermott, K.B., Norris, S.A., Shimony, J.S., Snyder, A.Z., Nelson, S.M., Barch, D.M., Schlaggar, B.L., Raichle, M.E., Petersen, S.E., Greene, D.J., Dosenbach, N.U.F., 2018. Spatial and Temporal Organization of the Individual Human Cerebellum. SSRN Electron. J. 100, 977-993.e7. https://doi.org/10.2139/ssrn.3188429

Mash, L.E., Linke, A.C., Olson, L.A., Fishman, I., Liu, T.T., Müller, R.A., 2019. Transient states of network connectivity are atypical in autism: A dynamic functional connectivity study. Hum. Brain Mapp. 40, 2377–2389. https://doi.org/10.1002/hbm.24529

Mathiowetz, V., Volland, G., Kashman, N., Weber, K., 1985a. Adult norms for the Box and Block Test of manual dexterity. Am. J. Occup. Ther. 39, 386–391. https://doi.org/10.5014/ajot.39.6.386

Mathiowetz, V., Weber, K., Kashman, N., Volland, G., 1985b. Adult Nonns For The Nine Hole Peg Test OfFinger Dexterity. Occup. Ther. J. Res. 5, 24–38.

Matsui, T., Murakami, T., Ohki, K., 2018. Neuronal Origin of the Temporal Dynamics of Spontaneous BOLD Activity Correlation. Cereb. Cortex 1–13. https://doi.org/10.1093/cercor/bhy045

Mattay, V.S., Fera, F., Tessitore, A., Hariri, A.R., Das, S., Callicott, J.H., 2002. Neurophysiological correlates of age-related changes in human. Neurology 58, 630–635. https://doi.org/10.1212/WNL.58.4.630

Mayhew, S.D., Bagshaw, A.P., 2017. Dynamic spatiotemporal variability of alpha-BOLD relationships during the resting-state and task-evoked responses. Neuroimage 155, 120–137. https://doi.org/10.1016/j.neuroimage.2017.04.051

Mayhew, S.D., Ostwald, D., Porcaro, C., Bagshaw, A.P., 2013. Spontaneous EEG alpha oscillation interacts with positive and negative BOLD responses in the visual-auditory cortices and default-mode network. Neuroimage 76, 362–372. https://doi.org/10.1016/j.neuroimage.2013.02.070

Minati, L., Grisoli, M., Bruzzone, M.G., 2007. MR spectroscopy, functional MRI, and diffusion-tensor imaging in the aging brain: A conceptual review. J. Geriatr. Psychiatry Neurol. 20, 3–21. https://doi.org/10.1177/0891988706297089

Mira-Dominguez, O., Mills, B.D., Carpenter, S.D., Grant, K.A., Kroenke, C.D., Nigg, J.T., Fair, D.A., 2014. Connectotyping: Model based fingerprinting of the functional connectome. PLoS One 9. https://doi.org/10.1371/journal.pone.0111048

Mo, J., Liu, Y., Huang, H., Ding, M., 2013. Coupling between visual alpha oscillations and default mode activity. Neuroimage 68, 112–118. https://doi.org/10.1016/j.neuroimage.2012.11.058

Moosmann, M., Ritter, P., Krastel, I., Brink, A., Thees, S., Blankenburg, F., Taskin, B., Obrig, H., Villringer, A., 2003. Correlates of alpha rhythm in functional magnetic resonance imaging and near infrared spectroscopy. Neuroimage 20, 145–158. https://doi.org/10.1016/S1053-8119(03)00344-6

Morcom, A.M., (Cam-CAN), C.C. for A. and N., Henson, R.N., 2018. Increased prefrontal activity with aging reflects nonspecific neural responses rather than compensation. J. Neurosci. 38, 7303–7313. https://doi.org/10.1101/156935

Morgan, V.L., Englot, D.J., Rogers, B.P., Landman, B.A., Cakir, A., Abou-Khalil, B.W., Anderson, A.W., 2017. Magnetic resonance imaging connectivity for the prediction of seizure outcome in temporal lobe epilepsy. Epilepsia 58, 1251–1260. https://doi.org/10.1111/epi.13762

Mueller, S., Wang, D., Fox, M.D., Yeo, B.T.T., Sepulcre, J., Sabuncu, M.R., Shafee, R., Lu, J., Liu, H., 2013. Individual Variability in Functional Connectivity Architecture of the Human Brain. Neuron 77, 586–595. https://doi.org/10.1016/j.neuron.2012.12.028

Mulert, C., Lemieux, L. (Eds.), 2010. EEG-fMRI: Physiological basis, techniques and applications. Springer.

Murphy, K., Birn, R.M., Handwerker, D.A., Jones, T.B., Bandettini, P.A., 2009. The impact of global signal regression on resting state correlations: Are anti-correlated networks introduced? Neuroimage 44, 893–905. https://doi.org/10.1016/j.neuroimage.2008.09.036

Murphy, K., Fox, M.D., 2017. Towards a consensus regarding global signal regression for resting state functional connectivity MRI. Neuroimage 154, 169–173. https://doi.org/10.1016/j.neuroimage.2016.11.052

Muschelli, J., Nebel, M.B., Caffo, B.S., Barber, A.D., Pekar, J.J., Mostofsky, S.H., 2014. Reduction of motion-related artifacts in resting state fMRI using aCompCor. Neuroimage 96, 22–35. https://doi.org/10.1016/j.neuroimage.2014.03.028

Muthukumaraswamy, S.D., Myers, J.F.M., Wilson, S.J., Nutt, D.J., Lingford-Hughes, A., Singh, K.D., Hamandi, K., 2013. The effects of elevated endogenous GABA levels on movement-related network oscillations. Neuroimage 66, 36–41. https://doi.org/10.1016/j.neuroimage.2012.10.054

Nalci, A., Rao, B.D., Liu, T.T., 2019. Nuisance effects and the limitations of nuisance regression in dynamic functional connectivity fMRI. Neuroimage 184, 1005–1031. https://doi.org/10.1016/j.neuroimage.2018.09.024

Nasiotis, K., Clavagnier, S., Baillet, S., Pack, C.C., 2017. High-resolution retinotopic maps estimated with magnetoencephalography. Neuroimage 145, 107–117. https://doi.org/10.1016/j.neuroimage.2016.10.017

Nikolaou, F., Orphanidou, C., Papakyriakou, P., Murphy, K., Wise, R.G., Mitsis, G.D., 2016a. Spontaneous physiological variability modulates dynamic functional connectivity in resting-state functional magnetic resonance imaging. Phil. Trans. R. Soc. A 374. https://doi.org/10.1098/rsta.2015.0183

Nikolaou, F., Orphanidou, C., Papakyriakou, P., Murphy, K., Wise, R.G., Mitsis, G.D., 2016b. Spontaneous physiological variability modulates dynamic functional connectivity in resting-state functional magnetic resonance imaging. Philos. Trans. R. Soc. A Math. Phys. Eng. Sci. 374, 20150183. https://doi.org/10.1098/rsta.2015.0183

Noble, S., Spann, M.N., Tokoglu, F., Shen, X., Constable, R.T., Scheinost, D., 2017. Influences on the Test-Retest Reliability of Functional Connectivity MRI and its Relationship with Behavioral Utility. Cereb. Cortex 27, 5415–5429. https://doi.org/10.1093/cercor/bhx230

Noll, D.C., Schneider, W., 1994. Theory, simulation, and compensation of physiological motion artifacts in functional MRI. Proc. - Int. Conf. Image Process. ICIP 3, 40–44. https://doi.org/10.1109/ICIP.1994.413892

O'Brien, I.A., O'Hare, P., Corrall, R.J.M., 1986. Heart rate variability in healthy subjects: Effect of age and the derivation of normal ranges for tests of autonomic function. Br. Heart J. 55, 348–354.

Ogawa, S., Lee, T.M., Kay, A.R., Tank, D.W., 1990. Brain magnetic resonance imaging with contrast dependent on blood oxygenation. Proc. Natl. Acad. Sci. USA 87, 9868–9872. https://doi.org/10.7566/JPSJ.84.064704

Okada, Y.C., Lahteenmäki, A., Xu, C., 1999. Experimental analysis of distortion of magnetoencephalography signals by the skull. Clin. Neurophysiol. 110, 230–238. https://doi.org/10.1016/S0013-4694(98)00099-6

Oken, B.S., Salinsky, M.C., Elsas, S.M., 2006. Vigilance, alertness, or sustained attention: physiological basis and measurement. Clin. Neurophysiol. 117, 1885–1901. https://doi.org/10.1016/j.clinph.2006.01.017

Olbrich, S., Sander, C., Matschinger, H., Mergl, R., Trenner, M., Schönknecht, P., Hegerl, U., 2011. Brain and body: Associations between EEG-vigilance and the autonomous nervous system activity during rest. J. Psychophysiol. 25, 190–200. https://doi.org/10.1027/0269-8803/a000061

Oldfield, R.C., 1971. The assessment and analysis of handedness: The Edinburgh inventory. Neuropsychologia 9, 97–113. https://doi.org/10.1016/0028-3932(71)90067-4

Omlor, W., Patino, L., Hepp-Reymond, M.C., Kristeva, R., 2007. Gamma-range corticomuscular coherence during dynamic force output. Neuroimage 34, 1191–1198. https://doi.org/10.1016/j.neuroimage.2006.10.018

Omlor, W., Patino, L., Mendez-Balbuena, I., Schulte-Monting, J., Kristeva, R., 2011. Corticospinal Beta-Range Coherence Is Highly Dependent on the Pre-stationary Motor State. J. Neurosci. 31, 8037–8045. https://doi.org/10.1523/JNEUROSCI.4153-10.2011

Orban, C., Kong, R., Li, J., Chee, M.W.L., Yeo, B.T.T., 2020. Time of day is associated with paradoxical reductions in global signal fluctuation and functional connectivity. PLOS Biol. 18, e3000602. https://doi.org/10.1371/journal.pbio.3000602

Özbay, P.S., Chang, C., Picchioni, D., Mandelkow, H., Chappel-Farley, M.G., van Gelderen, P., de Zwart, J.A., Duyn, J., 2019. Sympathetic activity contributes to the fMRI signal. Commun. Biol. 2, 1–9. https://doi.org/10.1038/s42003-019-0659-0

Parkes, L., Fulcher, B., Yücel, M., Fornito, A., 2018. An evaluation of the efficacy, reliability, and sensitivity of motion correction strategies for resting-state functional MRI. Neuroimage 171, 415–436. https://doi.org/10.1016/j.neuroimage.2017.12.073

Patriat, R., Molloy, E.K., Birn, R.M., 2015. Using Edge Voxel Information to Improve Motion Regression for rs-fMRI Connectivity Studies. Brain Connect. 5, 582–595. https://doi.org/10.1089/brain.2014.0321

Pauling, L., Coryell, C.D., 1936. The Magnetic Properties and Structure of Hemoglobin, Oxyhemoglobin and Carbonmonoxyhemoglobin. Proc. Natl. Acad. Sci. 22, 210–216. https://doi.org/10.1073/pnas.22.4.210

Pfurtscheller, G., Lopes da Silva, F.H., 1999. Event-related EEG / MEG synchronization and desynchronization : basic principles. Clin. Neurophysiol. 110, 1842–1857. https://doi.org/10.1016/S1388-2457(99)00141-8

Pinna, G.D., Maestri, R., Torunski, A., Danilowicz-Szymanowicz, L., Szwoch, M., La Rovere, M.T., Raczak, G., 2007. Heart rate variability measures: A fresh look at reliability. Clin. Sci. 113, 131–140. https://doi.org/10.1042/CS20070055

Pinto, J., Nunes, S., Bianciardi, M., Dias, A., Silveira, L.M., Wald, L.L., Figueiredo, P., 2017. Improved 7 Tesla resting-state fMRI connectivity measurements by cluster-based modeling of respiratory volume and heart rate effects. Neuroimage 153, 262–272. https://doi.org/10.1016/j.neuroimage.2017.04.009

Pitzalis, M.V., Mastropasqua, F., Massari, F., Forleo, C., Di Maggio, M., Passantino, A., Colombo, R., Di Biase, M., Rizzon, P., 1996. Short- and long-term reproducibility of time and frequency domain heart rate variability measurements in normal subjects. Cardiovasc. Res. 32, 226–233. https://doi.org/10.1016/0008-6363(96)00086-7

Pizzo, F., Roehri, N., Medina Villalon, S., Trébuchon, A., Chen, S., Lagarde, S., Carron, R., Gavaret, M., Giusiano, B., McGonigal, A., Bartolomei, F., Badier, J.M., Bénar, C.G., 2019. Deep brain activities can be detected with magnetoencephalography. Nat. Commun. 10, 1–13. https://doi.org/10.1038/s41467-019-08665-5

Pogosyan, A., Gaynor, L.D., Eusebio, A., Brown, P., 2009. Boosting Cortical Activity at Beta-Band Frequencies Slows Movement in Humans. Curr. Biol. 19, 1637–1641. https://doi.org/10.1016/j.cub.2009.07.074

Power, J.D., 2019. Temporal ICA has not properly separated global fMRI signals: A comment on Glasser et al. (2018). Neuroimage. https://doi.org/10.1016/j.neuroimage.2018.12.051

Power, J.D., Barnes, K.A., Snyder, A.Z., Schlaggar, B.L., Petersen, S.E., 2012. Spurious but systematic correlations in functional connectivity MRI networks arise from subject motion. Neuroimage 59, 2142–2154. https://doi.org/10.1016/j.neuroimage.2011.10.018

Power, J.D., Laumann, T.O., Plitt, M., Martin, A., Petersen, S.E., 2017a. On Global fMRI Signals and Simulations. Trends Cogn. Sci. 21, 911–913. https://doi.org/10.1016/j.tics.2017.09.002

Power, J.D., Lynch, C.J., Dubin, M.J., Silver, B.M., Martin, A., Jones, R.M., 2020. Characteristics of respiratory measures in young adults scanned at rest, including systematic changes and "missed" deep breaths. Neuroimage 204, 116234. https://doi.org/10.1016/j.neuroimage.2019.116234

Power, J.D., Mitra, A., Laumann, T.O., Snyder, A.Z., Schlaggar, B.L., Petersen, S.E., 2014a. Methods to detect, characterize, and remove motion artifact in resting state fMRI. Neuroimage 84, 320–341. https://doi.org/10.1016/j.neuroimage.2013.08.048

Power, J.D., Mitra, A., Laumann, T.O., Snyder, A.Z., Schlaggar, B.L., Petersen, S.E., 2014b. Methods to detect, characterize, and remove motion artifact in resting state fMRI. Neuroimage 84, 320–341. https://doi.org/10.1016/j.neuroimage.2013.08.048

Power, J.D., Plitt, M., Gotts, S.J., Kundu, P., Voon, V., Bandettini, P.A., Martin, A., 2018. Ridding fMRI data of motion-related influences: Removal of signals with distinct spatial and physical bases in multiecho data. Proc. Natl. Acad. Sci. U. S. A. 115, E2105–E2114. https://doi.org/10.1073/pnas.1720985115

Power, J.D., Plitt, M., Laumann, T.O., Martin, A., 2017b. Sources and implications of whole-brain fMRI signals in humans. Neuroimage 146, 609–625. https://doi.org/10.1016/j.neuroimage.2016.09.038

Power, J.D., Schlaggar, B.L., Petersen, S.E., 2015. Recent progress and outstanding issues in motion correction in resting state fMRI. Neuroimage 105, 536–551. https://doi.org/10.1016/j.neuroimage.2014.10.044

Power, J.D., Silver, B.M., Dubin, M.J., Martin, A., Jones, R.M., 2019. Distinctions among real and apparent respiratory motions in human fMRI data. Neuroimage 201. https://doi.org/10.1101/601286

Prokopiou, P.C., Pattinson, K.T.S., Wise, R.G., Mitsis, G.D., 2019. Modeling of dynamic cerebrovascular reactivity to spontaneous and externally induced CO2 fluctuations in the human brain using BOLD-fMRI. Neuroimage 186, 533–548. https://doi.org/10.1016/j.neuroimage.2018.10.084

Proudfoot, M., Rohenkohl, G., Quinn, A., Colclough, G.L., Wuu, J., Talbot, K., Woolrich, M.W., Benatar, M., Nobre, A.C., Turner, M.R., 2017. Altered cortical beta-band oscillations reflect motor system degeneration in amyotrophic lateral sclerosis. Hum. Brain Mapp. 38, 237–254. https://doi.org/10.1002/hbm.23357

Provencher, D., Hennebelle, M., Cunnane, S.C., Berube-Lauziere, Y., Whittingstall, K., 2016. Cortical thinning in healthy aging correlates with larger motor-evoked EEG desynchronization. Front. Aging Neurosci. 8, 1–8. https://doi.org/10.3389/fnagi.2016.00063

Pruim, R.H.R., Mennes, M., van Rooij, D., Llera, A., Buitelaar, J.K., Beckmann, C.F., 2015. ICA-AROMA: A robust ICA-based strategy for removing motion artifacts from fMRI data. Neuroimage 112, 267–277. https://doi.org/10.1016/j.neuroimage.2015.02.064

Quaegebeur, A., Lange, C., Carmeliet, P., 2011. The neurovascular link in health and disease: Molecular mechanisms and therapeutic implications. Neuron 71, 406–424. https://doi.org/10.1016/j.neuron.2011.07.013

Raichle, M.E., 2015. The Brain's Default Mode Network. Annu. Rev. Neurosci. 38, 433–447. https://doi.org/10.1146/annurev-neuro-071013-014030

Raj, D., Anderson, A.W., Gore, J.C., 2001. Respiratory effects in human functional magnetic resonance imaging due to bulk susceptibility changes. Phys. Med. Biol. 46, 3331–3340. https://doi.org/10.1088/0031-9155/46/12/318

Raj, D., Paey, D.P., Anderson, A.W., Kennan, R.P., Gore, J.C., 2000. A model for susceptibility artefacts from respiration in functional echo-planar magnetic resonance imaging. Phys. Med. Biol. 45, 3809–3820. https://doi.org/10.1088/0031-9155/45/12/321

Reland, S., Ville, N.S., Wong, S., Carrault, G., Carré, F., 2005. Reliability of heart rate variability in healthy older

women at rest and during orthostatic testing. Aging Clin. Exp. Res. 17, 316–321. https://doi.org/10.1007/BF03324616

Reuter-Lorenz, P.A., Park, D.C., 2010. Human Neuroscience and the Aging Mind : A New Look at Old Problems. J. Gerontol. Psychol. Sci. 65B, 405–415. https://doi.org/10.1093/geronb/gbq035.

Reuter, M., Rosas, H.D., Fischl, B., 2010. Highly accurate inverse consistent registration: A robust approach. Neuroimage 53, 1181–1196. https://doi.org/10.1016/j.neuroimage.2010.07.020

Reuter, M., Schmansky, N.J., Rosas, H.D., Fischl, B., 2012. Within-subject template estimation for unbiased longitudinal image analysis. Neuroimage 61, 1402–1418. https://doi.org/10.1016/j.neuroimage.2012.02.084

Riecker, A., Gröschel, K., Ackermann, H., Steinbrink, C., Witte, O., Kastrup, A., 2006. Functional significance of age-related differences in motor activation patterns. Neuroimage 32, 1345–1354. https://doi.org/10.1016/j.neuroimage.2006.05.021

Robinson, E.C., Jbabdi, S., Glasser, M.F., Andersson, J., Burgess, G.C., Harms, M.P., Smith, S.M., Van Essen, D.C., Jenkinson, M., 2014. MSM: A new flexible framework for multimodal surface matching. Neuroimage 100, 414–426. https://doi.org/10.1016/j.neuroimage.2014.05.069

Rosas, H.D., Liu, A.K., Hersch, S., Glessner, M., Ferrante, R.J., Salat, D.H., Van Der Kouwe, A., Jenkins, B.G., Dale, A.M., Fischl, B., 2002. Regional and progressive thinning of the cortical ribbon in Huntington's disease. Neurology 58, 695–701. https://doi.org/10.1212/WNL.58.5.695

Rossiter, H.E., Davis, E.M., Clark, E. V., Boudrias, M.H., Ward, N.S., 2014. Beta oscillations reflect changes in motor cortex inhibition in healthy ageing. Neuroimage 91, 360–365. https://doi.org/10.1016/j.neuroimage.2014.01.012

Rosso, A.L., Studenski, S.A., Chen, W.G., Aizenstein, H.J., Alexander, N.B., Bennett, D.A., Black, S.E., Camicioli, R., Carlson, M.C., Ferrucci, L., 2013. Aging, the Central Nervous System, and Mobility. Journals Gerontol. Med. Sci. 68, 1379–1386. https://doi.org/10.1093/gerona/glt089

Sailer, A., Dichgans, J., Gerloff, C., 2000. The influence of normal aging on the cortical processing of a simple motor task. Neurology 979–986.

Sakoglu, U., Calhoun, V.D., Pearlson, G.D., Kiehl, K.A., Wang, Y.M., Michael, A.M., 2010. A method for evaluating dynamic functional network connectivity and task-modulation: Application to schizophrenia. Magn. Reson. Mater. Physics, Biol. Med. https://doi.org/10.1007/s10334-010-0197-8

Sala-Llonch, R., Bartrés-Faz, D., Junqué, C., 2015. Reorganization of brain networks in aging: a review of functional connectivity studies. Front. Psychol. 6, 663. https://doi.org/10.3389/fpsyg.2015.00663

Salat, D.H., Buckner, R.L., Snyder, A.Z., Greve, D.N., Desikan, R.S.R., Busa, E., Morris, J.C., Dale, A.M., Fischl, B., 2004. Thinning of the cerebral cortex in aging. Cereb. Cortex 14, 721–730. https://doi.org/10.1093/cercor/bhh032

Salimi-Khorshidi, G., Douaud, G., Beckmann, C.F., Glasser, M.F., Griffanti, L., Smith, S.M., 2014. Automatic denoising of functional MRI data: Combining independent component analysis and hierarchical fusion of classifiers. Neuroimage 90, 449–468. https://doi.org/10.1016/j.neuroimage.2013.11.046

Salmelin, R., Hämäläinen, M., Kajola, M., Hari, R., 1995. Functional segregation of movement-related rhythmic activity in the human brain. Neuroimage. https://doi.org/10.1006/nimg.1995.1031

Satterthwaite, T.D., Elliott, M.A., Gerraty, R.T., Ruparel, K., Loughead, J., Calkins, M.E., Eickhoff, S.B., Hakonarson, H., Gur, R.C., Gur, R.E., Wolf, D.H., 2013. An improved framework for confound regression and filtering for control of motion artifact in the preprocessing of resting-state functional connectivity data. Neuroimage 64, 240–256. https://doi.org/10.1016/j.neuroimage.2012.08.052

Satterthwaite, T.D., Wolf, D.H., Loughead, J., Ruparel, K., Elliott, M.A., Hakonarson, H., Gur, R.C., Gur, R.E., 2012.

Impact of in-scanner head motion on multiple measures of functional connectivity: Relevance for studies of neurodevelopment in youth. Neuroimage 60, 623–632. https://doi.org/10.1016/j.neuroimage.2011.12.063

Savva, A.D., Kassinopoulos, M., Smyrnis, N., Matsopoulos, G.K., Mitsis, G.D., 2019. Effects of Motion Related Outliers in Dynamic Functional Connectivity Using the Sliding Window Method. J. Neurosci. Methods 108519. https://doi.org/10.1016/j.jneumeth.2019.108519

Scheeringa, R., Petersson, K.M., Kleinschmidt, A., Jensen, O., Bastiaansen, M.C.M., 2012. EEG Alpha Power Modulation of fMRI Resting-State Connectivity. Brain Connect. 2, 254–264. https://doi.org/10.1089/brain.2012.0088

Schmiedt-Fehr, C., Mathes, B., Kedilaya, S., Krauss, J., Basar-Eroglu, C., 2016. Aging differentially affects alpha and beta sensorimotor rhythms in a go/nogo task. Clin. Neurophysiol. 127, 3234–3242. https://doi.org/10.1016/j.clinph.2016.07.008

Schoffelen, J.M., Oostenveld, R., Fries, P., 2008. Imaging the human motor system's beta-band synchronization during isometric contraction. Neuroimage 41, 437–447. https://doi.org/10.1016/j.neuroimage.2008.01.045

Scholvinck, M.L., Maier, A., Ye, F.Q., Duyn, J.H., Leopold, D.A., 2010. Neural basis of global resting-state fMRI activity. Proc. Natl. Acad. Sci. 107, 10238–10243. https://doi.org/10.1073/pnas.0913110107

Schölvinck, M.L., Maier, A., Ye, F.Q., Duyn, J.H., Leopold, D.A., 2010. Neural basis of global resting-state fMRI activity. Proc. Natl. Acad. Sci. U. S. A. 107, 10238–43. https://doi.org/10.1073/pnas.0913110107

Scott, S.H., 2012. The computational and neural basis of voluntary motor control and planning. Trends Cogn. Sci. 16, 541–549. https://doi.org/10.1016/j.tics.2012.09.008

Ségonne, F., Dale, A.M., Busa, E., Glessner, M., Salat, D., Hahn, H.K., Fischl, B., 2004. A hybrid approach to the skull stripping problem in MRI. Neuroimage 22, 1060–1075. https://doi.org/10.1016/j.neuroimage.2004.03.032

Seidler, R.D., Bernard, J.A., Burutolu, T.B., Fling, B.W., Gordon, M.T., Gwin, J.T., Kwak, Y., Lipps, D.B., 2010. Motor control and aging: Links to age-related brain structural, functional, and biochemical effects. Neurosci. Biobehav. Rev. 34, 721–733. https://doi.org/10.1016/j.neubiorev.2009.10.005

Seitzman, B.A., Gratton, C., Laumann, T.O., Gordon, E.M., Adeyemo, B., Dworetsky, A., Kraus, B.T., Gilmore, A.W., Berg, J.J., Ortega, M., Nguyen, A., Greene, D.J., McDermott, K.B., Nelson, S.M., Lessov-Schlaggar, C.N., Schlaggar, B.L., Dosenbach, N.U.F., Petersen, S.E., 2019. Trait-like variants in human functional brain networks. Proc. Natl. Acad. Sci. https://doi.org/10.1073/pnas.1902932116

Seitzman, B.A., Gratton, C., Marek, S., Raut, R. V., Dosenbach, N.U.F., Schlaggar, B.L., Petersen, S.E., Greene, D.J., 2020. A set of functionally-defined brain regions with improved representation of the subcortex and cerebellum. Neuroimage 206, 116290. https://doi.org/10.1016/j.neuroimage.2019.116290

Shannon, B.J., Dosenbach, R.A., Su, Y., Vlassenko, A.G., Larson-Prior, L.J., Nolan, T.S., Snyder, A.Z., Raichle, M.E., 2013. Morning-evening variation in human brain metabolism and memory circuits. J. Neurophysiol. 109, 1444–1456. https://doi.org/10.1152/jn.00651.2012

Shmuel, A., Leopold, D.A., 2008. Neuronal correlates of spontaneous fluctuations in fMRI signals in monkey visual cortex: Implications for functional connectivity at rest. Hum. Brain Mapp. 29, 751–761. https://doi.org/10.1002/hbm.20580

Shmueli, K., van Gelderen, P., de Zwart, J.A., Horovitz, S.G., Fukunaga, M., Jansma, J.M., Duyn, J.H., 2007. Low-frequency fluctuations in the cardiac rate as a source of variance in the resting-state fMRI BOLD signal. Neuroimage 38, 306–320. https://doi.org/10.1016/j.neuroimage.2007.07.037

Silberstein, P., Pogosyan, A., Kühn, A.A., Hotton, G., Tisch, S., Kupsch, A., Dowsey-Limousin, P., Hariz, M.I., Brown, P., 2005. Cortico-cortical coupling in Parkinson's disease and its modulation by therapy. Brain

128, 1277–1291. https://doi.org/10.1093/brain/awh480

Smith, S.M., Beckmann, C.F., Andersson, J., Auerbach, E.J., Bijsterbosch, J., Douaud, G., Duff, E., Feinberg, D.A., Griffanti, L., Harms, M.P., Kelly, M., Laumann, T., Miller, K.L., Moeller, S., Petersen, S., Power, J., Salimi-Khorshidi, G., Snyder, A.Z., Vu, A.T., Woolrich, M.W., Xu, J., Yacoub, E., Uğurbil, K., Van Essen, D.C., Glasser, M.F., 2013. Resting-state fMRI in the Human Connectome Project. Neuroimage 80, 144–168. https://doi.org/10.1016/j.neuroimage.2013.05.039

Smith, Stephen M, Fox, P.T., Miller, K.L., Glahn, D.C., Fox, P.M., Mackay, C.E., Filippini, N., Watkins, K.E., Toro, R., Laird, A.R., Beckmann, C.F., 2009. Correspondence of the brain's functional architecture during activation and rest. Proc. Natl. Acad. Sci. U. S. A. 106, 13040–5. https://doi.org/10.1073/pnas.0905267106

Smith, S. M., Fox, P.T., Miller, K.L., Glahn, D.C., Fox, P.M., Mackay, C.E., Filippini, N., Watkins, K.E., Toro, R., Laird, A.R., Beckmann, C.F., 2009. Correspondence of the brain's functional architecture during activation and rest. Proc. Natl. Acad. Sci. 106, 13040–13045. https://doi.org/10.1073/pnas.0905267106

Smith, S.M., Nichols, T.E., Vidaurre, D., Winkler, A.M., Behrens, T.E.J., Glasser, M.F., Ugurbil, K., Barch, D.M., Van Essen, D.C., Miller, K.L., 2015. A positive-negative mode of population covariation links brain connectivity, demographics and behavior. Nat. Neurosci. 18, 1565–1567. https://doi.org/10.1038/nn.4125

Solis-Escalante, T., Müller-Putz, G.R., Pfurtscheller, G., Neuper, C., 2012. Cue-induced beta rebound during withholding of overt and covert foot movement. Clin. Neurophysiol. 123, 1182–1190. https://doi.org/10.1016/j.clinph.2012.01.013

Spinks, R.L., Kraskov, A., Brochier, T., Umilta, M.A., Lemon, R.N., 2008. Selectivity for Grasp in Local Field Potential and Single Neuron Activity Recorded Simultaneously from M1 and F5 in the Awake Macaque Monkey. J. Neurosci. 28, 10961–10971. https://doi.org/10.1523/JNEUROSCI.1956-08.2008

Sporns, O., 2013. The human connectome: Origins and challenges. Neuroimage 80, 53–61. https://doi.org/10.1016/j.neuroimage.2013.03.023

Stancák, A., Pfurtscheller, G., 1995. Desynchronization and recovery of β rhythms during brisk and slow self-paced finger movements in man. Neurosci. Lett. 196, 21–24. https://doi.org/10.1016/0304-3940(95)11827-J

Stebbins, G.T., Carrillo, M.C., Dorfman, J., Dirksen, C., Desmond, J.E., Turner, D. a, Bennett, D. a, Wilson, R.S., Glover, G., Gabrieli, J.D.E., 2002. Aging effects on memory encoding in the frontal lobes. Psychol. Aging 17, 44–55. https://doi.org/10.1037/0882-7974.17.1.44

Suárez, L.E., Markello, R.D., Betzel, R.F., Misic, B., 2020. Linking Structure and Function in Macroscale Brain Networks. Trends Cogn. Sci. 24, 302–315. https://doi.org/10.1016/j.tics.2020.01.008

Susi, G., de Frutos-Lucas, J., Niso, G., Ye-Chen, S.M., Toro, L.A., Chino Vilca, B.N., Maestú, F., Susi, G., de Frutos-Lucas, J., Niso, G., Ye-Chen, S.M., Toro, L.A., Chino Vilca, B.N., Maestú, F., 2019. Healthy and Pathological Neurocognitive Aging: Spectral and Functional Connectivity Analyses Using Magnetoencephalography, Oxford Research Encyclopedia of Psychology. https://doi.org/10.1093/acrefore/9780190236557.013.387

Tadel, F., Baillet, S., Mosher, J.C., Pantazis, D., Leahy, R.M., 2011. Brainstorm: A user-friendly application for MEG/EEG analysis. Comput. Intell. Neurosci. 2011. https://doi.org/10.1155/2011/879716

Tagliazucchi, E., Laufs, H., 2014. Decoding Wakefulness Levels from Typical fMRI Resting-State Data Reveals Reliable Drifts between Wakefulness and Sleep. Neuron 82, 695–708. https://doi.org/10.1016/j.neuron.2014.03.020

Tatti, E., Rossi, S., Innocenti, I., Rossi, A., Santarnecchi, E., 2016. Non-invasive brain stimulation of the aging brain: State of the art and future perspectives. Ageing Res. Rev. 29, 66–89.

https://doi.org/10.1016/j.arr.2016.05.006

Thompson, G.J., Magnuson, M.E., Merritt, M.D., Schwarb, H., Pan, W.J., Mckinley, A., Tripp, L.D., Schumacher, E.H., Keilholz, S.D., 2013a. Short-time windows of correlation between large-scale functional brain networks predict vigilance intraindividually and interindividually. Hum. Brain Mapp. 34, 3280–3298. https://doi.org/10.1002/hbm.22140

Thompson, G.J., Merritt, M.D., Pan, W.J., Magnuson, M.E., Grooms, J.K., Jaeger, D., Keilholz, S.D., 2013b. Neural correlates of time-varying functional connectivity in the rat. Neuroimage 83, 826–836. https://doi.org/10.1016/j.neuroimage.2013.07.036

Thompson, G.J., Riedl, V., Grimmer, T., Drzezga, A., Herman, P., Hyder, F., 2016. The Whole-Brain "Global" Signal from Resting State fMRI as a Potential Biomarker of Quantitative State Changes in Glucose Metabolism. Brain Connect. 6, 435–447. https://doi.org/10.1089/brain.2015.0394

Thulborn, K.R., Waterton, J.C., Matthews, P.M., Radda, G.K., 1982. Oxygenation dependence of the transverse relaxation time of water protons in whole blood at high field. Biochim. Biophys. Acta 714, 265–270. https://doi.org/10.1016/0304-4165(82)90333-6

Tong, Y., Frederick, B. de B., 2014. Studying the spatial distribution of physiological effects on BOLD signals using ultrafast fMRI. Front. Hum. Neurosci. 8, 1–8. https://doi.org/10.3389/fnhum.2014.00196

Tong, Y., Hocke, L.M., Frederick, B.B., 2019. Low Frequency Systemic Hemodynamic "Noise" in Resting State BOLD fMRI: Characteristics, Causes, Implications, Mitigation Strategies, and Applications. Front. Neurosci. 13. https://doi.org/10.3389/fnins.2019.00787

Tong, Y., Hocke, L.M., Nickerson, L.D., Licata, S.C., Lindsey, K.P., Frederick, B. de B., 2013. Evaluating the effects of systemic low frequency oscillations measured in the periphery on the independent component analysis results of resting state networks. Neuroimage 76, 202–215. https://doi.org/10.1016/j.neuroimage.2013.03.019

Toth, M., Kiss, A., Kosztolanyi, P., Kondakor, I., 2007. Diurnal alterations of brain electrical activity in healthy adults: A LORETA study. Brain Topogr. 20, 63–76. https://doi.org/10.1007/s10548-007-0032-3

Triantafyllou, C., Hoge, R.D., Krueger, G., Wiggins, C.J., Potthast, A., Wiggins, G.C., Wald, L.L., 2005. Comparison of physiological noise at 1.5 T, 3 T and 7 T and optimization of fMRI acquisition parameters. Neuroimage 26, 243–250. https://doi.org/10.1016/j.neuroimage.2005.01.007

Triantafyllou, C., Polimeni, J.R., Wald, L.L., 2011. Physiological noise and signal-to-noise ratio in fMRI with multi-channel array coils. Neuroimage 55, 597–606. https://doi.org/10.1016/j.neuroimage.2010.11.084

Tsvetanov, K.A., Henson, R.N., Jones, P.S., Mutsaerts, H.-J., Fuhrmann, D., Tyler, L.K., Cam-CAN, Rowe, J.B., 2019. The effects of age on resting-state BOLD signal variability is explained by cardiovascular and neurovascular factors. bioRxiv.

Tsvetanov, K.A., Henson, R.N.A., Tyler, L.K., Davis, S.W., Shafto, M.A., Taylor, J.R., Williams, N., Cam-Can, Rowe, J.B., 2015. The effect of ageing on fMRI: Correction for the confounding effects of vascular reactivity evaluated by joint fMRI and MEG in 335 adults. Hum. Brain Mapp. 36, 2248–2269. https://doi.org/10.1002/hbm.22768

Turchi, J., Chang, C., Ye, F.Q., Russ, B.E., Yu, D.K., Cortes, C.R., Monosov, I.E., Duyn, J.H., Leopold, D.A., 2018. The Basal Forebrain Regulates Global Resting-State fMRI Fluctuations. Neuron 97, 940-952.e4. https://doi.org/10.1016/j.neuron.2018.01.032

Valenza, G., Sclocco, R., Duggento, A., Passamonti, L., Napadow, V., Barbieri, R., Toschi, N., 2019. The central autonomic network at rest: Uncovering functional MRI correlates of time-varying autonomic outflow. Neuroimage. https://doi.org/10.1016/j.neuroimage.2019.04.075

Van de Moortele, P.F., Pfeuffer, J., Glover, G.H., Ugurbil, K., Hu, X., 2002. Respiration-induced Bo fluctuations

and their spatial distribution in the human brain at 7 Tesla. Magn. Reson. Med. 47, 888–895. https://doi.org/10.1002/mrm.10145

van Dijk, K.R.A., Sabuncu, M.R., Buckner, R.L., 2012. The influence of head motion on intrinsic functional connectivity MRI. Neuroimage 59, 431–438. https://doi.org/10.1016/j.neuroimage.2011.07.044

Van Essen, D.C., Smith, S.M., Barch, D.M., Behrens, T.E.J., Yacoub, E., Ugurbil, K., 2013. The WU-Minn Human Connectome Project: An overview. Neuroimage 80, 62–79. https://doi.org/10.1016/j.neuroimage.2013.05.041

Van Essen, D.C., Ugurbil, K., Auerbach, E., Barch, D., Behrens, T.E.J., Bucholz, R., Chang, A., Chen, L., Corbetta, M., Curtiss, S.W., Della Penna, S., Feinberg, D., Glasser, M.F., Harel, N., Heath, A.C., Larson-Prior, L., Marcus, D., Michalareas, G., Moeller, S., Oostenveld, R., Petersen, S.E., Prior, F., Schlaggar, B.L., Smith, S.M., Snyder, A.Z., Xu, J., Yacoub, E., 2012. The Human Connectome Project: A data acquisition perspective. Neuroimage 62, 2222–2231. https://doi.org/10.1016/j.neuroimage.2012.02.018

Van Veen, B.D., van Drongelen, W., Yuchtman, M., Suzuki, A., 1997. Localization of brain electrical activity via linearly constrained minimum variance spatial filtering. IEEE Trans. Biomed. Eng. 44, 867–880. https://doi.org/10.1109/10.623056

van Wijk, B.C.M., Beek, P.J., Daffertshofer, A., 2012. Differential modulations of ipsilateral and contralateral beta (de)synchronization during unimanual force production. Eur. J. Neurosci. 36, 2088–2097. https://doi.org/10.1111/j.1460-9568.2012.08122.x

Vanderwal, T., Eilbott, J., Finn, E.S., Craddock, R.C., Turnbull, A., Castellanos, F.X., 2017. Individual differences in functional connectivity during naturalistic viewing conditions. Neuroimage 157, 521–530. https://doi.org/10.1016/j.neuroimage.2017.06.027

Veldhuizen, R.J., Jonkman, E.J., Poortvliet, D.C., 1993. Sex differences in age regression parameters of healthy adults--normative data and practical implications. Electroencephalogr. Clin. Neurophysiol. 86, 377–84.

Vidaurre, D., Hunt, L.T., Quinn, A.J., Hunt, B.A.E., Brookes, M.J., Nobre, A.C., Woolrich, M.W., 2018. Spontaneous cortical activity transiently organises into frequency specific phase-coupling networks. Nat. Commun. 9. https://doi.org/10.1038/s41467-018-05316-z

Vidaurre, D., Smith, S.M., Woolrich, M.W., 2017. Brain network dynamics are hierarchically organized in time. Proc. Natl. Acad. Sci. 114, 201705120. https://doi.org/10.1073/pnas.1705120114

Vigneau-Roy, N., Bernier, M., Descoteaux, M., Whittingstall, K., 2014. Regional variations in vascular density correlate with resting-state and task-evoked blood oxygen level-dependent signal amplitude. Hum. Brain Mapp. 35, 1906–1920. https://doi.org/10.1002/hbm.22301

Wang, C., Ong, J.L., Patanaik, A., Zhou, J., Chee, M.W.L., 2016. Spontaneous eyelid closures link vigilance fluctuation with fMRI dynamic connectivity states. Proc. Natl. Acad. Sci. 113, 9653–9658. https://doi.org/10.1073/pnas.1523980113

Whittaker, J.R., Driver, I.D., Venzi, M., Bright, M.G., Murphy, K., 2019. Cerebral autoregulation evidenced by synchronized low frequency oscillations in blood pressure and resting-state fMRI. Front. Neurosci. 13, 1–12. https://doi.org/10.3389/fnins.2019.00433

Wilson, T.W., Heinrichs-Graham, E., Becker, K.M., 2014. Circadian modulation of motor-related beta oscillatory responses. Neuroimage 102, 531–539. https://doi.org/10.1016/j.neuroimage.2014.08.013

Winder, A.T., Echagarruga, C., Zhang, Q., Drew, P.J., 2017. Weak correlations between hemodynamic signals and ongoing neural activity during the resting state. Nat. Neurosci. 20, 1761–1769. https://doi.org/10.1038/s41593-017-0007-y

Wise, R.G., Ide, K., Poulin, M.J., Tracey, I., 2004. Resting fluctuations in arterial carbon dioxide induce significant low frequency variations in BOLD signal. Neuroimage 21, 1652–1664. https://doi.org/10.1016/j.neuroimage.2003.11.025

Wong, C.K., Zotev, V., Misaki, M., Phillips, R., Luo, Q., Bodurka, J., 2016. Automatic EEG-assisted retrospective motion correction for fMRI (aE-REMCOR). Neuroimage 129, 133–147. https://doi.org/10.1016/j.neuroimage.2016.01.042

Wong, C.W., DeYoung, P.N., Liu, T.T., 2016. Differences in the resting-state fMRI global signal amplitude between the eyes open and eyes closed states are related to changes in EEG vigilance. Neuroimage 124, 24–31. https://doi.org/10.1016/j.neuroimage.2015.08.053

Wong, C.W., Olafsson, V., Tal, O., Liu, T.T., 2013. The amplitude of the resting-state fMRI global signal is related to EEG vigilance measures. Neuroimage 83, 983–990. https://doi.org/10.1016/j.neuroimage.2013.07.057

Xia, C.H., Ma, Z., Ciric, R., Gu, S., Betzel, R.F., Kaczkurkin, A.N., Calkins, M.E., Cook, P.A., García de la Garza, A., Vandekar, S.N., Cui, Z., Moore, T.M., Roalf, D.R., Ruparel, K., Wolf, D.H., Davatzikos, C., Gur, R.C., Gur, R.E., Shinohara, R.T., Bassett, D.S., Satterthwaite, T.D., 2018. Linked dimensions of psychopathology and connectivity in functional brain networks. Nat. Commun. 9, 1–14. https://doi.org/10.1038/s41467-018-05317-y

Xia, Y., Chen, Q., Shi, L., Li, M.Z., Gong, W., Chen, H., Qiu, J., 2019. Tracking the dynamic functional connectivity structure of the human brain across the adult lifespan. Hum. Brain Mapp. 40, 717–728. https://doi.org/10.1002/hbm.24385

Xifra-Porxas, A., Kassinopoulos, M., Mitsis, G.D., 2020. Physiological and head motion signatures in static and time-varying functional connectivity and their subject discriminability. bioRxiv.

Yan, C.G., Cheung, B., Kelly, C., Colcombe, S., Craddock, R.C., Di Martino, A., Li, Q., Zuo, X.N., Castellanos, F.X., Milham, M.P., 2013. A comprehensive assessment of regional variation in the impact of head micromovements on functional connectomics. Neuroimage 76, 183–201. https://doi.org/10.1016/j.neuroimage.2013.03.004

Yeo, B.T.T., Tandi, J., Chee, M.W.L., 2015. Functional connectivity during rested wakefulness predicts vulnerability to sleep deprivation. Neuroimage 111, 147–158. https://doi.org/10.1016/j.neuroimage.2015.02.018

Yuan, H., Zotev, V., Phillips, R., Bodurka, J., 2013. Correlated slow fluctuations in respiration, EEG, and BOLD fMRI. Neuroimage 79, 81–93. https://doi.org/10.1016/j.neuroimage.2013.04.068

Zarahn, E., Aguirre, G.K., D'Esposito, M., 1997. Empirical Analyses of BOLD fMRI Statistics. Neuroimage 5, 199–212. https://doi.org/10.1006/nimg.1997.0264

Zeng, L.-L., Wang, D., Fox, M.D., Sabuncu, M., Hu, D., Ge, M., Buckner, R.L., Liu, H., 2014. Neurobiological basis of head motion in brain imaging. Proc. Natl. Acad. Sci. 111, 6058–6062. https://doi.org/10.1073/pnas.1317424111

Zhang, J., Huang, Z., Tumati, S., Northoff, G., 2019. Intrinsic Architecture of Global Signal Topography and Its Modulation by Tasks. bioRxiv.

Zilles, K., Armstrong, E., Schleicher, A., Kretschmann, H.J., 1988. The human pattern of gyrification in the cerebral cortex. Anat. Embryol. (Berl). 179, 173–179. https://doi.org/10.1007/BF00304699

Zimmerman, J.E., Thiene, P., Harding, J.T., 1970. Design and operation of stable rf-biased superconducting point-contact quantum devices, and a note on the properties of perfectly clean metal contacts. J. Appl. Phys. 41, 1572–1580. https://doi.org/10.1063/1.1659074